UNIVERSITY OF PALERMO

Department of Chemical, Management, Informatics and Mechanical Engineering

UNIVERSITY OF ERLANGEN-NUREMBERG

Chair of Manufacturing Technology

Fundamental investigation on the mechanical behavior of weld seams

PhD CANDIDATE

Ing Sergio Pellegrino

COORDINATOR

Ch. Mo Prof. Ing. Salvatore Gaglio

TUTOR

Ch. Mo Prof. Ing. Livan Fratini

CO-TUTOR

Prof. Dr.-Ing. habil. Marion Merklein

CYCLE XXVI

ACADEMIC YEAR 2015/2016

Als binationale Dissertation genehmigt von der Technischen Fakultät der Friedrich-Alexander-Universität Erlangen-Nürnberg

Tag der mündlichen Prüfung: 08/03/2016

Vorsitzende des Promotionsorgans: Prof. Dr. -Ing. habil. Marion Merklein

Gutachter:

Prof. Dr. Livan Fratini, Università degli Studi di Palermo

Prof. Dr.-Ing. habil. Marion Merklein, Friedrich-Alexander-Universität Erlangen-Nürnberg

Cotutelle

The joint supervision of thesis is a mode of carrying out the PhD, which involves the registration of the candidate in two universities, in two different countries, and the issuing of a qualification recognized by both states.

In order to apply for the admission under the joint supervision the candidate must be already registered in a PhD program, and both the involved countries must have already signed a mutual framework agreement. If these conditions exist, it is necessary to enter into an agreement for each student registered at joint supervision. The agreement must be prepared by the candidate together with the two tutors and approved by the Academic Senate and signed by the Rectors of the involved universities.

During the preparation of the thesis, the student is under the joint supervision of both the two tutors, one for each university. The student must stay alternately in the two institutions, to which the two tutors belong (and usually for equal periods). The oral defense takes place in front of a joint committee of university professors from both countries (at least two per side). The diploma can be unique or double, but in any case it must mention the existence of the joint supervision.

In Italy, the authority responsible for the drafting of agreements for joint supervision is the CRUI (Conference of Italian University Rectors).

This thesis is the result of a research study carried out under the joint supervision operated by the University of Palermo and the Friedrich-Alexander- Universität Erlangen-Nürnberg, and in particular between the departments of the “Chemical Engineering, Management, Computer Science, Mechanical Engineering (DICGIM)” and the “Lehrstuhl für Fertigungstechnologie (LFT)”. Prof. Livan Fratini (for the University of Palermo) and Prof. Marion Merklein (for FAU) were the tutors of this thesis.

Abstract

The solid state welding processes allow joints free from defects with reduced residual stresses and low distortion. However, such processes are generally characterized by a complex mechanical junction because of the particular material flow. Therefore, the design and optimization of the processes in which the solid bonding phenomenon occurs are difficult and requires a large number of tests. The purpose of this research is the description on the mechanical behavior of welded seams obtained through the friction stir welding (FSW) and linear friction welding (LFW) processes by analyzing the same phenomenon that occurs in both metallurgical processes, named the solid bonding phenomenon. The aim of this research is the development of a technique for the FSW and LFW processes, able to quantitative determine the weldability degree of a material as a function of the technological parameters of the processes. The description of this phenomenon has been done through the solid bonding criteria. The development and the applicability of the analytical bonding criteria, originally developed for different manufacturing processes, has been studied on the FSW and LFW processes in order to obtain an integrated numerical tool able to predict the occurrence of solid bonding starting from the process input parameters. LFW and FSW experimental campaigns AA6082 and AA6061 aluminum alloys were carried out with the aim to study the effects of the process parameters on the quality of the welded joints. Appropriate process windows have been defined for both the processes, to acquire the data needed to implement the integrated numerical tool of the processes. At the same time, a numerical model of the processes have been developed and set up, obtaining information on the field variables needed to implement the bonding criterion proposed. The experimental and numerical campaign led to an exhaustive knowledge of the material flow phenomena as function of the process operative parameters, thus obtaining effective design tools for both the solid state welding processes. The applicability of the pressure-time criterion has been tested on the FSW process and LFW process using the two different aluminum alloys. Additionally, the Neural Network was developed able to predict, starting from the evolution of temperature, strain, strain rate and pressure on the bonding line, the occurrence of the solid bonding as well as quantitative parameter Q providing information on the “quality” of the weld.

Index

1 Introduction

1.1 The Need to investigate the solid state bonding

The technologies of welding and cutting of metals represent one of the main sectors of the manufacturing industry. Therefore, developing an innovative supply chains for the welding technologies, it is a topic that the market looks with great attention in order to improve the reliability and competitive use of them.

The welding technology is a topic in continuous evolution in which the research field is always open. Nowadays, to improve efficiency and reduce the costs, new technologies such as the High Energy Density Welding process [1] and Solid State Process [2] have established their role within the market.

The European Union regulations for CO_2 emissions for 2021 request a reduction of about 40 % compared to the 2007 fleet average [3]. In this context, one promising approach to reach this goal is lightweight construction. The reduction of the vehicle mass leads to a significant saving of fuels and emissions. In order to reduce the weight of the body in white, different strategies are pursued. High strength materials are applied to crash-relevant parts to simultaneously reduce sheet thickness and mass. On the one hand, Aluminum, due to its light weight, is applied to bodyshell parts such as roofs or doors. Another approach is to use the most appropriate material such as aluminum, magnesium and carbon fiber reinforced plastics for each specific component. However, this last approach leads to new challenges regarding the joining technology.

Solid state joining and processing technologies are becoming the centre of attention of scientists and engineers involved with advanced lightweight structures. The main reason for that is the nature of such processes: since bonding and processing take place in the solid state, all metallurgical reactions involved in the melting and solidification are avoided, resulting in defect-free joints with better properties.

Some example of solid state welding methods [4] that do not involve the melting of the joined materials are the ultrasonic welding [5], the explosion welding [6], friction welding [7] (including friction stir welding and the linear friction welding), magnetic pulse welding [8], co-extrusion welding [9], diffusion bonding [10], exothermic welding [11], high frequency welding [12], induction welding [13], porthole die extrusion [14] and roll welding [15].

The main solid state bonding processes used in industry are: the Porthole Die Extrusion (PDE) [16], Accumulative Roll Bonding (ARB) [17], the Friction Welding (FRW) such as the Friction Stir Welding (FSW) [18] and the Linear Friction Welding (LFW) [19]. These processes will be therefore investigated in order to study the solid bonding phenomena.

Particular attention is paid to the friction welding processes (FRW), i.e. friction stir welding (FSW) and Linear friction welding (LFW). The FRW processes are a solid-state welding process that generates heat through mechanical friction between workpieces in relative motion to each other, with the addition of a lateral force called "upset". This allows plastically displacing and fusing the materials. Friction welding is used with metals and thermoplastics in a wide variety of aviation and automotive applications. The combination of fast joining times (in the order of a few seconds), and direct heat input at the weld interface, yields to relatively small heat-affected zones. Friction welding techniques are generally melt-free, which avoids grain growth in engineered materials, such as high-strength heat-treated steels. Another advantage of this technique is that the motion tends to "clean" the surface between the welded materials, which means that they can be joined with less preparation. During the welding process, depending on the method being used, small debris are forced out of the working mass (flash). Another advantage of FRW is that it allows different materials to be joined. This is particularly useful in aerospace, where lightweight materials such as aluminum are joined to high-strength steels.

These solid state welding processes, object of this work, do not provide the filler material and is governed by operating parameters of which the most important are the time, temperature and pressure.
Thanks to these new technologies, it has been possible to conceive and develop a whole new set of welded joints. With the FSW and LFW process is possible obtaining particular microstructure characteristics of the welded joints, to improve the mechanical properties and also to improve the production efficiency and integrity of the parts already tested.

All these processes have in common the same phenomenon: the solid bonding phenomena. This phenomenon is governed by some parameters such as time,

temperature, and pressure that individually or in combination produce coalescence of the base metal without significant melting of the base metals.

These processes are not only important for the current applications, but also for their future development in fields such as shipbuilding, railway and automobile production of electric motors, etc.

The solid state welding of seams represents a major manufacturing problem, inasmuch as it affects the productivity of the process, the resistance of the profile and the aspect of the surface.
Currently, the soundness of welded joints involves only destructive test methods, such as bending tests and tearing of the joints. These methods, far from being significant and repeatable, have the great disadvantage to give information only when the process has already been finished, at the very end of product development.
For this reason, criteria for predicting the welding quality are of particular interest. These criteria should implement processes which guarantee the minimum mechanical strength of the welds once the profile is produced in a definite set of operative conditions.
It follows that the progressive extension of the concept of weldability, the material ability to be welded, goes together with technological development.
The measurement of the material weldability degree is an innovative field which essentially focuses on the development of tests in order to characterize the welded materials.
The aim of this research is the development of a technique able to quantitative determines the weldability degree of a material as a function of the technological parameters of the welding process.

1.2 Overview of the solid state bonding

The solid state bonding processes such as Friction Stir Welding (FSW), Linear Friction Welding (LFW), Porthole Die Extrusion (PDE), and Accumulative Roll Bonding (ARB) are currently widely used in industry [20] due to their ability of not requiring the melting of the material, making them particularly suitable for all those materials difficult to weld with traditional techniques, such as alloys of aluminum,

magnesium and titanium. However, often the process is based on the knowledge of the operator rather than upon scientific knowledge. In fact, the solid bonding phenomenon has not been the subject of detailed studies.

In the last two decades, few studies were presented regarding the mechanical process of such techniques [21]. The researchers focused on numerical analyses aimed at highlighting strain, strain rate and stress distributions in the workpiece. Investigations on FSW process were mainly focusing on the geometry of the tool, while regarding the porthole die extrusion process investigations were giving attention to the porthole die and to the effectiveness of the occurring material flow. It should be observed that often the industrial design of such parts is carried out just on the basis of workers experience and skills; the studies of these processes with the aim of advanced FE tools can provide innovative solutions, allowing the production of more efficient parts. Nevertheless, it should be observed that the geometry of these parts is just one of the variables that strongly affect the effectiveness of the joints part and in particular the strength of the welding lines. The effectiveness of the joining parts is usually investigated via experimental destructive tests. In particular, bending tests and tearing of the joints are the most common methods, together with local mechanical investigations of the parts as micro-hardness tests and metallurgical observations. Overall, these methods are just ex post verifications which are developed when the tool has already been built and defined. In this way, in the last years [22], in order to set up definitively effective numerical tools, 3D thermo-mechanical models were completed with effective bonding criteria implemented in order to take into account the actual phenomena occurring during the solid bonding processes.

The first criterion for the production of sound joints is based on rules for die design. In particular, it is well known that the extrusion ratio, in the PDE process, between the welding zone and the die exit is the main factor for achieving a high weld quality. Another important aspect investigated by researcher is the achievement of adequate interface pressures in the welding zone. *Akeret* [23] indicated a critical pressure value equal to at least three times the flow stress of the material; *Bourqui et al.* [24] suggested a ratio of 0.5 between pressure in the welding chamber and at die entrance. The adoption of numerical analyses now allows an accurate evaluation of the plastic flow of the deforming material and, as a consequence, the application of more specific welding criteria. However, several problems arise with the validation of

these methods; among these are: welding strength depends not only on the mechanics of the process, the variability of the chemical composition, sometimes defects are due to oxides or inclusions dragged into the welding zone.
Due to the several variables mentioned above, a systematic comparison between welding quality prediction techniques has not been performed yet. While generic “rules” are still applied to particular cases and cannot be generalized, “criteria”, which are later described, have never put in relation by means of an adequate investigation and their practical effectiveness is still unknown.
After determining the welding surface via FEM analysis, some element variables such as pressure, effective stress and velocity must be determined. The methods such as Maximum pressure criterion, proposed by *Akeret* [23], Pressure–time criterion, proposed by *Plata and Piwnik* [25] and the Pressure–time–flow criterion have been studied and used to characterize the mechanical behavior of the solid bonding welded seams.

1.3 Thesis objectives

The aim of this research is the development of a technique for the FSW and LFW processes, able to quantitative determine the weldability degree of a material as a function of the technological parameters of the processes.

Within this work, a detailed survey of the literature, aimed at the identification of a suitable plan for the experiments to be performed has been conducted in order to implement the criteria that represent the solid bonding phenomena at the FSW process and LFW process.

Therefore experimental studies have been conducted in order to validate results from a numerical investigation.

The challenge of this work was due to the innovation of these methods which made difficult the establishment of the best method. The methods developed within the research can be applied to other processes where the metallurgical phenomena that govern the junctions are the same.

Friction stir welding and the linear friction welding technology have been a major boon to advanced industry since their introduction. In spite of their short history, they have found widespread applications in diverse industry sectors. Hard materials such as steel and other important engineering alloys can be now welded efficiently using these processes. Significant progress has also been made in the fundamental understanding of both welding processes and the structure and properties of the welded joints. The understanding of the solid bonding phenomena that occurs in both processes will be useful in reducing defects and improving uniformity of weld properties and, at the same time, expanding the applicability of these processes to new engineering alloys. With a better quantitative understanding of the underlying principles of heat transfer, material flow, tool-work piece contact conditions and effects of various process parameters, efficient tools have been devised.

The most important key problem that remains to be addressed is the fundamental knowledge of these processes and the knowledge of the evolution of the structure and properties that needs to be combined to build intelligent process control models with a goal to achieve defect free structurally sound and reliable welds. Tailoring weld structure and properties based on fundamental knowledge still remains an important milestone in these processes. Attainment of this important goal would require new, more reliable and efficient process sub-models and reliable sub-models to describe the evolution of structure and properties of the welded joints.

Current FSW process sub-models are complex, time consuming, and cannot be used in real time. Furthermore, they all suffer from lack of reliability of the predicted results because the underlying physics is highly complex and the current phenomenological models do not contain any model component designed to ensure compliance with experimental results.

Thus, the aim of this work is to establish a general environment for evaluating the criteria proposed in literature; it will be also discussed the sensitivity of those criteria to changes in local processing variables and the eventual existence of critical values which allow to assess the welding quality.

1.4 Thesis layout

In order to apply the analytical bonding criteria to the FSW and LFW processes, and so to obtain an integrated numerical tool able to predict the occurrence of solid bonding starting from the process input parameters, a detailed research activity on the solid state welding techniques has been developed.

This study is started with a preliminary analysis of the existing literature on the applicability of the bonding criteria paying particular attention to the processes in which the solid bonding criteria were applied: accumulative roll bonding (ARB) and porthole die extrusion (PDE) processes. After that, a detailed literature review on the FSW and LFW processes has been made in order to identify the full experimental plans, for both the processes, to obtain different quality of the welded joints to allow the applicability of the bonding criterion proposed in all welding condition. In particular, the aluminum alloys AA6082 and AA6061 have been chosen; then the most interesting joint configurations, both from an academic and an industrial point of view, have been considered. In particular, the butt joints for both the processes FSW and LFW; finally the most influent operative parameters, both technological and geometrical, have been selected to be engineered during the subsequent stages of the research work.

In order to apply the bonding criteria proposed to the FSW and LFW processes it has gone to the experimental part of this thesis. An experimental campaign has been focused on the previously considered case studies. At the same time, a numerical model of the processes have been developed and set up, obtaining information on temperature, strain, strain rate distributions, as well as on forces and on the material flow in order to implement the bonding criteria proposed.

Finally, the applicability of the pressure-time criterion has been tested on the FSW process and LFW process using the two different aluminum alloys. Additionally, a Neural Network was developed to predict the occurrence of the solid bonding and the quality of the welded obtained.

2 Solid state bonding phenomena: critical review

2.1 Introduction

Within this chapter, a detailed survey of the literature aimed at the identification of a suitable plan for the experiments to be performed has been conducted in order to implement the criteria that represent the solid bonding phenomena aimed at the identification of a suitable plan of the experiments to be performed to implement criteria that represent the solid bonding phenomena. A detailed study of the solid bonding phenomenon has been done focusing on the:

- Operating parameters that influence this phenomenon
- Main processes in which the solid bonding phenomenon occurs
- Characterization of the welded joints with these types of process

Therefore it was developed an analysis of the literature of the processes where the solid bonding phenomenon occurs. The porthole die extrusion process has been studied paying particular attention at all of process parameters that influence the junction. For instance, the porthole die geometries allowing obtaining larger welding pressures than the ones usually got with conventional equipment were studied. Anyway, it should be observed that porthole die geometry is just one of the variables that strongly affect the effectiveness of the extruded part and in particular the strength of the welding lines: the extrusion ratio, the portholes number, the extrusion speed, the bearing length, the billet temperature and mandrel shape are actually further variables to be considered in the design of extrusion processes of complex parts.

Regarding the accumulative roll bonding process particular attention was paid to the microstructural evolution and mechanical properties of aluminum alloys processed in different ARB cycles. The importance of the rolling-ratio and the temperature process has been examined and also the two mechanisms that occur in the ARB process which differ from other high straining processes. The first mechanism is the effect of severe shear deformation just below the surface.

The other mechanism is the introduction of new interfaces. A large number of interfaces are introduced by several ARB cycles.

Particular attention was paid at the friction stir welding process and the linear friction welding process. A complex study regarding these processes have been made aimed at the identification of a suitable plan for the experiments to be performed has been conducted in order to implement the criteria that represent the solid bonding phenomena.

2.2 Solid bonding based processes

2.2.1 Porthole Die Extrusion process

2.2.1.1 Process description

The extrusion of hollow or semi-hollow profiles is a common industrial process which is often made by using the "porthole die". The porthole die technique consists of two elements, the matrix and the mandrel [26]. The support that forms the profile is divided into two parts. For hollow profiles of the matrix, an opening similar to the shape of the outer contour profile can be found, while the inner contours are determined by the shape of the mandrel.

The material within the matrix is pushed by a punch, and therefore the material is forced to pass through the portholes, which facilitates flow of the material. In order to allow the material flow from the initial section of the mandrel to the bearing of the matrix, the portholes are "milled" by the mandrel [16]. The material flow is then separated from the legs of the matrix and once exceeded the legs, the material flow is directed to the welding chamber where it will be welded [27]. The welding material is actualized in the welding chamber, under proper conditions of temperature and pressure. If the appropriate conditions of temperature and pressure are achieved, the welding process takes place in a solid state condition. The welding lines in the longitudinal extruded profiles are determined. The quality of the extruded joints obtained with this process is closely related to the efficiency of the mechanical longitudinal welds [28]. In recent years, several studies on the "porthole dies" extrusion processes have been done. Many of these studies are focused on the highlighting of strains, strain rate and the distribution of tensions in the die and inside the portholes via Finite Element Analysis (FEA).

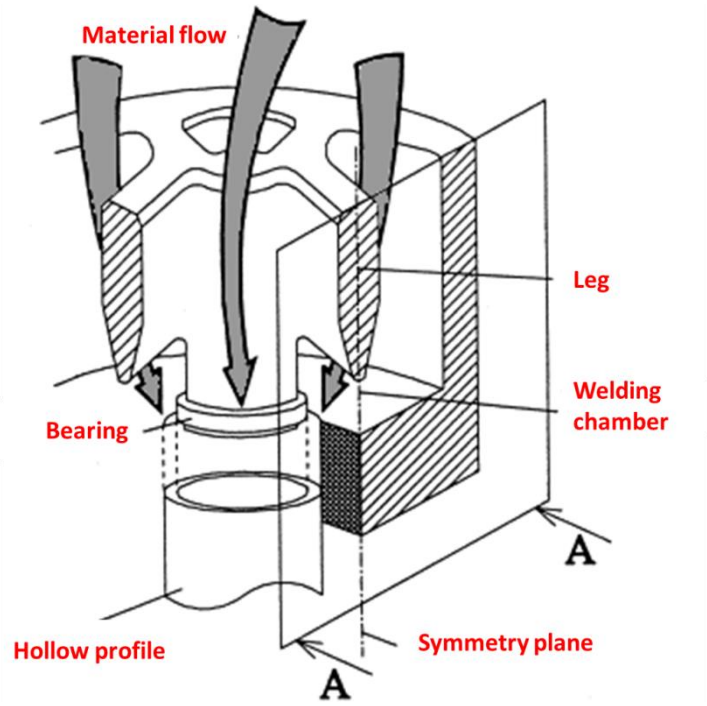

Figure 2.1 Porthole die extrusion process. [26]

2.2.1.2 Literature review

Kim and Ikeda [29] and also *Uyyuru and Valberg [30]* studied, through numerical and experimental tests, the material flow of this process. The importance that the material flow has on the quality of the resulting product has been demonstrated. Objectives of these studies were also the search for a relationship between the geometry of the porthole and the material flow, for example to highlight the occurrence of cracks or dead zones [31].

Xie et al. [32] studied the effects of that patch pockets in the die porthole had on the material flow. The temperature at the exit of the welding chamber and the load of extrusion has been investigated. The authors compared the results obtained with the same process without the pockets in the die porthole thus having an overview of possible changes on the geometry of the die.

Donati [33] and *Kloppenborg* [34] studied on the mold design starting from a careful study of the material flow through an innovative numerical model visco-plastic.

These studies are particularly important considering that, often the industrial design of the molds is performed only on the basis of the knowledge and skills of workers.

With appropriate geometries of molds it can be reached different pressure values in the welding chamber so it can improve the quality of the welded seams comparison welded joints obtained using conventional equipment. The geometry of the die, however, is only one of the variables that influence the process and in particular the mechanical properties of the weld: the others variables are also the extrusion ratio, the number of portholes, the extrusion speed, the length of the bearing, the temperature at which the molds are brought, the material and the height of the welding chamber.

The design of the welding chamber has a key role in this process. *Ambrogio et al.* [35] studied that, is fundamental having to reach the best compromise between the research of optimal force on the mold and the conditions of higher pressures. In fact, as regards the research of optimal force, it would require a tight welding chamber while to obtain the ideal pressure and a complete filling of the die wide welding chamber are require. In this contest, the height of the welding chamber is a fundamental parameter that influences the quality of the extruded piece.

Valberg [14] began to study the solid state bonding phenomenon in this process, paying particular attention to the values of pressure at the interface that can be reached in the welding chamber.

Buffa and Donati [36] have described the different solid-state bonding conditions found in the porthole die extrusion process and in friction stir welding process. In particular, in extrusion, the welding occurs between two oxide-free seams in similar conditions of temperature, strain and strain rate. In FSW, in turn, the flowing material bonds on a contaminated surface which is heated and compressed by the action of the tool shoulder. The observed differences in various field variables can be related to the peculiar process conditions which have been considered in the two processes (extrusion ratio, tool rotation speed and tool feed rate in FSW).

2.2.2 Accumulative Roll bonding process

2.2.2.1 Process description

In recent years many techniques of severe plastic deformation [37] have been proposed and tested. The methods used and promising in terms of industrial

application as a method for production of ultrafine grained materials [38] are the Equal Channel Angular pressing (ECAP) and the Accumulative Roll Bonding (ARB). The Severe Plastic Deformation (SPD) is a promising technique for the production of bulk metallic material with an ultrafine grain (UFG) structure because it introduces a very large plastic strain, while maintaining the original geometry. The most important strengthening mechanisms, which lead to the high strength of materials processed by any SPD technique, are work hardening induced grain refinement.

The innovative potential of UFG materials for advanced applications in engineering and medicine is high, and the production of these materials is becoming more and more economically feasible [39]. By increasing the production rate, UFG materials can be widely used for industrial applications [40].

Accumulative Roll-Bonding is a relatively new severe plastic deformation (SPD) process.Accumulative Roll Bonding (ARB) is a process in which two sheets of material are overlapped and rolled at 50 % of their deformation. This welding process has characteristics almost similar to a lamination. The difference is that, initially, the two metal sheets after passing through the rollers are welded forming the final laminate, of course with reduced thickness compared to the beginning based on the rolling ratio imposed. The two metal sheets are dragged by friction by the two rolling cylinders which rotate in the opposite direction with an angular velocity of equal module.

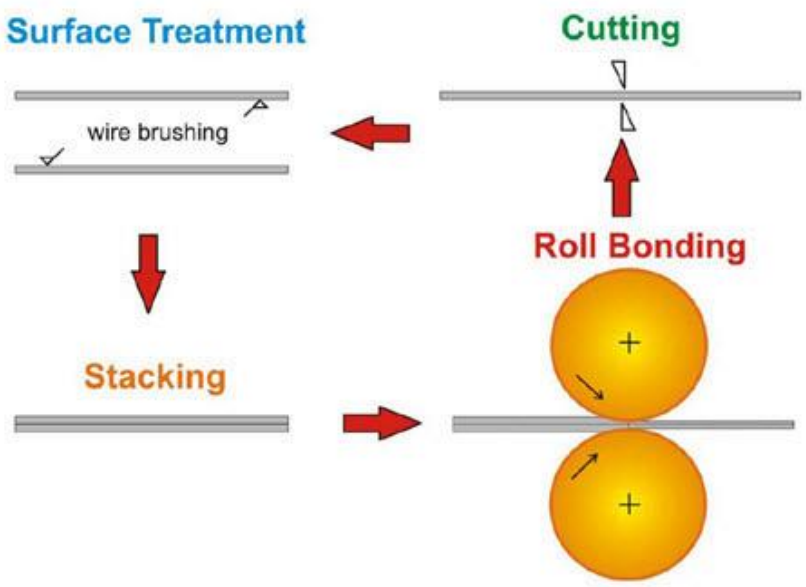

Figure 2.2 ARB process. [41]

The distance between the two rollers is less than the initial thickness of the two sheets. The metal sheets passing through the two cylinders undergo a crushing, an enlargement and elongation, that increases the speed in the rolling direction according with the condition of invariability of the volume which requires that the material flow that passes through the input section is equal to that of the material flow that passes through the outlet section. The state of plane strain in this process is considered. The size of these metal sheets depends only on the power and the dimensions of the rolling mill.

The ARB process shown is schematically represented in Figure 2.2. The process is cyclical; the main phases of the process are:

- Wire brushing of sheet surfaces in order to remove the oxide layer;
- Stacking of two sheets on top of each other;
- Rolling
- Sheet cutting

A strip is neatly placed on top of another strip. The adjoining surfaces of the two sheets are pre-treated in order to enhance bond strength. The two layers of material are joined together by rolling, as in a conventional roll-bonding process. Then, the rolled sheet is cut along the direction perpendicular to the rolling one in order to obtain two identical sheets. The cut strips are again surface-treated, stacked and roll-bonded. The whole process is repeated for a fixed number of times. In most cases, the process is repeated up to 10 times.

The process of ARB must be conducted at an elevated temperature. The temperature is below the re-crystallization of the material. In this way the accumulated tension is canceled [42]. A low temperature would result in a reduction in ductility and insufficient bond strength.

There is a critical rolling reduction in one pass roll-bonding, below which it is difficult to achieve sufficient bonding. The critical reduction depends on the materials and processing temperatures. Usually, more than 35 % reduction for each pass is necessary, so that the rolling-force becomes bigger when compared with the conventional rolling.

Sheet deformation mainly occurs in the rolling direction. There is no need for an increase in the sheet width since the sheets are wide enough and the broadening is prevented by high frictional resistance. It should be pointed that if the sheets metal is

relatively wide, it can be assumed that there is only an increase in length and no increase in the width of a sheet during rolling. The increase in width [43] can therefore be considered as negligible when the width is much bigger than the length of deformation zone.

The physical and mechanical properties of the nano-structured materials are higher if compared with mechanical properties of conventional metallic materials. Generally the decrease of grain size of the material produce the increase of mechanical strength (the law of Hall Petch) but a loss of ductility is resulted.
Different parameters influence the effectiveness of the ARB process. The latter can be quantitatively evaluated through the analysis of microstructure and mechanical properties. The most important ARB process parameters include: process temperature, percentage reduction per cycle, number of ARB cycles, roll diameter and roll speed, initial material condition before rolling, surface roughness of the sheets as well as oxide layer.
Process temperature is a key variable influencing the microstructure, thermal stability, mechanical properties as well as the quality of the metal sheet bonding. An optimal process temperature usually has to be determined for every material. It is trade-off between good bonding and a good thermal stability. The highest hardness is reached when the rolling is performed at the lowest possible temperature, although, for aluminum alloys, better bonding is obtained at temperatures higher than 200 °C. The reasons for softening include dynamic recovery and/or partial re-crystallization during pre-heating and rolling. Higher temperatures enhance grain growth thus decreasing the potential for a rapid grain refinement. The sheet temperature affects bonding by influencing the adhesion of the oxide layer of the parent metal. In particular the strength of the bond between the oxide and the strip decreases with temperature with beneficial effects for the bonding quality.

2.2.2.2 Literature review

Severe plastic deformation (SPD) define a class of fabrication techniques that produce nanocrystalline materials by means of plastic deformation often under high pressure and relatively low temperatures [44]. The most common severe plastic deformation techniques are: Equal Channel Angular Extrusion (ECAE) [45], High

Pressure Torsion (HPT), Repetitive Corrugation And Straightening (RCS) [46], Cyclic Extrusion Compression (CEC) [47], Torsion Extrusion [48], Severe Torsion Straining (STS) [49], Cyclic Closed-Die Forging (CCDF) [50], Super Short Multi-Pass Rolling (SSMR) [51] and Accumulative Roll Bonding (ARB) [52]. It is worth pointing out that SVP can be used only with materials with certain potential to plastic deformation. The basic mechanisms behind these techniques are aimed to increase the dislocation density within the original material through intense plastic deformation. In order to reduce the strain field associated with dislocation structure, it recovers into cell wall structures and deformation shear bands. Through room temperature the recovery of the recrystallization occur, these microstructures can further transform into low-angle and high-angle grain boundaries [53]. A number of elemental and alloy systems (nickel, copper, aluminum, and magnesium) have been produced by severe plastic deformation methods. It has been shown that the grain sizes of these bulk systems are in the order of 100 µm. additionally, the mechanical properties of the processed alloys significantly increase. As an example, ARB aluminum alloys with ultra-fine grains showed large strength at room temperature, up to 3.7 times larger than that of the parent materials [52].

In spite of the variety of different SPD processes, three processes have attracted the industrial and academic researches more than the others, namely ECAE, HPT and ARB. Figure 2.3 presents a schematic configurations of the three processes and the attainable plastic strain [44].

Process name	Schematic representation	Equivalent plastic strain
Equal channel angular extrusion (ECAE) (Segal, 1977)		$\varepsilon = n\frac{2}{\sqrt{3}}\cot(\varphi)$
High-pressure torsion (HPT) (Valiev et al., 1989)	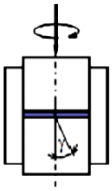	$\varepsilon = \frac{\gamma(r)}{\sqrt{3}}, \gamma(r) = n\frac{2\pi r}{t}$
Accumulative roll-bonding (ARB) (Saito, Tsuji, Utsunomiya, Sakai, 1998)	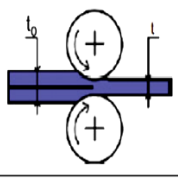	$\varepsilon = n\frac{2}{\sqrt{3}}\ln\left(\frac{t_0}{t}\right)$

Figure 2.3 Summary of major SPD processes. [44]

One of the first papers regarding the ARB process is dating to 1998. *Saito et al* .[52], have faced the problem of creating a material with ultrafine structure through this process. The various stages of the process that consists of three cycles are showed. In each cycle a reduction 50 % of the material thickness was subjected with the ARB process. The results obtained show the possibility to produce the bulk aluminum with ultra-fine grained structure and unusual strength by the ARB process.

The possibility to produce the bulk steel sheets with ultra-fine grains by ARB process was investigated by *Saito et al.* [15]. As known, steel is the most used structural material, hence, the ultra-grain refining of steel is greatly desired in many fields. The ultra-grain refining and strengthening produced on steels could largely reduce the weight of any constructions, and the strengthening without alloying elements would be preferable for recycling. The authors concluded that ARB is very useful process for high straining and ultra-grain refining, and most of structural metallic materials with ultra-fine grains could be easily achieved by ARB.

Mechanical properties of UFG steels were shown based on *Tsuji's* experimental data [54]. UFG steels are usually characterized by very high strength but limited uniform tensile ductility when they have single phase structure. The limited uniform elongation was understood in terms of early plastic instability, which is an inevitable feature of the UFG single-phased materials. The paper conclusions clearly indicated that the studies of the UFG steels should be focused on "multi-phase" in future.

Tsuji [42] studied also the role of shear strain in grain refinement of aluminum during ARB. The through thickness distribution of redundant shear strain of the ARB processed aluminum sheets was quantitatively evaluated. With an increasing number of ARB cycles the amount of shear strain and the number of shear strain peaks increase and the distribution of shear strain becomes more complicated. It was clearly demonstrated that shear strain greatly affects the ultragrain refinement by ARB. The grain size distribution through thickness is phased due to the shear strain distributions. The role of shear strain in grain refinement was considered from the viewpoints of equivalent strain, strain gradient and strain path.

Regarding the experimental tests performed, the Aluminum alloys [55] and the steel [56] were used. The ultimate tensile strength was compared for each material tested. In all three experimental tests, an increase of the tensile strength greater than 80 % compared to the material that did not undergo the process has been obtained. An increase of the strain hardening showing the decreasing of the elongation [57].

Salvatori [56] issues on nanotech-IT an article regarding the Roll Bonding. The author studied that the SPD techniques are able to producing nanostructured massive materials which present not only high properties of mechanical strength but also high values of ductility, excellent superplastic properties, good toughness and fatigue strength. In addition, the author writes, that this process offers interesting applications in the aerospace, transportation industry, in metal forming, in the medical field and in the production of magnets. *Azushima* [44] have faced this topics in a keynote paper in 2008.

Chen and Wu [58] conducted a study on the ability to recrystallization of the aluminum alloys and also the solid state phenomena during the ARB process. The two alloys have been subjected to the ARB process. A marked improvement on the tensile strength have been obtained, in the specific case, the tensile strength increases were respectively about 70 % and 150 % compared to the initial condition. Their aim was to demonstrate that, a discarded material, with poor quality mechanical properties, could potentially be recovered after having undergone several cycles of Accumulative Roll Bonding [59].

2.2.3 Friction Stir Welding process

2.2.3.1 Process description

Friction Stir Welding (FSW) is a solid state welding process patented by The Welding Institute in Cambridge (UK) in 1991 [60]. The friction stir welding process is a solid bonding process. The coalescence between the parties of the metal sheets is produced by the heat generated by the friction between two surfaces in relative motion between them [61]. This process is becoming increasingly important due to the exceptional results obtained for the mechanical junction of materials, such as aluminum alloys, referred as "not weldable" with conventional welding technologies. The main advantages of this welding technique are:

- The ability to produce joints of high quality in a very short time
- The absence of filler rod
- The ability to weld most common materials

- The possibility to weld dissimilar materials between them and non-weldable alloys with traditional techniques, such as titanium alloys
- The possibility to realize joints of different geometries

Through FSW it is possible to obtain sound joints out of several light alloys and to join different materials in terms of both chemical composition and supply state (fused, extrusions, laminates, and foams). These materials, when subjected to conventional welding technologies are problematic, presenting hot cracking, porosity and distortions. The process was originally developed to weld “not weldable” aluminum alloys, as 2xxx [62], 5xxx [63], 6xxx [64], 7xxx [65] and 8xxx [66] alloys and hybrid joints [67]. Due to the high quality of the obtained joints, other alloys have been tested as magnesium [68], titanium [69] and nickel based superalloys [70]. For these reasons this technique is finding wide applications in industry, in particular, wide range of applications such as in aerospace components, ship, railway or automobile parts: applications can be found also in electric motors development, cooling elements, food industry field and all industries making use of light alloys.

The machine tool used for the process is a milling machine with a vertical axis, providing the possibility to apply a load on the tool. The joining process, for two or more pieces, occurs with the use of a properly designed tool. In the Friction stir welding process the tool consists of a shoulder and of a rotating element of generally cylindrical shape or conical shape named pin, which is inserted between the mating sides of the sheets to be welded.

The metal sheets are fastened to a support plate so as to oppose the lateral component of the force exerted by the tool. The rotating tool moves forward along the welding line generate the junction. Of course the trajectory of the tool could also assume curvilinear profiles.

The process starts with a plunge phase figure 2.4 where the tool approaching to the separation surface of the sheets, generating the contact between the side surface of the pin with the thickness of the metal. The pin must be completely immersed in the sheets, so the tool is in contact along the entire sheets thickness.

The heat generated by the friction between the rotating tool and the material brings the metal in the malleable state, without reaching the melting point of the metal. The tool is then advanced along the welding line and, by rotating, drag the metal that is mixed, the so-called stirring, and transferred by 180 °C from the leading edge to the trailing edge of the pin.

The shoulder, scraping on the surface of the metal sheets, generates the heat required for the plasticization of the metal. The shoulder being of a diameter greater than the pin prevents the material outflow from the welding area. The combined action of mixing by the pin and the vertical pressure exerted by the shoulder determines the formation of the junction in the solid state. A peculiar material flow is obtained because of the tool action. The material in the leading edge is dragged around the tool many times before being deposited in the trailing edge. In this way a circular flow is obtained in the horizontal plane. Looking at a transverse section of the joint, two zones can be identified, called advancing side and retreating side. In the advancing side, the rotation speed and feed rate tool are in the same direction; vice versa, in the retreating side, the two speeds are discordant. Due to the rotation of the pin, the material is dragged around the tool before being left at the advancing side, where the actual solid bonding takes place and the weld consolidates once the tool left. The temperatures reached during the process and the plastic deformation carried out by the tool, influence both the microstructure of the alloy, both the joint strength. In fact, the temperatures reached and the severe plastic deformations induced on the material near the tool allow producing a zone at the center of the weld seam characterized by equiaxic and very fine grain. This grain refinement results from a process of dynamic recrystallization, and results in an increasing of the mechanical characteristics in the nugget zone.

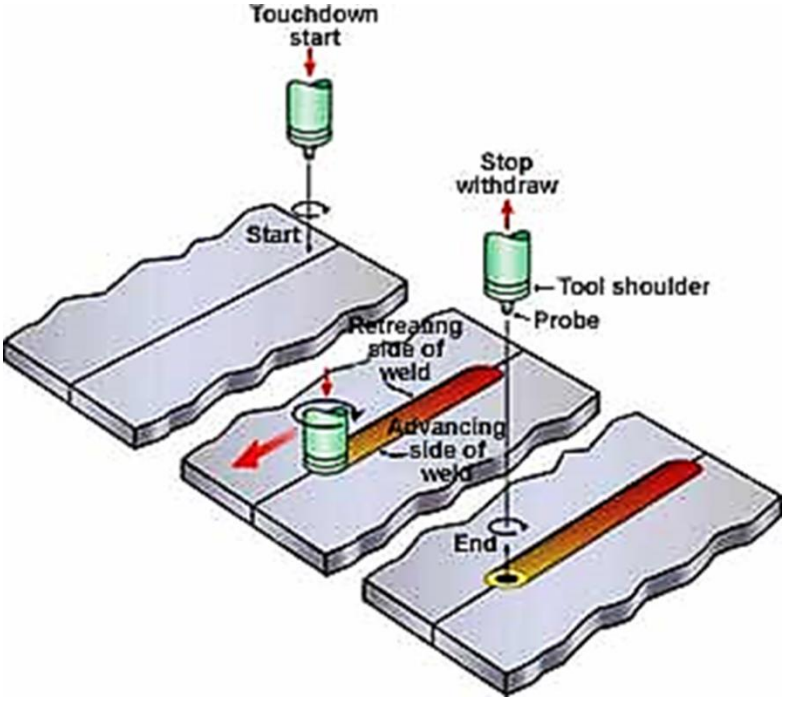

Figure 2.4 Schematic of the friction stir welding process. [71]

The tool is not inserted perfectly perpendicular to the sheets, but with at an angle, side angle nuting, which generally varies from 1 ° to 3 °. The angle of nuting is done to avoid creating a fillet weld and to facilitate the material flow below the pin and under the shoulder.

Selection and optimization of process parameters are related to several aspects, such as the material to be welded and the joint morphology. Important parameters to be set up are the tool size (both shoulder and pin), the tool rotational speed, the tool feed rate (welding speed) and the tool penetration depth or Force superimposed on the tool.

The choice of the material tool depends on the materials to be welded. The geometrical characteristics of the tool are:

- A cylindrical body that is inserted into the tool-shoulder on the welding machine;
- The press and strip actions on top of the sheets, called "skin", are carried out by the “Shoulder”. This part is in charge of generating the heat and preventing the escape of plasticized material from the area of the joint. It is the part of the tool responsible for the forging.
- The stirring action of the material affects one part of the tool named “Pin”. This part penetrates into the material and, through the rotary motion around its own axis, stirs the material. It is the part of the tool responsible of the material flow lines.

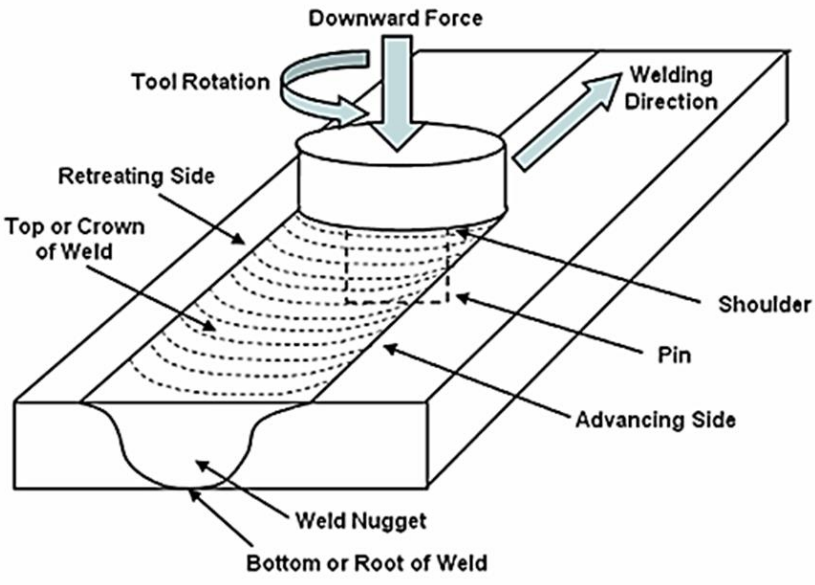

Figure 2.5 Schematic drawing of friction stir welding. [72]

2.2.3.2 Literature review

Considering its various advantages, many studies have been performed on FSW [73]. They are mainly to understand the process itself, especially the effect of process parameters (tool geometry, tool materials, rotation speed, moving speed, tool angle, base materials and their arrangement in the advancing or retreating sides, base material thickness [74].) on the quality of welding (temperature distribution, material flow or deformation, microstructure, residual stress, defects, texture [75]) and studies on the macroscopic performance of friction stir welded automotive sheets.

Mishra and Çam [76] propose a careful study on the friction stir welding process. The authors have analyzed the geometrical and the process parameters of the process, the tool geometry, the microstructure and the classic defects which can arise in a joint of FSW. In particular the mechanisms responsible for the formation of the junction in FSW processes and also the microstructural refinement and the final mechanical properties of the welded joint have been examined [77].

The authors have shown that the maximum temperature reached, in correspondence of the central part of the welded joint, is a function of the ratio between the tool rotation speed [rpm] and the speed of advance named feed rate [mm / min] along the weld line: in general, with increase of this ratio, it increases the maximum temperature. In general, when this ratio increases the maximum temperature reached increases. In particular if such a relationship grows for the decrease of the feed rate, the time contact between the material and the tool increases so consequently also increases the time during which a part of the piece is located at the highest temperature.

Mahoney et al. [78] have successfully welded a sheets of aluminum alloy AA 7075 developing an study of the microstructure aimed at highlighting the quality of the joint produced.

According to the microstructure of the grains, three areas in a FSW joint were identified: a defined area shuffled nugget, an area called thermo-mechanically altered TMAZ and a heat affected zone HAZ called. In the central area (Nugget) a total recrystallization has occurred. The nugget is characterized by a fine grain structure and equiaxed, with diameter between three and ten microns, and resistance to breakage may even reach 110 % of that of the base material. Between the nugget and the heat affected zone there is the TMAZ, which was affected by heat input due

to the heat generated by the tool, both the mechanical deformation due to direct contact with the pin. At the sides of the thermo-mechanically affected zone is located the HAZ, which is affected solely of the heat flow generated by the welding process. It is therefore subject to only a thermal cycle, without undergoing any deformation.

Reynolds et al. [79] have studied the process paying particular attention to the microstructure, the material flow and at the temperatures reached during the process to identifying the conditions in which welding takes place in the solid state. The study was validated on experimental tests of aluminum alloys that were subject to mechanical tests. The authors have shown that the material also flows vertically. In fact, in this process there is a vertical material flow. From the top surface of the sheet thickness, the material is forced downward by the tool moving and, at the same time, from the lower zone, the material flows upward.

In the same year, *Heinzi et al.* [80] conducted a study on the microstructure and mechanical properties of joints made with FSW technique of aluminum alloy AA 6013. The investigation through optical microscope transmission by performing a grain size in the heat-affected zones was carried out. Through the microstructural investigation, the authors have understood that the rotation of the pin causes that the cross section of the welding joints is not symmetrical with respect to the welding line. An Advancing side and a Retreating side have been defined, i.e. the side where the feed rate is respectively concordant and discordant with the peripheral speed of rotation of the pin. The mechanical tests like the micro-hardness and tensile strength, for the characterization of welded joints were carried out.

Hassan et al. [81] have studied the effects of the main variables of welding process, in addition to the geometric form of the tool, on microstructure and mechanical properties in the area nugget. The tests using an aluminum alloy AA 7010 were performed. The authors found that the parameters that have most influence the FSW process can be divided into two categories:

- Tool geometry
- Welding parameters

Both the parameters have important effects on the material flow and on the temperature distribution, thus determining the microstructural evolution of the welded joints. For the success of the weld are decisive tool rotation speed (ω, rpm) and the feed rate (v, mm / min). The first is responsible for the mixing of the material, in

particular by increasing the tool rotation speed higher temperatures are reached during the process, with consequent increase of heat and mixing.

Balasubramanian [82] has established the relationship that exists between the base material properties and process parameters of FSW process. An experimental campaign using five different types of aluminum alloys (AA 1050, AA 6061, AA 2024, AA 7039 and AA 7075) using different combinations of process parameters was conducted. The joints made were analyzed by checking the quality and so being able to get to the empirical relationships between the base metal properties and the process parameters in order to establish, in first, which is the right set of process parameters to obtain joints without defects [83]. It is fair to note that, at present, only the empirical relationships can be used to predict the parameters of FSW process to produce sound joints.

Regarding measured mechanical properties within and around the FSW zone, many researches have been performed. For aluminum alloys, *Sato and Kokawa* [84] reported that the FSW zone of 6063-T5 aluminum alloys had reduced strength and ductility compared to the base material. The reduction in strength and ductility of the FSW zone of 6XXX series aluminum alloys was also observed for 6056 aluminum alloys by *Cabibbo et al.* [64].

However, *Hirata et al.* [63] found that formability in FSW 5083 aluminum alloys was improved by grain refinement in the stir zone while the flow stress was lowered [85].

As for dual-phase steels, *Park et al.* [86] examined that the weld zone showed higher strength with less ductility, alike conventional mild steels [87]. As for magnesium alloys, the evolution of bigger grain size has been observed in the weld zone, resulting in lower hardness in the stir zone [88].

Finally, as far as numerical modeling of FSW is regarded, again an extremely limited number of papers are found in literature.

Goetz and Jata [89] have been studied the FSW of Ti-6Al-4V modeling and comparing to aluminum alloys using a finite element model. The model was used to predict the tool and workpiece temperatures for various tool rpms and plunge rates,

as well as loads and deformation behavior [90]. The effect of various tool materials was also examined with respect to tool and workpiece temperature response.

Nandan and Roy [91] have been modeled a three-dimensional visco-plastic flow of metals and the temperature fields in friction stir welding. The equations of conservation of mass, momentum, and energy were solved in three dimensions using spatially variable thermophysical properties and non-Newtonian viscosity. Non-Newtonian viscosity for the metal flow was calculated considering strain rate, temperature, and temperature-dependent material properties. The computed profiles of strain rate and viscosity were examined from the existing literature on thermomechanical processing [92]. The heat and mass flow during welding was found to be strongly three-dimensional. Significant asymmetry of heat and mass flow, which increased with welding speed and rotational speed, was observed. Convective transport of heat was an important mechanism of heat transfer near the tool surface. The numerically simulated temperature fields, cooling rates and the geometry of the thermomechanically affected zone agreed well with independently determined experimental values.

Buffa [93] proposed a continuum based FEM model for friction stir welding process, that is 3D Lagrangian implicit, coupled, rigid-viscoplastic. This model is calibrated by comparing with experimental results of force and temperature distribution, and then is used to investigate the distribution of temperature and strain in heat affect zone and the weld nugget. The model correctly predicts the non-symmetric nature of FSW process, and the relationships between the tool forces and the variation in the process parameters. It is found that the effective strain distribution is non-symmetric about the weld line while the temperature profile is almost symmetric in the weld zone.

Buffa and Fratini developed a thermomechanically coupled, rigid-visco-plastic, three-dimensional finite element model [93] to study the effect of tool geometry and welding velocity on material flow pattern and the grain-size distribution in the welded joints [94].

Xu et al. [95] through the numerical simulation of the of the FSW process have characterized the material flow around the rotating tool. The patterns of material flow

simulated with finite element method have been imposed, a concrete response with the experimental observations was found. The simulation results also showed that the material flow tends to pass around and behind the pin from the closing side, rather than from both sides of the pin.

Zhang et. al. [96] have been studied the 3D material flow under different process parameters in the FSW process of 1018 steel by using rate-dependent constitutive model. The numerical results indicate that the border of the shoulder can affect the material flow near the shoulder-plate interface. The mixture of the material in the lower half of the friction stir weld can benefit from the increase in the angular velocity or the decrease in the welding speed [97]. The authors understood also that flaws may occur when the angular velocity is very high or the translational velocity is very small. When the angular velocity applied on the pin is small or the welding speed is high, the role of the extrusion of pin on transport of the material in FSW becomes more important. Swirl or vortex occurs in the tangent material flow and may be easier to be observed with the increase in the angular velocity of the pin.

Zhao et al. [98] studied the effect of tool pin design on the weldability and mechanical properties of welded 2014 Al plates. Cylindrical and tapered tool pins did not ensure effective mixing in the vertical direction leading to wormholes at the base of the TMAZ [99]. However, when tapered tools with threads were used, defect free welds were obtained. Other studies have also confirmed that tools with screw threads generate more heat and improve flow of the softer material by exerting a downward force. Since the material flows mainly on the retreating side, insufficient plasticity and material flow results in a ‘‘wormhole” on the advancing side [100]. This effect becomes more prominent at low temperatures due to sluggish flow of materials. The choice of pin angle, which is the angle between the conical surface of the pin and its axis, is another important parameter which influences the FSW process [101]; increasing the angle leads to a more uniform temperature distribution along the vertical direction, which helps in reducing distortion [102]. An angle of ’40 is thought to be optimum for 7xxx aluminum alloys.

Tool	Cylindrical	Whorl™	MX triflute™	Flared triflute™	A-skew™	Re-stir™
Schematics				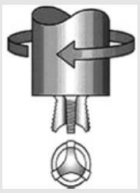		
Tool pin shape	Cylindrical with threads	Tapered with threads	Threaded, tapered with three flutes	Tri-flute with flute ends flared out	Inclined cylindrical with threads	Tapered with threads
Ratio of pin volume to cylindrical pin volume	1	0.4	0.3	0.3	1	0.4
Swept volume to pin volume ratio	1.1	1.8	2.6	2.6	Depends on pin angle	1.8
Rotary reversal	No	No	No	No	No	Yes
Application	Butt welding; fails in lap welding	Butt welding with lower welding torque	Butt welding with further lower welding torque	Lap welding with lower thinning of upper plate	Lap welding with lower thinning of upper plate	When minimum asymmetry in weld property is desired

Figure 2.6 A selection of tools designed at TWI. [103]

Nicholas [104] *and Thomas* [105] have focused on some of the variants of FSW process, in particular the further innovation that could be provided in the joining technology for the aerospace industry and so widespread benefits resulting from the application of FSW in for example, aerospace, shipbuilding, automotive and railway industries have been discussed.

2.2.4 Linear Friction Welding process

2.2.4.1 Process description

Linear Friction Welding (LFW) is a solid state welding process that works by oscillating one workpiece relative to another whilst under a large compressive force. These layers are plasticized by a combination of applied force and frictional heating, occurring when reciprocating linear motion is generated between the two adjoining parts (Figure 2.7). Linear Friction Welding was patented in 1929 [106], but the description of the process was unclear. The revised concept was recorded in 1960, but it was still unclear due to the difficulty in generating the reciprocal linear motion [107]. The Caterpillar Tractor Company [108] spoke of this process in a patent. However, the patent was focused on the machine that generates the linear reciprocating motion and not on the process of welding. In fact, a patent search has

shown that there are no currently valid patents that protect the foundations of the LFW process.

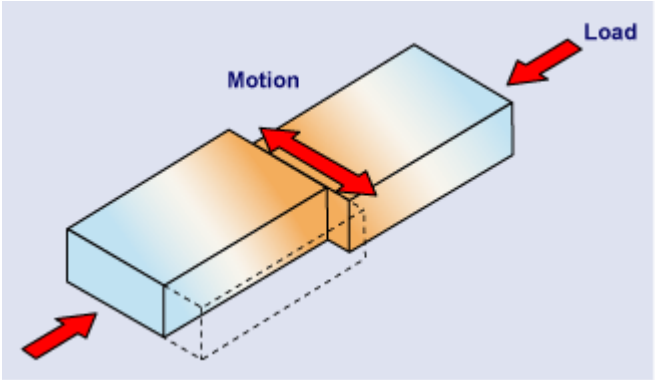

Figure 2.7Schematic illustration of the LFW process. [109]

The LFW process is a joining process in which the two pieces are placed in contact by means of axial action and, therefore, placed in mutual reciprocating linear motion. The formation of a uniform weld bead is obtained due to increasing the axial thrust. The weld bead consisting of the plasticized material, part of which is ejected to the interface named flash. When a reciprocating motion occurs under an assigned pressure, a significant amount of heat is produced. Due to the concurrent effect of oscillation and pressure, the material at the interface is forced to flow out of the joint. Part of this plasticized material, called flash, is removed during welding. In this way, any pre oxidized surface and other impurities are removed through the flash, allowing intimate contact between the materials and the creation of the joint.

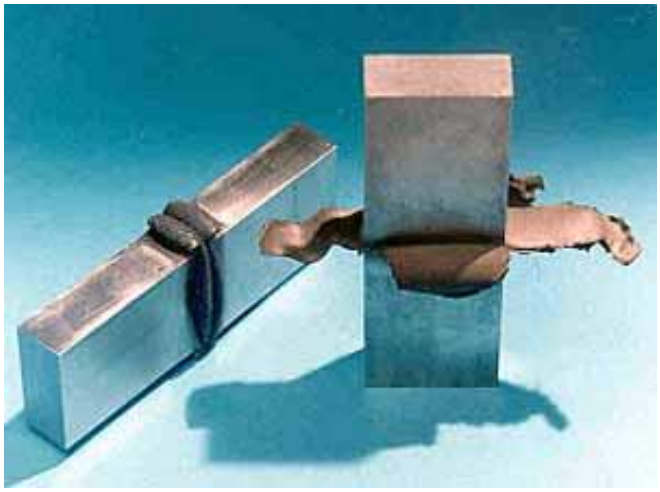

Figure 2.8 Fabrication of LFW welded specimens. [109]

Different phases can be identified during the process [110].

1. ***Preparation phase***: The specimens are clamped together under a small compressive force in order to determine the specimen position and set the machine zero (datum). The specimens are then retracted in order to leave a small separation distance between the pieces (retract).
2. ***Conditioning Phase***: the oscillatory motion of one specimen begins, and the parts are placed in contact with a small force [111] for an assigned time.
3. ***Frictional Phase***: the compressive action increases up to a set value generating heat at the interface. The material softens at the interface and a material flow out from the joint as flash. This loss of material from the welding zone causes an axial-shortening of the pieces (called burn-off). This phase ends when the burn off reaches a predetermined distance. Due to the crucial role played by this phase for the effectiveness of the process, a deeper analysis can be performed. In particular, The “frictional phase” can be further divided into three distinct sub-phases, depending on the behavior of the material [112].

    I. *Initial Phase*: At the beginning, the two materials are put into contact under pressure. During this sub-phase, heat is generated due to the peaks and valleys rubbing. The actual contact area significantly increases due to the wear of the roughness and no axial-shortening of the specimens is present. If the frequency of the alternative motion is too low for a given axial force, the generated heat is insufficient to compensate the losses for conduction and irradiation. This condition does not allow the material softening, causing the failure of the passage to the next sub-phase.

    II. *Transition Phase*: when a sufficient frictional heat is produced, in the previous sub-phase, the temperature at the interface increases and, consequently, the resistance of the material decreases. Some particles begin to be expelled at the interface and the Heat Affected Zone (HAZ) expands. The real contact area is considered to be 100 % of the cross section. In these conditions of temperature and pressure, the axial load is overly high for the plasticized material.

III. *Equilibrium Phase*: the plasticized material is ejected from the interface as flash due to the oscillatory motion and the applied pressure. During this sub-phase the axial shortening of the specimens begins as a consequence of the ejected material. In the softened area of the interface a uniform weld bead (i.e. flash) is formed. Instability may appear at this stage, due to an irregular temperature distribution. If temperature increases too much, an excessive extrusion of plastic material is obtained.

4. ***Forging Phase***: the relative motion is stopped instantly, and the specimens are aligned very quickly. Usually a forging strength is applied to consolidate the welding. The force is maintained for a time set to consolidate the joint. The force value can be equal to or greater than the friction force.

An important feature of the LWF process, as well as for others friction welding processes, is that it does not present any fusion of the parts to be bonded [7]. In this way, the junction takes place in the solid state [113], with several advantages over fusion welding techniques often characterized by well-known solidification problems (e.g. porosity, hot cracking, segregation, etc..). Moreover, for many materials, the strong deformations in the weld region during the welding enable recrystallization phenomena, resulting in a fine microstructure and in enhanced mechanical properties with respect to the base material [114].

Other benefits include the speed of execution of the process itself [115] (e.g. less than 10 seconds for the Ti-6Al-4V4 [116] and about 1.5 seconds for aluminum alloys [117]) and its good repeatability. Due to the expulsion of oxides during the movement, controlled atmosphere is not required even when welding reactive materials as titanium alloys.

On the other hand, one of the main drawbacks of the process is the high cost of the equipment. In fact, the process is generally limited to niche applications such as the production of bladed disks for aircraft engines. However, the machines used for the process have undergone a significant reduction in costs and this can lead to a wider industrial application of the process. Finally, a further disadvantage of the process is that it can be noisy [118].

Components machined from solid titanium are expensive due to the large amount of material that is purchased compared to the amount that remains after machining. LFW reduces the material required to produce a component by joining smaller

workpieces to produce a component, which is subsequently machined to the desired dimensions, as shown in figure 2.21. Currently, the LFW process is an established technology for the manufacture of titanium alloy integrated bladed disks (blisks) for aero-engines [119]. However, due to the significant cost saving that can be achieved when fabricating components [120], LFW is finding increasing interest from other industrial sectors, particularly for the joining of the aluminum alloy. Despite this interest, the process has experienced limited additional industrial implementation [121], which is partly due to a lack of fundamental scientific understanding of LFW [122]. The rapid nature of the process and the fact that the interface of the workpiece cannot be observed during welding means the using physical experiments alone may fail to provide adequate insight into the LFW process.

Furthermore, the LFW process is under development for assembling nickel-based super-alloys [123]. However, the interest in the process is growing, especially for applications where other alloys or non-metallic materials are used.

In recent years the LFW process has gained importance because it reduces the material waste of the processing. Consider, an example, to the realization of a piece "L" of a material not weldable. The only way to achieve it would be to extract it from a full piece, but, of course, the amount of unused material would be considerably greater than the one used. However, as is well known, especially in aviation is the rule Buy to Fly Ratio [124]. This is the reason why this process has always more industrial applications in the recent years [125]. The price of the machine is rather high and the machine can be devoted only to the process of LFW this is only problem represented.

Regarding the linear friction welding process, the interest about this process is mainly in the aeronautical field, because the convenience of the rule of "buy to fly ratio". With this type of process is possible to weld metal like titanium, material not used because of the price and because most of the material waste is unusable. In the aeronautics field, for 100 Kg of titanium purchased only 10 % is actually used. In fact, in the conventional machining operations undergone by a titanium piece, nearly 90 % of the material is throw out, because unusable.

2.2.4.2 Literature review

Vairis and Frost from University of Bristol are most active researchers regarding the linear friction welding process [110]. The experimental tests on a material whose chemical composition is made up of titanium, aluminum and vanadium (Ti 6Al 4V) was studied by the authors. In the first article the relations existing between technological parameters such as the amplitude and frequency of oscillation and the applied pressure were investigated. In addition to the technological parameters also the physical conditions that develop during the process, conditions that lead to the creation of the flash expelled during the test have been studied. The importance of the minimum power required in order to generate the conditions to obtain the welding and also the importance of forging pressure which is implemented at the end of the process to obtain a homogeneous welding seams have been investigated by the authors.

Particular attention was paid to the pressure of forging [111], because when the powers during the tests are low, needs to be high the pressure of forging in order to compensate and achieve the chemical and physical conditions to obtain the bonding phenomenon. In the second article, the performance of the material flow has been studied, regarding the same titanium alloy Ti-6Al-4V. In the article, the formation of the flash starting from the study of the morphology and the state of the material during and after the process has been showed.

The comparison of three control methods for a friction-welding machine has been carried out by *Bayindir and Ates* [126]. The conventional automatic control, based on a programmable logic controller, and peripheral interface controller system were set up to design a friction welding machine. In the study, it has been observed that these systems worked successfully and the peripheral interface controller system showed the best performances.

As the joints characterization is regarded, a few papers can be found focusing on different materials.

In the study of *Sahin* [127], an experimental set-up was designed and produced to achieve the friction welding of components having equal dimensions. The set-up was

designed as a continuous drive, and the transition from friction to forging stage can be done automatically. In the experiments, high-speed steel (HSS-S 6-5-2) and medium-carbon steel (AISI 1040) were used to produce a mixed joint (Figure 2.23). Post-weld annealing was applied to the joints at 650 °C for 4 h. Firstly, the process windows to obtain sound welded joints has been investigated and the optimum welding parameters for the joints were obtained. Later, the strengths of the joints were determined by tension, fatigue and notch-impact tests, and results were compared with the tensile strengths of materials. Then, hardness variations and microstructures in the post-weld of the joints were obtained and examined.

Corzo [128] conducted a study on the rules of fracture occurring in the process of Linear Friction Welding in Titanium alloys applicable in the aeronautics field. The research discussed, has paid attention to the microstructure of the joint in particular the mechanical analysis of the heat affected zone has been done, highlighting the high hardness and a characterization of the morphological structure in which there is recrystallization. Their study has led them to assert that in the majority of cases, when the break is located in the welding line, low toughness values of the material which, consequently, breaks due to fragility occurring and propagation of a crack has been showed [129].

Regarding the LFW process, *Wanjara and Jahaz* published a study on the morphological analysis, through scanning electron microscope (SEM), of the joints produced with different technological parameters [114].

Ma, Li et al [130] studied the microstructure of the welded joint with the process of LFW. The material used was a titanium alloy (Ti-6Al-4V). The study that led covered the extruded material in the form of flash, and in a phase composed of the hybrid phase alpha plus beta phase was observed. The authors also investigated the place of the break of the material during the tension tests [131]. The material presented showed that the fracture occurs in the base material, far from where welding takes place. The same authors conducted a study similar however on steel (45), obtaining similar results to those already achieved with the titanium alloy.

The same authors [132] conducted a study regarding the numerical simulation of the LFW process using a titanium alloy (TC4). The process parameters, the evolution of

the temperature on the specimen during the test and especially the axial shortening of the specimen have been simulated. The survey was conducted through software that works both as a code is implicit explicit.

Lang et al. [133] have addressed the microstructural evolution of a titanium alloy, the TC11, welded with a Linear Friction Welding process. The material used was the titanium alloy (Ti-6Al-4V) (Figure 2.26). With this study a complete transformation from the alpha phase to beta phase was shown. In this article the authors show that no dynamic recrystallization was observed in the thermo-mechanically affected zone. The material extruded in the form of flash was studied, observing the hybrid material phase (composed of the alpha phase plus beta phase). The authors conclude that some defects, such as kiss bonding and porosity, occurred in the joint at relatively low amplitude of oscillation.

In the research of *Romero* [134] a detailed investigation for the influence of the forging pressure on the microstructural, microhardness, and residual stress development in linear friction welded Ti–6Al–4V has been performed. In this paper, the energy dispersive synchrotron X-ray diffraction scans were performed in the three main directions across the welds to characterize the residual stress development. The experimental results identified a strong relationship between forging pressure, residual stresses and weld microstructure, whereby the residual stresses, the width of the weld region, and the α - Ti texture strength in the weld region generally decreased with the increase in forging pressure.

A study on superalloy was conducted by *Chamanfar et al.* [135]. Linear friction welding (LFW) was used to join the nickel-base superalloy, WASPALOY. Under the experimental conditions used in their investigation, temperature was recorded by inserting thermocouples at different locations from the weld interface, indicating that the temperature in the weld area reached up to 1280 °C, which is at least 50 °C below the melting point of the bulk alloy. However, this temperature is well above the liquation temperature of the low melting point components in the alloy (1245 °C). As a result, liquation may occur in linear friction welded (LFWed) WASPALOY. Furthermore, according to the SEM and X-ray mapping results, LFW altered the chemical composition, morphology and size of the γ′ precipitates at a location of

2 mm from the weld interface. It was determined that γ′ coalescence at 2 mm from the weld interface played a role in decreasing the microhardness (by 30 %) relative to the base metal.

The investigation carried out by *Mary and Jahazi* [136] is focused on LFW of a widely used Ni-based superalloy, namely IN-718. Commercial blocks IN-718 alloy were linear friction welded under optimized processing conditions. In their paper, the evolution of the welded joint microstructure was investigated using optical and scanning electron microscopy.

In particular, the visual examinations and macroscopic observations of microstructure evolution in the transverse section revealed a specific shape and a dual nature for the flash due to the presence of oxide layers expelled during the beginning of the equilibrium phase from the parts interface.

The aim of the study of *Rotundo* [137] was to evaluate the possibility of using the linear friction welding (LFW) technique to produce sound joints on a 2124 Al / 25 vol. % SiCp composite. The MMC joints were subjected to microstructural and mechanical characterization, including hardness, tensile and fatigue tests, without any post-weld heat treatment. In the articles it was shown that the joint efficiency was higher than 80 %, both in respect to the ultimate tensile strength and fatigue strength at 107 cycles. Furthermore, the authors have demonstrated that the fracture occurred in the Thermo-Mechanically Affected Zone (TMAZ), with a relevant reduction in the elongation to failure.

In the papers by *Jun et al.* [138, 139], the study of residual strains in AA 2024 / AlSiCp linear friction welds was carried out using a novel approach based on eigenstrain.

Synchrotron X-ray and neutron diffraction were used to measure the interplanar lattice spacing in the welds and to deduce the residual elastic strains as a function of the distance from the bond line. The limited experimental datasets were combined with eigenstrain-based FE modelling in order to reconstruct the complete strain states in the entire components. The article shows that the approach based on

eigenstrain is a powerful basis for reconstructing full-field residual strain/stress distributions in engineering structures.

Ceschini [140] have made a study on the characterization of Friction Stir Welding joints and Linear Friction Welding joints. In particular, a matrix composite aluminum alloy and particulate reinforced ceramic have been investigated. Two composite materials obtained by melting process, then extruded and heat treated T6: AA 6061 / 20 % vol.Al2O3p and AA 7005 / 10 % vol.Al2O3p have been welded by the FSW process. The LFW joints have been made of a composite material with a matrix of aluminum alloy and particulate reinforced silicon carbide, obtained through powder metallurgy, and then, forged and heat-treated T4 AA 2124 / 25 % vol.SiCp. The effects of welding on the microstructure of the joints, using techniques of optical microscopy with image analysis and scanning electron microscopy (SEM) with energy dispersive microprobe (EDS) have been done. Impact tests with Charpy pendulum instruments were conducted. The study of the mechanisms of damage was performed by means of SEM analysis of the fracture surfaces. Both welding processes have given welded joints free from defects. The microstructure of the welds was found to be dependent on the characteristics of initial microstructural composites and also by the type of welding process used. In the case of the material composite AA 6061 / 20 % Al2O3p and AA 7005 / 10 % Al2O3p, welded by FSW, a substantial increase of resiliency, than the base material, as a result of refinement of the grains of the matrix, the reduction of the average size of the particles of reinforcement and their angularity, induced by the welding process was observed. The material composite AA 2124 / 25 % SiCp, welded by LFW, presented toughness values comparable with those of the base material, as a result, especially, the limited effects of welding on the size and distribution of the particles of reinforcement.

Computational numerical modelling offers a pragmatic method for understanding what is happening during the rapidly evolving process [141]. For example, LFW models have been used to provide insight into the residual stress formation [142], strain rates [143], flash morphology [144], flash formation rates [145], thermal fields [146], microstructure evolution [147] and interface contaminant removal [148].

According to the literature, there are three primary approaches that can be used to model the LFW process. The first approach, as evidenced by the early work by *Varis and Frost* [112] involved modelling only one workpiece, which was oscillated against a non-deformable surface, as illustrated in figure 2.9a. This approach allows for quicker computational times as only half of the geometry is modelled. The problem, however, is that the coefficients of friction need to be known so that the thermal aspects of the model during phase 1 can be predict accurately.

As computational power increased, many authors expanded on the early approach to develop the second modelling approach, which considered both workpiece [149] as illustrated in figure 2.9b. Many of the problems with this approach are the same as the first. For example, despite considering both workpiece, models of this type show that they never truly merge during phase 2 and 3, as happens in reality for man [133], meaning the flow behavior after the workpiece merge to each other is still not considered.

The third approach, as show in figure 2.9c, was developed by *Turner and Gebelin* [141], who noticed that prior to the workpiece merging there is negligible macroscopic plastic deformation, at least for the titanium alloy. Once a viscous layer is formed the process may be modelled as a single-body due to there being full contact between the two workpiece. A temperature profile needs to be mapped onto the single-body model to account for the heat generated prior to merging. This is vital, as the temperature profile will result in a low flow-strength for the material at the centre. This enables the material at the centre to deform in preference to the surrounding material, allowing the single body to represent two individual workpiece. Due to the merging of the interface material being modelled, this approach considers the true interface flow behavior and produce much better replications of the flash morphology for Ti-6Al-4V workpiece[144]. The limitation of this approach is that the stages prior to workpiece merging are not modelled.

The majority of the investigations into the LFW process, modelling and experimental, have focused on characterising the primary process inputs, namely the amplitude, frequency, applied force / pressure and burn-off [150]. The effects of the workpiece geometry where often neglected. To the authors' knowledge, only two journal

publications specifically comment on the geometric effect; and both were concerned with titanium alloys.

Karadge et al. [151], for an identical combination of process inputs, showed that the post-weld interface grain size and the thickness of the thermos-mechanically affected zone increased when larger workpiece were used.

Sorina-Müller [148] compared the interface temperatures between a prismatic and a blade-like geometry, the larger prismatic geometry had a higher peak temperature. The reasons why these phenomena occurred were not investigated in any significant detail. Furthermore, when 2D modelling Ti-6Al-4V linear friction welds, [125] noticed ripples in the flash morphology, which was not observed by [143]. The only major difference between the models was the size of the workpiece used, the in-plane width was larger in the work by [143].

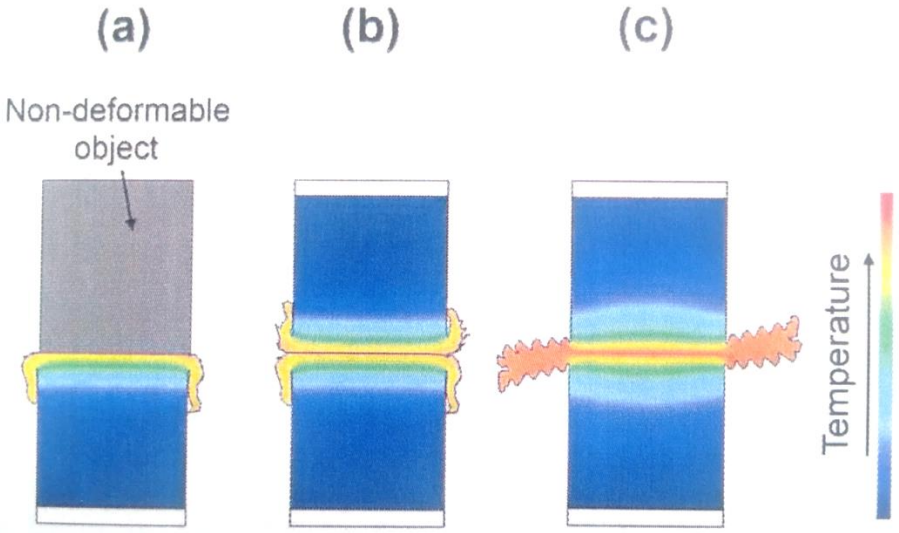

Figure 2.9 Modelling approaches: (a) one workpiece, (b) two workpiece, (c) a single body representing two workpiece [143]

2.3 Analysis of the solid bonding criteria

After have analyzed the solid state welding processes, the research has been focused in the study of the criteria which represent the solid bonding phenomena.

The characterization of the solid state bonding phenomena can be found in the literature for processes such as Accumulative Roll Bonding (ARB) or Porthole Die Extrusion (PDE).

Donati and Tomesani [152] studied the relationship between product quality and die designs in extruded aluminum profiles with welded seams. The quality of the joint obtained depends strongly on a different selection of the operating parameters, both geometrical both technological. Using different combinations of process parameters a different quality of the weld was found (defective or defect-free). *Jeong* et al. [153] studied the welding pressures through 3D simulation of the non-steady state and compared with experimental results. The objective of this study was to analyze the metal flow and to predict the welding pressure of the workpiece by FE simulations and experiments. The authors found that the welding pressure grows larger with regard to the increase in billet temperature.

Liu et al. [28] conducted an research that was aimed to get an insight into the longitudinal weld seam formation during extrusion through porthole dies and to evaluate the factors determining the quality of the weld seams.

The authors found that when the ram speed increased, the mean stresses and temperatures on the welding plane in the welding chamber increased, which was reflected in the increases in extrusion pressure and extrudate temperature, being beneficial to the solid-state bonding at the weld seams. Tensile tests confirmed that extrusion at a higher ram speed led to enhanced transverse tensile strength and strain of the extruded square tube, as a result of improved bonding at the longitudinal weld seams.

The formation of the longitudinal weld seams during extrusion through a porthole die is a solid-state bonding process. The weld quality depends on the complex combinations of thermal and mechanical parameters inside the portholes and particularly inside the welding chamber of the die with a set of geometrical parameters. It is practically impossible to get access to the space inside the porthole die and, therefore, direct experimental investigations of metal flow and weld seam formation in porthole dies are restricted. In such a situation, computer simulation based on the finite element (FE) method can play a unique role in revealing the evolution and distribution of temperature, pressure, metal velocity and effective

stress inside the porthole die. DEFORM 3D software was successfully used for this purpose to investigate the effect of extrusion process parameters and die geometry on the weld quality during the extrusion of the AA 6082 aluminum alloy into an H-shaped profile with a longitudinal weld seam [154]. With reference to the results from the tensile tests and crack growth tests of the same H section [155], a welding parameter K_{ad} that took the pressure, effective stress and welding chamber height into account was proposed to be a criterion for the prediction of the weld quality and for the discrimination between good and poor welds. DEFORM 3D was used in another investigation on metal flow and weld seam formation in the transient state during the extrusion of the AA 7003 aluminum alloy with respect to the effects of billet temperature, bearing length and product wall thickness on extrusion load, welding pressure and surface quality [153].

Ceretti et al. [22] showed how to properly simulate the bonding phenomena that occur in a Porthole Die extrusion process. The solid bonding phenomenon that occur in this process have been studied through matrices modular in which was possible to modify the geometrical parameters of the reference matrix, in order to vary the conditions in which the weld occurred. In this way, the variables that had a great influence on the process could be identified. The analysis was conducted by a phenomenological point of view, identifying one by one of the critical parameters for the obtaining of a welding defect-free, in order to derive design rules for the process in question.

As the time needed for diffusion to proceed is highly limited in the welding chamber [156], adhesive bonding under pressure may be the predominant mechanism. Thus, the contact time between two metal streams is expected to have a minor effect on the welding quality. Of more importance to the weld quality are the yielding of the material that is a function of temperature and the welding pressure affected by the dimensions of the welding chamber. Values higher than critical ones must be applied in the welding chamber to crush the asperities (roughness) of the metal streams through plastic deformation and to realise strong adhesion between the two neighbouring metal streams. Of course, the critical welding pressure required decreases as the yielding strength of the workpiece decreases or the temperature on the welding plane in the welding chamber increases.

Below, the three solid bonding criteria mostly used are described briefly.

2.3.1 Maximum pressure criterion

This criterion considers as parameter discriminating only the maximum pressure at the interface of the joint to be welded. If this value exceeds a critical limit, which depends only on the material state at that specific point considered, the welding can be considered good.

$$\mathrm{Pm} = \max\left(\mathrm{p_i}\right) > \mathrm{Cost.}$$

equation 2.1

To the knowledge of the authors, no experimental verifications of such model have been produced. In a FEM analysis, the criterion can be eventually normalized, by rating pressure to the effective stress in a specific point; in this case we have: *P*mn = max (p_i/σ_i). In order to avoid errors due to local scattering on P_i and σ_i values on the chamber width, the application of this criterion, as performed by the authors, was made by evaluating the maximum of the mean values of pressure and effective stress on the same width direction.

Akeret [157] has found that when this value exceeds a critical threshold, which depends only on local conditions and instantaneous conditions of the material, the welding can be considered optimal. This criterion is significantly longer applied in industrial practice because of its simplicity.

The effectiveness of this criterion for ARB processes has been investigated by different authors [158] which produced lightweight pieces, using high-strength metal for the safety and reliability of micro-parts. It is fair to note that, due to the simplicity, this criterion is not particularly suitable for processes characterized by complex material flow [159], such as PDE and FSW. Accordingly, this criterion was not considered in this study.

2.3.2 Pressure-time criterion

This criteria, proposed by *Plata and Piwnik* [25], is based on integral in time of the relationship between the contact pressure and the flow stress of the material. Plata using as a parameter discriminating (*W*) calculated as the integral in time of the contact pressure (p), estimated for actual material stress (σ_{eff}) calculated on the welding surface of the material.

$$w = \int_0^t \frac{p}{\sigma eff} * dt(s)$$

equation 2.2

When the parameter (*W*) above defined reaches a limit value (*Wlim*), the material is welded. This criterion has been widely used by different authors.

Donati and Tomesani [160] and *Jeong et al.* [153] studied the effectiveness of the pressure-time criterion in the PDE process through mechanical and metallurgical investigations to validate the approach proposed. The influence of the length of the bearing on the welding pressure and on the temperature of the billet in a porthole die extrusion process with of hollow profiles to predict the welding pressure have been studied. The results obtained have shown that it is possible to correctly simulate the solid bonding phenomena that occur during this process.

Ceretti et al. [161] determined the critical value of the criterion through experimental tests of accumulative roll bonding process of AA 6061. In particular, tests of flat rolling composed of two rectangular specimens aluminum alloy AA 6061 were carried.

The limit curve obtained was used and implemented for the extrusion of hollow profiles complexes (PDE).

D'Urso [162], [163] implemented a new process for the identification of the pressure-time criterion in depending of temperature through an experimental-simulation strategy on the aluminum alloy AA 6082. This was possible due to the experimental tests of rolling followed by FEM simulations of the process of the identified case studies by identifying a exponentially limit curve.

Buffa and Fratini [164] studied the solid state bonding in friction stir welding process. The solid state bonding is obtained between an undeformed “cold” material, already placed in the advancing side of the joint, and the “hot” material flow incoming from

the retreating side. Proper conditions of pressure, temperature, strain and strain rate are needed in order to get the final effective bonding. In the paper experimental tests on butt joints made out of AA 6061-T6 aluminum alloys are used to identify the sets of process parameters resulting either in sound or poor joints. The same process conditions have been simulated used an already developed model in order to highlight the actual bonding line and the values of the main field variables determining the soundness of the joints. Finally a correlation between process parameters values, field variables values and joint effectiveness is made.

Donati and Tomesani [165] in their work summarizes the outcome of recent research by the authors on modeling the formation of seam welds in aluminum extrusion and on evaluating the related mechanical properties on the final products. A profile with a seam weld in the middle section was produced with different die designs in order to investigate the relation between die design and local welding parameters, such as contact pressure, temperature, time of contact, strain and strain rate paths. The local welding conditions were evaluated by complete thermo-mechanical 3D FEM simulation of the processes. Specimens were extracted from the profiles and tensile tested, the resulting mechanical properties being discussed with respect to the local welding conditions. The possibility to adopt criteria for assessing the welding quality is discussed, together with the effect of high speed damage cracking.

Although the authors cited have found satisfactory results, [154] have pointed out that this approach is sometimes able to provide incorrect predictions when high velocity gradients nodal are observed.

2.3.3 Pressure-time-flow criterion

As noted before *Donati and Tomesani* [154] have shown that the pressure-time criterion emphasizes the role dead zones of the material in a PDE matrix, in which the residence time of the material tend to infinity. Consequently, the correction factor of the speed was introduced, highlighting that the material flow that passes through a generic point should also be considered otherwise would result in an error.

$$w = \int_0^t \frac{p}{\sigma eff} * dt(s) * v$$

equation 2.3

The validity of this approach was demonstrated on experimental PDE tests made and discussed by *Valberg* [14]. Special H profiles were produced by changing the geometry of the bearing and the width of the central section, so as to create a different window of operating conditions to obtain joints with different welding quality. The results showed that is possible to predict the solid bonding phenomena that occur during a PDE process using this criterion. The effectiveness of this criterion has not been tested on industrial case studies.

In the study by *Buffa and Pellegrino* [166] have applied two bonding criteria to FSW starting from the local value of the main field variables calculated through a specifically developed 3D numerical model of the process. Their applicability and effectiveness have been assessed through an experimental and numerical campaign carried out with the main process parameters varying in a wide range.

The pressure–time–flow criterion was demonstrated to be better suited for FSW processes when large welding speed is used.

2.4 Challenges identified

The purpose of this phase of the study is to define the specific aspects of the research. In particular, a careful analysis of the existing literature regarding the welding processes in the solid state was performed. This analysis has been done in order to identify the weld joints that have to be realized with solid bonding phenomena. The focus is on the process of friction stir welding and linear friction welding. Therefore, the choice of materials, including those usually considered "difficult" to be welded with traditional techniques such as aluminum alloys, titanium, magnesium and steel; choice of the configuration of the joints (i.e. mixed joints) and the geometry of the specimens. Particular attention was paid to the choice of the various process parameters in order to obtain different quality of welded joints. The effects by operating parameters selected on the fundamental characteristics of the welded joints so as to obtain joints "excellent" and others that are defective is going

to show. In fact, the research will focus on case studies identified. This will be followed by choosing the right set of technological parameters and geometry in order to obtain intentionally different quality of welded joints.

- There are few case studies exclusively intended to study the solid bonding phenomenon.
- The criteria that represent the conditions in which the solid state welding occur are limited.
- The few case studies are directed exclusively to the accumulative roll bonding process and porthole die extrusion process.

In this way, the research will focus on the friction stir welding process and Linear Friction Welding process. In particular, the case studies will be identified, choosing a set of technological parameters and geometrical parameters for each process, in order to obtain different quality of the welded joint. The experimental tests of the case studies will be develop, and the mechanical analysis of the welded joints and the microstructure analysis will be performed.

The aim is to use the results of the numerical models, of the microstructural investigations and the bonding criteria in order to determine the solid bonding phenomena occurring during the friction stir welding process and the linear friction welding process. The results obtained from the FE model must correspond to the results obtained from the experimental tests, so that the solid bonding criterion proposed can be implemented to describe the bonding phenomena that occur in the FSW and LFW. The neural network construction is also provided, useful tool able to provide information about the welded joint by means of the solid bonding phenomenon.

2.5 Neural network

Perform an experimental tests involves a considerable cost, such as the materials for the equipment. Therefore, it becomes essential to have tools able to reduce the number of such experiments, with consequent a costs reduction. The finite element codes are a very important tool, because it can reproduce quite closely the real

processes machining. Regarding the study of the solid bonding phenomena, it could be advantageous to support the finite element method with another tool that it provides information on the success of the weld or also some characteristics of the welded joints. In order to identify the success of the solid bonding of the welded joints and the quality of the welded seams a supervised multilayer feedforward networks based on a backpropagation algorithm have been built up [167].

The information regarding the final characteristics of the welded joints, like welded or not-welded, could optimize the numerical simulation analysis, for example, changing the operating parameters to achieve the desired condition. Through the combined use of FEM codes and neural networks is possible to reproduce the machining process and to provide the final characteristics of the welded joints. A neural network is a mathematical model that operates the interconnections of the input variables and returns the output values. Each input variable corresponds to a so-called artificial neuron, while groups' neurons form a layer.

Ney [168] faced the problem of interpretation of the discriminating criteria for the training and the output of the neural network, so the interpretation of the structure of the neural network itself. The problem was to find a suitable structure of the neural network which can be connected to a number of well-established techniques in statistical pattern recognition, as the potential functions, kernel density and continuous mixture density. The formation of the output of the neural network attempt to approximate the probability posterior class to a classic statistical approach. This work extends these connections introducing and analyzing new criteria, such as maximize the probability of class and to minimize the residual error rate. These criteria are defined between the probability density functions. Furthermore, these criteria can be interpreted in terms of weighted Quasi-maximum likelihood estimations have been found, where the weights depend non-linearly way on the parameters of the model that need to be trained.

Frosini and Petrecca [169] studied the possibility of using neural networks to control the torques of induction motors. In particular, neural networks have been used to detect any abnormalities of torques. *Ayhan et. al.* [170] have been used other neural networks to identify the mean value of the load torque stationary. These networks were trained and validated on data collected by an induction motor three-phase

1.5 kW. A good agreement between the experimental values and calculated results has been found.

Okuyucu et al. [171] and *Boldsaikhan et. al.* [172] in two different work has implemented the artificial neural network (ANN) to analyze the correlation between the parameters of the Friction Stir Welding process (FSW) of aluminum alloy plates and the mechanical properties of the welded joint. The input parameters of the model were the feed rate and the tool rotation speed. The outputs of the ANN model were the mechanical properties of the welded joints obtained: tensile strength, yield strength, elongation, and hardness of the welded seams. A good performance of the model ANN has been achieved. The model can be used to calculate the mechanical properties of the welded aluminum plates with a process having as input variables the technological parameters of the process. The results obtained from the experimental tests have been compared with the results measured by the ANN and the simulations of the process getting a good agreement.

Also interesting is the study that *Malinov and Sha* [173] led in 2004. Artificial neural networks (ANN) for the modeling of titanium alloys have been applied. In particular as input data have been used: the diagrams for titanium alloys time-temperature transformation (TTT); the correlation between processing parameters and titanium alloy properties with the alloy γ-TiAl; diagrams of fatigue for alloy Ti-6Al-4V; the corrosion resistance of titanium alloys. For each tests an appropriate combination of input and output to the network has been chosen. In particular multi-layer networks that have been trained with a set of complete data from the published literature were created. Neural networks proposals have achieved good performance, in fact, different effects have been modeled, including: the influence of alloying elements on the kinetics transformation of titanium alloys; the influence of the process parameters, the composition of the alloy and the working temperature on the mechanical properties of titanium alloys; the influence of microstructure, temperature, surface treatments and the stress ratio on fatigue life. These models of artificial neural networks combined with programs for the optimization of the inputs to achieve desirable combinations of output have been implemented. These are useful and powerful tools to solve practical applications in the titanium alloys field.

Buffa and Fratini [174] have proposed a prediction of the mechanical properties and microstructural through the use of artificial neural networks in FSW processes of titanium alloys in double phase. In fact, the authors, in order to achieve the cost savings and an efficient process design, developed a numerical simulation of the process combined with a neural network. An artificial neural network properly formed and connected to the 3D FEM model for the FSW process of titanium alloy Ti-6Al-4V has been developed, with the aim to predict the values of microhardness and microstructure of the welded joints to vary of the main process parameters. The input data used were obtained from the FE models: for every point examined the values of the variables of interest have been calculated. A good agreement between the experimental values and calculated results was found.

The finite element simulations are an effective tool to study the variables that influence the solid bonding phenomena [175], such as temperature, time, strain, pressure and strain rate. The numerical simulations provide the ability to compare the values of these variables at the varying of the operating parameters of the processes. These data will be used as input to the neural network. The goal of the NN is the prediction of the solid bonding phenomena using a generic set of process parameters. The aim of this work is to be able to correctly represent the solid bonding phenomena occurred during the experimental campaigns of LFW and FSW carried out, as regards both the dynamics of the processes, through finite element simulations, as regards either the success or failure of the weld and the quality of the weld. Therefore, it is possible to understand the significant importance of this study, which allows to implement numerically different processes of solid state welding. In this way, it is possible to reduce the number of tests to do, with the consequent economic saving, but is also a tool able to provide information on the quality of the welded joints, freeing, by testing procedures definitely more costly and lengthy. The prediction of sound weld or defect weld through the neural network is also an independent tool compared to welding criteria found in the literature, thus exceeding the limit of such expressions, or the applicability of analytical formulas only in specific conditions. The combined use of finite element codes and neural networks is therefore a very useful tool for the representation and description of the solid bonding phenomenon.

3 Friction stir welding experiments

3.1 Introduction

3.1.1.1 Application of the solid bonding criteria examined to the FSW process

The research was focused in the processes of Linear Friction Welding and Friction Stir Welding. The application of the solid bonding criteria on the process of FSW and LFW has been proposed.

In this chapter the case study will be identify aimed at the identification of a suitable plan for the experiments to be performed in order to implement the criteria that represent the solid bonding phenomena at the FSW process. The third chapter of this thesis will be divided into a first part, called Experimental set-up, where it will be described the experimental campaign carried out

In particular, the effects of operating parameters on the fundamental aspects of the process in order to obtain different quality of the welded joints: "excellent" joints and others that present defective. The selection of the set of technological and geometrical parameters in order to obtain intentionally different quality of welded joints it will be highlight.

The literature review, at this point of the investigation, has contributed to the identification of case studies identified. In particular, the aim was to highlight the influence of process parameters on the quality of the welded joint.

How it was cited above, the study that Buffa and Donati [36] have done, it has been important to understand the influence of the process parameters because the authors have analyzed the operating parameters of the FSW process. The optimal geometry and the welding speed, to improve the nugget using aluminum alloys, as well as the mechanical bonding has been studied. Also

In the second paragraph of the third chapter, the welded joints by FSW will be characterized. Also in this case the state of the art has contributed to the characterization of the FSW weld seams such as the work done by Chen and Yang [176]. The authors have pointed out the conditions that cause the typical defects during the FSW process and the influence on the mechanical properties of the joint.

A low heat input leads to the generation of the tunnel and/or of the "kissing bond" phenomenon was discovered. The "kissing bond" phenomenon defect is particularly difficult to be identified with non-destructive testing. Finally, in addition to the tool rotation speed and the feed rate also the angle of inclination of the tool, nuting angle, have been studied noting that influence the heat input during the process.

The FEM simulations of the FSW process of the case studies identified by the software DEFORM 3D will be performed. The solid bonding criteria identified will be implemented in the process. As regards the FEM simulations, to study the numerical models present in the literature and in particular that of the Buffa and Fratini group was useful.

In the third paragraph of this chapter, the numerical analysis of case studies previously identified experimentally will be developed. Following the study of *Fratini and Buffa* [93] that proposed a FEM model 3D Lagrangian implicit, coupled rigid viscoplastic, for the Friction Stir Welding process. This model has been calibrated by comparing the experimental results of strength and temperature distribution. So to study the temperature distribution and deformation the FEM model was used. The FEM model correctly predicts the non-symmetric cross section of the FSW process and also correctly simulated the relations between the tool forces and the variation of the process parameters. With the FEM model is also possible to detect the distribution of the effective strain that is not symmetric respect to the welding line, while the temperature distribution is almost symmetrical in the welding area.

Finally, the applicability of the criteria solid bonding and neural networks will be proposed as a fundamental tool for an efficient process design.

3.2 Experimental set up

As far as friction stir welding is regarded, during doctoral period, the experimental campaigns were carried out. In particular, experimental activities permitted to draw process windows for two aluminum alloys, AA6061 and AA6082.

A dedicated experimental campaign was carried out measuring the temperature trend and energy input. The mechanical characteristics were analyzed in order to identify the proper process parameters ranges for effective solid bonding.

A numerical analysis of the process was carried out in order to set up a robust numerical model and to investigate the evolutions of the most relevant field variables, namely temperature, strain, strain rate.

3.2.1 Used materials

The aluminum for its light weight is used for trains, planes, cars and boats. However, the aluminum is never found in the metallic state, but always combined with other elements, mainly for oxygen. Thanks to its exceptional properties, aluminum is essential for many types of applications. In fact, the main properties of aluminum are:

- Lightweight;
- Unbreakable;
- Corrosion resistance;
- Good thermal conductor;
- Resistant to temperature changes;
- Protect from light, air, humidity, from microorganisms without altering the taste of the content;
- It is easy to handle and possesses optimal characteristics for recycling.

The choice of materials for use in the transportation industry has become important in recent years, due to of rapid progress in the various technologies. Aluminum is already entered in the aircraft, in fact, one of the key parameters in the design of the aircraft was the relationship between engine power and the weight of the aircraft (called specific power) from this it hints at the importance of 'use of lightweight materials on them. Figure 3.1 shows how in a modern airplane the percentage of aluminum uploads also over 80 %.

Airplane	Aluminium % weight	Steel % weight	Titanium % weight	Composite % weight	Other % weight
Boeing 747	81	13	4	1	1
Boeing 757	78	12	6	3	1
Boeing 767	80	14	2	3	1
Boeing 777	70	11	7	11	1
DC-10	78	14	5	1	2
MD-11	76	9	5	8	2
MD-12	70	8	4	16	2

Figure 3.1 Material composition of the structure of a modern aircraft [105]

Aluminum alloys are alloys in which aluminum (Al) is the predominant metal. The typical alloying elements are copper, magnesium, manganese, silicon, tin and zinc. There are two principal classifications, namely casting alloys and wrought alloys, both of which are further subdivided into the categories heat-treatable and non-heat-treatable. About 85 % of aluminum is used for wrought products, for example rolled plate, foils and extrusions. Cast aluminum alloys yield cost-effective products due to the low melting point, although they generally have lower tensile strengths than wrought alloys. The most important cast aluminum alloy system is Al–Si, where the high levels of silicon (4.0–13 %) contribute to give good casting characteristics. Aluminum alloys are widely used in engineering structures and components where light weight or corrosion resistance is required.

Alloys composed mostly of aluminum have been very important in aerospace manufacturing since the introduction of metal-skinned aircraft. Aluminum-magnesium alloys are both lighter than other aluminum alloys and much less flammable than alloys that contain a very high percentage of magnesium.

Aluminum alloy surfaces will develop a white, protective layer of aluminum oxide if left unprotected by anodizing and/or correct painting procedures. In a wet environment, galvanic corrosion can occur when an aluminum alloy is placed in electrical contact with other metals with more negative corrosion potentials than aluminum, and an electrolyte is present that allows ion exchange. Referred to as dissimilar-metal corrosion, this process can occur as exfoliation or as intergranular corrosion. Aluminum alloys can be improperly heat treated. This causes internal element separation, and the metal then corrodes from the inside out. Aircraft mechanics deal daily with aluminum alloy corrosion.

Aluminum alloy compositions are registered with The Aluminum Association. Many organizations publish more specific standards for the manufacture of aluminum alloy, including the Society of Automotive Engineers standards organization, specifically its aerospace standards subgroups and ASTM International.

The fundamental aluminum properties are: excellent electrical and thermal conductivity, low specific weight and corrosion resistance.

Regarding the thermal and electrical conductivity, it is possible to evaluate the influence of the main impurities present in the aluminum taking into account the fact that each element has a different influence. It is worth noticing that thermal conductivity is a key feature to the LFW process as it determines how the heat produced at the interface between the specimens diffuses in the joint going “away” form the welding area:

- elements with minimal effect: Ni, Si, Zn, Fe;
- elements with average effect: Cu, Ag, Mg;
- elements with high impact: Ti, V, Mn, Cr.

An important aspect concerning on the thermal conductivity, is the ratio Fe/Si: in fact, in order to ensure the highest thermal conductivity to the alloy, the ratio must be kept constant and equal to 1.5; otherwise, the conductivity drops dramatically. This behavior is due to the formation of an intermetallic compound, which if present in the alloy in the dispersed phase, subtracts a certain impurities amount thus improving the conductivity.

The specific weight is a second crucial point for aluminum and its alloys, as the impurities can cause a change in the specific weight of pure aluminum.

As part of this thesis, the AA6061 and the AA6082 we have been studied. This two aluminum alloys belong at the family of alloys of 6000.

Aluminum alloys 6xxx series constitute a hybrid between the 4xxx and 5xxx, because the main elements of alloys are magnesium and silicon (Al-Mg2-Si). This class is suitable for the heat treatment, with the aim of achieving the desired formation of precipitates, such as to improve the mechanical characteristics. The most widespread of such class is the alloy 6061 (P-AlMg1SiCu 0.60 % Si, 0.30 % Cu, 0.20 % Cr) which also contains copper, to further improve the mechanical characteristics, and chromium to control the intergranular structure. This aluminum alloy is an excellent compromise between mechanical properties, weldability and mechanical strength, making it suitable for plastic machining, heat treatment and structural use.

Aluminum alloy 6082 is a medium strength alloy with excellent corrosion resistance. It has the highest strength of 6000 series alloys. Alloy 6082 is known as a structural

alloy. In plate form, 6082 is the alloy most commonly used for machining. As a relatively new alloy, the higher strength of 6082 has seen it replace 6061 in many applications. The addition of a large amount of manganese controls the grain structure which in turn results in a stronger alloy. It is difficult to produce to produce thin walled, complicated extrusion shapes in alloy 6082. The extruded surface finish is not as smooth as other similar strength alloys in the 6000 series. In the T6 and T651 temper, 6082 machines well and produce tight coils of sward when chip breakers are used.

In particular, the composition of the two utilized alloys are reported in Table 3.1

Alloy	Si	Fe	Cu	Mn	Mg	Cr	Zn	Ti	Al
AA6061	0.40-0.80	0.0-0.70	0.15-0.40	0.0-0.15	0.80-1.20	0.04-0.35	0.0-0.25	0.0-0.15	remainder
AA6082	0.7-1.3	0.5	0.1	0.4-1	0.6-1.2	0.25	0.2	0.1	remainder

Table 3.1 Composition alloys

The mechanical properties of the materials have been studied to modeling of the plastic characteristics of AA6082 and AA6061 for the friction stir welding process. For the numerical investigation of the friction stir welding process flow curves at elevated temperatures have been calculated. To model the plastic behavior of the material, these flow curves must provide a dependency in the temperature and strain rate as well. A servo mechanical hydraulic testing machine, the Gleeble 3500 of Dynamic Systems Inc. was applied for the tests. For the elongation local measurement the optical system ARAMIS, GOM GmbH was used. According to the process temperatures during the friction stir welding, we varied the test temperature from 25 °C until 500 °C (25, 150, 300, 400 and 500 °C) in dependency of three different strain rates of 0.1 s^{-1}, 1 s^{-1} and 6.5 s^{-1} (Fig. 3.2).

For the statistic coverage three tests were performed for each parameter combination. Based on the results of the tensile tests, which are performed according to the standard DIN EN ISO 6892-2 [177]. The flow curves for AA6082 have been modeled applying the Hockett- Sherby criteria [178] for the interpolation. Hereby, a very high accuracy with a R^2-value of more than 99.0 % was accomplished.

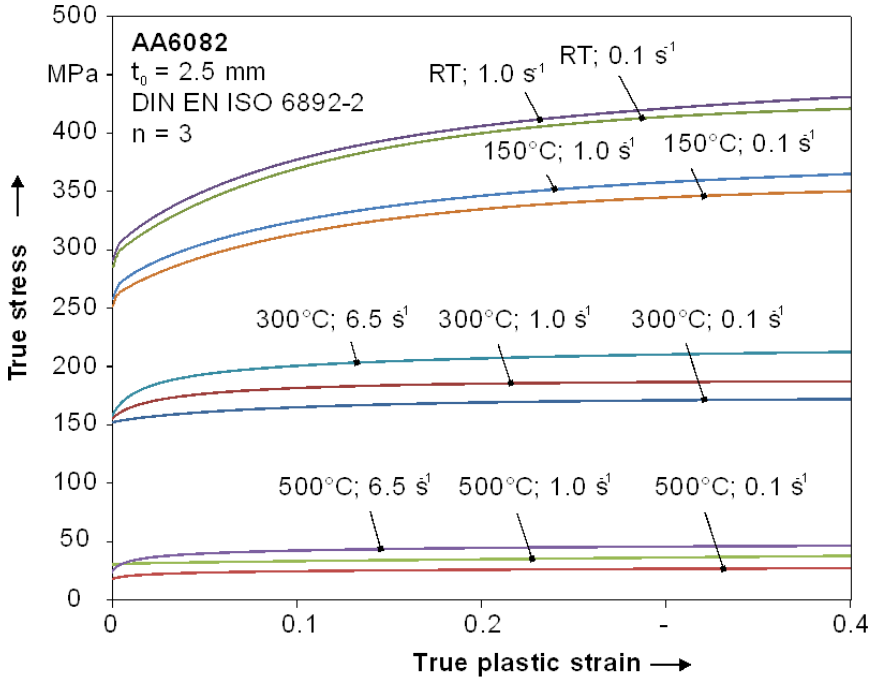

Figure 3.2 Flow curves in decency of temperature and strain rate according to the standard DIN EN ISO 6892-2 for AA6082

For the characterization of the general material characteristics uniaxial tensile tests were carried out. To detect the influence of the anisotropic behavior, the standardized dog-bone like specimens were cut parallel, perpendicular and in 45 ° to the rolling direction.

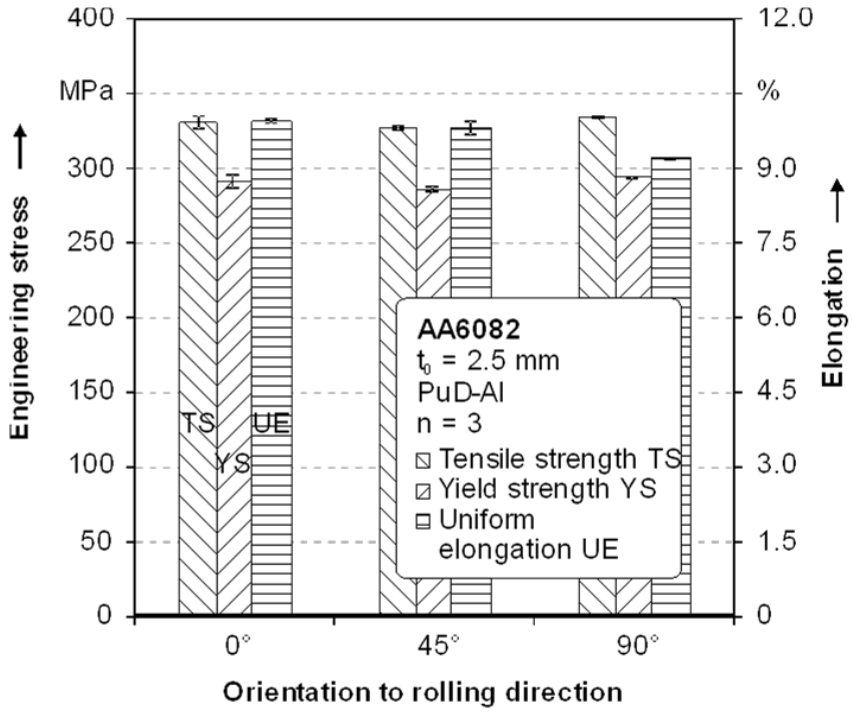

Figure 3.3 Material parameters of the hardenable aluminum alloy AA 6082 according to the standard PuD-Al

For the characterization the standard PuD-Al in the automotive industry the parameters of the tensile test according to the automotive standard PuD-Al for aluminum alloys is applied. The pre-load 5 MPa, the velocity modulus 10 MPa/s, the testing rate before yielding 10 MPa/s, the elongation for yielding 0.5 % and the elongation rate after yielding 0.667 % / s was used. In order to evaluate information after necking and flow stresses at higher strains for better approximation of the elongation, the optical measurement 2D-system Aramis©, GOM mbH Braunschweig, Germany is applied. For the statistical coverage three tests were performed for each parameter combination.

A well-known test setup for simple shear tests of wrought sheet metal is based on the American Society for Testing and Materials standard ASTM B831 [179]. The ASTM standard for single shear testing was developed primarily to investigate the behavior of aluminum products under shear loading using a single shear zone. The original ASTM sample is used in a tension testing machine, where the shear stress is calculated from the uniaxial tensile force. This planar simple shear experimental setup can be realized on a universal testing machine with a built-in clamping device, as, for example, developed by [180]. The uniaxial load of the machine enforces a parallel movement of two lateral grips [181]. The crosshead motion was adjusted at a constant machine speed of 0.1 mm / min which leads to a shear strain rate of 0.001 s^{-1}.

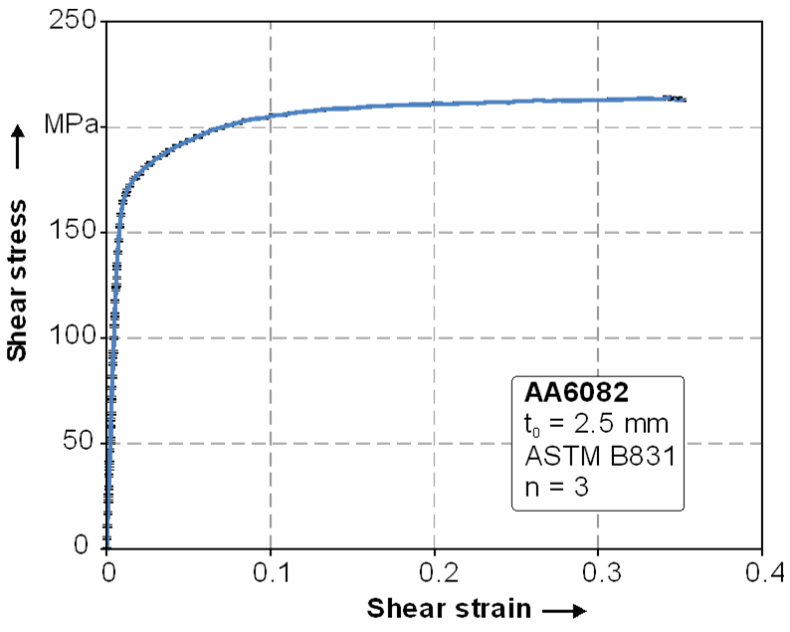

Figure 3.4 Shear stress according to ASTM B831 for the hardenable aluminum alloy AA6082

Each test was repeated at least three times so the result is average of the three tests. Regarding the investigation of the stress states in the σ1-σ2 plane, the shear tests have been developed to study the second and forth quadrants of the plane. The planar shear test specimens according to a modified ASTM specimen proposed by [182] have been used in this study.

Biaxial tensile test is a testing in which the sample is stretched in two distinct directions to obtain the mechanical characteristics of anisotropic materials. The biaxial testing machine described in [183] was used for the determination of yield locus diagrams at room temperature. The standard samples in AA6082 were obtained by sheet thickness of 2.5 mm using laser cutting. The specimens were first coated with white paint and graphite to create a stochastic pattern and subjected to a drying operation in order to be used with the software ARAMIS. Each test was repeated at least three times so the result is an average of the three tests.

σ_0 [MPa]	σ_{45} [MPa]	σ_{90} [MPa]	σ_b [MPa]	r_b	r_0	r_{45}	r_{90}
263.52	268.33	270.83	267.42	0.7112	0.581	0.925	0.785

Table 3.2 Experimental results for yield loci modelling of AA6082

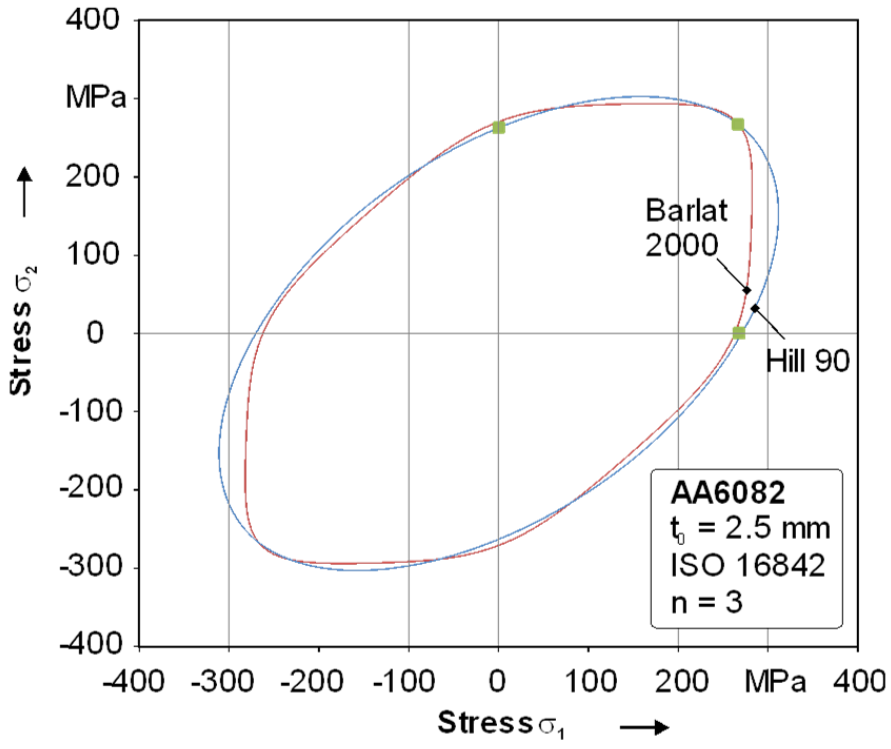

Figure 3.5 Yield surface according to Barlat 2000 and Hill 90 for AA6082

Regarding the characterization for the forming simulation the yield surfaces predicted using the two yield criteria Barlat-2000 [184] and Hill-90 [185] has been developed. The two yield criteria are compared with the corresponding experimental data in Fig 3.3, Fig 3.4 and Tab 3.2 respectively. The material parameters employed in the yield functions can be obtained in more than one way. The parameters can be obtained by curve fitting to either the r-values or the yield stresses (at various orientations with respect to the rolling direction).

A similar procedure was used for the characterization of AA6061. The following table 3.3 summarizes the mechanical properties of the two aluminum alloys.

Properties	AA6061	AA6082
Density [g/m3]	2.70	2.70
Melting temperature [°C]	650	555
Thermal expansion coeff. [K^{-1}]	$23.4*10^{-6}$	$24*10^{-6}$
Young modulus [GPa]	70	70
Thermal conductivity [W/m*K]	166	180
Electrical resistance [Ω*m]	$0.040*10^{-6}$	$0.038*10^{-6}$
Yield stress [MPa]	276	275
Tensile strength [MPa]	310	334
Elongation [%]	12	11
Shear strength [MPa]	207	210
Vickers hardness [HV]	110	130

Table 3.3 Mechanical properties

The variation of the two material flow stresses as a function of temperature has been taken into account in order to explain the mechanical behavior of the joint obtained with varying process parameters [186].

The elastic modulus of aluminum alloys also depends on the elements content: Ni, Fe, Cu, Si, and Mn provide an increase in the Young's modulus of the alloy, proportional to the respective elastic modulus. It is also to be noted that, in virtue of the crystal lattice type, the material may have a favorable behavior for the low temperature applications. In particular, as temperature decreases, resilience does not vary appreciably while the ductility and mechanical strength grow for almost all materials. Aluminum and its alloys, have remarkable features of drawability, ductility,

malleability. In fact, it is suitable for all the plastic operations in cold and hot processing.
The working tool of the aluminum is not difficult, however must be used a high cutting speeds thus requiring a robust machine.

The good castability of the aluminum and its alloys makes them suitable for the classical foundry material. In this technological process, due to the high shrinkage coefficient, pure aluminum is less usable than its alloys.
Finally, one of the most important drawbacks when processing aluminum alloys is the affinity to oxygen. Aluminum oxide (alumina) creates an extremely hard layer on the surface of aluminum sheets or specimens. Its elevated hardness and higher melting point makes some aluminum alloys not weldable by traditional fusion welding processes. For this reason, other joining techniques are usually utilized (e.g. adhesive bonding, nailing, riveting, etc.).

Defects related to the traditional welding process include:

- Cutting: a groove merged in the base metal adjacent to the base of the joint and not filled with the base metal.
- Inclusion of slag: a solid particle nonmetallic remains trapped in the weld metal or between weld metal and the base metal.
- Porosity: defect in the shape of the cavity formed by trapped gas during the process of solidification.
- Overlap: the protraction of the weld metal over the head, face or root of the weld joint.
- Defect removal from the support: damage caused by the removal of the support base of the coupling used to withstand the molten metal.
- Cavity shrinkage: cavity caused by the natural shrinkage in weld metal during solidification.
- Inclusions oxide: oxide particles surface that have not been merged and that are trapped in the weld metal.
- Failure of fusion (LOF) condition characterized by incomplete fusion of the metal.
- Insufficient of penetration (LOP): condition in which the weld penetration is below specification.

- Craters: areas of depression at the ends of the weld or in the sump of molten metal.
- Spray: particles of molten metal that are ejected during heating and which do not become part of the weld.
- Insufficient filling: a depression on the face of the weld or on the surface of base in the weld metal, which extends to beneath the surface of the adjacent base metal.

3.2.2 Specimens geometry

It has been preceded with the choice of the right set of geometric parameters in such a way as to obtain intentionally different quality of welded joints.

To the geometric parameters belong:

- the geometry of the pin;
- the size of the shoulder;
- geometry of welding joints

The sheets thickness was 2.5 mm. Butt joints were obtained out of aluminum alloys AA6061-T6 and AA 6082-T6, 100 mm x 200 mm in dimensions.

As regards the tool geometrical parameters, on the basis of experimental results obtained with other alloys, and on the basis of simulations carried out [94], it was decided to realize the shoulder with a diameter of 10 mm while a pin conical shape with an conical angle of 30 ° and a major base diameter equal to 3.5 mm. Such tool geometries allow the proper material flow from the front of the pin to the rear. The height of the pin is fixed to 2 mm, since the thickness of the sheet to weld is 2.5 mm, so a pin height greater than 2 mm would lead to a too pointed pin, and then to a resistant section of the pin, towards the tip, not sufficient to resist the stresses to which it is subjected during the process. The tool geometry is shown in the figure 3.8. Given the high a stress to which is subject the tool for its realization has been chosen a H13 steel. The tool, have been made using a lathe. The tool, before being used, will be subjected to a hardening process. The quenched to 1020 °C is performed to make the harder the surface of the tool and to avert the possibility that the tool is

exposed to excessive dimensional variations due to the stresses which it is subjected during use.

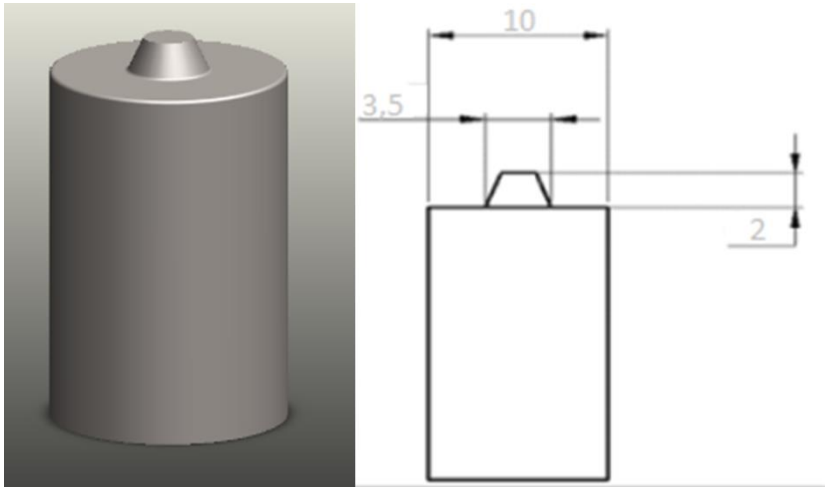

Figure 3.6 FSW tool used

3.2.3 Process parameters

The effects of the operating parameters have been highlighted on some of the fundamental aspects of the process in order to obtain "excellent" joints and defective joints. We proceeded with choosing the right set of geometric and technological parameters in order to obtain intentionally different quality of welded joints. As regards to the technological parameters is chosen a tilt angle of the tool (angle nuting) of 2 °. For the execution of the joints have been used the following process parameters:

Parameter	***Value***
Feed rate V [mm/min]	100, 200, 400
Rotational speed R [rpm]	1000; 500
Nuting angle	2°
Tool sinking [3]	2.2

Table 3.4 Process parameters ranges

A properly designed clamping fixture was utilized in order to fix the specimens to be welded on a milling machine Mazak Nexus 410 A. The steel plates composing the fixture where finished at the grinding machine in order to assure a uniform pressure distribution on the fixed specimens. Fig.3.7 shows the welded sheet at the end of the process.

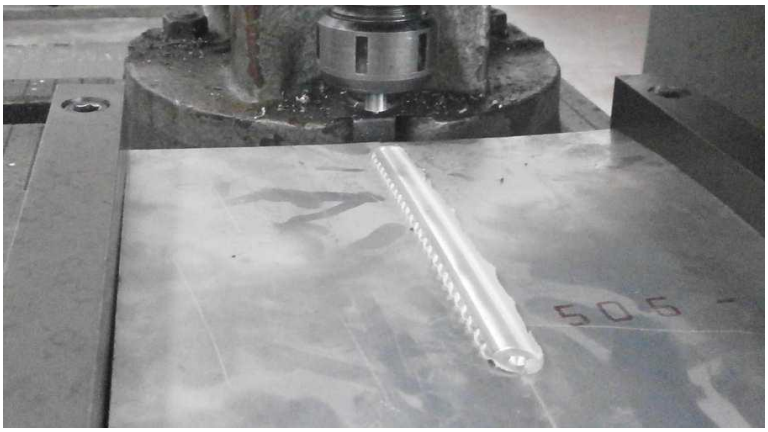

Figure 3.7 Utilized clamping fixture and welded joint

Each test was repeated three times and from each different specimen was cross-sectioned perpendicularly to the welding direction. Macro observations were aimed to analyze the material area involved in the process mechanics; furthermore, through the micro observations, the presence of flow defects was investigated. In order to obtain such results the specimens were hot mounted, polished and finally etched with Keller reagent and observed by a LM

3.2.4 Joints analysis

For all the considered case studies, the produced welds were properly prepared for micro and macro observations. In particular, the preparation cycle was performed through a specimens cutting, resin embedding, polishing and chemical etching.

The investigation methods regarding the metallurgy are designed to deepen the knowledge of the intrinsic properties of metals such as structures and mechanical and physical properties. The analysis can be conducted macroscopically and microscopically. The observation of the samples is done with the metallographic microscope, which differs from the microscope common because the metal sample can be observed only for reflection.

The optical microscope allows the observation of crystal grains and any precipitate alloy. The welded sheets were cut and were then extracts some specimens being careful that the weld line of junction of the two sheets was orthogonal to the blade of the miter saw. In this way they were obtained the specimens suitable for metallographic analysis.

The next step was to embed in a resin matrix phonological, by the use of a mold of cylindrical shape. A machine for hot embedding, REMET IPA 30 (Figure 3.8a) and an epoxy resin were used. In particular, maximum temperature of 175 °C and a pressure of 4.5 bar were selected. This operation has been done to perform the analysis of metallography along the cross section of the specimens, which we recall measure just 2.5 mm, it would be impossible to perform the operation of polishing and the positioning of the specimen without to be embedded. In any embedded were inserted three samples with, the same technological parameters.

The embedded specimens were polished by means of polishing an operation that consists in treating the surface of the specimens with abrasive papers of various grit according to a predetermined sequence. TAKEN MECAPOLp260 (Figure 3.8b) was used for fine grinding and polishing.

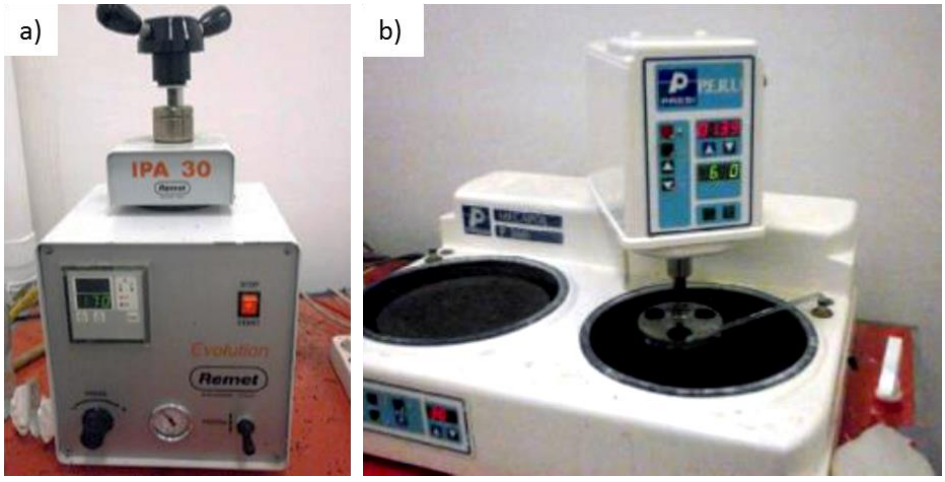

Figure 3.8 a) REMET IPA 30 machine and b) TAKEN MECAPOLp260 machine

The specimens are grinding and then polishing used an alumina solution. After the polishing step, the samples have a perfectly lapped surface, and therefore it cannot be examined by optical microscopy because light would be reflected. In order to perform the analysis it is necessary to proceed with a chemical etching selectively eroding the most reactive phases and highlighting the structure of the material. In the case of aluminum alloys, the Keller solution (1 cm^3 HF, 1.5 cm^3 HCl, 2.5 cm^3 HNO3 and 95 cm^3 H2O) was used as reagent. The specimen was immersed into this acid for an assigned time. The immersion time for AA6082 was 90 s.

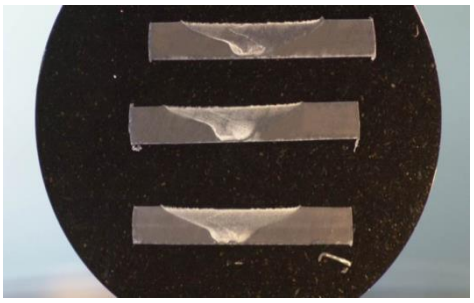

Figure 3.9 Example of weld samples embedded, polished and subjected to acid

3.3 Similar joints: AA6061 and AA6082

3.3.1 Process windows

Three different conditions were observed as a result of the experimental welding campaign. In particular, when the combination of the process parameters resulted in too low heat input, a “cold” weld was obtained. In this condition named “Not bonding test”, either no bonding or only partial bonding in the top area of the cross section of the specimen was observed. The “insufficient heat test” was a second different condition that was observed. In the cross section of these joints is more likely that flow defects due to an insufficient heat flow, as the known tunnel defect, occur. Finally, sound joints were obtained with increasing heat input, i.e. increasing the tool rotational speed and/or decreasing the feed rate

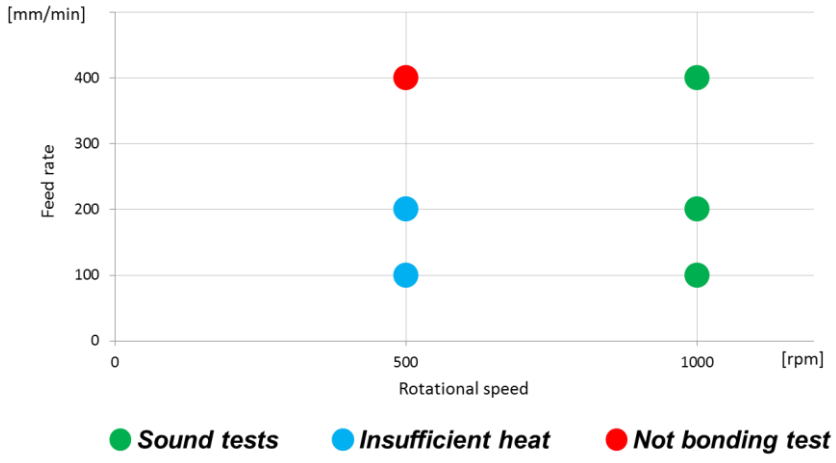

Figure 3.10 Process windows for AA6061 and AA6082

Figure 3.10 reports the experiments carried out with varying the rotational speed tool and feed rate as well as the obtained output. The process parameters shown in the figure have been used for both aluminum alloys

3.3.2 Temperature trends analysis

Temperature trend during the processes was monitored using a thermocouple inserted into a blind hole at a distance of 7 mm from the weld line figure 3.11.

Thermocouples are temperature sensors formed by connecting two different thermal conductive materials. The thermal contact has been obtained by welding (electric discharge) the two materials. A K-type thermocouple (Chromel (Ni-Cr) (+) / Alumel (Ni-Al) (-)) was used. These thermocouples allow a wide measuring range varying from -200 °C to 1260 °C.

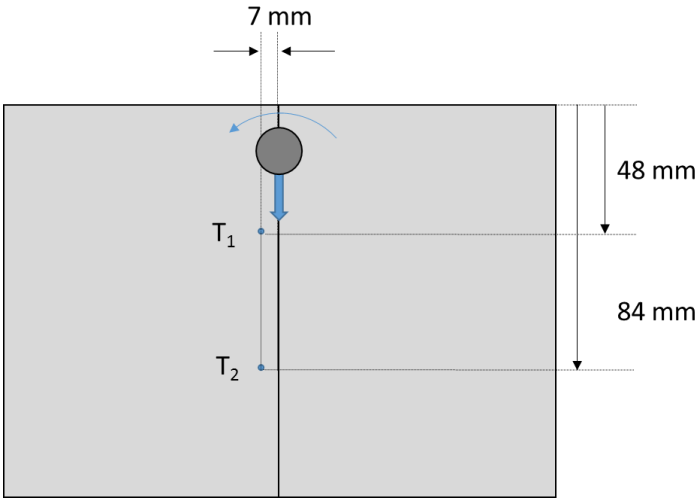

Figure 3.11 Thermocouple position

In the Figure 3.12 the measured temperatures are reported for the material AA6082. Solid lines are used for sound tests, while dotted lines are used for tests characterized by insufficient heat and the dash-dot lines indicate the limit conditions for bonding (defect joints).

Maximum peak temperature equal to 370 °C was measured using a rotational speed tool of 1000 rpm and feed rate of 100 mm/min.

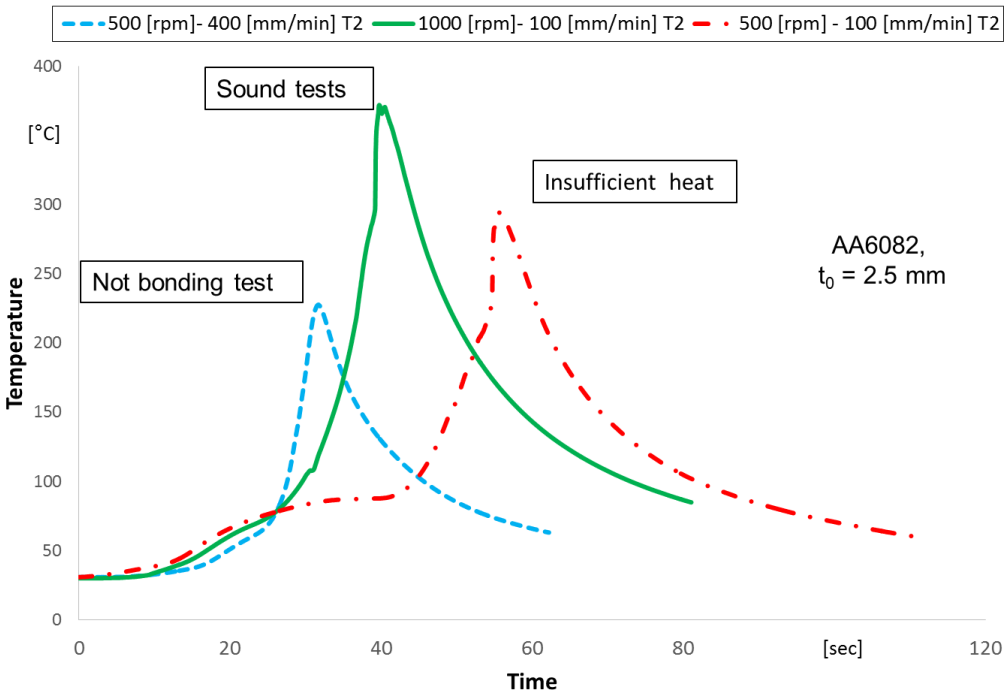

Figure 3.12 Measured temperatures for the AA6082 alloy

It is interesting that the temperature reached during the process influences the quality of the welded joint. In particular with a right set of operating parameters it can get a sound joint.

In fact, you can see on the figure 3.12 that from the hottest process parameters 1000 [rpm]-100 [mm/min] sound test occur, the joint at medium temperature 500 [rpm] -100 [mm/min] defect joint occur and finally with the colder process parameters 500 [rpm]-400 [mm/min] not bonding joint is obtained.

3.3.3 Macroscopic analysis and Micrographic analyses

A detailed analysis of both macro and micro images of the joints permit to highlight a peculiar process mechanics occurring in these cases. A sort of inverse extrusion mechanics occurs with an upward metal flow and a very thin bottom metal layer in which often cracks are present.

In the FSW process, if an insufficient heat generation level is reached, due to the interaction between tool and workpiece, the material flow results ineffective giving

rise to typical defects named tunnel defects; in other words, an incomplete material filling is observed under the tool pin head. Furthermore, for too large values of heat flux a reduction in the joint resistance is observed; an accurate micro and macro analysis of the obtained joints permitted to interpret the occurring phenomena. For large values of heat flux the following observation are derived:

- an enlargement of both the thermo-mechanically affected zone (TMAZ) and of the heat affected zone (HAZ) is observed;
- a subsequent enlargement of the average value of the grain size is obtained;
- local micro-fusions are noticed.

All the mentioned effects concur to reduce the joint strength

In the following, the obtained results will be presented referring to test on the basis of the acquired macro and micro images and, in this way, the overall material flow occurring during the process utilizing the conical pin will be outlined. Furthermore indications will be given on the effect of the considered technological parameters, namely the tool rotation speed and the tool feed rate, on the observed material flow.

3.3.3.1 AA6061

A detailed observation of the material microstructure in the joint section of two friction stir welded AA6061-T6 sheets allows discerning a few different areas. As seen before, the weld nugget has a strong influence on the joint mechanical properties; therefore the analysis and prediction of the weld microstructure are definitely relevant for effective joints design. How it has been explained above, chapter 2, four characteristic areas of the joints can be identified: the base material, the heat affected zone, thermo-mechanically affected zone and the weld zone (Nugget).

Each experiment was repeated three times and macro and micrograph were developed on the obtained jointed specimens with the aim to highlight the different material microstructures all along the joint section; the specimens were polished and attached with chromic acid reagent and observed by a light microscope.

In figure 3.13, in turn, the cross section of one the sound results is reported, the test was developed with the following operative parameters: R=1000 rpm, V=400 mm/min, θ=2°.

The different material zones are quite discernible in Figure 3.13: An irregular central zone, called nugget area is present close to the joint vertical symmetry plane, characterized by very small grains with no particular orientation; two lateral quite small areas (TMAZ) characterized by distorted irregular grains; again two lateral quite large areas (HAZ) characterized by dendrites oriented normally to the generated heat flux and finally, all around, the base material.

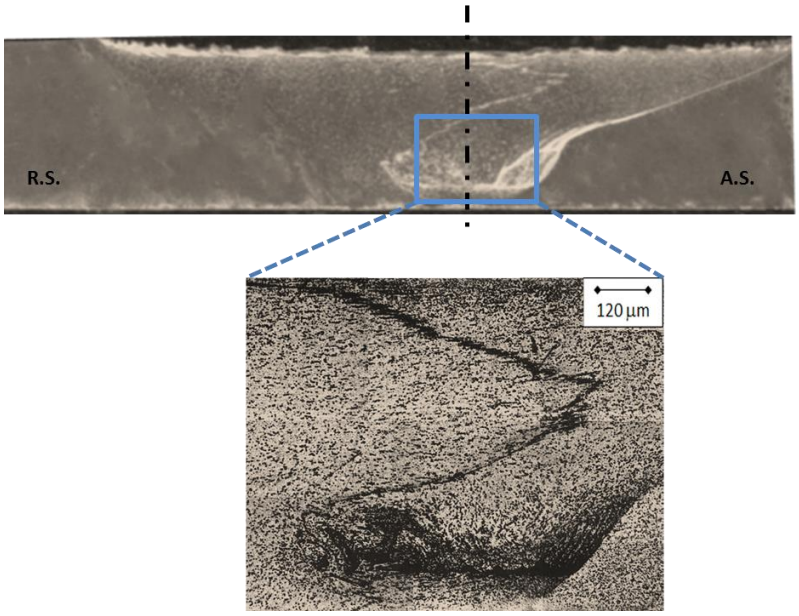

Figure 3.13 Macro and micro image of a transverse section of the "Sound joint" 1000 rpm-400 mm/min case study

It can be observed that the overall effect of conical pins is a more regular material flow occurring in the transverse joint section: in particular regular onion rings were observed. Complete circles are clearly discernible and no more swirl phenomena are observed at the bottom of the joints. Such phenomenon is fundamentally due to the downward action determined on the material by the conical surface of the tool in its rotating and translating movement. The cone angle of the pin induces a vertical downward movement of the material which allows a more effective material flow and avoids swirl phenomena at the bottom of the joint.

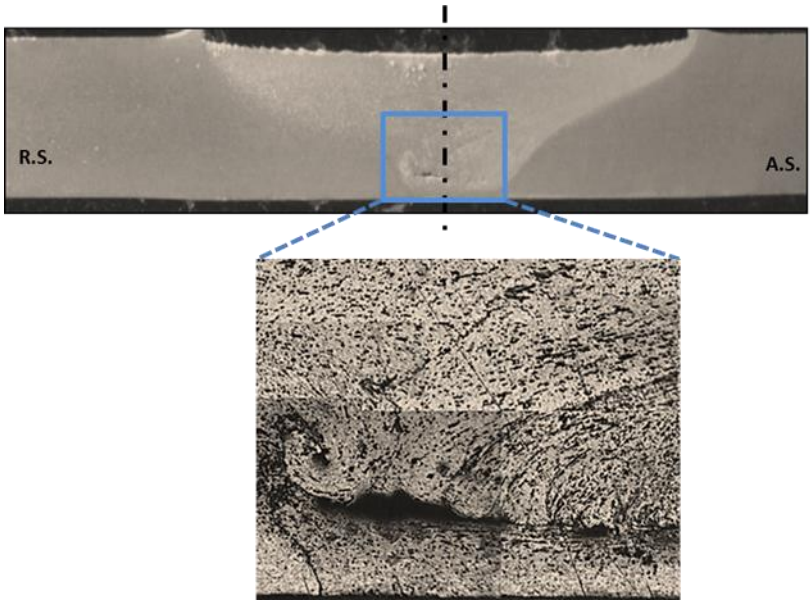

Figure 3.14 Macro and micro image of a transverse section of the “Insufficient heat joint” 500 rpm-100 mm/min case study

Regarding the second welded joints condition " Insufficient heat joint ", a reduction in the joints resistance is observed; an analysis macro images of the joints permit to highlight a peculiar process mechanics occurring in these cases figure 3.14.

The insufficient heat condition is when a low heat was conferred to the joint and so the correct material flow is not occurred. A sort of inverse extrusion mechanics occurs with an upward metal flow and a very thin bottom metal layer in which often cracks are present. The specimen showed a good mechanical characteristics but metallurgical analysis has showed the lack of weld “seam” continuity at the interface.

Finally, the third condition when the combination of the process parameters resulted in too low heat input is shown in the figure 3.15. The joint obtained using as the operational parameters 500 rpm and 400 mm/min is shown. Increasing the feed rate tool up to 400 mm/min, the generated heat is lower so different quality joints are obtained. Almost no continuous bonding is obtained in the cross section. These indicate insufficient heat input was given to the joint. It is worth noting that the insufficient amount of generated heat during the process can cause defects in the weld area difficult to detect by non-destructive analysis methods. From the performed observations it is seen that the wide range of tool feed rate value and tool rotation speed value utilized permitted to analyze three different welding conditions: in the 1000 rpm and 400 mm/min case study a sound weld is observed in all the zones of the transverse section, with no tunnels at the bottom of the joint.

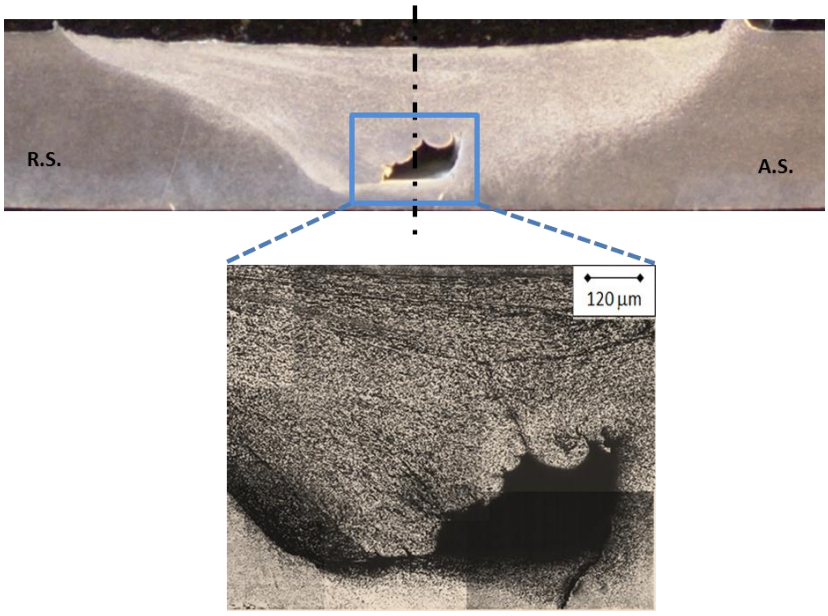

Figure 3.15 Macro and micro image of a transverse section of the "Not bonding test" 500 rpm-400 mm/min case study

With the 500 rpm and 100 mm/min case study a small tunnel is found close to the bottom of the pin, while, for the 500 rpm and 400 mm/min case study, a significant flow defect is observed. In these conditions the defect cannot be described as a tunnel, but rather it is just an incomplete filling of the advancing side. In the micro magnification it is possible to see the material "trying" to fill the gap. Because of the insufficient heat flow the material cannot flow properly.

Finally, the obtained results are summed up in a general overview.

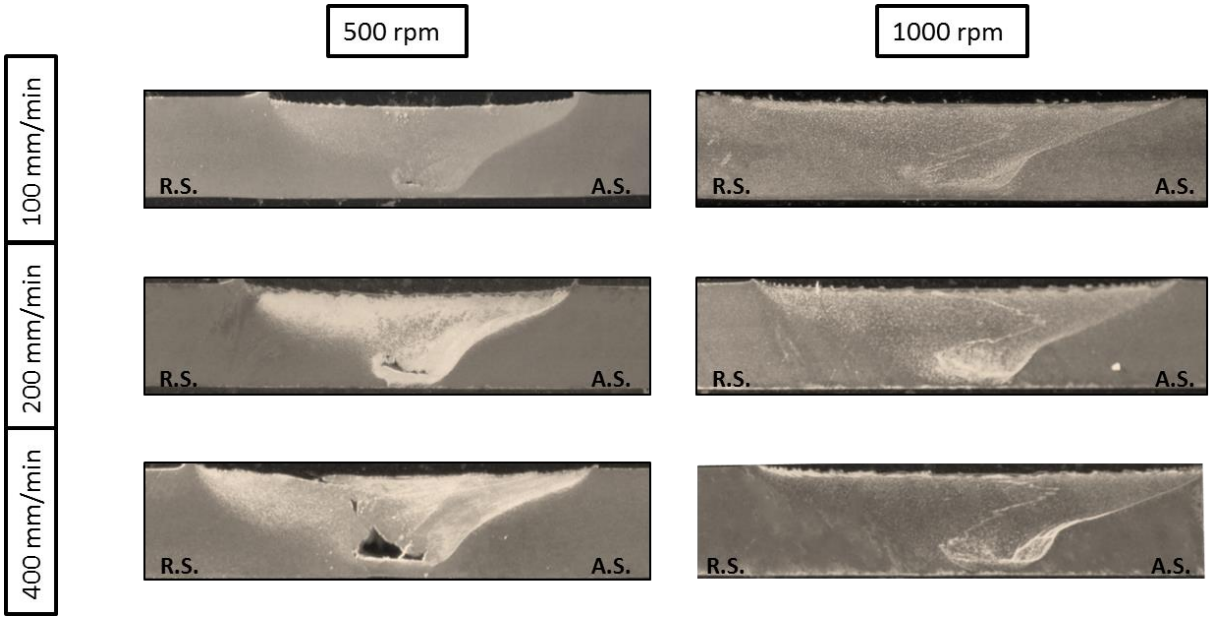

Figure 3.16 Etched cross section of the analyzed case studies for the AA6061

3.3.3.2 AA6082

As shown previously for the aluminum alloy AA6061 the results obtained with the aluminum alloy AA6082 are reported. In order to assess the applicability of the considered bonding criteria to FSW welding experiments were carried out as indicated in Table 3.4.

In figure 3.17, in turn, the cross section of one the sound results is reported, the test was developed with the following operative parameters: R=1000 rpm, V=400 mm/min, θ=2 °.

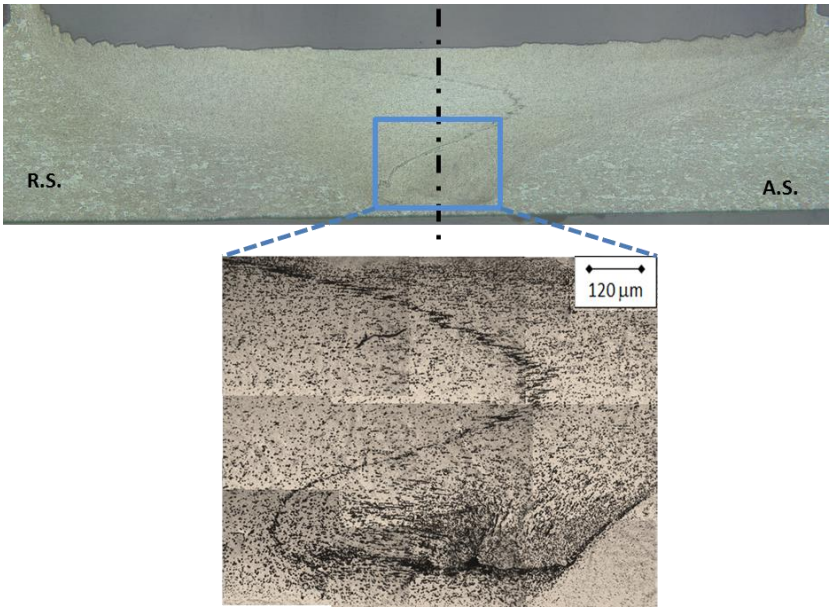

Figure 3.17 Macro and micro image of a transverse section of the "Sound joint" 1000 rpm-400 mm/min case study

As far as the central zone in the Advancing side is regarded, it is expected that the tool action moves back the aluminum material from the retreating side (R.S.) towards the advancing one (A.D.): such phenomenon is particularly evident in the top layers, close to the shoulder surface and decreases all along the sheet thickness. This denotes that the highlighted material flow – from the retreating side towards the advancing one – decreases along the sheet thickness from the top layers to the bottom ones. Such decreasing flow is due to the shoulder action which is stronger than the pin one as the shoulder acts on a much larger surface and at larger radial distances from the tool axis. It should be observed that part of the material coming from the advancing side is forced to move forward with respect to the tool pin in the

welding direction in a sort of extrusion process mechanics: the larger is the revolutionary pitch of the considered FSW process, the stronger results such phenomenon. As far as bottom zone, a few considerations can be developed. It should be observed that the aluminum material coming from the retreating side has got a vertical component due just to the tool cutting angle since a conical pin is utilized; part of the flux close to the bottom of the blanks is obliged to change its direction at the bottom of the sheets close to the bottom zone moving upwards towards the advancing side.

In Figure 3.18 a joint produced using operating parameters 500 rpm and 100 mm/min is shown. The tunnel defect is present in the cross section of the welded joint.

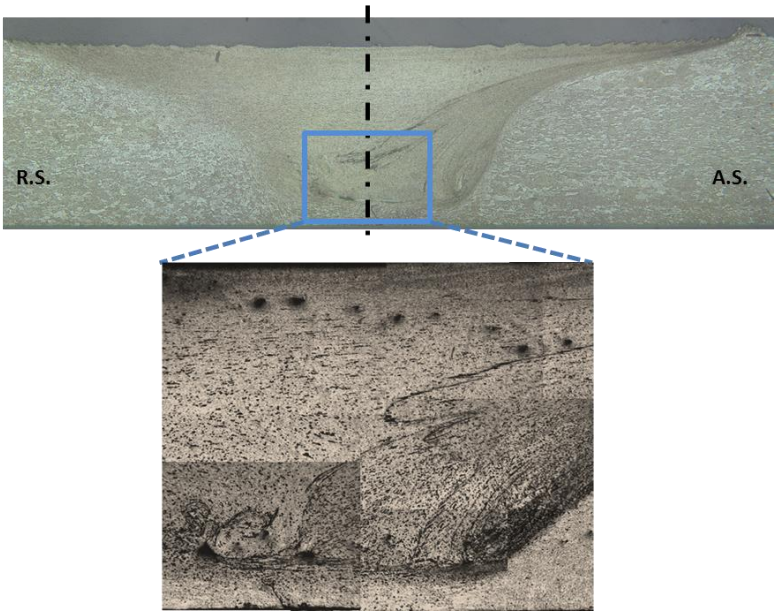

Figure 3.18 Macro and micro image of a transverse section of the "Insufficient heat joint" 500 rpm-100 mm/min case study

As for the aluminum alloy AA6082, with these process parameters the joint shown in figure appears to be good. The "insufficient heat" condition is not reached. The small void observed at the bottom of the pin for the AA6061 due to an insufficient heat conferred to the weld is not observed for this test.

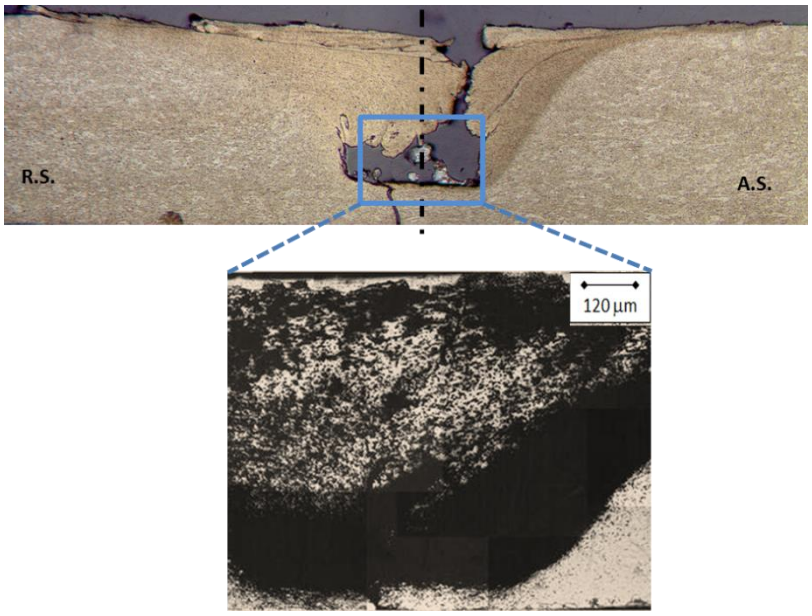

Figure 3.19 Macro and micro image of a transverse section of the "Not bonding test" 500 rpm-400 mm/min case study

Further increasing the feed rate tool up to 400 mm/min, the generated heat turns out to be insufficient for the weld. A not welded joint because of insufficient amount of heat during the process is shown in Figure 3.19; the operating parameters used are 500 rpm and 400 mm/min. In particular, the not bonding test has a very large void area at the bottom of the pin and a crack is visible starting from the bottom of the joint and reaching the top surface

In Figure 3.20, as an example, a micrograph of the nugget zone occurring for the FSW process conditions (1000 rpm, 400 mm/min), is reported. An enlarged scale is utilized in order to better highlight the grain borders and dimensions: an average grain size of about 10 µm was measured.

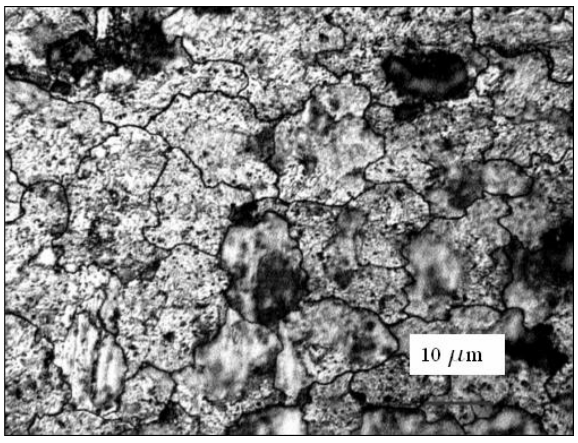

Figure 3.20 Micrograph of the nugget zone of the FSW joint 1000 rpm-400 mm/min

Finally, the obtained results are summed up in a general overview.

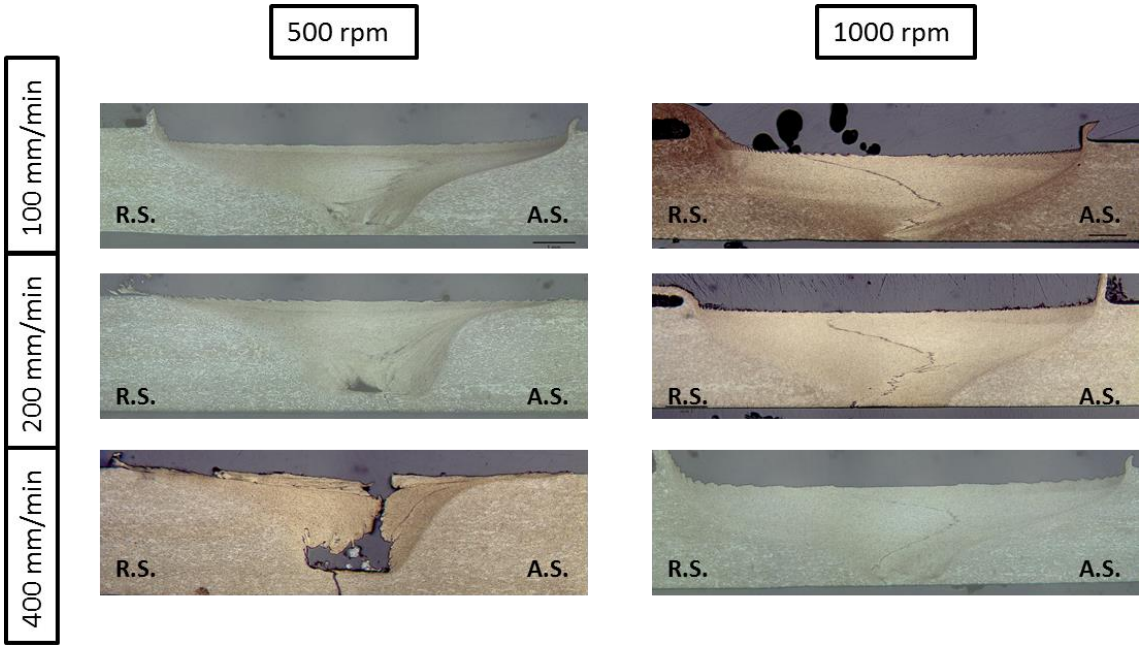

Figure 3.21 Etched cross section of the analyzed case studies for the AA6082

As it can be seen, the three welds characterized by rotation equal to 500 rpm are characterized by flow defects. Looking at insufficient heat test, for 500 rpm and 200 mm/min a tunnel defect is visible at the bottom of the pin, while a very small void can be observed in the same area for test 500 rpm and 100 mm/min. In turn, the three welds produced with rotation equal to 1000 rpm are defect free.

3.3.4 Uniaxial Tensile analyses

The machine where are carried out the tensile tests of the welded specimens, is consists essentially of a closed frame very rigid, with the uprights can slide on columns on which the movable cross-member. This is controlled with very precise movement by an electric motor through mechanical transmission or through hydraulic transmission. There is the possibility to vary the speed of the moving crosshead. The specimen, according to size the bar or sheet or other form, is gripped by two jaws (controlled mechanical or pneumatic) in such a way that, during application of the load, the specimen tends to be increasingly stuck between two equipment on each jaw. The two jaws are integral respectively with the movable cross-member element and a very rigid but sensitive to the load, said load cell. The load cell is, in turn,

embedded in the frame of the machine. When the cross-member is made to move, the test specimen is put into traction. The types of tensile curve that can be obtained from a material subjected to tensile test in a universal machine of the indicated type can be variable in function of the "history" of the material. The machine used in our tests of traction is a hydraulic press.

3.3.4.1 AA6061

The produced welds underwent tensile tests in order to assess the effectiveness of the bonding obtained during the process. In Figure 3.22 the obtained results are reported as percentage of the ratio between the UTS of the tested joint and the one of the base material. The three defect free welds, i.e. the ones obtained with rotation equal to 1000 rpm, have a similar resistance, ranging between 72 % and 74 %. On the other hand, a decreasing trend is found for the case studies characterized by rotation of 500 rpm. In particular, the resistance of test characterized of 500 rpm and 100 mm/min is only slightly lower than the one of the sound joints. As the welding speed increases, the defect becomes larger and a dramatic drop of the UTS is observed till an almost zero value is observed for test 500 rpm and 400 mm/min.

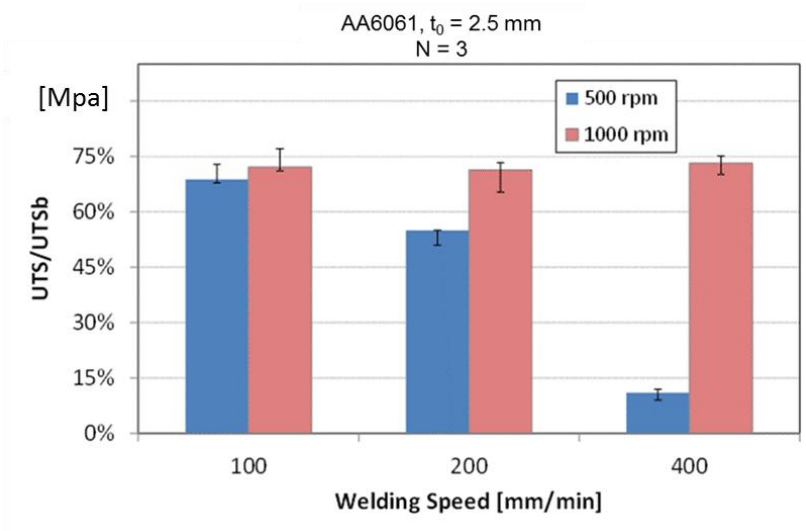

Figure 3.22 Tensile test results for the considered case studies AA6061.

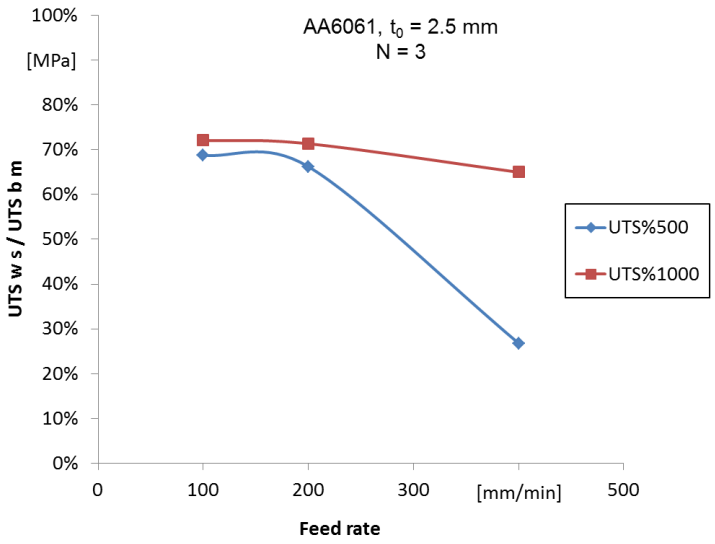

Figure 3.23 UTSws/UTSbm vs. Feed rate AA6061

In Figure 3.23 the influence of the tool feed rate is shown; the tests were developed assuming R=1000 rpm and 500 rpm, θ=2 °. A maximum value of the joint resistance is observed: actually for low values of the tool feed rate micro-fusions and uncontrolled Si precipitations reducing the joint strength, are observed. On the other hand for large values of V an insufficient heat flux is generated. It has been observed that the Si particles density in the nugget area decreases with the increasing of V; furthermore the average size of Si particles has been measured varying from 7 μm to 12 μm, and this value increases with the increasing of the R value. Such observations have to be explained with the different levels of specific heat power conferred for each test.

3.3.4.2 AA6082

Ultimate tensile strength results have been reported in the following figures.

How it can be seen from the figures the welded specimen characterization of 500 rpm and 400 mm/min the welding was not occurred. A moderate decrease of the UTS from 1000 rpm to 500 rpm is reached.

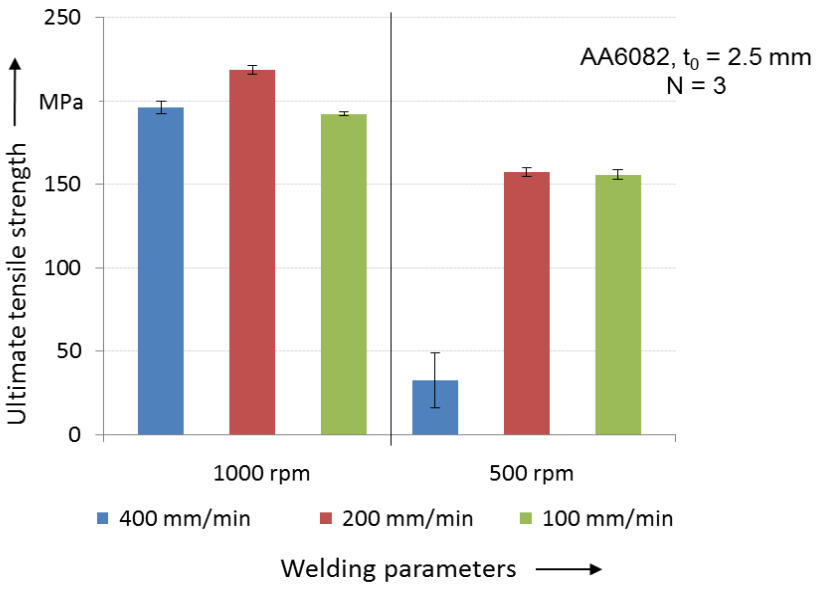

Figure 3.24 Ultimate Tensile test results for the considered case studies AA6082

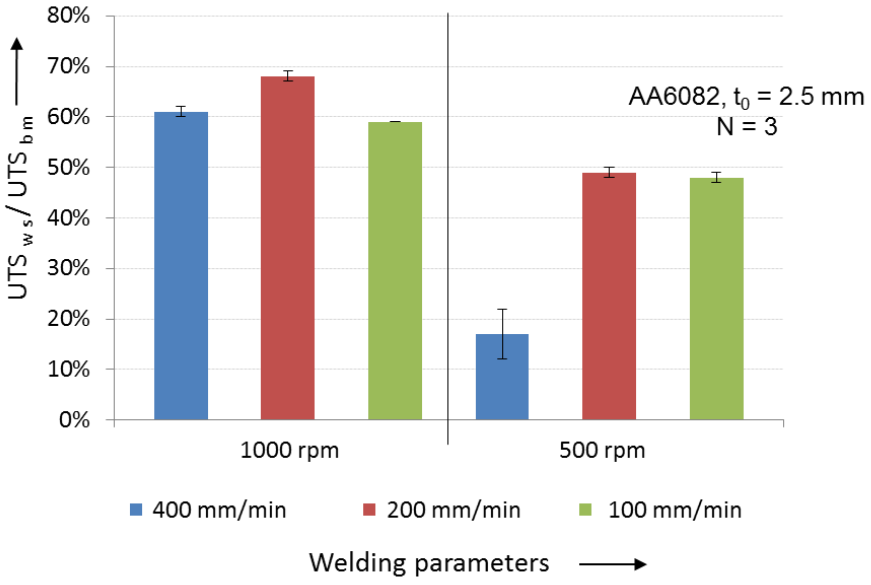

Figure 3.25 UTSws/UTSbm vs. welding parameters AA6082

The ratio between the UTS of the tested joint and the one of the base material have been reported in the graph.

For 1000 rpm highest value of the ratio in 200 mm/min feed rate. Minimal decrease of the ratio when decreasing the welding temperature regarding the welded specimens characterized 1000 rpm of tool rotation speed.

3.3.5 Microhardness analyses

For each of the developed joints hardness tests were developed with the aim to investigate the mechanical properties of the welding zone. In particular different hardness tests were developed on the equatorial plane of the joints at different distances from the symmetry plane towards both the retreating side of the joint and the advancing one.

In particular, for the Vickers microhardness a straight pyramid diamond indenter with a square base with a vertex angle of 136° is used.

The Vickers hardness value through the following formula is calculated:

$$HV = \frac{2P \sin\left(\frac{136}{2}\right)}{{d_m}^2}$$

equation 3.1

Where P is the applied load, measured in kg and d_m is the average value of the diagonals. It was chosen to apply a load of 0.5 kg in relation to the material of the specimens, for a holding time of about 30 s.

3.3.5.1 AA6061

The microhardness trends of the tested joint characterized of 1000 rpm of tool rotation speed have been reported in the following figure 3.26. It should be observed that the welding process softens significantly the material and the hardness is reduced from 110 HV to 90 HV, for V = 400 mm/min, to 85 HV for V = 200 mm/min and to 80 HV for V = 100 mm/min in the joint axial zone. Such behavior explains the strength reduction of the welded joints with respect to the base material.

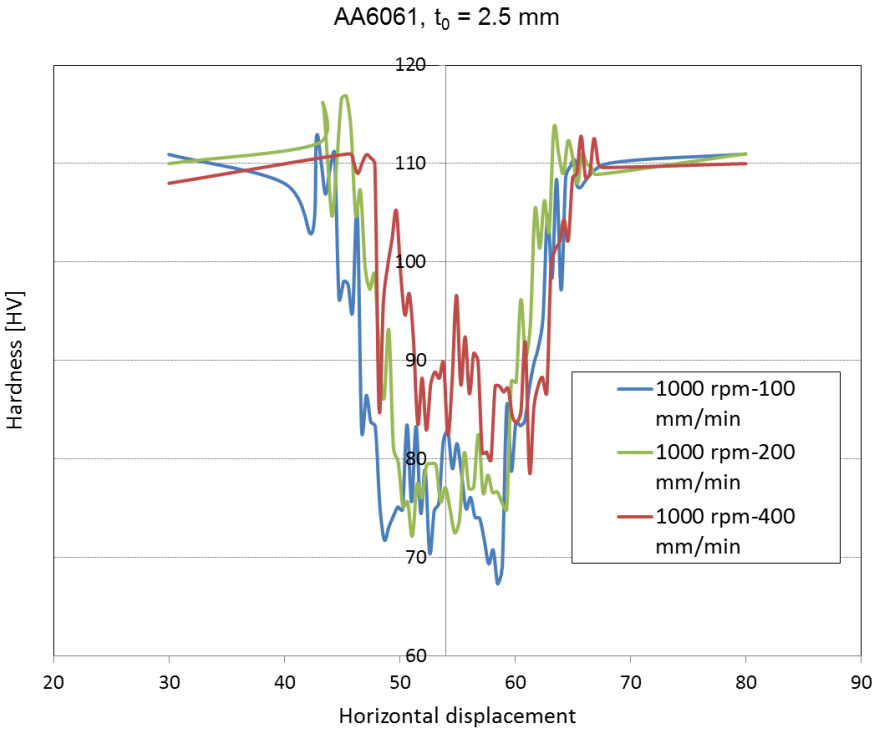

Figure 3.26 Hardness test results for the 1000 rpm case studies AA6061.

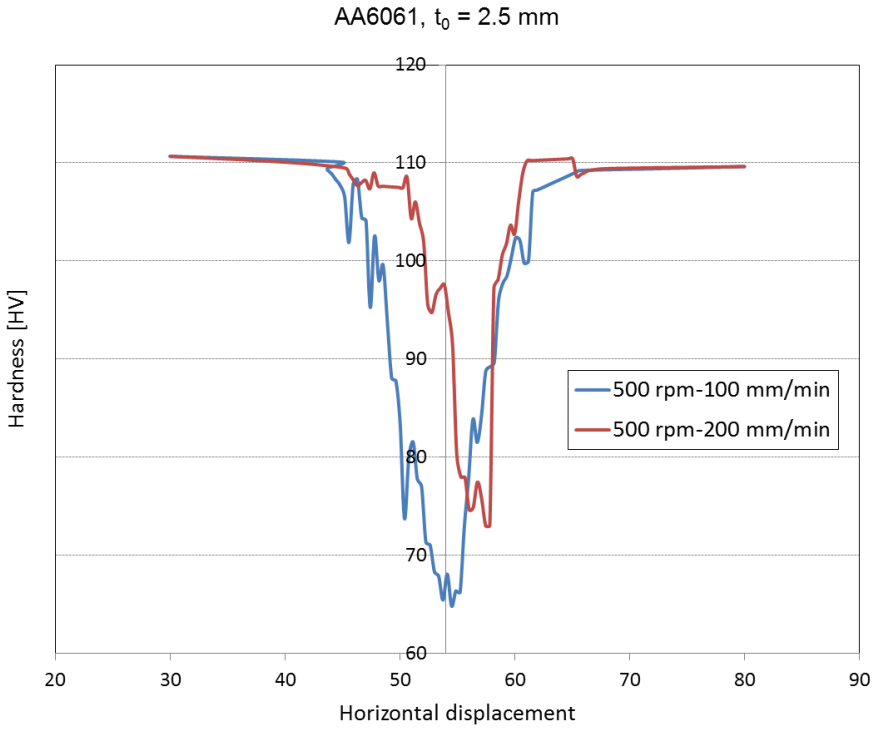

Figure 3.27 Hardness test results for the 500 rpm case studies AA6061.

The microhardness trends of the tested joint characterized of 500 rpm of tool rotation speed have been reported in the following figure 3.29.

In this cases, it should be observed that the welding process softens significantly the material and the hardness is reduced from 110 HV to 75 HV, for V= 200 mm/min, to 70 HV for V= 100 mm/min in the joint axial zone.

It can be seen the symmetric behavior of the hardness and decrease of the values on the welding area and a moderate decrease of the hardness from lower to higher process temperature. The minimum values of hardness for the welded joints with 500 rpm decrease of the HAZ.

3.3.5.2 AA6082

The microhardness test of the tested joint characterized of 1000 rpm of tool rotation speed and 100 mm/min of feed rate have been reported in the following figure 3.28. It should be observed that the welding process softens significantly the material also for the AA6082 and the hardness is reduced from 130 HV to 90 HV.

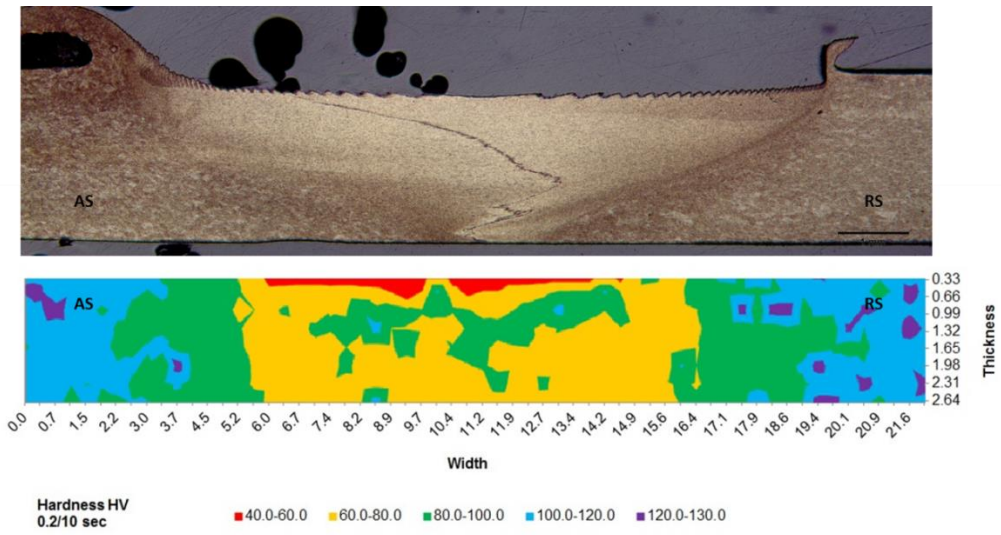

Figure 3.28 Hardness test results for the "Sound joint" 1000 rpm-100 mm/min case study

A sound weld is observed in all the zones of the transverse section with no tunnels at the bottom of the joint.

The microhardness test of the joint characterized of 500 rpm and 200 mm/min have been reported in the following figure 3.29. In this case, it should be observed that the

welding process softens significantly the material and the hardness is reduced from 130 HV to 75 HV. A small avoid is present in the cross section of the joint.

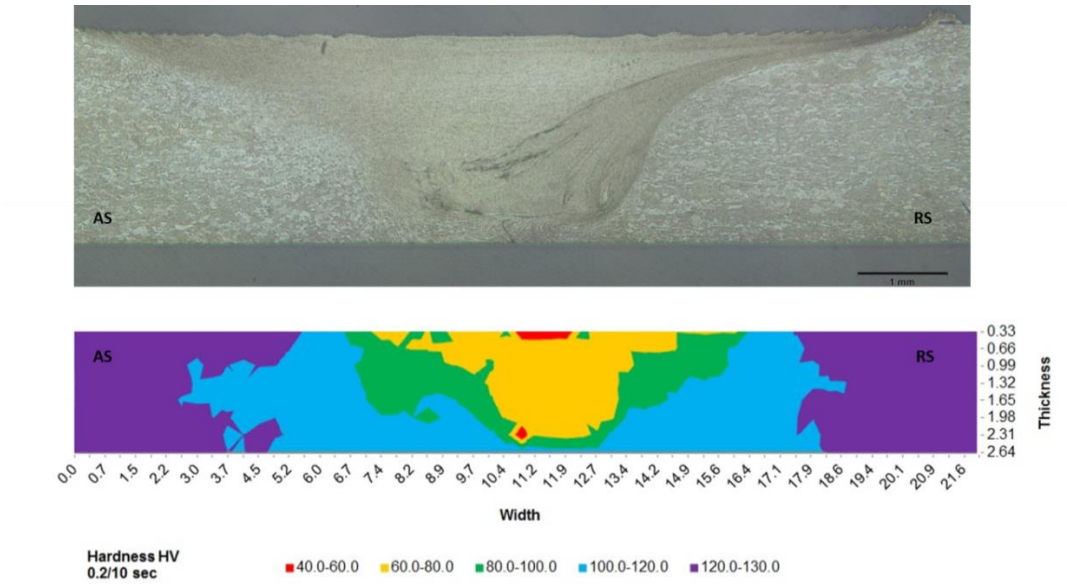

Figure 3.29 Hardness test results for the "Insufficient heat joint" 500 rpm-200 mm/min case study

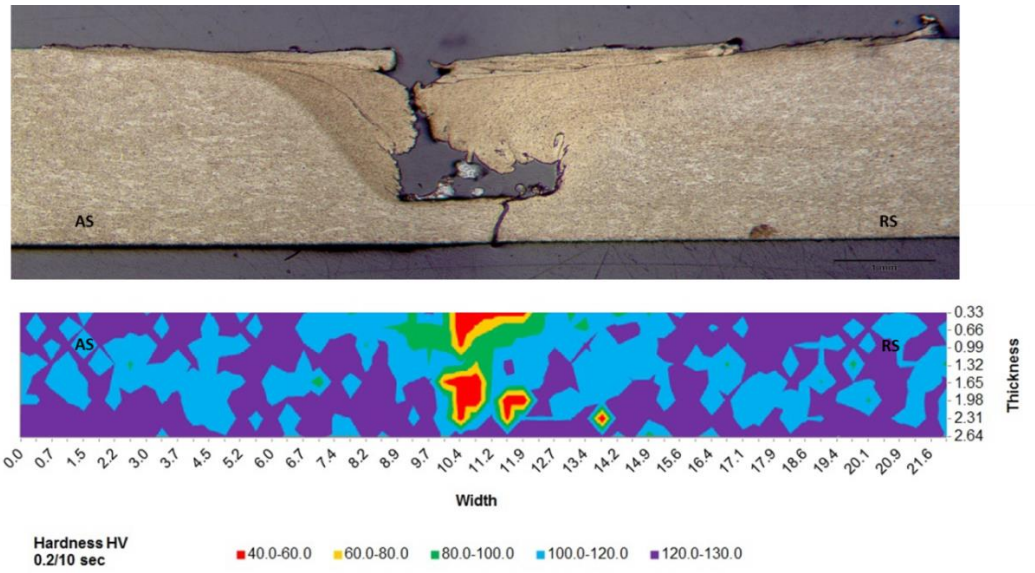

Figure 3.30 Hardness test results for the "Not bonding test" 500 rpm-400 mm/min case study

For the welded joint characterized of 500 rpm and 400 mm/min the microhardness result is reported figure 3.30.

The test has a very large void area at the bottom of the pin and a crack is visible starting from the bottom of the joint. The process parameters are not able to modify the properties of the joint. The hardness remains nearly that of the base material

3.4 Numerical Analysis

Friction Stir Welding is a quite complex process both for the heat generation aspect and for the deformation one; the former is influenced by many parameters, technological (tool rotational speed, feed rate, etc.), and related to tool and workpiece materials (thermal properties, friction couple, etc.), and the actual generation process is still quite unclear. The latter is very different from the one that can be observed in the most of other processes because it is been estimated that very high strain and strain rates can be reached at temperatures of about 400-500 °C, making hard a correct material flow characterization.

A fully 3D FEM model for the FSW process is proposed [93, 102], that is thermo-mechanically coupled and with rigid-viscoplastic material behavior. A unique feature of this model is the representation of sheet seam (abutting edges) as a continuum. This continuum hypothesis avoids the numerical instabilities that result from the discontinuities present at the edge of the two sheets. Predicted results are compared with the experimental data to validate this model.

The commercial FEA software DEFORM-3DTM, Lagrangian implicit code designed for metal forming processes, is used to model the FSW process. The workpiece is modeled as a rigid visco-plastic material, and the welding tool is assumed rigid. This assumption is reasonable as the yield strength of the sheet (conventionally aluminum alloy) is significantly lower than the yield strength of the tool (tool steel or carbide). The following is a summary of equations governing the material behavior.

A rigid-visco-plastic material model with Von Mises yield criterion and associated flow rule is used. The rigid-viscoplastic finite element formulation is based on the variational approach.

The FSW modeling is divided into two stages: 1) sinking stage and, 2) welding (advancing) stage. In other words, FSW is modeled in this research from its initial

state to steady state. During the sinking stage the tool first moves down vertically at 0.1 mm/sec with a rotating speed of 1000 rpm or 500 rpm, then, during welding or advancing stage, the rotating tool moves along the weld line (seam) joining the two workpieces. Before these two stages, the tool is tilted 2 ° about the vertical axis, namely the nuting angle. The sinking stage is modeled to obtain high enough temperature for the subsequent welding process and the advancing stage is modeled to investigate the thermo-mechanical phenomena in the formation of weld nugget.

For the thermal characteristics of the AA6082 and AA6061 aluminum alloys taken into account, the following values were utilized: thermal conductivity k1 = 180 [N/(s °C)] and thermal capacity c = 2.4 [N/ (mm^2 °C)] for the AA6082 while k1 = 166 [N/(s °C)] and thermal capacity c = 2.3 [N/ (mm^2 °C)] for the AA6061 taken from literature for aluminum alloys. No variation of k1 and c with temperature was taken into account; this assumption linearizes the thermal equation and results in better convergence. A rigid-viscoplastic temperature and strain rate dependent material model is employed. The friction stir welding simulation is carried out to study the influence of different process parameters using the generated material data during the base material characterization. The flow curves at elevated temperatures data (Figure 3.2 regarding the AA6082) are used in the numerical model so as to obtain a faithful simulation of the process done experimentally. With increasing temperature and decreasing strain rate a significant drop of the initial yield stress and the yield stress level itself is observed. Until a temperature of 150 °C the resistance of the material versus a further plasticization increases. This strain hardening is shown by a growth of the flow curve (Fig. 3.2). With higher temperature the strain hardening decreases for 300 °C and vanishes for 500 °C. These effects can be explained by thermally induced recovery mechanisms. Due to the increasing temperature and therefore thermal energy the dislocation movements, which represent the plastic deformation, avoid the obstacles of the crystal structure more easily. The required force for the dislocation movement through the face-centered or cubic-centered lattice of the aluminum matrix is reduced. The strength of the material therefore decreases. The reduced strain hardening effect or softening is a result of dynamic recovery mechanisms during the test.

These mechanisms lead to softening effects, which increases with higher temperature and low strain rates. With increasing strain rate the material strength increases due the reduced time for dynamic recovery.

The value of the heat transfer coefficient is not very important in FSW due to the fact that the tool quickly reaches a steady state temperature very close to the sheet temperature, resulting in a poor thermal exchange between the tool and the workpiece. A preliminary sensitivity analysis for different interface heat exchange coefficient value confirmed that there were no significant variations of temperature as interface heat exchange coefficient changes.

In order to obtain the desired vertical material flow, a conical pin shapes smooth can be adopted. Based on previous experimental campaign, the following tool design was utilized (see Figure 3.6): a pin height of 2 mm, a major pin diameter equal to 3.5 mm, a shoulder diameter equal to 10 mm. The tool was modeled as rigid body and meshed, for the thermal analysis, with about 3,000 tetrahedral elements.

During the modeling of workpiece, a “single block” continuum model (sheet blank without a gap) is used in order to avoid contact instabilities due to the intermittent contact at the sheet-sheet and sheet-tool interfaces. In particular, a single sheet has been considered and the rotating tool once completed the sinking phase, moves forward welding a crack left behind the pin as it advances along the welding line. The sheet blank, width of 60 mm, a thickness of 2.5 mm and length of 90 mm, was meshed with about 12,000 tetrahedral elements with single edges of about 0.625 mm; in this way about four elements were placed along the sheet thickness. A non-uniform mesh with adaptive re-meshing was adopted with smaller elements close to the tool and a remeshing referring volume was identified all along the tool feed movement (Figure 3.31). Experience in previous FEM simulation shows that a coarser mesh leads to incorrect results and a finer mesh results in unaffordable computation time without significant improvement of simulation results.

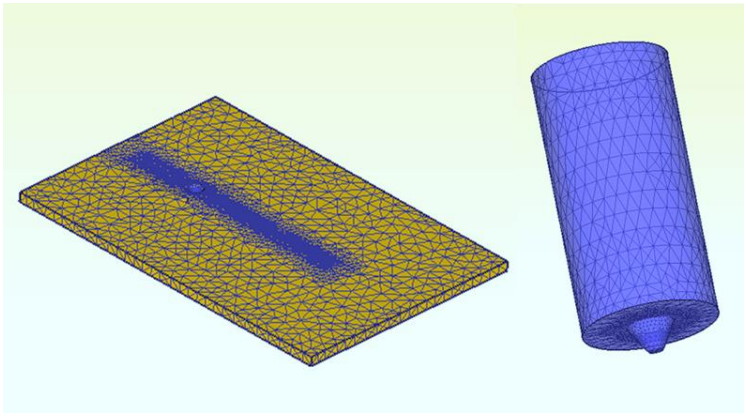

Figure 3.31 The FE continuum model

A constant shear friction factor of 0.46 is used for tool-sheet interface on the basis of a previous experimental thermal characterization and a numerical sensitivity analysis for the shear friction factor m. All the simulations are performed using the same experimental procedure and process parameters figure 3.10. Advancing velocity of the tool was varied to investigate its effect on the weld zone.

A key step in to development of the FEM model of the FSW process is to assign the proper boundary conditions. The software used to assign a variety of parameters, such as heat transfer, pressure and forces, which allow you to manage different conditions. In the specific case it has gone to the allocation of the conditions that emulate the physical contact between the machine tool and the workpiece. The boundary conditions have to assign the speed nodal equal to zero (figure 3.34). Such conditions should be assigned to particular areas of the workpiece so as to prevent the translation of the material because of the forces that occur between workpiece and the die.

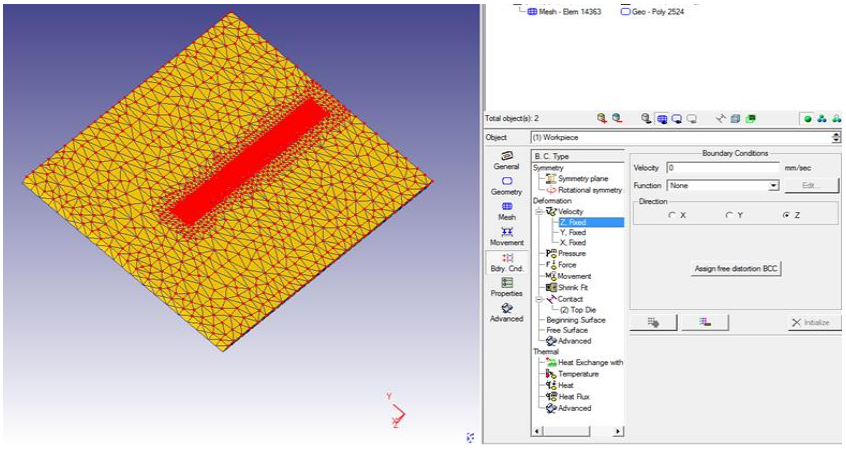

Figure 3.32 Boundary conditions in the FSW model

The proposed model has been calibrated with several experimental tests. In particular, in the following, the procedure to obtain a proper m coefficient to be introduced in the shear factor friction model is described; such coefficient was determined on the basis of an inverse identification approach [187]. The experimental plan (Figure 3.10), at the varying of the tool rotational speed and feed rate, was carried out, and each developed test was thermally characterized monitoring the conferred heat flux utilizing two embedded thermocouples, at 7 mm from the welding line respectively.

At the end of the simulation the material flow was investigated through the analysis of the nodes position and the main field variables history that they experience. The “point tracking” option of the software DEFORM-3DTM was utilized. The points P1 and P2 have been identified, in the same position of the thermocouples hole, to study the temperatures variables figure 3.33.

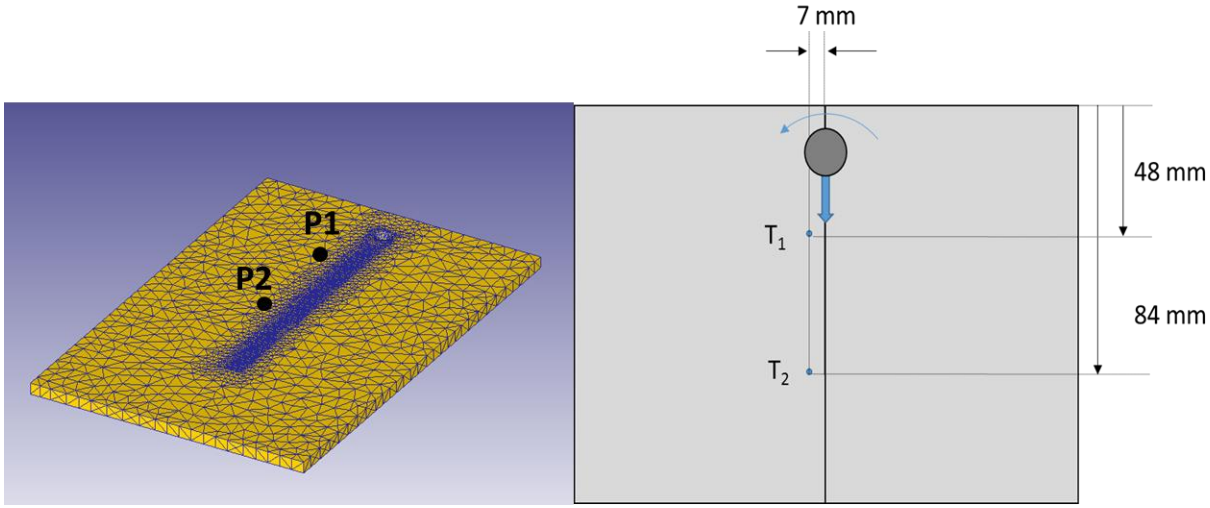

Figure 3.33 Temperatures study in the FSW model

The local value of temperature for a given reference points and time was calculated. Figure 3.34 shows the distribution of the above cited field variable in the sound welded specimens characterized by 500 rpm of tool rotation speed and 200 mm/min of feed rate.

The temperature predicted by the proposed model was compared to the experimental results (Figure 3.34). It is observed that the predicted temperature matches the experimental results very well. The time gap between the experimental results and the numerical ones is due to the thermocouple that begins to record the

experimental temperature prior of the contact piece-tool, while the numerical result started to record during the second stage (above cited welding stage), in which is divided the FSW model. It has to be noticed that although the comparisons were performed using an AA6082-T6 aluminum alloy, it can be reasonably accepted that the validity of the thermal model is not strongly affected by the use of a different aluminum alloy. This is because that there is no significant difference in thermal properties between 6XXX series aluminum alloys. Furthermore, it is reasonable to assume that the same friction factor can be used for the contact interface between the tool material and the sheet when using different aluminum alloys.

It is seen that the temperature, calculated at the reference point P1, are quickly increased to around 190 °C for the joint as the experimental result. For the second point P2, the maximum temperature increasing up to 230 °C, confirming by the experimental test.

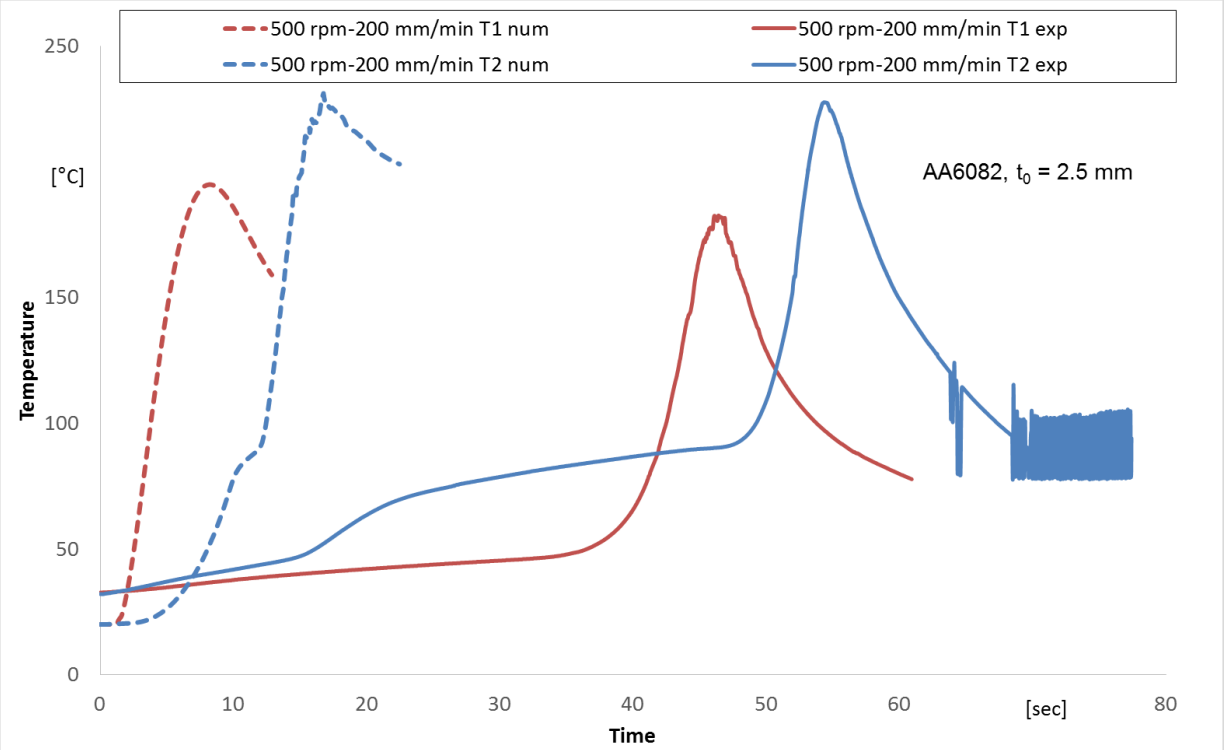

Figure 3.34 Temperature histories at 7 mm from the welding line for R=500 rpm and V=200 mm/min Exp vs Num.

In order to highlight the material flow due to the FSW processes, i.e. the nodes movements induced by the tool action and the main field variables history they

experience, the “node tracking option” of the software DEFORM-3DTM was utilized, highlighting for a set of nodes initially placed along the sheets separation line in a transverse section, their final position after deformation. The reference transverse section was taken after 40 mm of weld length, i.e. after the process reached the steady state. In particular, six observation points were selected, equally spaced along the joint thickness, and their deformation history was followed during their interaction with the welding tool. Figure 3.35 shows the considered points in the transverse section of the modeled joint.

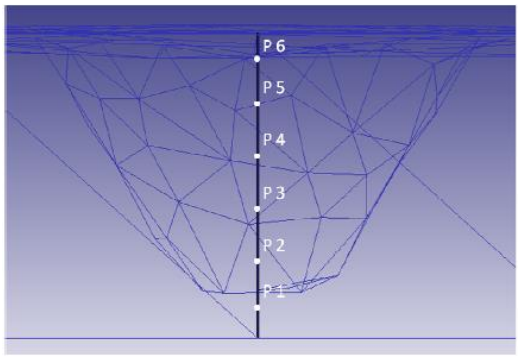

Figure 3.35 Observation points on the sheets separation line at the beginning of the welding simulation

The reasons for the different behavior described above, (macro analysis AA6061 chapter), have been investigated through the numerical model. First the temperature distribution in the top surface of the joints is shown for the three considered case studies (Fig. 3.36).

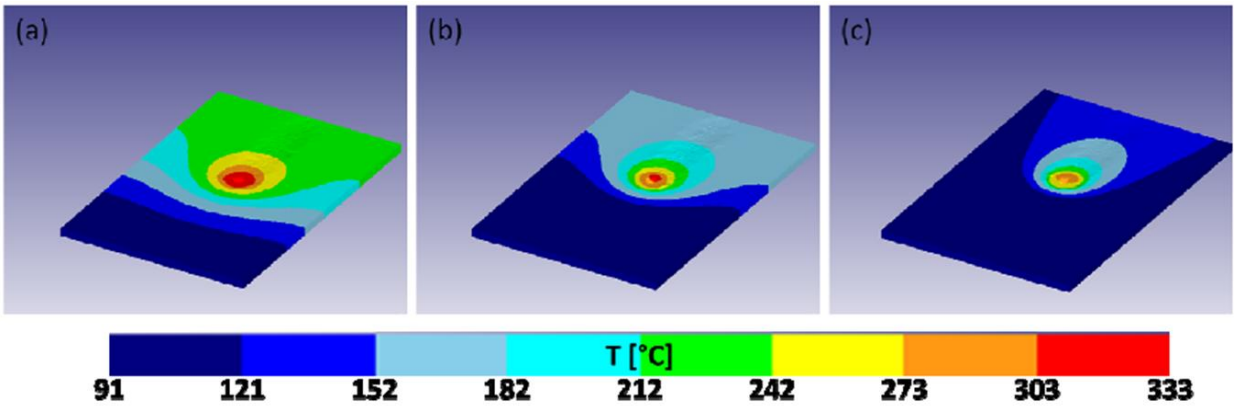

Figure 3.36 Temperature distributions on the joints top surface for the considered case studies AA6061: (a) 1000 rpm-400 mm/min, (b) 500 rpm-100 mm/min and (c) 500 rpm-400 mm/min

As expected a decreasing temperature is calculated at the increasing of the tool feed rate. In particular maximum temperature in the joints ranges from about 330 °C to about 280 °C. In the latter condition, corresponding to the 400 mm/min case study, the material does not reach a proper softened state in order to flow around the tool that works as a “mill” rather than as a stirring tool.

In order to analyzed more in depth the material flow induced by the thermo mechanical action of the tool, the movement and final position of the six observation points shown in Fig. have been investigated. In the next figure 3.37 the final position of the initial sheets separation line is visible along with the final position of the observation points, for each case study. It is worthy notice that the six points do not lie in the same transverse sections. However, being the weld continuous along the weld seam, the trace shown in figure 3.37 represents the actual position of the initial separation plane.

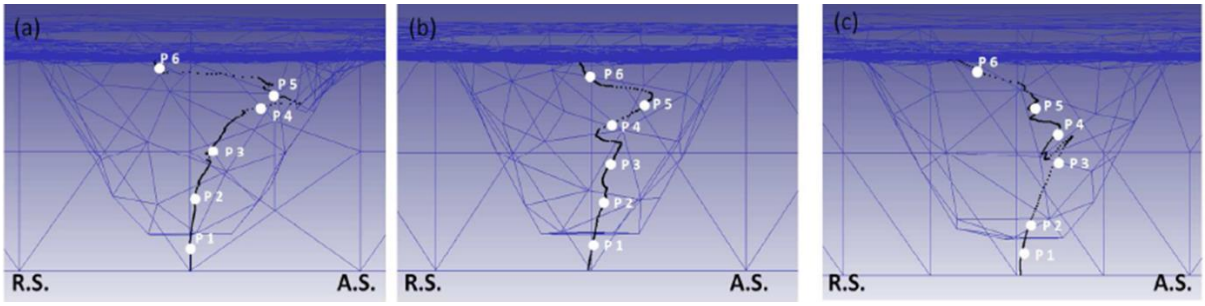

Figure 3.37 Final position of the initial sheets separation line and of the six observation points AA6061: (a) 1000 rpm-400 mm/min, b) 500 rpm-100 mm/min and (c) 500 rpm-400 mm/min

A few observations can be made from the above figure 3.37. First, for all the welds the final position of P1 is not significantly different form its original position. This is because it is located below the bottom of the pin, and then is only partially influenced by the material flow. Then, only for the 1000 rpm-400 mm/min case study the actual welding line is mostly located at the advancing side. The other two case studies show a more vertical line. In particular, the welding line is characterized, for the 500 rpm-400 mm/min case study, by a less regular trend, especially between points P3 and P4. Additionally, a large distance with points coarsening is found between points P2 and P3. As the black line itself is made of separate points, the line coarsening, resulting in increased distance between P2 and P3, indicates that material in that area underwent a too large deformation with consequent void creation due to insufficient material flow. A quantitative analysis was performed calculating the main

field variables histories, namely temperature, strain and strain rate, for the six observation points and for all the case studies (Fig.3.35).

Looking at the temperature distributions it arises that, for each weld, the six observation points experience similar histories during the process. On the other hand, at the varying of the case study there is a change both in the maximum value reached, as already observed in Fig. 3.36. It is known that temperature plays a key role in solid bonding. However, for the considered case studies, the reasons for the localization of the defects at the bottom of the joint have to be searched in the effect of the other variables, namely strain and strain rate.

As far as the former is regarded, the maximum value reached is in the area of P4 and P5, which is close to the top surface of the joint but not on the top of that. In this area the material is significantly affected by the action of the tool shoulder, which is still quite close; additionally the pin action is maximized by the larger diameter due to the conical shape. As far as P2 and P3 are regarded, they represent the points undergoing the minimum strain in the joint, not considering P1 which, as already noticed, is not heavily involved in the material flow being below the tool pin bottom surface. In this way P2 and P3 are located in the joint area which is more likely to experience an insufficient material flow.

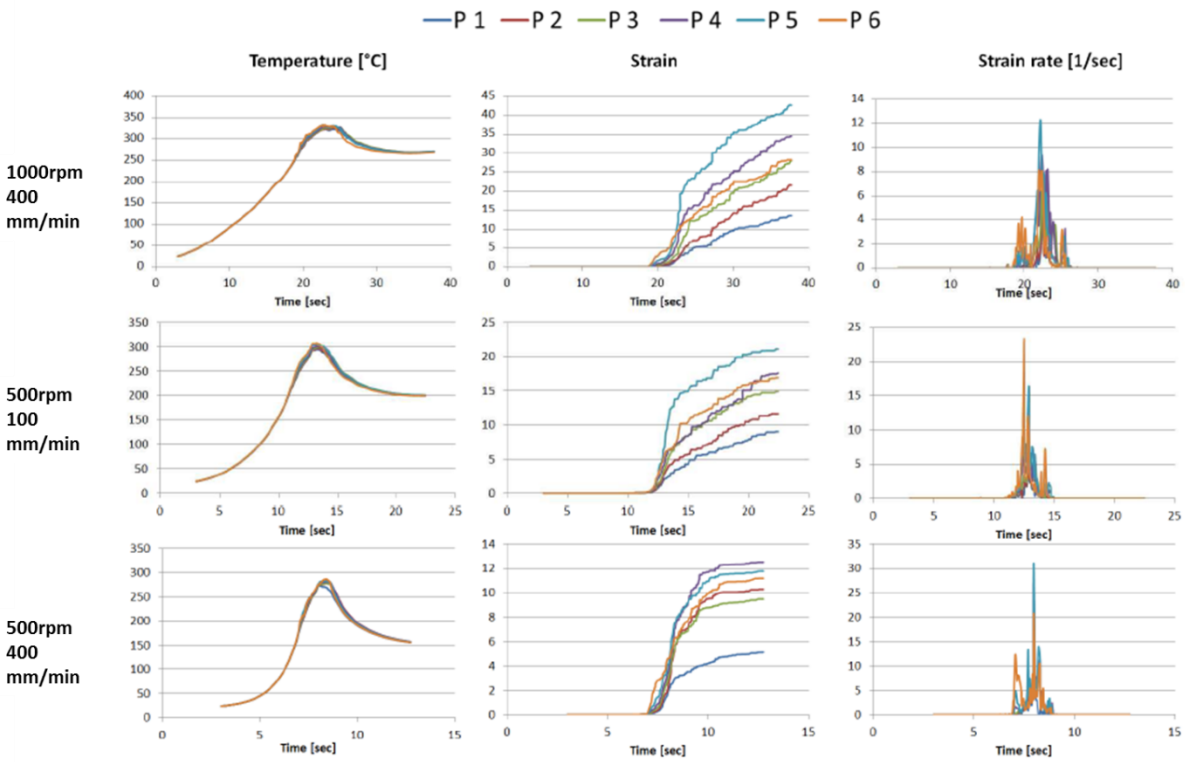

Figure 3.38 Temperature, strain and strain rate histories for the six observation points and for the case studies AA6061: 1000 rpm-400 mm/min, 500 rpm-100 mm/min and 500 rpm-400 mm/min

Overall, the strain values decrease at the increasing of the tool feed rate, being the same amount of material involved into the rotational motion of the tool for less rounds.

Finally it is worthy notice that such large values of strain can be calculated assuming a constant behavior of the flow stress for given temperature. This approach has been already utilized for other FSW models known in literature [102].

Looking at the strain rate, an overall trend opposite with respect to the strain is found, as it increases at the increasing of the tool feed rate. This is due to the enhanced mechanical effect of the tool, being the component of the prophetic speed of the tool due to the rotation the same and the one due to the advancing speed larger [102]. Focusing on each joint, consistently with what found for the strain, it is observed that maximum values are reached by the points close to the top surface, once again indicating the bottom of the joint as the area where the occurrence of a defect is more likely.

3.5 Applicability criteria solid bonding

A welding criterion was considered, namely the pressure–time (W) criterion. This criterion is based on integral in time, that, in order to perform the calculation, have been approximated with sums over smalltime intervals. Eq. (1) represents the pressure–time criterion.

$$W = \int_0^t \frac{p}{\sigma} dt \cong \sum_j \frac{p_j}{\sigma j} \Delta t_j$$

equation 3.2

Where p is the contact pressure at the interface, σ is the flow stress of the material in the given temperature, strain and strain rate conditions. Hence, W can be considered as the “equivalent time”, calculated with proper weights of pressure and temperature (i.e. the flow stress) for the occurrence of solid bonding.

In order to calculate, for each of the observation points highlighted in Fig. 3.37, the value of the welding criterion, the material flow occurring during the FSW process must be properly predicted. Buffa et al. [164] proved the effectiveness of the developed model for the prediction of the material flow by comparing the calculated

results with experimental measurements of the zig-zag line due to the oxides particles dispersed in the transverse section. Following the approach proposed in the above cited paper, the reference points were tracked during the process. It is worth noticing that the observation time interval begins as the points experience non-zero pressure values, i.e. before the tool reaches the reference transverse section. By the same token, the observation period ends after the tool leaves the reference section and pressure drops to zero. This behavior is due to the peculiar FSW process mechanics: the material close to the sheets separation line rotates together with the tool for a certain number of rounds, depending on the selected combination of process parameters; the rotation begins in the retreating side. Then the material is left at the advancing side of the joint. In fact, the latter is the area at which fracture occurs during tensile tests of sound joints. Fig. 3.39 shows the evolution of the tracking line, initially laying on the ideal separation surface between the sheets, till the final position reached by the six reference points (test 1000 rpm-400 mm/min).

Process time and the x coordinate (welding direction) are provided for each figure. The origin x = 0 is set when the tool axis correspond to the considered transverse section. It is necessary to observe that at the beginning the reference line is in the leading edge of the joint while at the end it lays on the trailing edge.

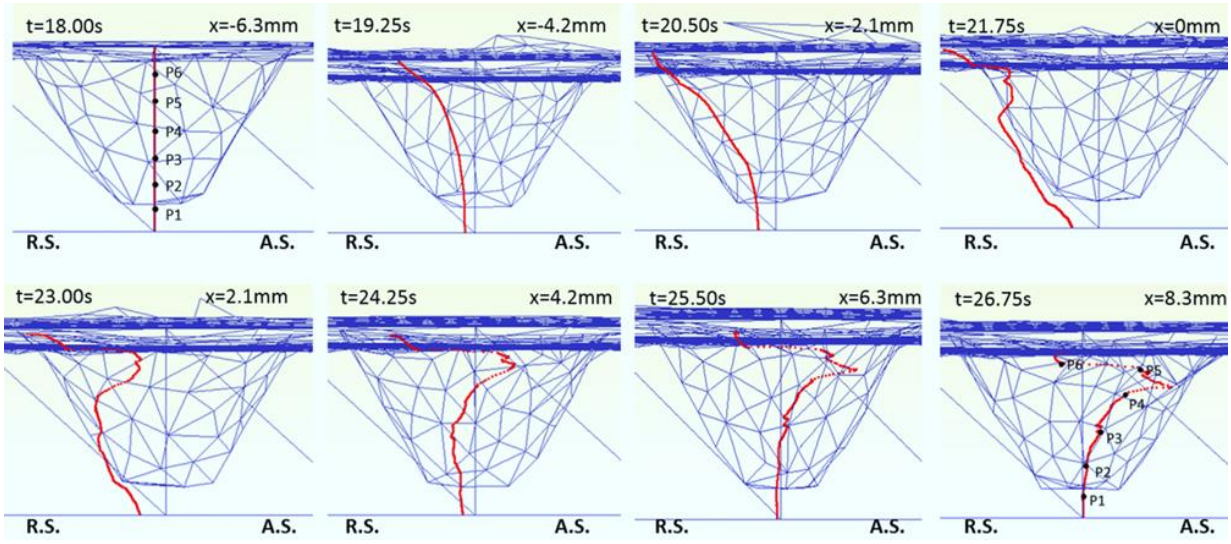

Figure 3.39 The identified points for the "node tracking option" – test 1000 rpm-400 mm/min.

The local value of the flow stress for a given reference point and time was calculated starting from the local values of temperature, strain and strain rate. The figure 3.40 a,

b and c show, for case study C1000-400, the distribution of the above cited field variables in the reference transverse section, right after the material closed the crack behind the tool

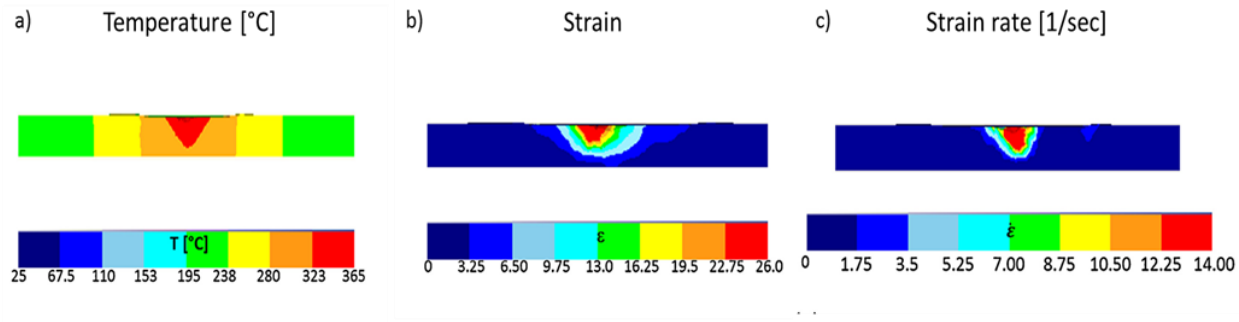

Figure 3.40 Temperature, strain and strain rate distribution in the transverse section test 1000 rpm-400 mm/min.

The field variables distribution highlights some of the characteristics of the FSW process: temperature is symmetric respect to the welding line; in turn, strain and strain rate peaks are shifted towards the advancing side.

Temperature start increasing as the welding tool approaches the considered transverse section and starts decreasing during the last part of the deformation, i.e. when the tool pin left the reference section and only the effect of the tool shoulder is present.

Then, for the P5 point, positioned in the upper half of the joint thickness, it can be stated that the tool shoulder (and not just the pin) has a significant influence on the evolution in time of the main field variables. Smaller time intervals are observed for points located closer to the bottom of the joints indicating that, in those areas, the main mechanical effect is due to the pin. Besides, also the final value of the accumulated strain is lower for points closer to the bottom of the joints, starting from about 3.5 (see Fig. 3.38).

As far as the contact pressure is considered, it is worth noticing that the separation line between the sheets (see again the red line in Fig. 3.39) changes both in shape and direction during the welding process. Consequently, the contact pressure must be calculated considering the change in the direction normal to this line for each of the considered points. It is worth noticing that the utilized software does not allow the extrapolation of the contact pressure between two “moving flows” of the same

deformable object. For this reason, the values of the mean stress were used to obtain the contact pressure value.

The final results of this procedure are shown in Fig. 3.41a in which the evolution of the normal pressure of P5 is considered for test 1000 rpm-400 mm/min. In Fig. 3.41b the flow stress characterizing P5 during the bonding process and deriving from the simultaneous effect of temperature, strain and strain rate, is shown.

Large values of pressure are observed during the deformation. At the same time, the flow stress is below 100 MPa. Starting from t = 18 s, the flow stress decreases with increasing temperature; then a maximum, corresponding to the strain rate peak, and a minimum, when temperature reaches the highest peak, are observed. Finally, it starts increasing again after strain rate drops to zero and temperature starts decreasing. In this way, the welding parameters W can assume values larger than 1.

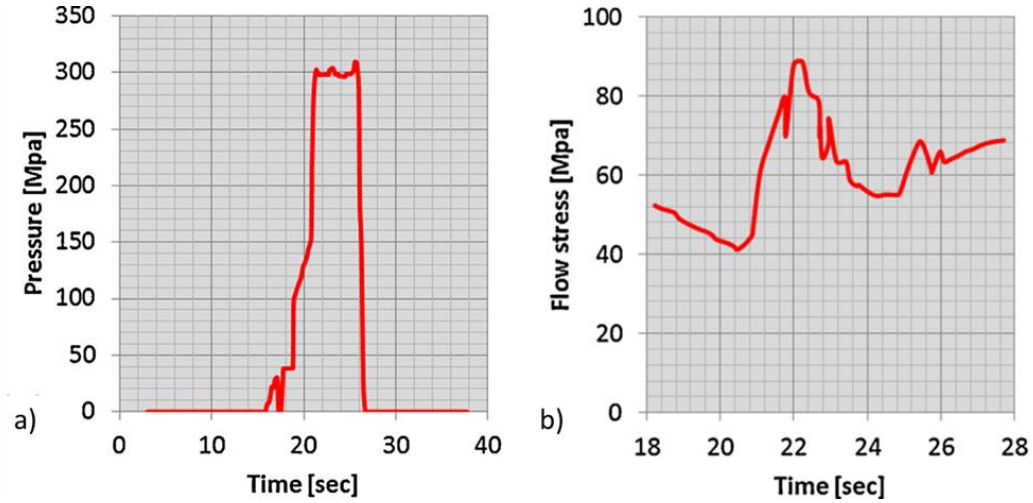

Figure 3.41 Evolution in time of (a) pressure and (b) flow stress for P5 – test 1000 rpm-400 mm/min.

3.5.1 Time–flow criterion to AA6082

In order to assess the applicability of the considered bonding criteria to FSW welding experiments were carried out as indicated in figure 3.10. The figure 3.21 shows the macrographs of the etched cross sections for all the analyzed case studies. In this paragraph, the W values calculated for the six observation points of each case study are reported as regard the welded joints obtained with the aluminum alloy 6082. For

the considered alloy, the critical value W_{LIM}=W_{LIM}(T) was taken from literature [162]. The utilized analytical expression is the following:

$$W^{LIM} = 332{,}621.59T^{-1.96} \; ; \qquad R^2 = 0.98$$

equation 3.3

Fig. 3.42, 3.43, 3.44, 3.45, 3.46 and 3.47 show the calculated W parameter and the threshold curve for the observation points investigated. To easily understand the application of the bonding criterion, each figure shows the results of experimental macro analysis of the welded test, the results of the numerical simulation with the final position of the six observation points, the uniaxial tensile tests result and the results of the W parameter in dependency of the temperature. The temperature corresponding to each point is the average value of the temperatures calculated during the time interval corresponding to non-zero pressure values. A few observations on the obtained values can be made. First, for all the tests, P1 is the point characterized by the lowest W value. This is consistent with what experimentally observed: at the bottom of the joints the least favorable conditions for solid bonding occurs, in terms of temperature, pressure and velocity. That is why if a flow defect is observed, it is located in that area.

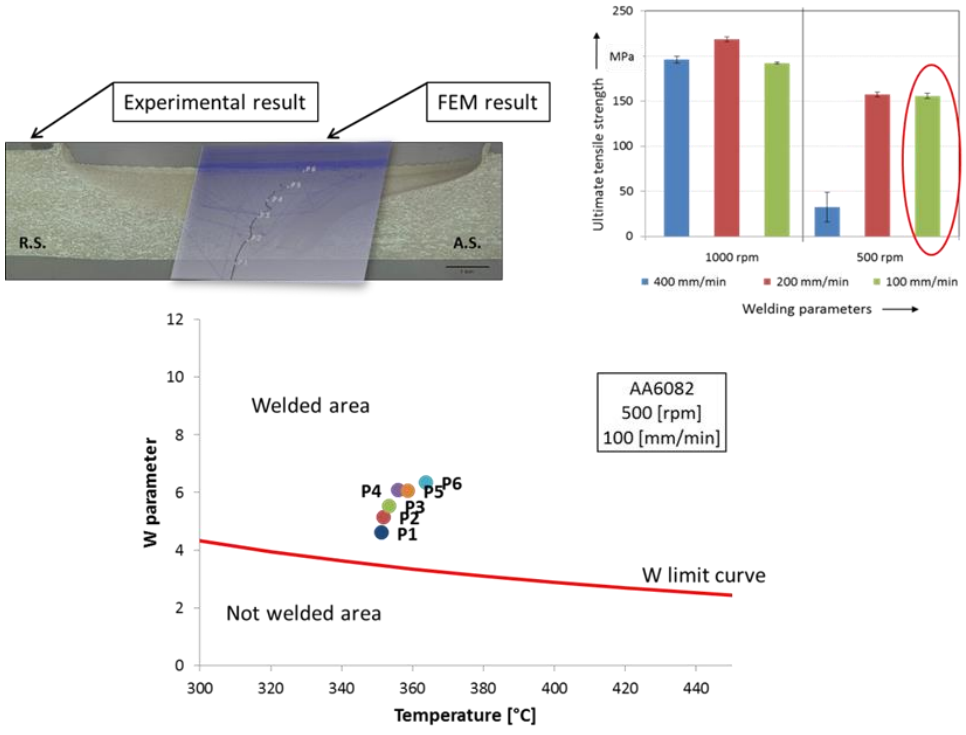

Figure 3.42 Calculated W parameter and threshold value limit curve for the test 500 rpm-100 mm/min.

For the aluminum alloy AA6082, with the process parameters of 500 rpm and 100 mm/min the joint shown in figure appears to be good. The "sound joint" condition is reached and the small void is not observed at the bottom of the pin for this test such as it has been observed in the same obtained welded joint using the AA6061. Regarding the tensile test result, a moderate decrease of the UTS from 1000 rpm to 500 rpm is reached. A satisfying prediction is obtained for this test, being all the observation points above the limiting curve.

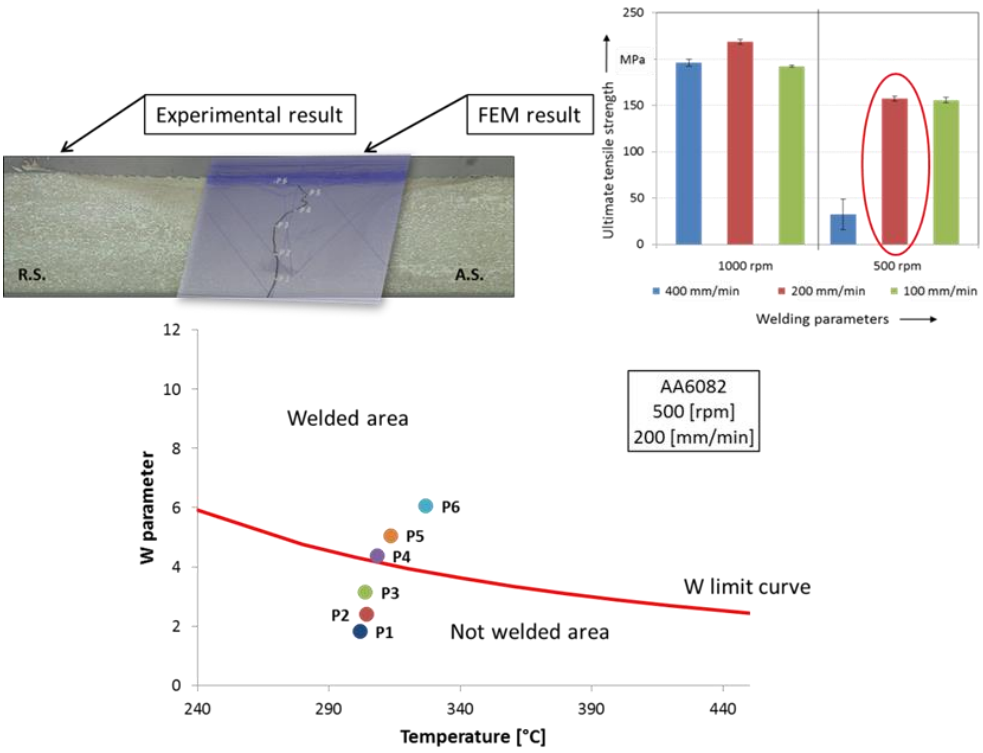

Figure 3.43 Calculated W parameter and threshold value limit curve for the test 500 rpm-200 mm/min.

Looking at insufficient heat test, for 500 rpm and 200 mm/min a tunnel defect is visible at the bottom of the pin. The tensile tests results are almost similar to those of the previous test. Anyway, the tunnels defect alters the quality of the welded joint. The tunnel defect of test corresponds to the points P1 and P2, which are below the curve. The remaining observation points are above the curve indicating a sound weld in those areas. The only exception is P3 for test, which is below the limit curve. In this case, this behavior it can be explained due to the relevant closeness of the P3 point to the material flow defect.

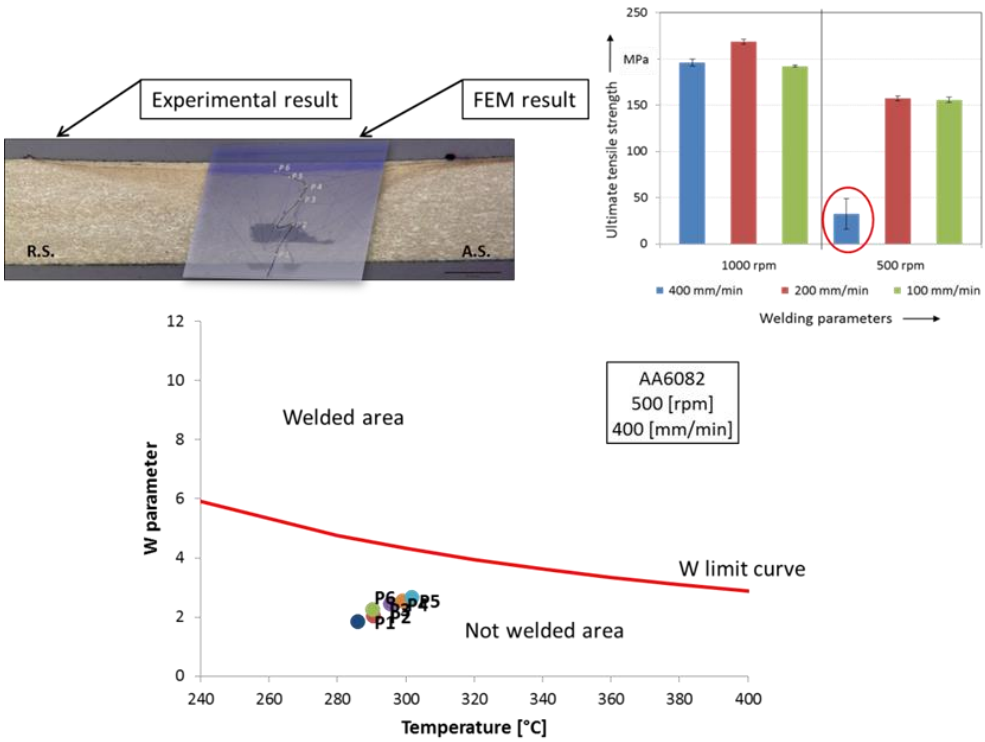

Figure 3.44 Calculated W parameter and threshold value limit curve for the test 500 rpm-400 mm/min.

Further increasing the feed rate tool up to 400 mm/min, the generated heat turns out to be insufficient for the weld. A not welded joint because of insufficient amount of heat during the process is shown in Figure 3.44. How it can be seen from the figure the welded specimen characterization of 500 rpm and 400 mm/min the welding was not occurred. All six observation points are below the W limit curve, which correctly describes the solid bonding phenomena that not occurred in this process parameters combination.

Finally, regarding the sound tests characterized by 1000 rpm of tool rotation speed are shown in the Fig 3.45, 3.46 and 3.47. The Piwnik and Plata criterion predict correctly the solid bonding phenomena that occurred in these tests. All the eighteen observation points are above the W limit curve.

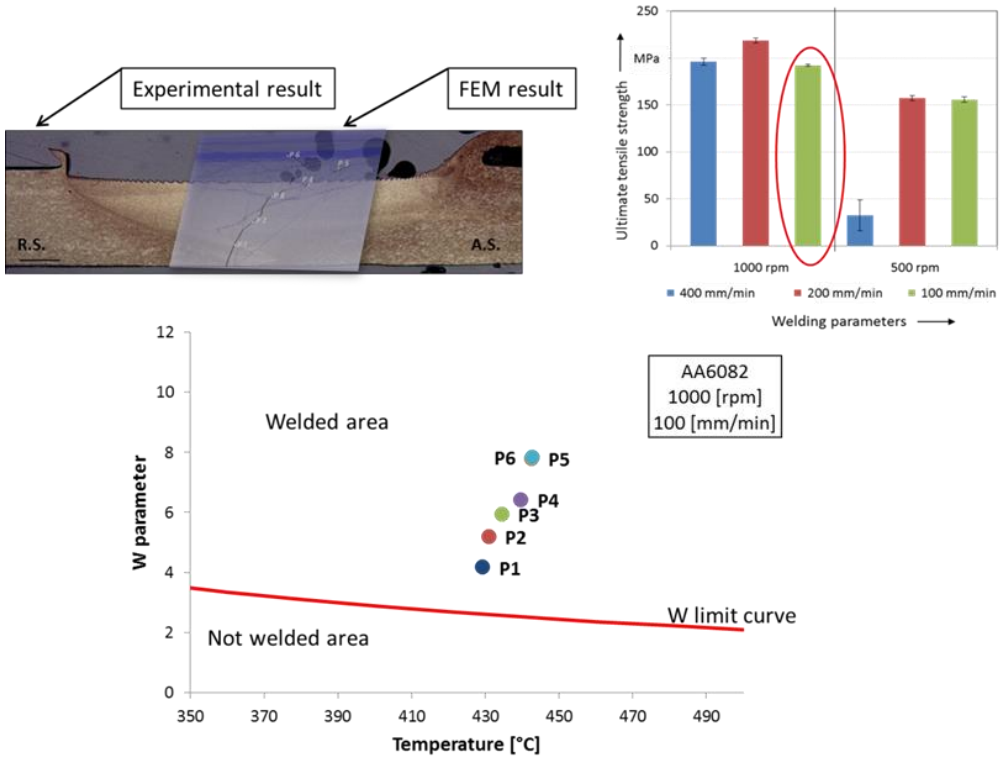

Figure 3.45 Calculated W parameter and threshold value limit curve for the test 1000 rpm-100 mm/min.

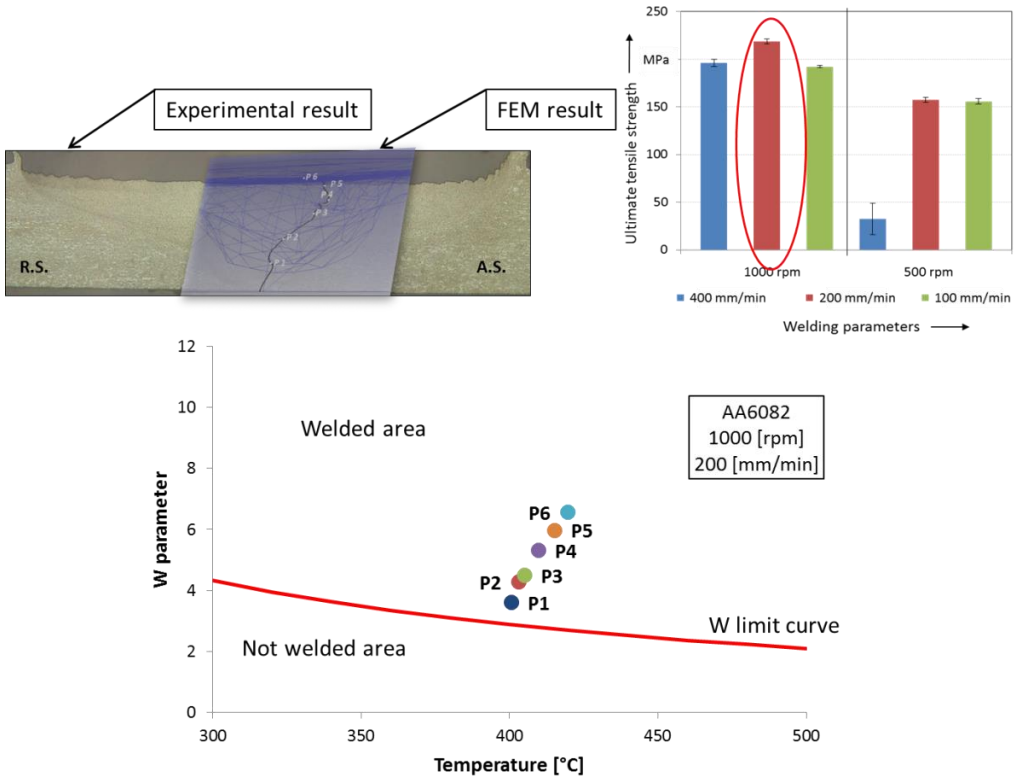

Figure 3.46 Calculated W parameter and threshold value limit curve for the test 1000 rpm-200 mm/min.

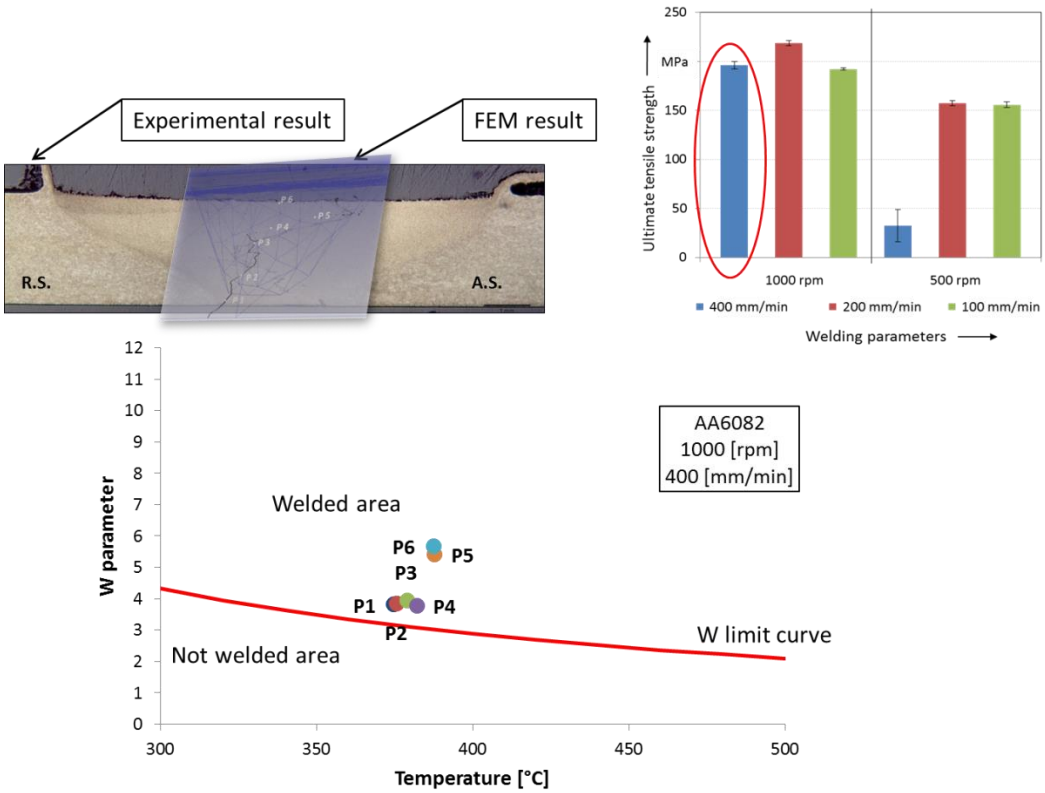

Figure 3.47 Calculated W parameter and threshold value limit curve for the test 1000 rpm-400 mm/min.

For this aluminum alloy, AA6082, the consistency of the results with respect both to the experimental evidences and to the expected effect of the process parameters, in terms of heat input conferred to the joints, permits to state that the W parameter is suited to predict the solid bonding phenomena occurring in FSW processes.

3.5.2 Time–flow criterion to AA6061

The bonding parameter W was calculated, for the six observation points highlighted in figure 3.35, using the numerical results shown in the previous paragraph. As far as the W parameter is regarded, i.e. the one based on the Pivnik and Plata criterion, a threshold value was taken from literature. In particular, as briefly discussed in the introduction paragraph, Ceretti et al. [161] use droll bonding tests on AA6061 to determine the critical value as a function of temperature. A regression was carried out obtaining the following analytical expression:

$$W_{lim} = 4.9063e^{-0.0017\,T} \qquad T > 320°C$$

equation 3.4

Fig. 3.48, 3.49, 3.50, 3.51, 3.52 and 3.53 show the calculated W parameter and the threshold curve for the observation points investigated using the same figure style used in the previous paragraph.

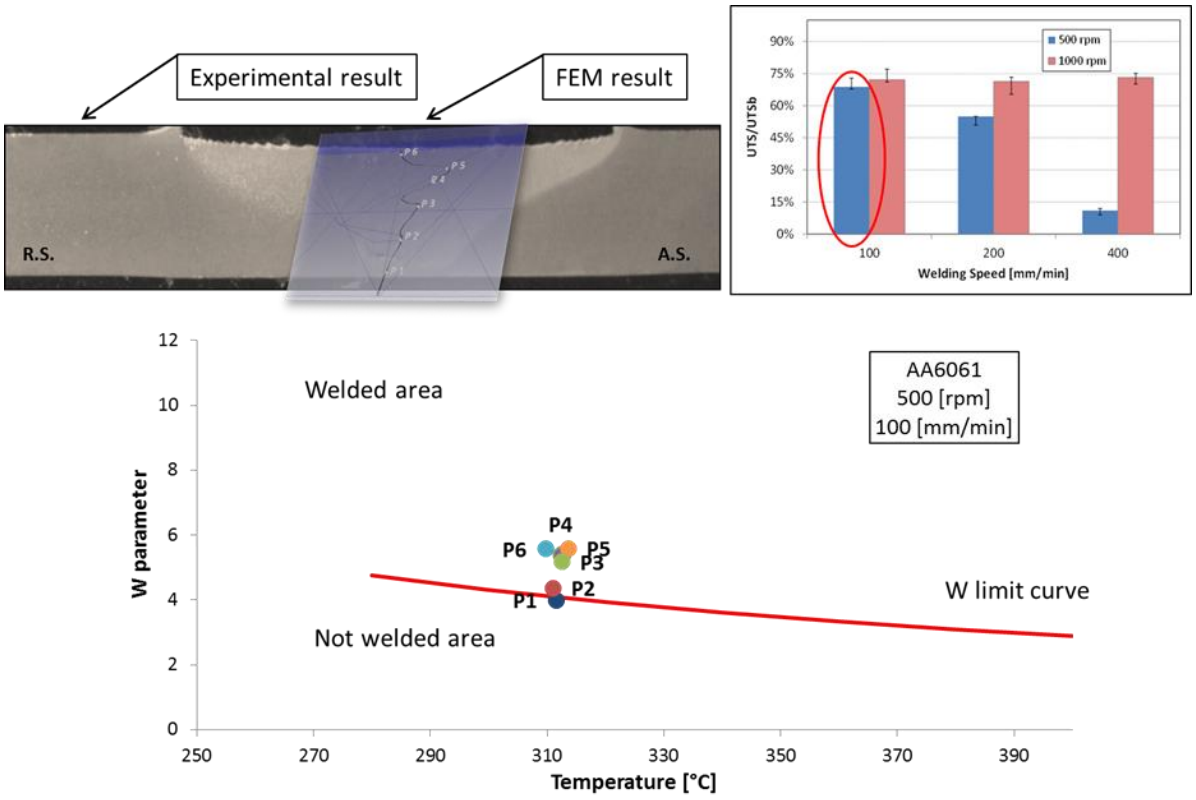

Figure 3.48 Calculated W parameter and threshold value limit curve for the test 500 rpm-100 mm/min.

As it have been say above regarding the experimental results of the FSW of AA6061, the three welds characterized by rotation equal to 500 rpm are characterized by flow defects. Looking at test above, a very small void can be observed in the bottom area of the cross section. The small void observed for test 500 rpm-100 mm/min is due to an insufficient heat conferred to the weld. As a consequence the material below the pin was too “cold” and was not properly mixed by the tool. Regarding the tensile test result, the resistance of test is only slightly lower than the one of the sound joints. A satisfying prediction is obtained for this test. The small void defect of test corresponds to the points P1, which are below the curve. The remaining observation points are above the curve indicating a sound weld in those areas.

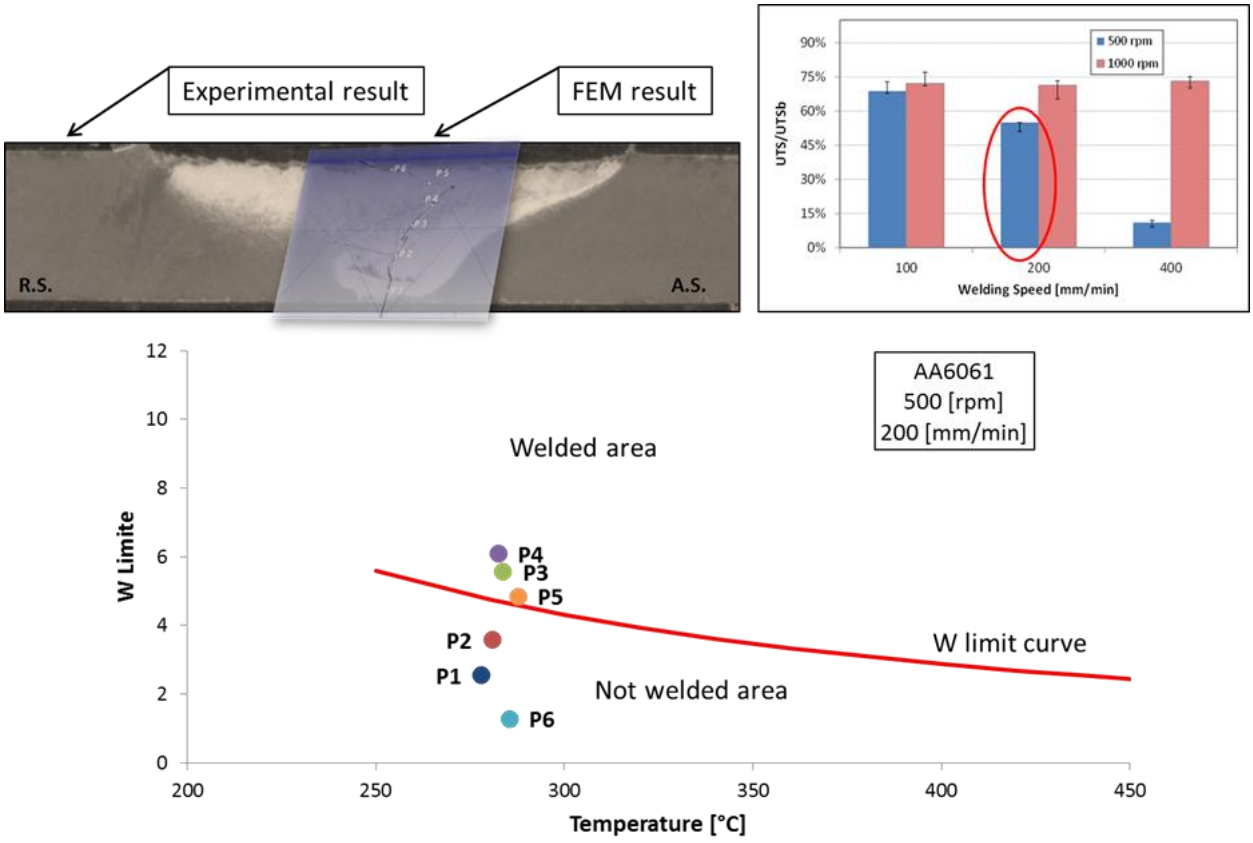

Figure 3.49 Calculated W parameter and threshold value limit curve for the test 500 rpm-200 mm/min.

Looking at test characterized by 500 rpm and 200 mm/min a tunnel defect is visible at the bottom of the pin. As the weld becomes colder, i.e. with increasing welding speed, the void becomes larger assuming the name of tunnel or “wormhole”. As the welding speed increases, the defect becomes larger and a dramatic drop of the UTS is observed. A satisfying prediction is obtained for test 500-200. The tunnel defect of test corresponds to the points P1 and P2, which are below the curve. The remaining observation points are above the curve indicating a sound weld in those areas. The only exception is P6 for test, which is well below the limit curve. For all the performed tests, maximum pressure in the direction orthogonal to the sheets separation line is observed at about mid thickness. Being P6 close to the top surface of the joint, small values of pressure are calculated inhibiting reaching the expected bonding parameter value.

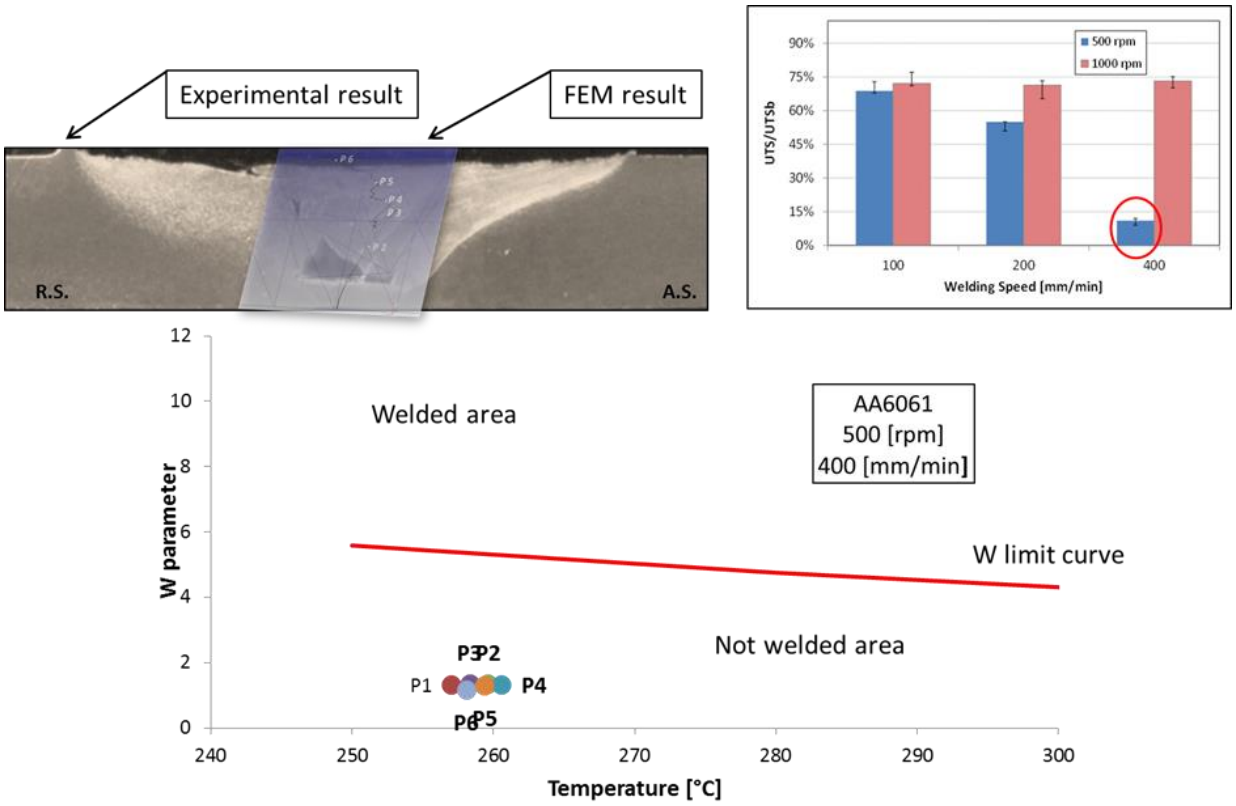

Figure 3.50 Calculated W parameter and threshold value limit curve for the test 500 rpm-400 mm/min.

The test characterized by 500 rpm and 400 mm/min has a very large void area at the bottom of the pin and a crack is visible starting from the bottom of the joint and reaching the top surface. As the welding speed increases, the defect becomes larger and a dramatic drop of the UTS till an almost zero value is observed for test. A satisfying prediction is obtained for this test. In particular, all the points of test are below the W limit curve, correctly indicating that solid bonding was not reached.

In turn, the three welds produced with rotation equal to 1000 rpm are defect free.

A sound weld, corresponding to tests characterized by 1000 rpm-100 mm/min (fig 3.51), 1000 rpm-200 mm/min (fig 3.52) and 1000 rpm-400 mm/min (fig 3.53) of operating parameters. This test has a similar resistance with the other sound tests, ranging between 72 % and 74 %. The network correctly predict test, being all the observation points above the limiting curve.

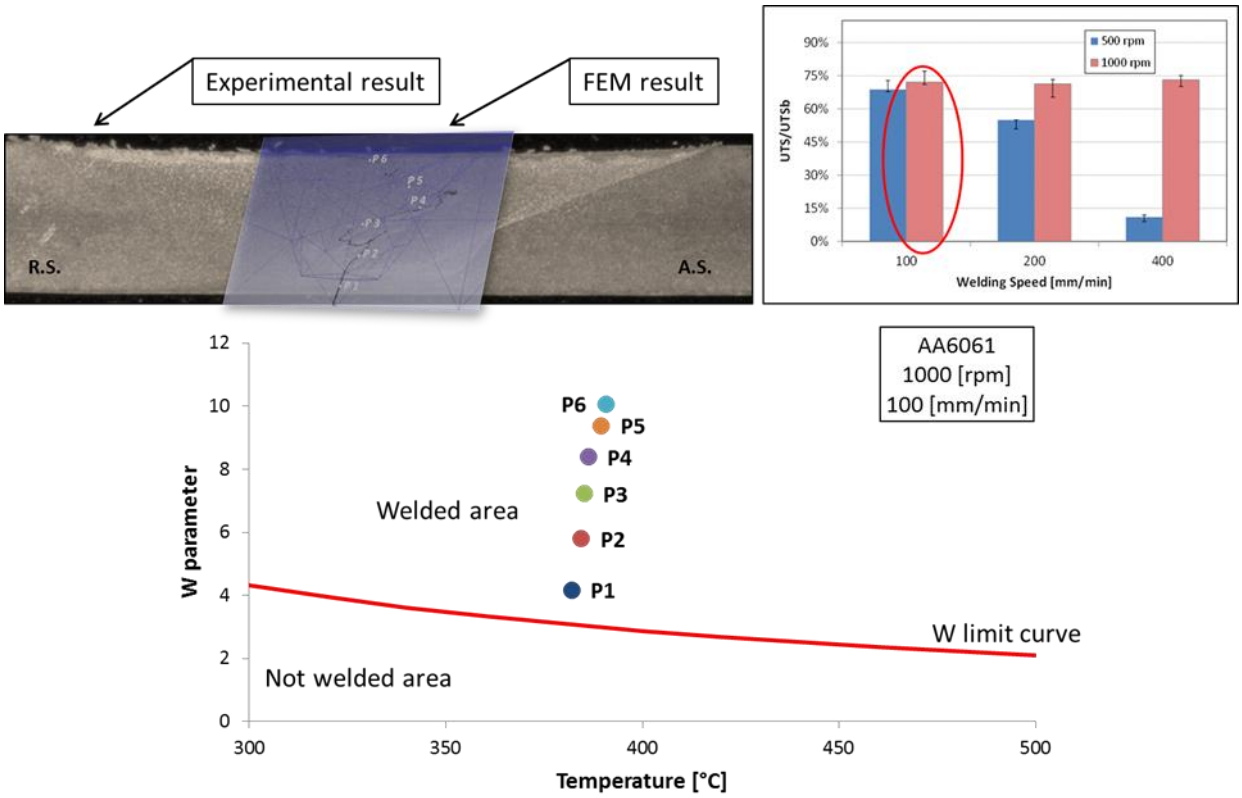

Figure 3.51 Calculated W parameter and threshold value limit curve for the test 1000 rpm-100 mm/min.

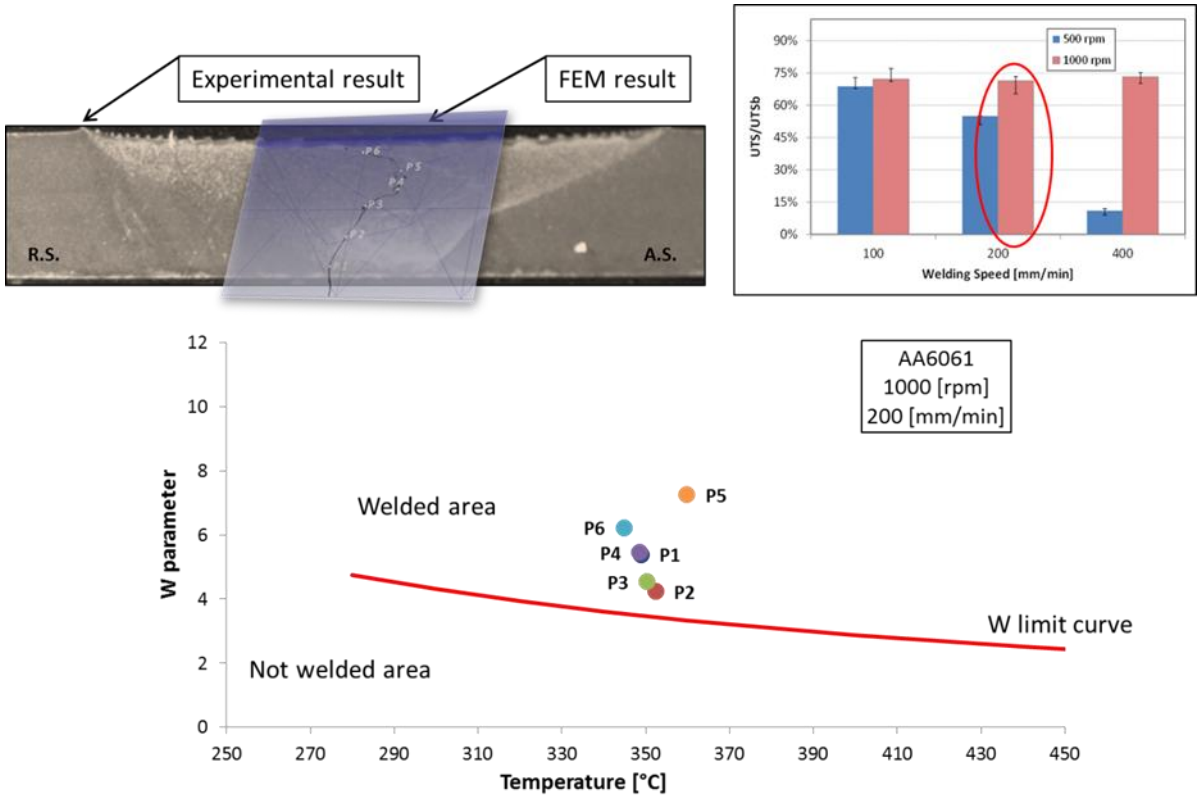

Figure 3.52 Calculated W parameter and threshold value limit curve for the test 1000 rpm-200 mm/min.

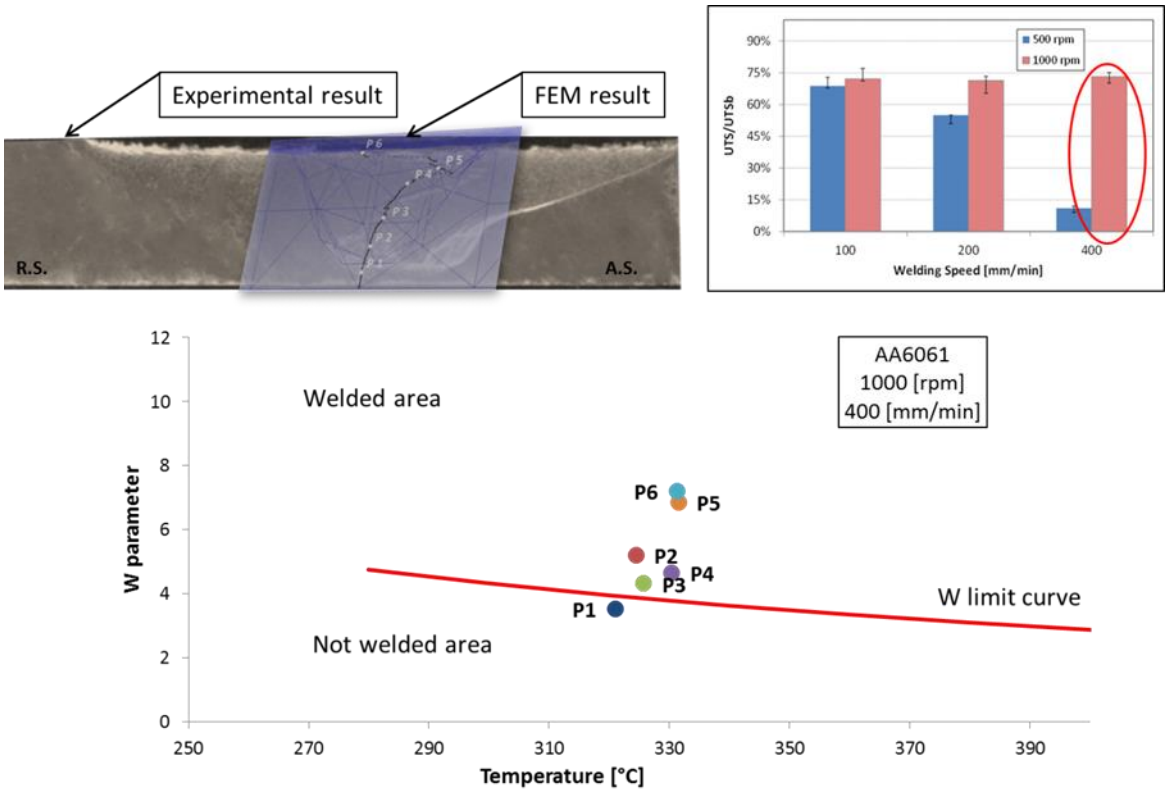

Figure 3.53 Calculated W parameter and threshold value limit curve for the test 1000 rpm-400 mm/min.

The consistency of the results with respect both to the experimental evidences and to the expected effect of the process parameters, in terms of heat input conferred to the joints, permits to state that the W parameter is suited to predict the solid bonding phenomena occurring in FSW processes.

3.6 Neural Networks

How it has already been said in the previous chapters of this thesis, the solid state bonding occurs in different manufacturing processes, as solid state welding processes, e.g. Friction Stir Welding (FSW), Linear Friction Welding (LFW), Rotary Friction Welding (RFW), extrusion of hollow profiles (PDE) and rolling of multiple sheets (ARB). For all the mentioned processes, the activation of this phenomenon results in peculiar advantages over more traditional processes. Solid bonding is triggered by proper values of specific field variables at the contact interface between

the parts joined that are usually characterized by better microstructural properties with respect to the base material.

In this paragraph, a neural network is set up, trained and used to predict the bonding occurrence starting from the results of specific numerical models developed for the ARB process, PDE process and FSW process. The Plata-Piwnik criterion was used in order to define a quantitative parameter taking into account the effectiveness of the bonding. This Neural Network developed is able to provide, for each point of the transverse sections of the joints, a qualitative output indicating occurrence of solid state welding as well as a quantitative output based on the Piwnik and Plata criterion indicating the level of “soundness” of the weld.

The results of the experimental and numerical campaign on FSW using the aluminum alloys 6061 that have been showed in the previous paragraph are used for develop the NN.

A rigid visco-plastic material model was utilized to simulate the ARB process and PDE process. In particular a strain, strain rate and temperature dependent flow stress was utilized.

For the thermal characteristics of the considered AA6061-T6 aluminum alloy, the following values were utilized: thermal conductivity k=180 [N/(s°C)] and thermal capacity c=2.4 [N/(mm2°C)] taken from literature; no variation of k and c with temperature was taken into account. This assumption makes the thermal problem linear speeding up the numerical solution at each time increment. When applicable, a constant interface heat exchange coefficient of 11 [N/(mm-s-°C)] was utilized for the contact between the deformable parts and the rigid dies. Additionally, thermal exchange with environment was considered, with coefficient equal to 0.02 [N/(mm-s-°C)].

3.6.1 Numerical campaign on Accumulative Roll Bonding (ARB)

As far as the Roll Bonding process is regarded, experimental data were taken from the paper by *D’Urso et al.* [162]. In the paper, two sheets were rolled together to a final welded sheet thickness of 10 mm. The tests were carried out at the varying of the initial sheets thickness, in order to obtain different rolling ratio values - ranging

from 50 % to 83.3 % - and of sheets temperature - ranging from 300 °C to 530 °C. A chart was built indicating effective bonding and failed tests as a function of temperature and the Piwnik and Plata parameter W.

The numerical model for the Roll Bonding process was developed, using Deform 2DTM , starting from the experimental campaign developed by *D'Urso et al*.[162]. A plane strain approach was selected and, similarly to what done for the previous model, the two sheets were modeled as a "single block". Two refinement mesh windows were used close to the rolls in order to get an average element size of 0.2 mm in that area. A constant time increment of 0.001 s was used. A shear friction model was adopted with value equal to 0.8. The heat exchange coefficient with environment was set equal to zero because of the isothermal conditions of the experimental tests. An initial temperature correspondent to the considered case study condition was given to the sheet.

The temperature at which bonding is obtained is indicated for each rolling ratio value. We developed numerical simulation for three temperature values lower than the threshold value and three values larger. When three values were not available, all the available values were simulated. Table 3.5 shows the 34 case studies taken into account.

Initial thickness [mm]	***Threshold temperature [°C]***	***Temperature of considered case studies [°C]***
12	520	530, 510, 490, 470.
13	490	530, 510, 490, 470, 450, 430.
14	420	470, 450, 430, 410, 390, 360.
15	380	430, 410, 390, 360, 330, 300.
16	340	410, 390, 360, 330, 300.
18	320	390, 360, 330, 300.
20	300	360, 330, 300.

Table 3.5 Roll Bonding parameters used for the numerical campaign

Finally, due to the stationary conditions of the rolling process, just one point for each case study was taken into account for the analysis of the field variables histories leading to the bonding. The point P1 was placed along the horizontal symmetry line, i.e. on the separation surface between the two sheets, as illustrated in Figure 3.54 together with the process model. The position of the point is indicated at the initial time increment considered (t0) and after the bonding process took place (t1).

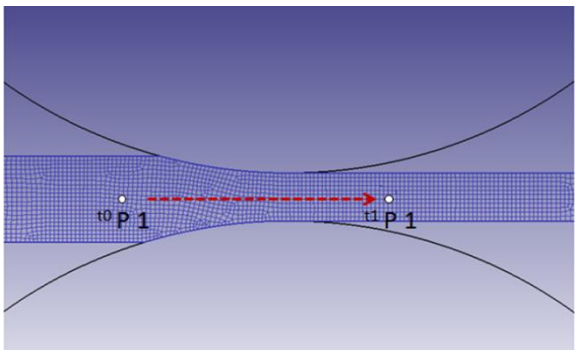

Figure 3.54 Observation point on the sheets separation line for the roll bonding process

As far as the roll bonding process is regarded, a similar approach used for the FSW process was followed. Due to the steady state nature of the process and to the relatively simple material flow, just one tracking point for each process condition was utilized. In particular, the selected point P1 lies on the initial separation line between the sheets (Figure 3.54, initial time t0) and, during the process, moves horizontally as indicated by the red dotted line in Figure 3.54. The final position (t1) corresponds to the time increment at which the bonding process is completed. For the roll bonding process the pressure that generates the welding can be easily calculated considering the stress in the vertical direction. The histories of strain, strain rate and pressure are reported in Figure 3.55 for the case study obtained with initial thickness of 16 mm and temperature of 390 °C.

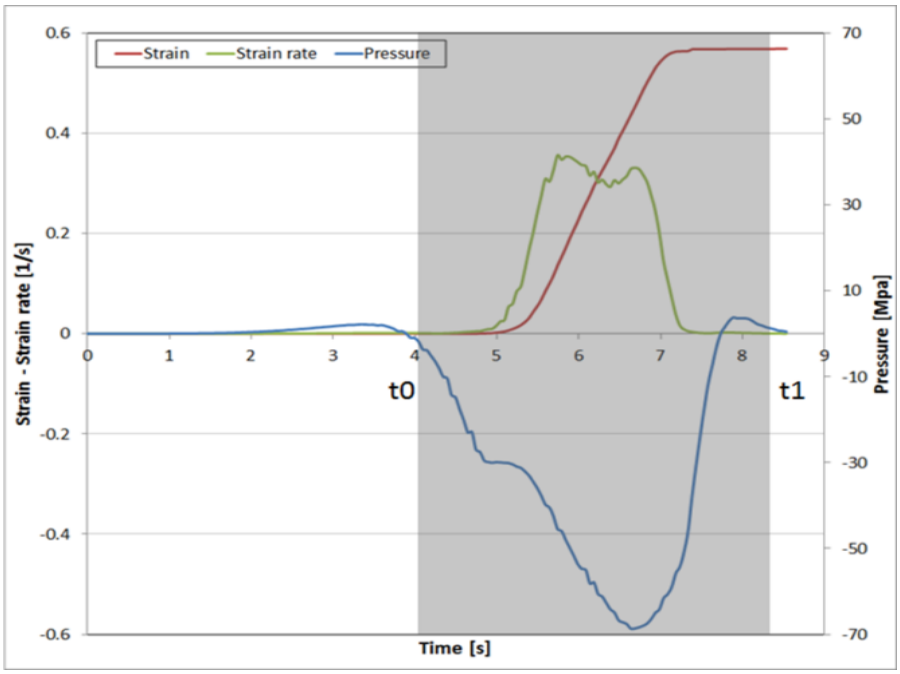

Figure 3.55 Field variables histories for the ARB process, case study characterized by initial thickness of 16 mm and temperature of 390 °C

The shaded area between t0 and t1 is the one considered for the data extraction. These process conditions results in sound bonding. Temperature is not shown as the experiments were conducted under isothermal conditions. Although smaller strain values are observed, the similar trends of the observed field variables with respect to FSW clearly show that the two techniques, characterized by totally different process mechanics, induce the same solicitations in the material in order to obtain the solid bonding.

3.6.2 Numerical campaign on Porthole Die Extrusion (PDE)

The experimental data for the PDE process were taken for the paper by *Ceretti et al.* [22]. In particular PDE tests were conducted at the varying of the Welding Chamber Height (WCH) and the Rib Thickness (RT) on AA6061 aluminum alloy. Other technological and geometrical parameters were kept constant as it will be better detailed in the following paragraph. The weld limit was experimentally obtained and numerical simulations were run at the varying of the above cited geometrical parameters in order to highlight the process conditions resulting in effective bonding or in defective parts. The numerical model for PDE was developed starting from the results found in the paper [22] by Ceretti et al. as indicated in Table 3.6.

Parameter	*Value*
Welding chamber width [mm]	140
Hole Width [mm]	30
Welding chamber height [mm]	30, 50
Rib Thickness [mm]	30, 60
Billet temperature [°C]	480
Dies Temperature [°C]	450
Punch Speed [mm/s]	8

Table 3.6 PDE parameters used for the numerical campaign

As far as the modeling of the process is regarded, Deform 2DTM was again used taking advantage of the existing symmetry. A refining mesh window was placed close to the rib with minimum element size of about 0.2 mm. A constant time increment of 0.001 s was used. The same material model used for ARB was selected. A shear friction model was selected with friction factor equal to 0.4. Five tracking points have been considered for the monitoring of the field variables evolution.

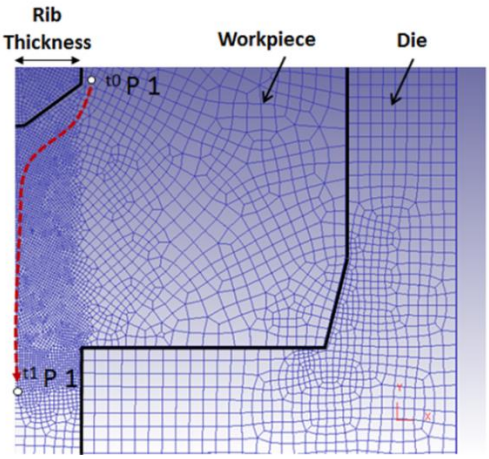

Figure 3.56 Sketch of the observation point flow for the PDE process

Figure 3.56 shows the sketch of the movement of one of the observation points as well as the mesh of the utilized model. The points were placed on the vertical symmetry plane of the model, i.e. where the solid binding occurs, under the rib. The points were “back tracked” when the process already reached the steady state, and continued till pressure dropped to zero.

Finally, a slightly different approach was followed for the PDE process. The five considered tracking points were placed along the bonding line, i.e. that vertical symmetry axis of the process, and “tracked back” to their starting position. This approach was followed in order to be sure that the observed points are involved in the bonding phenomenon at the contact interface between the two adjoining metal flows. In Figure 3.57 the field variables histories are reported for the case study characterized by WCH = 50 mm and RT = 60 mm.

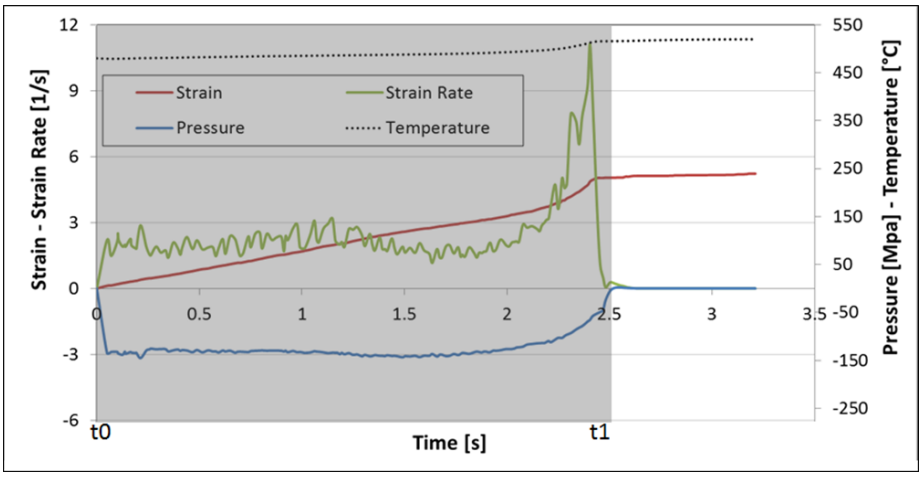

Figure 3.57 Field variables histories for the PDE process, case study characterized by WCH = 50 mm and RT = 60 mm.

Looking at the evolution of the monitored field variables again a similar trend is found with respect to the two previous processes, indicating that different process mechanics can result in similar thermo-mechanical histories for the material.

3.6.3 Neural network implementation

Artificial neural network (ANN) can perform highly complex mappings of nonlinearly related data by inferring subtle relationships between input and output parameters without prior definitions. It is able to generalize from a limited quantity of training data to predict overall trends and functional relationships.

A significant advantage of the ANN approach is that there is no need to have a well-defined process for algorithmically converting an input to an output. Rather, it needs only a collection of representative examples of the desired mapping. The ANN then adapts itself to reproduce the desired output when presented with training sample input. Based on these observations, the development of a neural network has been evaluated as the most effective for the prediction of the bonding phenomenon in three completely different processes. The neural network was designed with the aim to get two separated outputs: a qualitative output, indicating if the bonding process for the considered observation point occurred; a quantitative output, indicating the level of “soundness” of the bonding. In order to build the latter indicator, a parameter Q was defined starting from the Piwnik and Plata parameter W [25] for each observed point i:

$$Q_i = \frac{W_i}{W_i^{LIM}}$$

equation 3.5

where

$$W = \int_0^t \frac{p}{\sigma} dt \cong \sum_j \frac{p_j}{\sigma j} \Delta t_j$$

equation 3.6

W_{LIM} is the critical value of W that must be reached in order to obtain the solid bonding (eq. 3.4). It is worthy notice that a summation was used instead of the integral due to the discrete time increments j used for the simulations.

The training data set was build calculating an average value of the considered field variable for a specific tracking point and a given process, according to the following:

$$T_i = \frac{\int_{t0}^{t1} T dt}{t1 - t0} \cong \sum_j \frac{T_j \Delta t_j}{t1 - t0}$$

equation 3.7

$$p_i = \frac{\int_{t0}^{t1} p dt}{t1 - t0} \cong \sum_j \frac{p_j \Delta t_j}{t1 - t0}$$

equation 3.8

$$\varepsilon_i = \frac{\int_{t0}^{t1} \varepsilon dt}{t1 - t0} \cong \sum_j \frac{\varepsilon_j \Delta t_j}{t1 - t0}$$

equation 3.9

$$\dot{\varepsilon}_i = \frac{\int_{t0}^{t1} \dot{\varepsilon} dt}{t1 - t0} \cong \sum_j \frac{\dot{\varepsilon}_j \Delta t_j}{t1 - t0}$$

equation 3.10

In this was 36 data are derived from FSW (6 points, 6 process conditions), 34 from ARB (one point, 34 process conditions) and 20 from PDE (5 points, 4 process conditions).

A supervised multilayer feed-forward networks based on a back-propagation algorithm have been built. The network architecture consists of 5 hidden layers: the input layer is characterized by 4 neurons corresponding to the average values of temperature, strain, strain rate and pressure as calculated in eq. (3.7), (3.8), (3.9) and (3.10). Then 3 hidden layers are placed, with 5, 4 and 3 neurons, respectively. Finally an output layer, with 2 neurons corresponding to the qualitative “welded-not welded” output and the quantitative Q parameter is found. All the data were normalized to assume values between -1 and 1. Each layer is fully connected to the next and, according to the back-propagation rule, the weights of the connections linking a neuron belonging to a certain layer to a neuron belonging to the next are adjusted in the learning stage with the aim to minimize the error between the desired

output and the calculated one. In Figure 3.60 the architecture of the utilized neural network is shown.

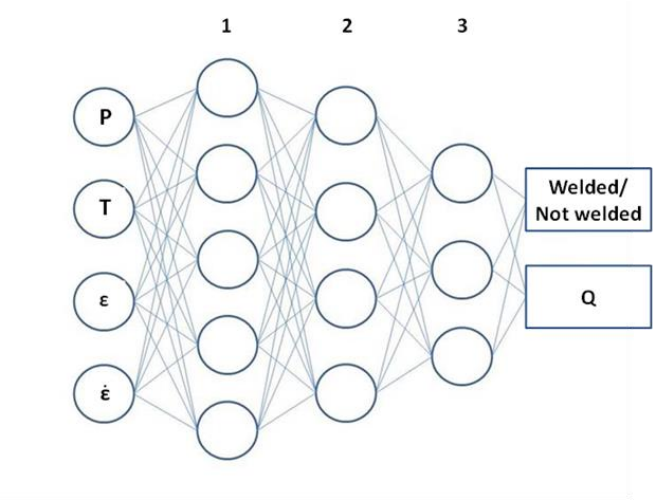

Figure 3.58 Architecture of the Utilized Neural Network

It has to be underlined that the topology of the utilized network has been defined on the basis of an optimization procedure aimed to improve the network performances: in particular the number of the hidden layers and the number of neurons have been determined, during the training stage, on the basis of the best performance following an analytical hierarchical procedure (AHP) [188]. As a matter of fact, if the architecture is too small, the network may not have sufficient degrees of freedom to learn the process correctly. On the other hand, if the network is too large, it may over fit the data.

As far as the training is regarded, it was developed providing to the network the input data coming from the simulations, as previously described; target data came from the experimental observations (welded/not-welded qualitative output) and combined experimental and numerical results (Q parameter). About 13 % of the available input and target data were used for the test of the network. In particular, 4 observation points for each process were selected, including both sound and not effective bonding.

Table 3.7 shows the 12 data used for the test of the network. For each observation point, the correspondent process parameters are given together with the target output. As far as FSW is regarded, points P1 and P2, namely the closest points to the bottom of the joint, have been chosen for different process conditions. As a

matter of fact when insufficient heat is given to a joint, the so called tunnel defect is found at the advancing side close to the bottom tip of the tool pin.

Id	*Point*	*Process*	*Process Parameters*	*Welded*	*Q*
1	P 1	PDE	WCH=30mm RT=30mm	N	0.27
2	P 2	PDE	WCH=30mm RT=60mm	N	0.30
3	P 2	PDE	WCH=50mm RT=60mm	Y	2.73
4	P 4	PDE	WCH=50mm RT=60mm	Y	2.68
5	P 1	RB	S_i =13mm T=450°C	N	1.04
6	P 1	RB	S_i =14mm T=390°C	N	1.04
7	P 1	RB	S_i = 15mm T=300°C	N	0.87
8	P 1	RB	S_i = 20mm T=330°C	Y	1.62
9	P 1	FSW	R=500rpm v=200mm/min	N	0.77
10	P 1	FSW	R=500rpm v=400mm/min	N	0.29
11	P 2	FSW	R=1000rpm v=100mm/min	Y	3.95
12	P 1	FSW	R=1000rpm v=200mm/min	Y	1.36

Table 3.7 Observation points selected for the test of the developed Neural Network

The two outputs of the developed Neural Network are compared with the expected output in figure 3.59 a and b.

As it can be observed, a perfect prediction of the occurrence of the bonding is found for all the case studies (Fig. 3.59a). Looking at the Q parameters, the network shows a satisfactory prediction capability (Fig. 3.59b). The maximum difference between the calculated target and the one predicted by the NN is found for ID 5 and 6. It is noted that these points are experimentally not bonded, as correctly predicted by the qualitative network output. The calculated Q parameter, although very close to a value of 1, corresponding to the limit condition, is slightly above this threshold. On the contrary, the network prediction is, for both points, equal to 0.93, indicating that a sound solid bonding did not occur. This is the reason why, especially for “edge” process conditions”, the presence of two separate outputs guarantees a better understanding and prediction of the occurring phenomenon.

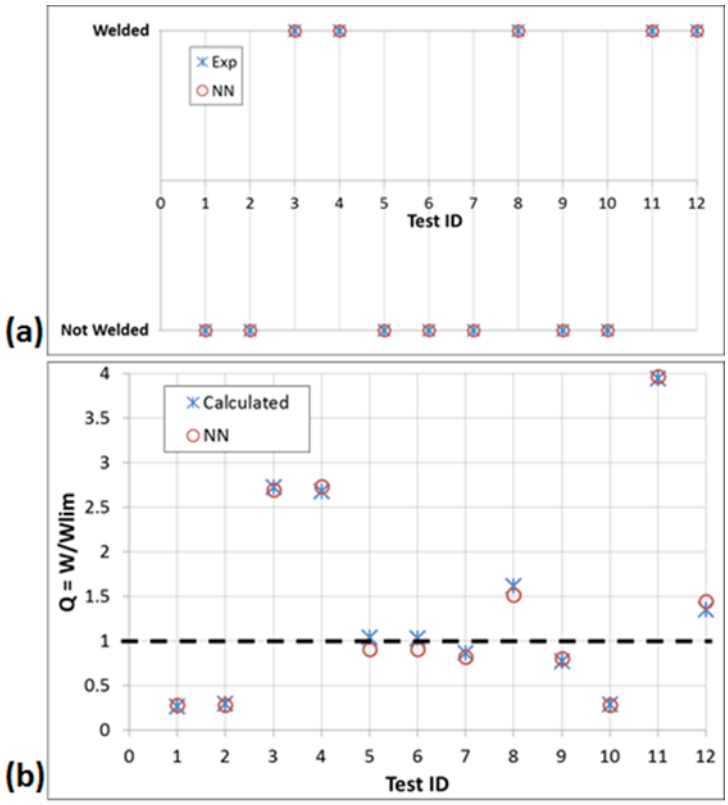

Figure 3.59 Comparison between expected output and Neural Network response: (a) Q parameter and (b) sound solid bonding occurrence

Finally, focusing on the FSW process, namely ID 9, 10, 11 and 12, the two not bonded zones found for ID 9 and 10 are correctly predicted by the network. From the figure 3.16 it is seen that a tunnel defect is present in the weld characterized by 500 rpm-200 mm/s, while a significantly larger tunnel is found in the weld characterized by 500 rpm-400 mm/s. Being the selected observation points P1 for both the case studies (see again Table 3.7), the incorrect bonding is quantitatively predicted for both. Additionally, the Q parameter is smaller for the ID 10, being about 25 %.

4 Linear friction welding experiments

4.1 Introduction

4.1.1.1 Application of the solid bonding criteria examined to the LFW process

For linear friction welding process, in first, the case studies have been identified and the set of technological and geometrical parameters in order to obtain different quality of the welded joint have been selected. Also regarding the LFW process, the state of the art has been useful for the identification of the welded joints.

Romero [134] from the University of Manchester performed a research based on the material from Vairis. The microstructures of the joints and residual stresses that occur during the process of LFW have been investigated. The research described has been useful to study the influence of pressure on the process.

The mechanical analysis and the microstructure analysis of the welded seams obtained by LFW process have been developed (chapter 4.3).

A similar study was conducted by *Chamanfar* [135]. The research has been based on the study of the mechanical properties and microstructure of welded joints with LFW process. This type of study was carried out under different process conditions. To study the process, the temperatures reached during the various tests have been detected. This work was carried out using special metal, like the Waspaloy. In this study, through different process conditions, the microstructural changes level has been showed.

At the same time the FEM numerical simulations of case studies identified by the software DEFORM 3D were performed (chapter 4.4). The solid bonding criterion examined was implemented in order to study the bonding phenomena that occur in LFW process. To implement the FEM numerical simulations, has been useful to study the numerical models present in the literature.

Sorina-Müller [148] has simulated the entire linear friction welding process using the titanium alloy Ti6Al2Sn4Cr6Mo in two conditions (β; α + β). The finite element method has been used to implement the simulation. In particular, a thermo-mechanical transient 3D analysis was conducted. Two different geometries of the

contact area (prismatic and knife as) have been simulated. The results are analyzed and compared with experimental data including profiles microstructure, hardness and axial shortening.

4.2 Experimental set up

As far as linear friction welding, the experimental campaigns were carried out in order to apply the solid bonding criteria proposed. In particular, experimental activities permitted to draw process windows for aluminum alloys, AA6082.

A dedicated experimental campaign was carried out measuring the temperature trend and energy input during the process. The mechanical characteristics were analyzed in order to identify the proper process parameters ranges for effective solid bonding.

4.2.1 Used materials

LFW joints were obtained out of AA6082-T6 aluminum alloy specimens. The base material was characterized, at room temperature, by a yield stress of 276 MPa and an ultimate tensile stress (UTS) of 323 MPa. Although weldable by traditional fusion welding techniques, this material shows very poor resistance in the welded area. Structural applications require more performing joints and solid state processes can represent an effective solution.

In particular, the composition of the utilized alloy is reported in Table 4.1

Alloy	Si	Fe	Cu	Mn	Mg	Cr	Zn	Ti	Al
AA6082	0.7-1.3	0.5	0.1	0.4-1	0.6-1.2	0.25	0.2	0.1	remainder

Table 4.1 Composition alloys

The mechanical properties of the material is shown in Table 4.2

Properties	AA6082
Density [g/m^3]	2.70
Melting temperature [°C]	555
Thermal expansion coeff. [K^{-1}]	24*10^{-6}
Young modulus [GPa]	70
Thermal conductivity [W/m*K]	180
Electrical resistance [Ω*m]	0.038*10^{-6}
Yield stress [MPa]	276
Tensile strength [MPa]	323
Elongation [%]	11
Shear strength [MPa]	210
Vickers hardness [HV]	114

Table 4.2 Mechanical properties

4.2.2 Specimens geometry

The used specimens were CNC machined from bars having 20 mm x 20 mm cross section. The specimen geometry can be divided into two parts: a base, intended to be fixed by screws to machine supports (specimen motion is reciprocating and vertical translational for the bottom and top specimen, respectively); the actual element to be welded, whose dimensions are reported in the following:

Bottom: height 10 mm, length 10 mm and width 7 mm. Top: height 10 mm, length 10 mm and width 7 mm

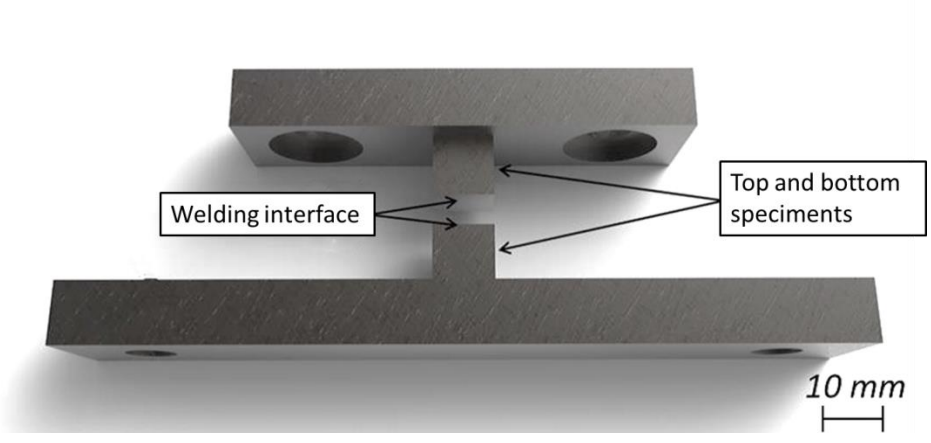

Figure 4.1 LFW specimens

Structural applications require more performing joints and solid state processes can represent an effective solution. In order to develop the experimental campaign, a previously in-house designed and built LFW machine was equipped with measuring sensors [189].

4.2.3 Process parameters

The determination of a process window highlighting the combination of process parameters needed in order to obtain different quality of welded joints was the first aim of this research. Variable oscillation frequency and applied pressure were used during the tests, while constant oscillation amplitude, specimen geometry and process time were selected. Oscillation frequency [f], pressure at the specimen interface [p] and process time [t] were varied according to Table 4.3

Parameter	***Value***
Frequency f [Hz]	36, 45, 58
Pressure p [MPa]	20, 30, 40, 50, 60
Amplitude A [mm]	2
Time t [sec]	1.25

Table 4.3 Process parameters

For each test the starting condition corresponded to a distance of the two contact surfaces equal to 0.5 mm. Once the oscillation reached the steady state the oleo-dynamic actuator valve was opened via software and pressure was applied. The contact between the two specimens was considered as starting time for the temporized pneumatic clutch. In this way the burn-off time was utilized for tests control and stop. During the deceleration phase an additional pressure, equal to 20 % of the test pressure, was given to the joint for 5 s. Each test was repeated three times and good repeatability was found in terms of sound/ poor weld obtainment.

In this way a process window was built with varying oscillation frequency and interface pressure. In the obtained graph a different marker was utilized to indicate sound joints, cold joints (low heat input) and instability conditions (excess of heat input).

The joints were cross-sectioned and macrographs were used to analyze the material zones modified by the process. The presence of flow defects were investigated

through micrographs. In order to obtain such results the specimens were hot mounted, polished and finally etched with keller reagent (1 cm^3 HF, 1.5 cm^3 HCl, 2.5 cm^3 HNO3 and 95 cm^3 H2O) and observed by a LM.

4.2.4 Joints analysis

For all the considered case studies, the produced welds were properly prepared for micro and macro observations. In particular, the preparation cycle was performed through a specimens cutting, resin embedding, polishing and chemical etching. So the specimens were first cut. The obtained samples were embedded into a thermosetting resin. This operation makes it manageable during polishing and during observation by optical microscope. For a good result of the sample it is necessary to clean the surfaces in the proximity of the cut in order to remove waste materials such as shavings and burrs. In order to facilitate the adhesion between resin and sample, degreasing of the outer surface with solvents, e.g. acetone or nitro solvent, is recommended. A machine for hot embedding, REMET IPA 30 (see Figure 3.8a) and an epoxy resin were used. In particular, maximum temperature of 175°C and a pressure of 4.5 bar were selected. TAKEN MECAPOLp260 (see Figure 3.8b) was used for fine grinding and polishing. The specimens are grinding and then polishing used an alumina solution. After the polishing step, the samples have a perfectly lapped surface, and therefore it cannot be examined by optical microscopy because light would be reflected. In order to perform the analysis it is necessary to proceed with a chemical etching selectively eroding the most reactive phases and highlighting the structure of the material. In the case of aluminum alloys, the keller solution was used as reagent. The specimen was immersed into this acid for an assigned time. The immersion time for AA6082 was 90 s.

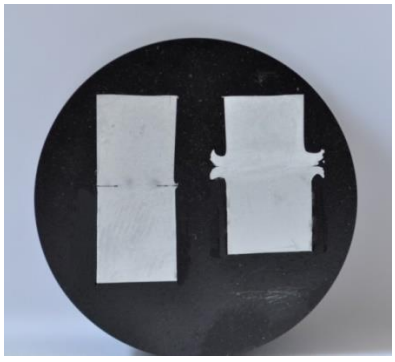

Figure 4.2 Example of weld samples embedded, polished and subjected to acid

4.3 Similar joint: AA6082

4.3.1 Process windows

Three different conditions were observed as a result of the experimental welding campaign. In particular, when the combination of the process parameters resulted in too low heat input, a “cold” weld was obtained. In this condition, either no bonding or only partial bonding in the central area of the cross section of the specimen was observed. Sound joints were obtained with increasing heat input, i.e. increasing oscillation frequency and/or pressure. Finally, when an excess of heat was conferred to the joint an “instability” condition was observed. In this case the significant material softening results in excess of burn off till specimen collapsing under the applied pressure during the last phase of the process.

Figure reports the experiments carried out with varying pressure and frequency as well as the obtained output

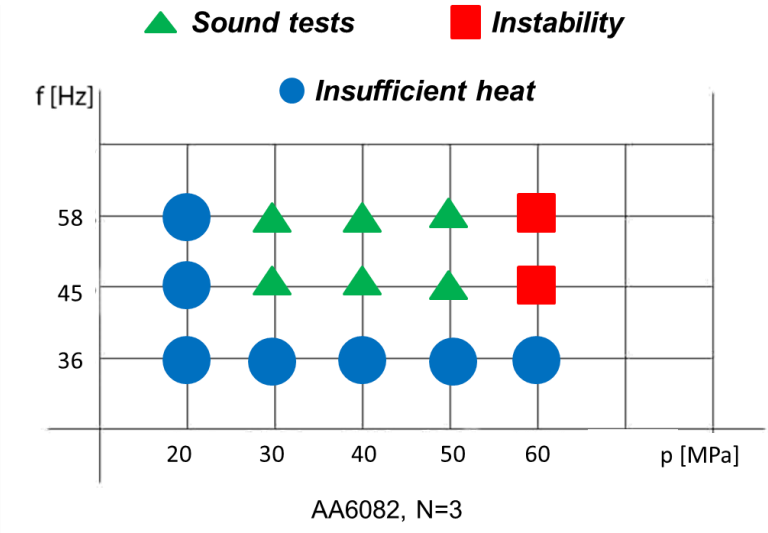

Figure 4.3 Process windows for AA6082

4.3.2 Temperature trends analysis

Temperature in the top specimen was monitored during the process using a thermocouple inserted into a blind hole at a distance of 6 mm from the interface.

Thermocouples are temperature sensors formed by connecting two different thermal conductive materials. The thermal contact has been obtained by welding (electric discharge) the two materials. A K-type thermocouple (Chromel (Ni-Cr) (+) / Alumel (Ni-Al) (-)) was used. These thermocouples allow a wide measuring range varying from -200 °C to 1260 °C.

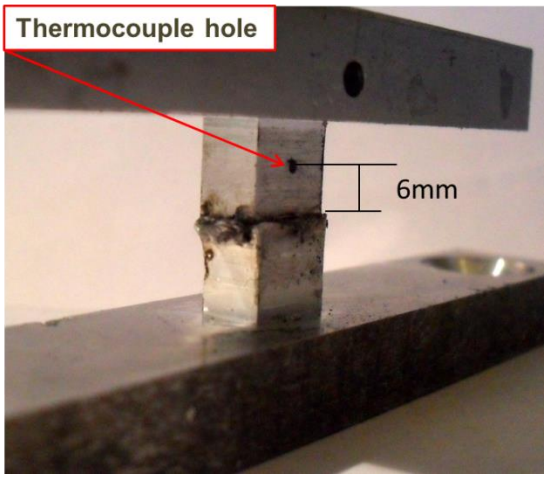

Figure 4.4 Thermocouple position

In the Figure 4.5 the measured temperatures are reported for the material.

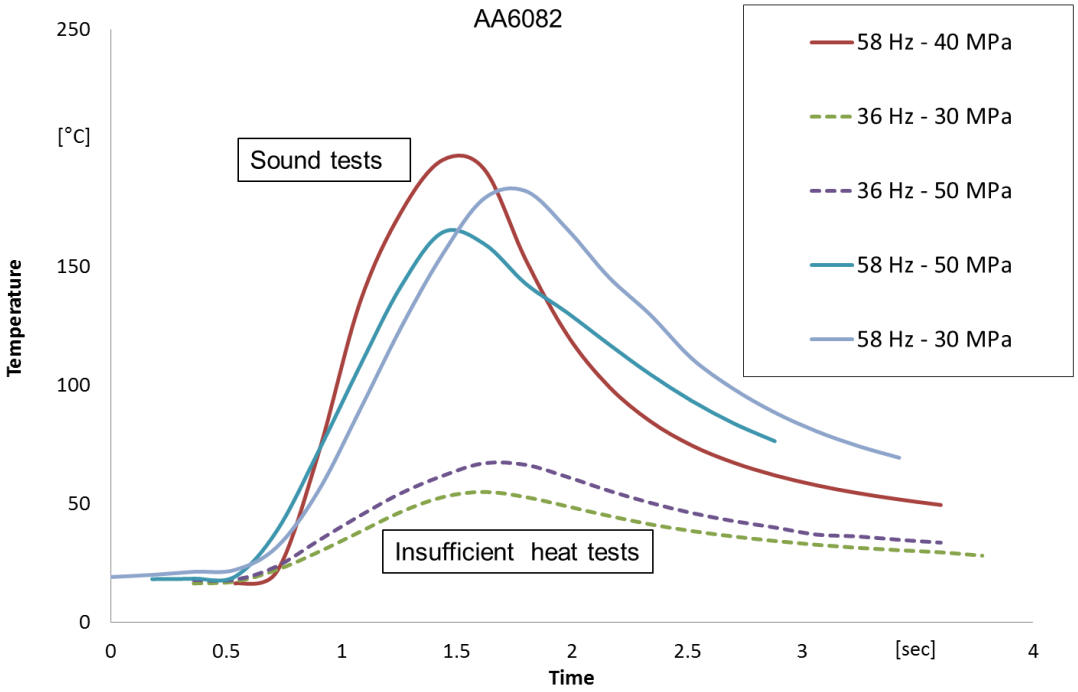

Figure 4.5 Measured temperatures for the AA6082 alloy

Solid lines are used for sound tests, while dotted lines are used for tests characterized by insufficient heat. Maximum peak temperature equal to 195 °C was measured using oscillation frequency of 58 Hz and an interface pressure of 40 MPa with both alloys.

It is interesting noticing that fixing the frequency at 58 Hz, temperature increases with increasing pressure from 30 MPa up to 40 MPa, while decreases when interface pressure increases up to 50 MPa. This effect is due to the large amount of flash expelled at higher pressure, causing significant thermal energy losses. The conclusion that the welding temperature decreases with increasing the pressures, over a certain threshold value, is further supported by J. Romero [134].

4.3.3 Macroscopic analysis

The mechanical deformation in the process of LFW is very peculiar. The joints were characterized by the presence of plastically deformed flash. The flash was extruded both in the parallel and normal direction relatively to the oscillation movement. For some joints, the flash was also expelled from the corners. The formation of the flash is a necessary condition to obtain good joints, even if the amount of material coming from the central area is higher than that coming from the peripheral areas.

Following, some results of the experimental campaign with AA6082 are showed, highlighting the three different conditions observed.

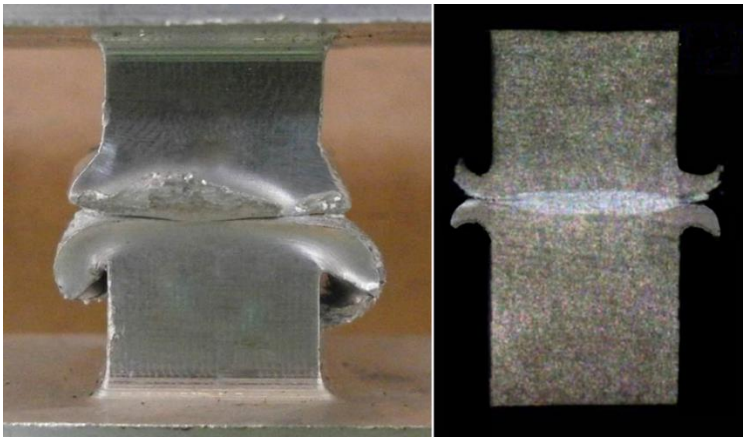

Figure 4.6 “Sound joint“ (58 Hz and 50 MPa)

First, a sound joint obtained with the process parameters of oscillation frequency 58 Hz and the interface pressure of 50 MPa is shown in Figure 4.6. An abundant formation of flash is observed in the joint picture and micrograph of the transverse section.

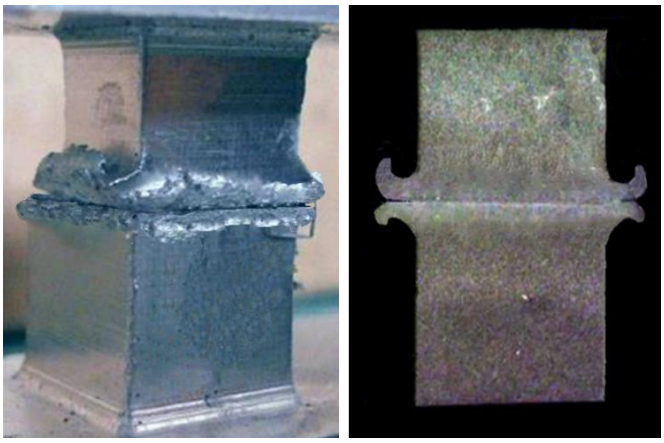

Figure 4.7 “Sound joint“ (45 Hz and 50 MPa)

The joint produced using an oscillation frequency of 45 Hz and an interface pressure of 50 MPa is shown in Figure 4.7. A correct formation of flash, as well as a thick weld line, that separates the two specimens, is observed. The joints welded show less flash with respect to the ones obtained with f=58 Hz because of the reduced heat input and consequent softening of material.

The second condition is when an excess of heat was conferred to the joint an “instability” condition was observed. In this case the significant material softening results in excess of burn off till specimen collapsing under the applied pressure during the last phase of the process.

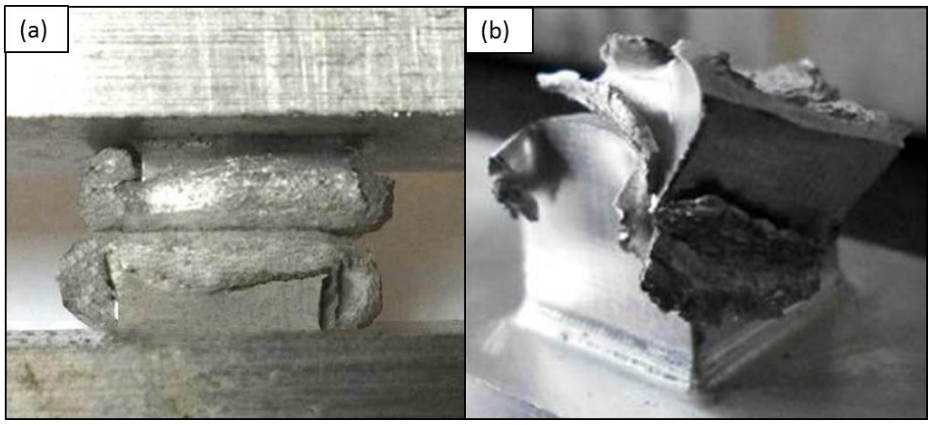

Figure 4.8 “Instability joint“ characterized by a) 45 Hz and 60 MPa and b) 58 Hz and 60 MPa

In the figure 4.8 the two joints characterized of instability are showed. An instable weld is shown in the figure 4.8a using oscillation frequency of 45 Hz and interface pressure of 60 MPa. Using the same pressure but increasing the frequency up to 58 Hz Figure 4.8b it is observed that the top specimen has collapsed preventing the formation of a weld.

Finally, the third condition when the combination of the process parameters resulted in too low heat input is shown in the figure. The joint obtained using as the operational parameters 58 Hz and 20 MPa is shown in Figure 4.9. Almost no flash is produced and no continuous bonding is obtained in the cross section. This indicates insufficient heat input was given to the joint. The specimen shown a good mechanical characteristics but metallurgical analysis has shown the lack of weld “seam” continuity at the interface.

Figure 4.9 “Insufficient heat joint“ (58 Hz and 20 MPa)

Decreasing the oscillation frequency down to 36 Hz, the generated heat is lower so different quality joints are obtained. In Figure 4.10 the top surface of the bottom specimen after the process is shown used 36 Hz of oscillation frequency and 60 MPa of interface pressure. A partially welded area can be observed in the center of the specimen surface. This indicates the onset of the bonding phenomenon that could not be completed because of the insufficient softening.

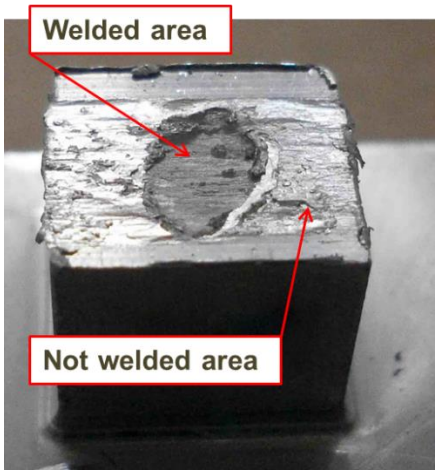

Figure 4.10 “Insufficient heat joint“ (36 Hz and 60 MPa)

It is worth noting that the insufficient amount of generated heat during the process can cause defects in the weld area difficult to detect by non-destructive analysis methods.

4.3.4 Micrographic analyses

The micrographic examination was carried out to investigate the material microstructural modifications and the defects after the process. In particular, the grain size was investigated and compared to that of the base material. For this analysis, an optical microscope and a dedicated imaging analysis software were used to acquire the images and for the measurements, respectively. Four characteristic areas of the joints can be identified: the parent material (PM), the heat affected zone (HAZ), thermo-mechanically affected zone (TMAZ) and the weld zone (WZ). Figure shows the typical material zones in an AA6082 joint

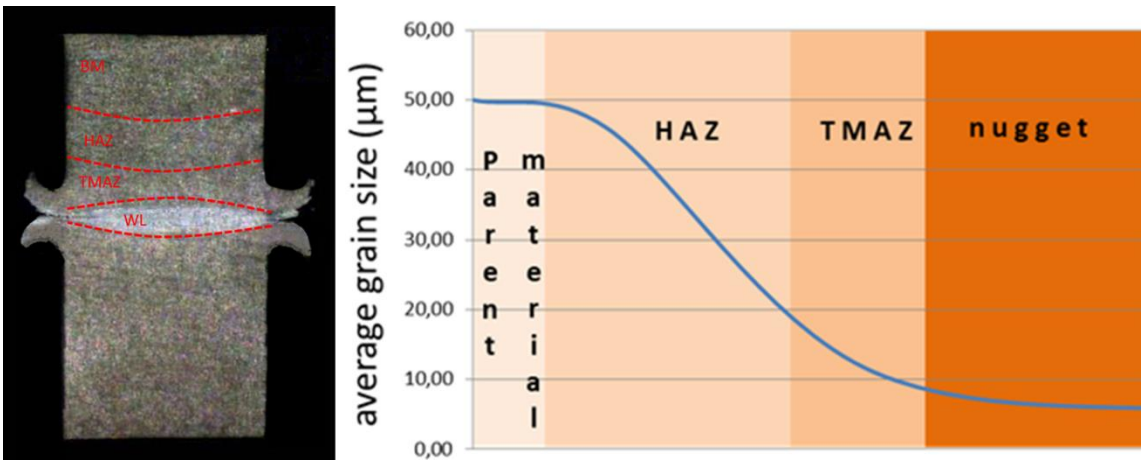

Figure 4.11 Typical material zones and graph on the average grain size AA6082

The microstructure and the mechanical properties or other properties do not undergo variations in the base material area. While, in the heat affected zone (HAZ) Fig 4.12a the microstructure change due to the temperature gradient generated during the welding in fact the average grain size changes due to the heat effects. However, in this zone no plastic deformation is optically visible.

In the thermo-mechanically affected zone (TMAZ) Fig 4.12b, the material was subjected to more heat than in the HAZ due to the proximity to the interface. In this zone, also a clear plastic deformation is observed. A further refinement of the average grain size is observed.

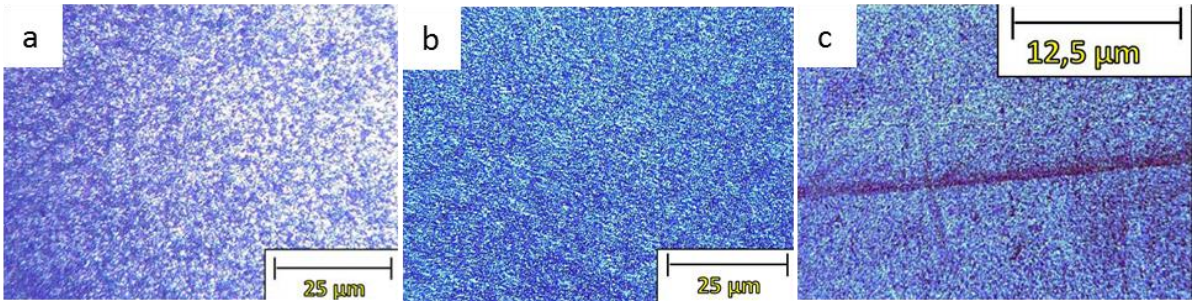

Figure 4.12 Micrograph of the a) HAZ (magnification 125x), b) micrograph of the TMAZ (magnification 125x) and c) micrograph of the WZ and flash (magnification 62.5x)

Finally, in the weld zone (WZ) Fig 4.12c, the microstructure is very different from the other parts of the welded joint. This is due to dynamic recrystallization. It should be noted that the dynamic recrystallization occurs when proper temperature gradient and plastic flow are generated.

4.3.5 Microhardness analyses

The microhardness measurements of the welded joints were carried out. In particular, for the Vickers microhardness a straight pyramid diamond indenter with a square base with a vertex angle of 136 ° is used (Figure 4.13). The test was chosen due to the dimension of the specimens. The small size imprint obtained on the piece is measured by a microscope-indenter combined apparatus (Figure 4.13).

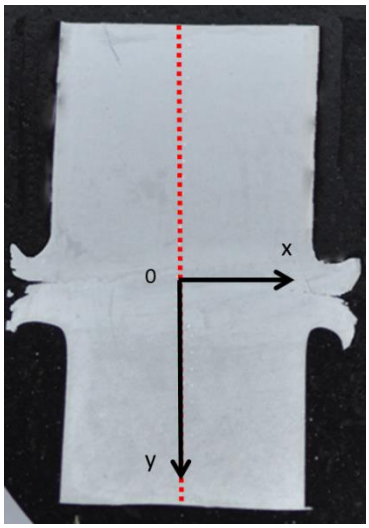

Figure 4.13 Imprint obtained on the piece and the relative points to microhardness test

The Vickers hardness value through the following formula is calculated:

$$HV = \frac{2P \sin\left(\frac{136}{2}\right)}{{d_m}^2}$$

equation 4.1

Where P is the applied load, measured in kg and d_m is the average value of the diagonals. It was chosen to apply a load of 0.5 kg in relation to the material of the specimens, for a holding time of about 30 s. Micorhardness was measured along the central axis of the joint transverse section, with a distance between the measurements points equal to 0.5 mm.

The microhardness trend of AA6082 welded joint is shown in Figure 4.14. How it can be seen in the Figure 4.14, the hardness decrease in the welding area approximately 37.5 % compared to the base material. The combined effect of the severe plastic deformation and recrystallization plays a very important role in the microhardness distribution.

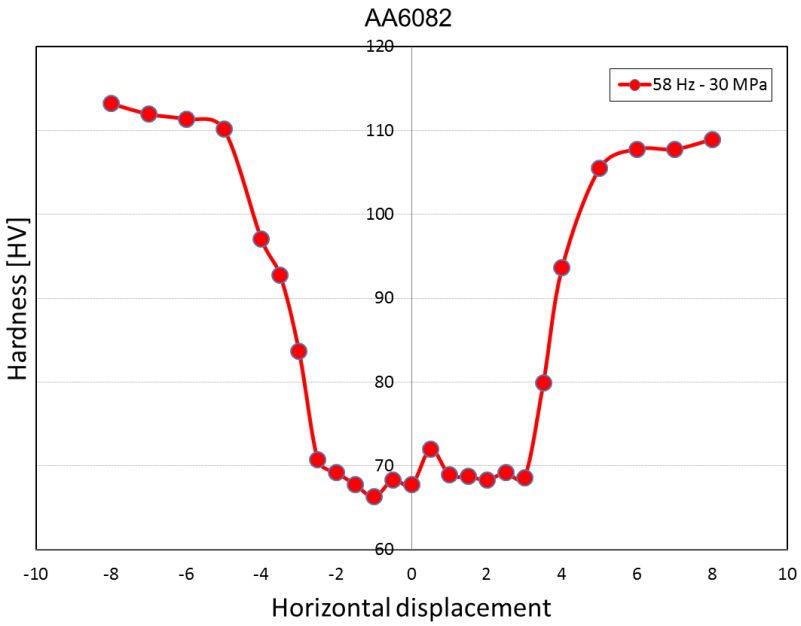

Figure 4.14 Hardness joint 58 Hz, 30 MPa

4.4 Numerical Analysis

Numerical modeling of linear friction welding (LFW) was conducted using the FEA DEFORM-3DTM commercial software, an implicit Lagrangian code designed to simulate metal forming processes. The coupled thermo-mechanical analysis with rigid-viscoplastic strain, strain rate and temperature dependent material behavior were performed using AA6082-T6 and AA6061-T6. The effects of the processing parameters on the temperature evolution and axial shortening of LFW joints were numerically investigated.

The simulations of the processes LFW were carried out starting from experimental tests for the AA6082.

The workpiece, reproducing the top specimen Fig 4.1, was modeled as a rigid visco-plastic object. A longitudinal symmetry plane was introduced in order to save CPU time [190]. The actual dimensions of the top specimen were reproduced.

The bottom specimen was modeled as a rigid plate 60 mm in width, 2.5 mm in thickness and 90 mm in length. With this assumption, significant saving in CPU time can be achieved with acceptable accuracy in the field variables prediction [190]. This

choice was made in order to simplify the contact condition avoiding numerical instabilities due to the deformable-deformable object contact.

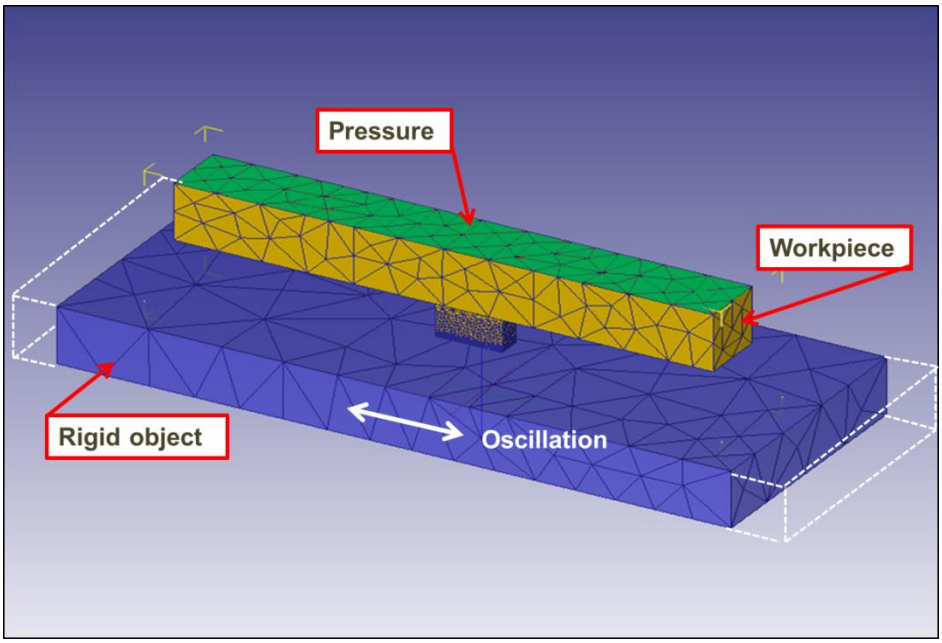

Figure 4.15 The FE continuum model

The software allows only discretization with tetrahedral elements, (linear shape functions). It was necessary to introduce a denser discretization close to the welding surface where high gradient of the main field variables exist. Additionally, a re-meshing referring volume was identified all along the specimen movement. Furthermore, it was necessary to make preliminary tests, with increasing mesh density, to determine the optimal dimension of the finite elements in these critical areas. Consequently, two windows with different discretization are created. The model has approximately 32.000 elements with the smallest elements characterized by edge of about 0.15 mm. The specimen is constrained against x and y translation for 7/8 of its height for increased stability, while an axial load was imposed on the top surface of the workpiece along the z axis.

For the thermal characteristics of the AA6082 and AA6061 aluminum alloys taken into account, the following values were utilized: thermal conductivity k1 = 180 [N/(s °C)] and thermal capacity c = 2.4 [N/ (mm2 °C)] for the AA6082 while k1 = 166 [N/(s °C)] and thermal capacity c = 2.3 [N/ (mm2 °C)] for the AA6061 taken from literature for aluminum alloys. No variation of k1 and c with temperature was taken into account; this assumption linearizes the thermal equation and results in better

convergence. A rigid-viscoplastic temperature and strain rate dependent material model is employed.

$$\sigma = KT^{A}(\dot{\varepsilon})^{B}(\varepsilon)^{C}$$

equation 4.2

Where K = 2.69 E10, A = -3.3155, B = 0.1324 and C = 0.0192, are material constants determined by a numerical regression based on experimental data. As it can be seen, an increase in temperature leads to a decrease in flow stress (A<0). On the contrary, an increase in both strain and strain rate leads to an increase in flow stress (B>0, C>0). As the friction factor at the interface is regarded, a dedicated procedure, developed by some of the authors and fully described in [190] for AA2011, was used. As a result, a temperature dependent friction factor was found:

$$m = \begin{cases} 0.2, & T < 220\ °C \\ \dfrac{-0.185T}{T-420}, & 220\ °C < T < 355\ °C \\ 1, & T > 355\ °C \end{cases}$$

equation 4.3

A friction window was used to simulate the real physical contact conditions, i.e. the top specimen contact surface varies with time according to the oscillation frequency Fig. 4.16. Outside the friction window, the constant shear friction factor was set equal to zero. A constant time increment of 0.0001 s was used for all the simulations. No heat exchange was considered between the top and bottom objects because of the symmetry of the process. The oscillation was assigned to the bottom specimen while the pressure was applied to the upper surface of the top specimen.

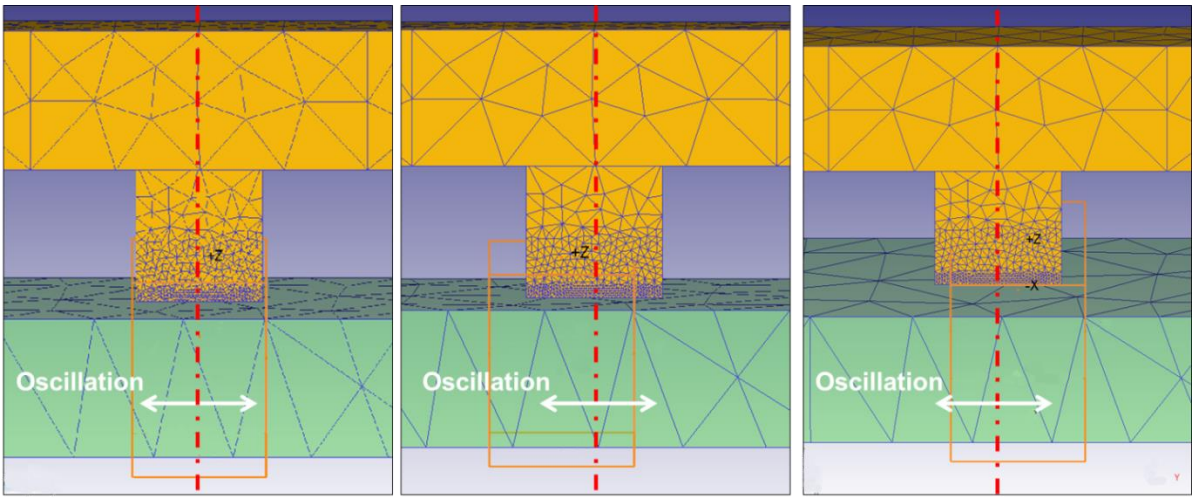

Figure 4.16 Boundary condition

In the following a comparison of the flash (shape and length) and the temperature trend obtained by experimental analysis and numerical simulation is carried out.

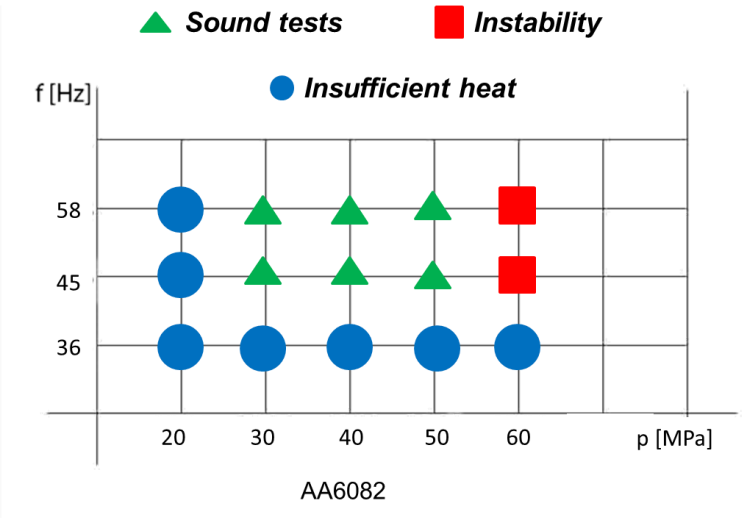

Figure 4.17 Experimental and numerical campaigns

The weld quality has been studied through the parallel observation of the temperature reached after 1.5 seconds, when the oscillation of the rigid die of the model is stop, and flash morphology.

At the end of the simulation the material flow was investigated through the analysis of the nodes position and the main field variables history that they experience. The “point tracking” option of the software DEFORM-3DTM was utilized. A point P1 has been identified, in the same position of the experimental thermocouple hole, to study the temperature variables figure 4.18.

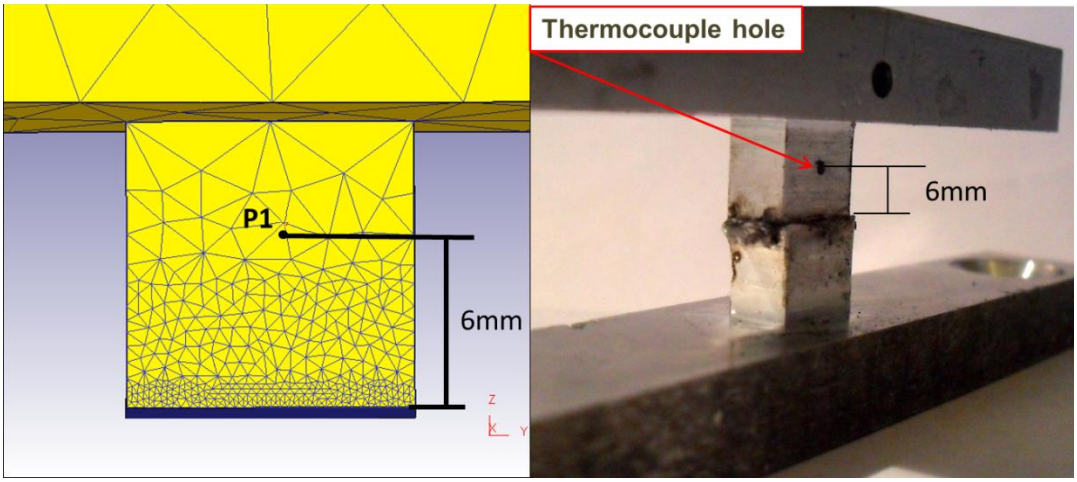

Figure 4.18 Temperatures study in the LFW model

The local value of temperature for a given reference point and time was calculated. Figure 4.19 show, the distribution of the above cited field variable in the sound welded specimens characterized by 58 Hz of oscillation frequency and 30 MPa, 40 MPa and 50 MPa of interface pressure.

The temperature distribution highlights the same characteristics of the numerical result and the experimental result of the LFW process.

It is seen that the temperature, calculated at the reference point P1, are quickly increased to around 200 °C for the sound joint characterization of 58 Hz and 40 MPa as the experimental result. For the second sound joint, decreasing the interface pressure value down to 30 MPa, the temperature reached is around 180 °C confirming by the experimental test. Finally, for the third sound joint the temperature reached decrease due to the generation of the flash down to 170 °C. In this case the numerical temperature trend is a little bit higher than the experimental temperature trend due to convergence problems arise due to self-contact and folding occurring in the deformable object.

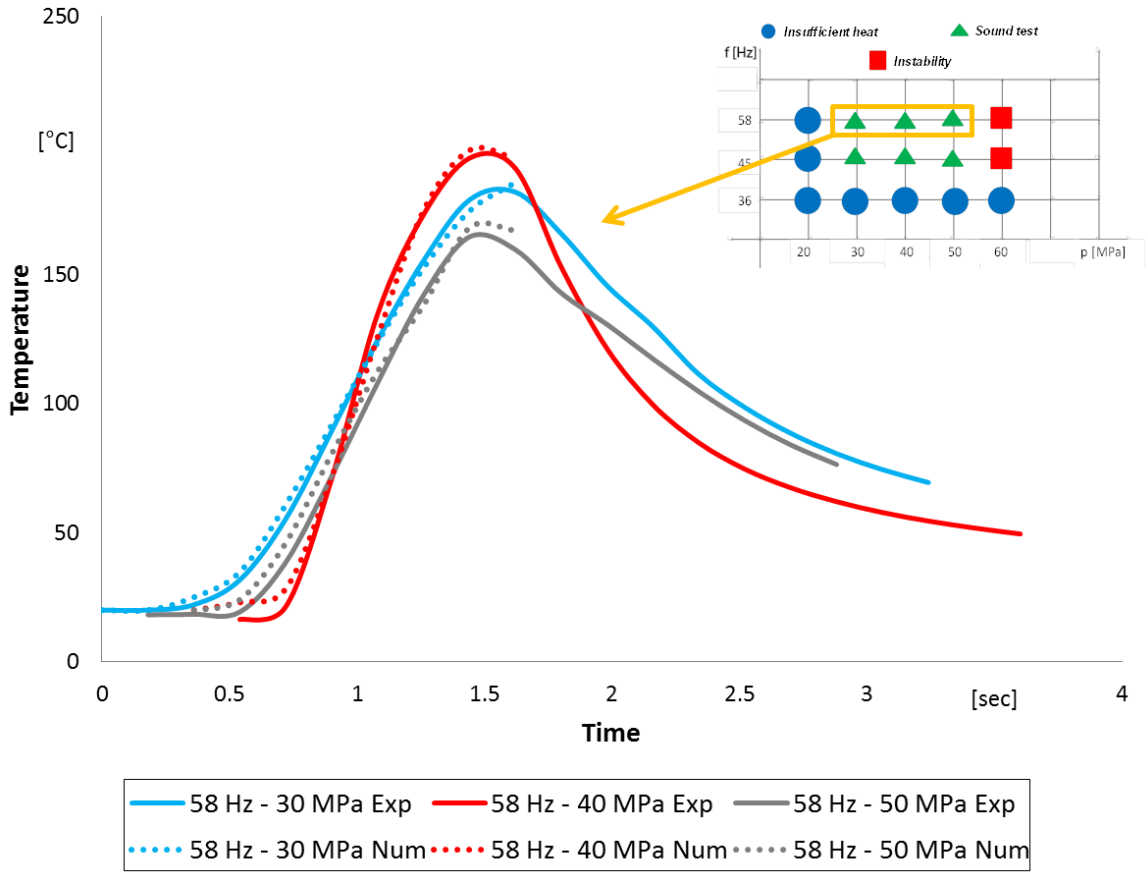

Figure 4.19 Temperature histories at 6 mm from the welding interface, Exp vs Num

Figures 4.20a, 4.21a and 4.22a show the distribution of temperature, strain, and strain rate in the specimen, at the end of the process for the case study characterized by frequency 58 Hz and interface pressure 40 MPa. The histories of the above cited field variables, calculated for point P2, i.e. the point initially located at the center of the contact surface, are reported in Figures 4.20b, 4.21b and 4.22b for the case study characterized by frequency 58 Hz and interface pressure 40 MPa. The field variables distribution highlights some of the characteristics of the linear friction welding process: temperature, strain and strain rate are higher at the welding surface. It is seen that temperature at the interface quickly increases to about 400 °C for the test characterized by f=58 Hz and p=40 MPa. The maximum temperature level is reached, for all the specimens, as the reciprocating motion stops, when the additional pressure is applied.

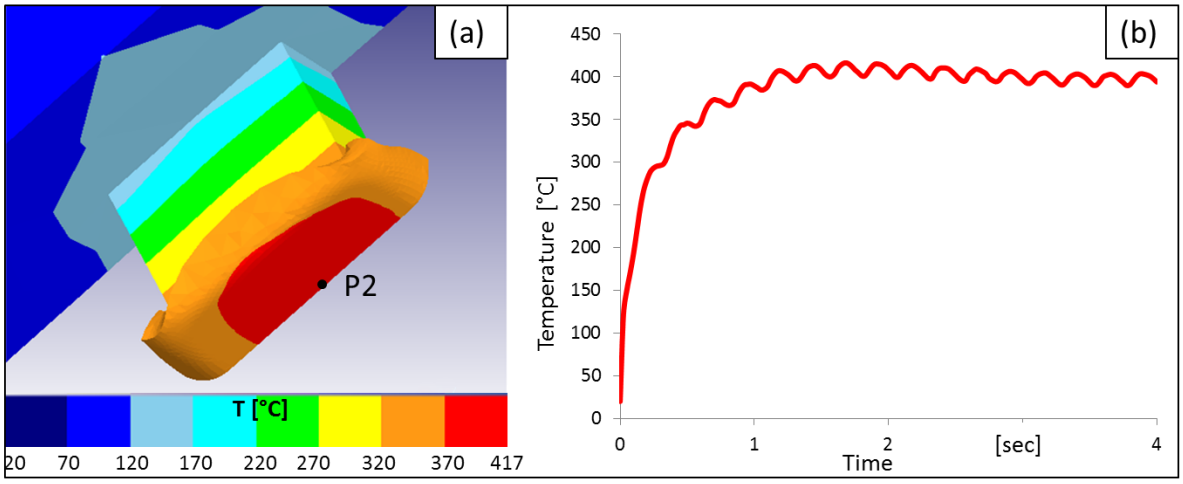

Figure 4.20 Temperature distribution in the specimen and evolution in time for P2-(58 Hz and 40 MPa)

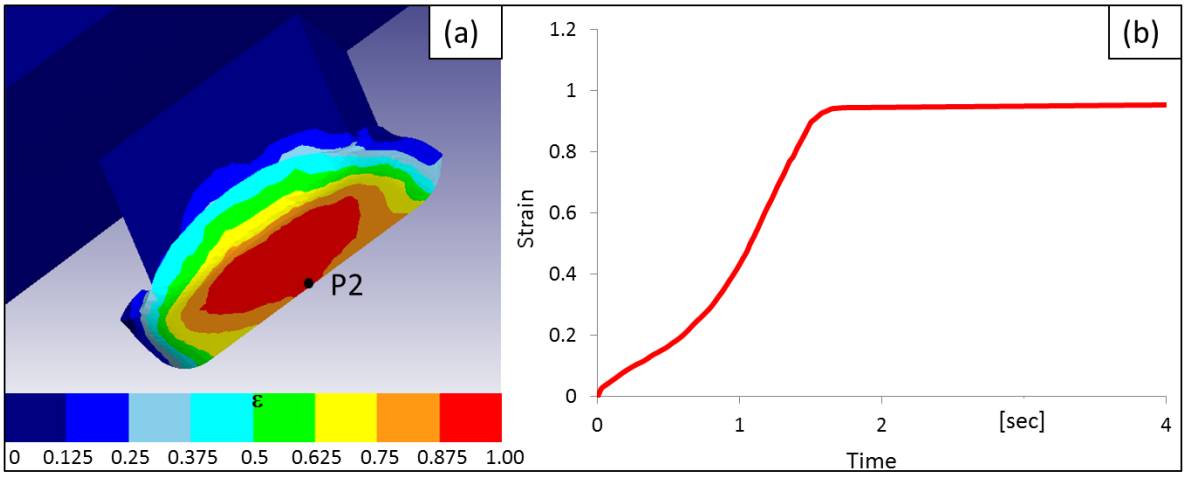

Figure 4.21 Strain distribution in the specimen and evolution in time for P2 – (58 Hz and 40 bar)

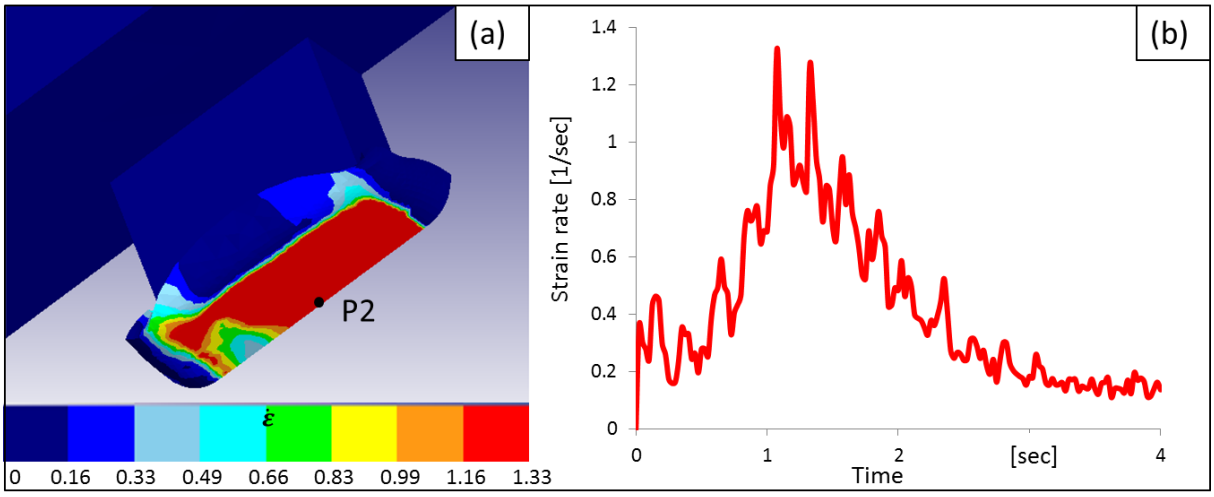

Figure 4.22 Strain rate distribution in the specimen and evolution in time for P2 – (58 Hz and 50 bar)

Two main zones can be identified regarding the effective strain figure 4.21: the zone still in in contact with the bottom specimen experience very high strain values; on the other hand, the zones of the material belonging to the flash, which have been in contact with the bottom specimen for a smaller time, show lower values.

The values of temperature, strain and strain rate, during the process, were collected and used to calculate the flow stress σ at each time increment.

With this process parameters a significant amount of flash is produced (Figure 4.23a).

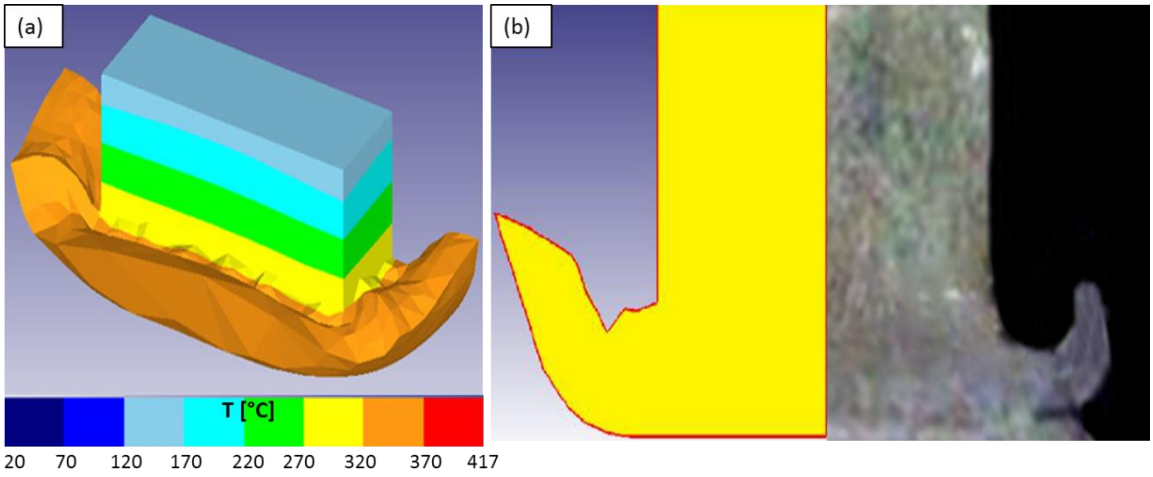

Figure 4.23 Experimental-numerical comparison, 58 Hz and 40 MPa

The experimental-numerical comparison of specimen geometry is shown in the figure 4.23b. It is worth noting that in the 3D isometric view showed in figure, the external

part of the flash is visible. Although a larger amount of heat is produced, when the material is extruded as flash, the latter is quickly cooled down by the surrounding environment.

4.5 Applicability criteria solid bonding

The pressure-time (W) welding criterion was utilized

$$W = \int_0^t \frac{p}{\sigma} dt \cong \Sigma W_j \cong \sum_j \frac{p_j}{\sigma j} \Delta t_j$$

equation 4.4

At the end of the simulation showed in the paragraph 4.4, the material flow was investigated through the analysis of the nodes position and the main field variables history that they experience. The “point tracking” option of the software DEFORM-3DTM was utilized, highlighting, for a set of points initially placed at the contact interface, their final position after deformation. Ten points were identified and monitored throughout the process as shown in figure 4.24.

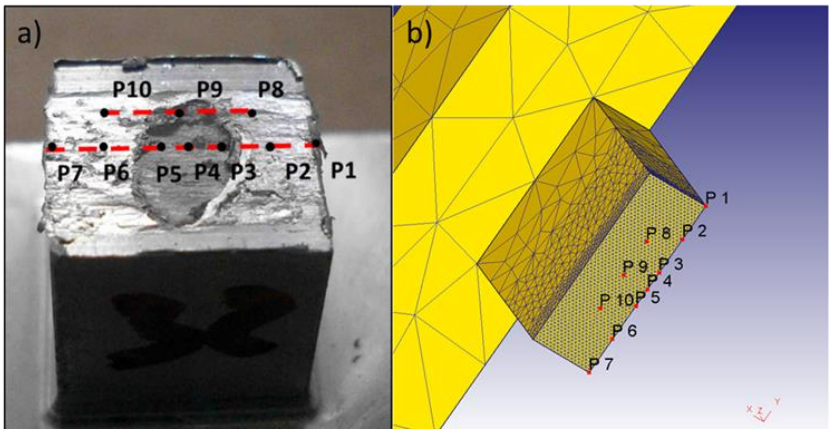

Figure 4.24 The identified points for the “point tracking” option

A time step of 0.01 s was selected to extract the data for each of the identified points (Fig. 4.24) and calculate the sum indicated in eq. 4.4.

So, in order to apply the bonding criterion proposed, the value of the welding criterion was calculated for each of the observation points and the final position of the observation points was highlighted. In this way, 150 values were obtained. As already mentioned, due to the relatively simple material flow, ten tracking point for each process condition were utilized. Figure 4.25 shows the final position of the

observation points for the case study characterized by frequency of 60 Hz and pressure of 40 MPa.

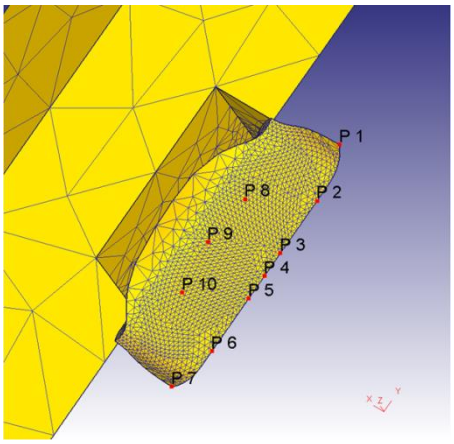

Figure 4.25 Final position of the identified points (58 Hz – 40 MPa)

In the linear friction welding process the pressure p generating the solid bonding (Eq. 4.4) can be easily calculated considering the actual contact pressure at interface.

The values of temperature, strain and strain rate, during the process, were collected and used to calculate the flow stress σ at each time increment j (Eq. 4.4).

4.5.1 Time–flow criterion to AA6082

In order to assess the applicability of the considered bonding criterion to LFW welding experiments were carried out as indicated in Table 4.3.

The bonding parameter W was calculated, for the ten observation points highlighted in fig. 4.24, using the numerical results shown in the previous paragraph. As far as the W parameter is regarded, i.e. the one based on the Pivnik and Plata criterion, a threshold value was taken from literature. In particular, as briefly discussed in the introduction paragraph, Ceretti et al. [161] use droll bonding tests on AA6082 to determine the critical value as a function of temperature. A regression was carried out obtaining the following analytical expression:

$$W^{LIM} = 332{,}621.59T^{-1.96} \; ; \qquad R^2 = 0.98$$

equation 4.5

The fig. 4.26 to 4.40 show the calculated W parameter and the threshold curve for the observation points investigated for each process parameter combination. To

easily understand the application of the bonding criterion, each figure shows the results of experimental macro analysis of the welded test, the results of the numerical simulation and the results of the W parameter in dependency of the temperature. The temperature corresponding to each point is the average value of the temperatures calculated during the time interval corresponding to non-zero pressure values.

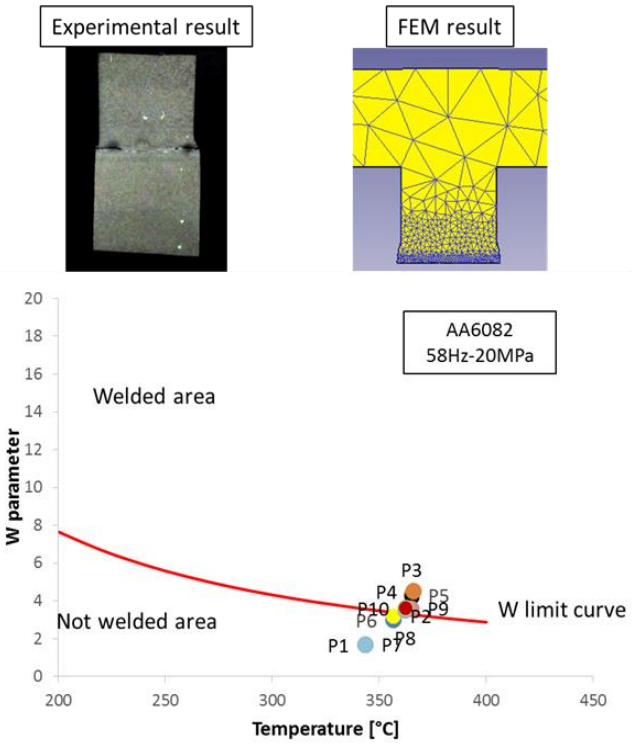

Figure 4.26 Calculated W parameter and threshold value limit curve for the test 58 Hz-20 MPa.

As it has been said above, the weld characterized by 58 Hz of frequency and 20 MPa of contract pressure is characterized by insufficient heat. The optical observation (Figure 4.9) has been shown that material continuity is obtained at the center of the transverse section. Although this is considered a “not welded” joint, as compared to a sound joint, it can be stated that solid bonding occurred at the center of the joint. As it can be seen in the Graph above, the points P3, P4 and P5, i.e. the points laying at the center of the contact area, are in the welded area of the graph while the point P9 that laying in the peripheral part of the center of the contact area, coincides with the limit. The all other points are below the W limit curve. It can be concluded that the prediction of the bonding criterion is correct.

Keeping the frequency and increasing the contact pressure it is obtained a sound joint. The network correctly predict test, being all the observation points above the

limiting curve. Only the points P1 and P7 are below the limit curve because are expelled by flash.

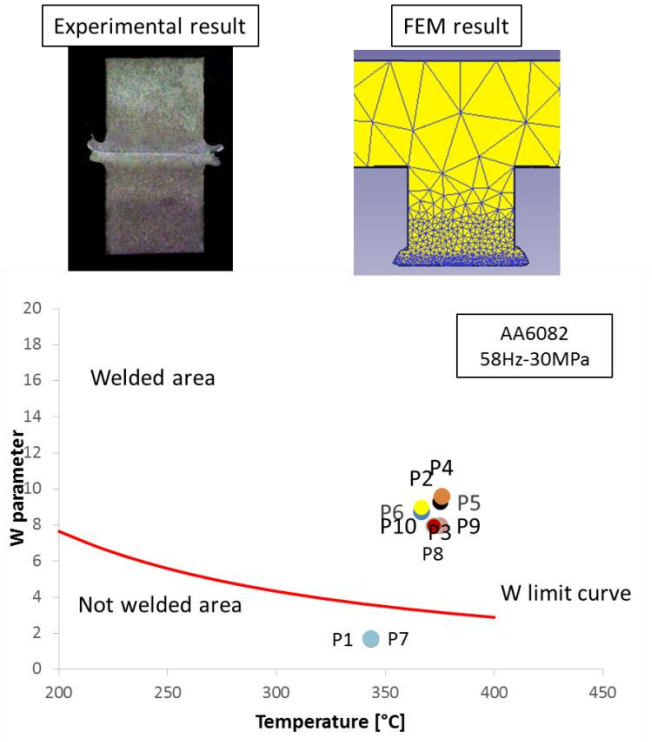

Figure 4.27 Calculated W parameter and threshold value limit curve for the test 58 Hz-30 MPa.

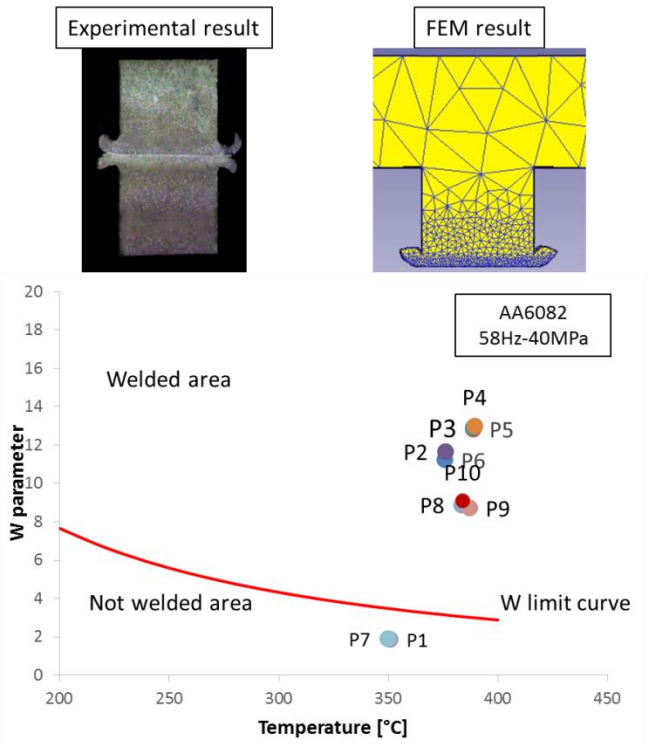

Figure 4.28 Calculated W parameter and threshold value limit curve for the test 58 Hz-40 MPa.

Increasing the contact pressure up to 40 MPa the same condition that it has been shown in the figure4.28 is found. A sound joint is obtained and this is correctly predicted by the bonding criterion proposed. Also in this case the point P1 and P7 are expelled in flash and so are not welded

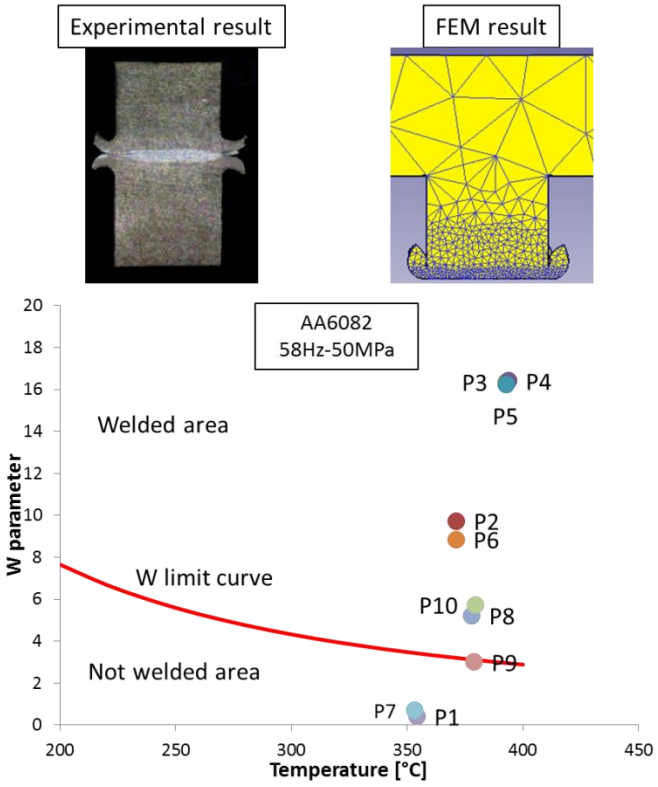

Figure 4.29 Calculated W parameter and threshold value limit curve for the test 58 Hz-50 MPa.

The welded joint characterized by 58 Hz of frequency and 50 MPa of contact pressure is a sound test. This joint is characterized by a large amount of flash figure 4.6. In this case the identified points in the central area, P3, P4 and P5 are welded. The points P8, P9 and P10 are expelled by the flash generated in the perpendicular direction to the linear motion direction of the bottom specimen. The W parameter being calculated as a summation in time, so it is easily understand that the point P9 is first point of the peripheral area of the welding interface, to be expelled by the flash. The points P2 and P7 are welded and the points P1 and P7 are expelled by the flash generated in the direction of the linear motion of the bottom specimen.

Finally, as regards the joints characterized of 58 Hz of frequency, the instability condition is reached increasing the contact pressure up to 60 MPa.

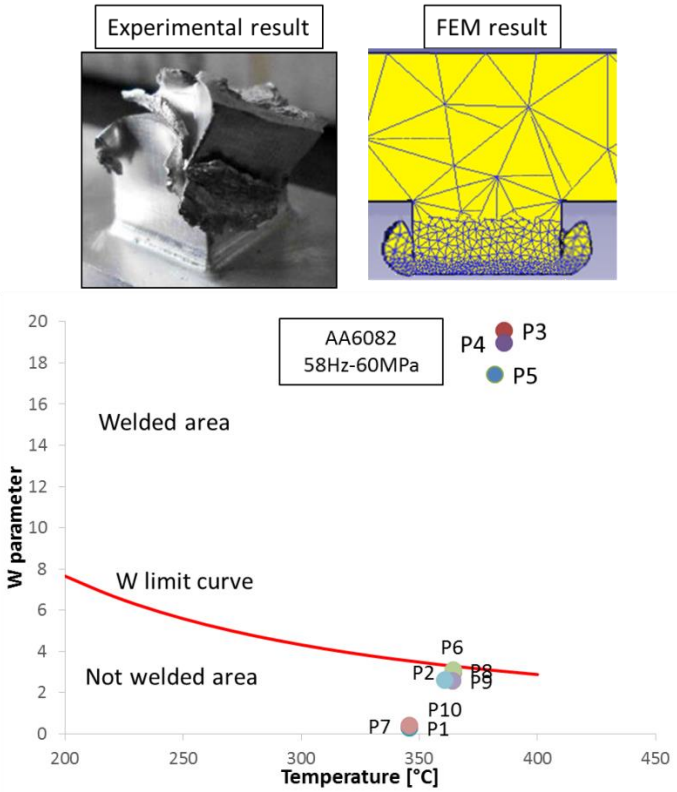

Figure 4.30 Calculated W parameter and threshold value limit curve for the test 58 Hz-60 MPa.

In this case the phenomenon described for the test 58 Hz-50 MPa it is even more emphasized. In fact, all the identified points are below the limit curve because are expelled by the generated flash except the three points P3, P4 and P5 laying to the centre of the interface surface. Moreover, the W values reached by these points are really high. This effect will be studied in the next paragraph through the neural network tool.

The weld characterized by 45 Hz of frequency and 20 MPa of contract pressure is characterized by insufficient heat. From the optical observation shows that material continuity is not obtained at the center of the transverse section. As it can be seen in the Graph above, all the identified points are below the W limit curve. It can be concluded that the prediction of the bonding criterion is correct.

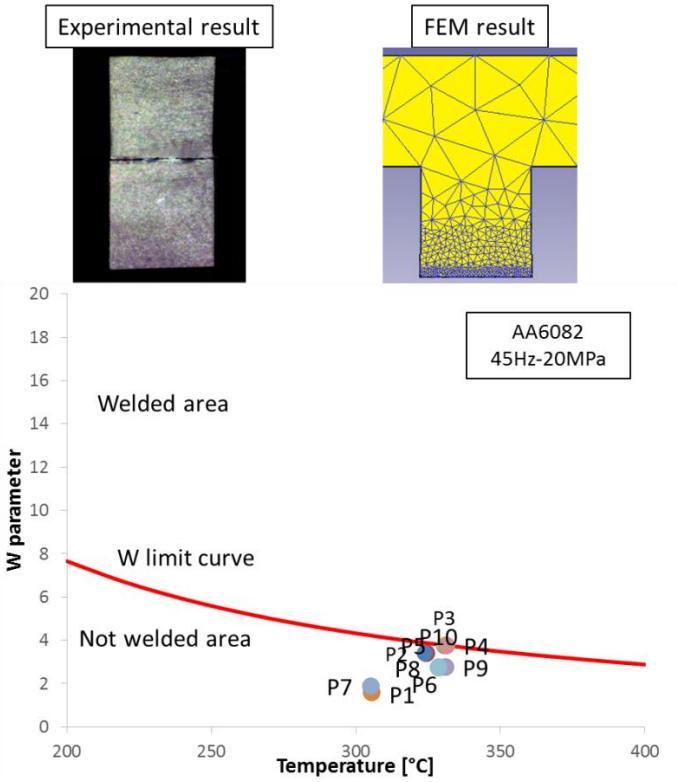

Figure 4.31 Calculated W parameter and threshold value limit curve for the test 45 Hz-20 MPa.

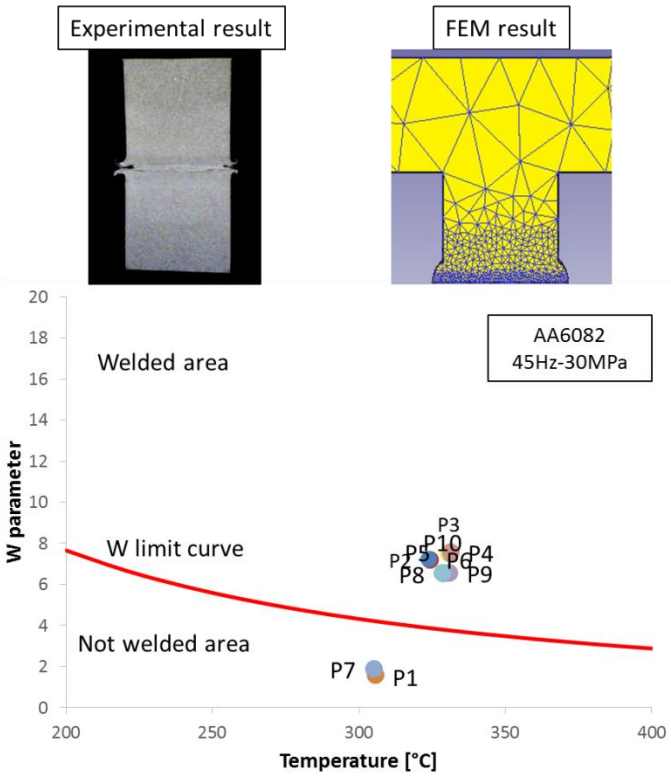

Figure 4.32 Calculated W parameter and threshold value limit curve for the test 45 Hz-30 MPa.

Keeping the frequency and increasing the contact pressure it is obtained a sound joint. The weld characterized by 45 Hz of frequency and 30 MPa of contract pressure is characterized by a correct bonding condition.

The network correctly predict the test, being all the observation points above the limiting curve. Only the points P1 and P7 are below the limit curve because are expelled by flash.

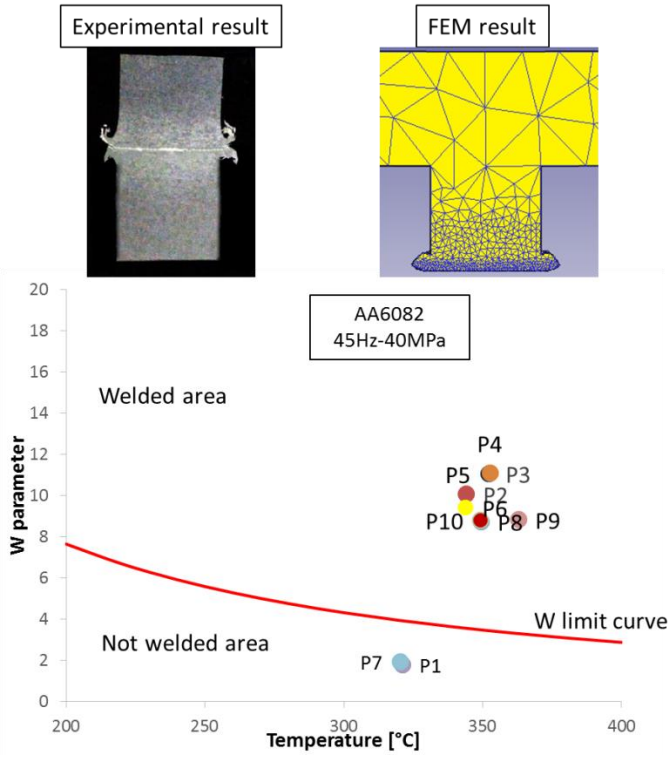

Figure 4.33 Calculated W parameter and threshold value limit curve for the test 45 Hz-40 MPa.

Increasing the contact pressure up to 40 MPa the same condition has seen before is presenting. A sound joint is obtained and this is correctly predicted by the bonding criterion proposed. Also in this case the point P1 and P7 are expelled in flash and so are not welded.

The welded joint characterized by 45 Hz of frequency and 50 MPa of contact pressure is a sound test. A sound joint is obtained and this is correctly predicted by the bonding criterion proposed. Also in this case the point P1 and P7 are expelled in flash and so are not welded.

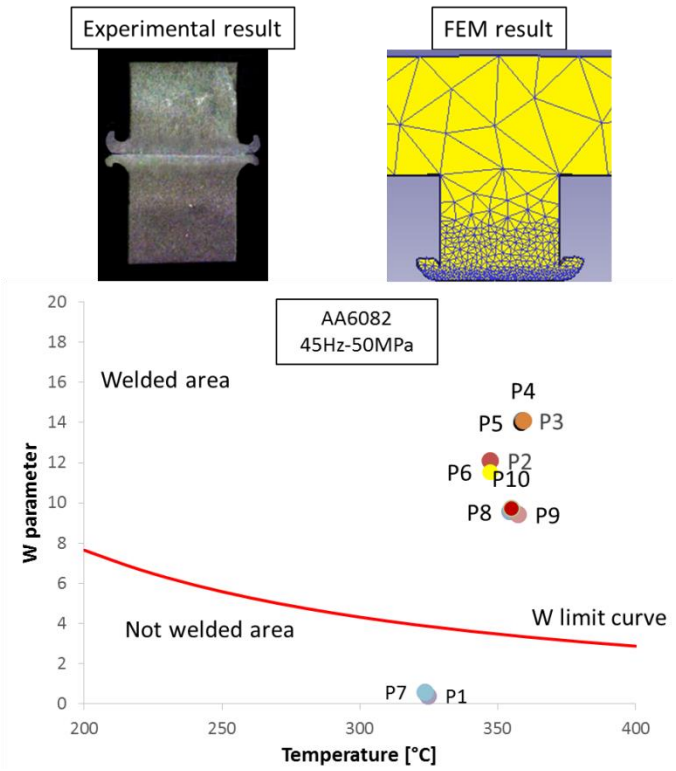

Figure 4.34 Calculated W parameter and threshold value limit curve for the test 45 Hz-50 MPa.

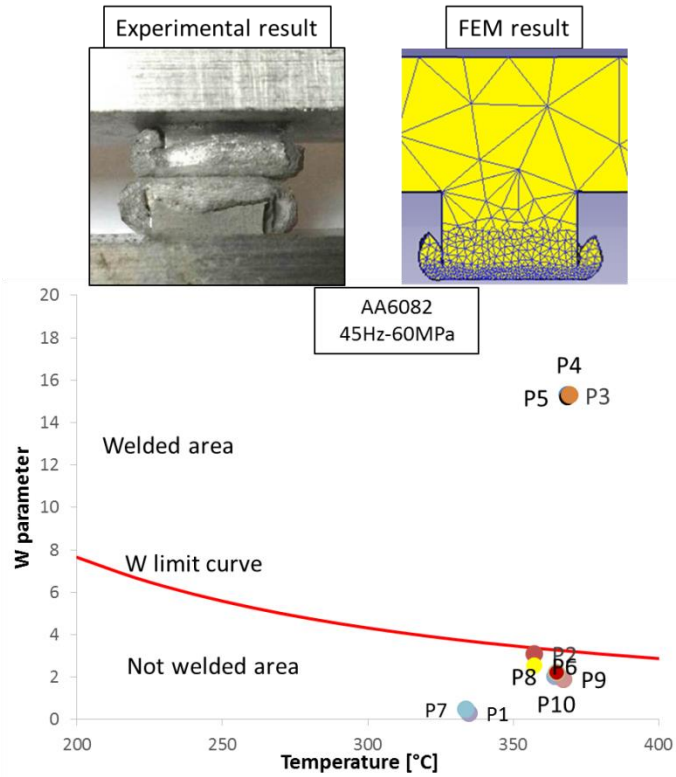

Figure 4.35 Calculated W parameter and threshold value limit curve for the test 45 Hz-60 MPa.

Finally, as regards the joints characterized of 45 Hz of frequency, the instability condition is reached increasing the contact pressure up to 60 MPa. In this case all

the identified points are below the limit curve because are expelled by the generated flash except the three points P3, P4 and P5 laying to the centre of the interface surface.

Decreasing the frequency down to 36 Hz, the insufficient heat condition is reached independently of the contact pressure choice. In the next figures, the experimental results, the numerical results and the bonding criterion results of the identified points are shown for each parameter combinations kept the frequency to 36 Hz. In the all case the W limit value is not reached, describing correctly the experimental condition occurred.

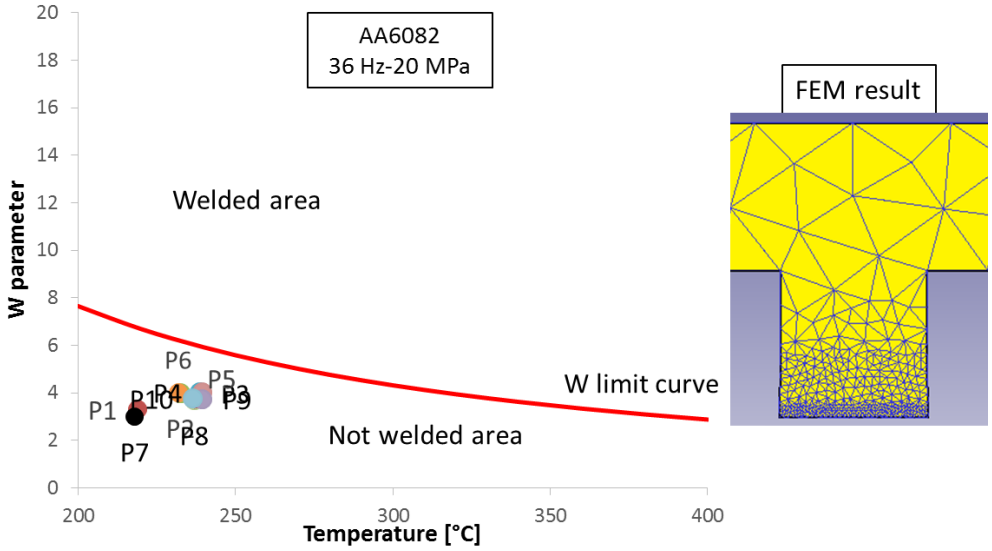

Figure 4.36 Calculated W parameter and threshold value limit curve for the test 36 Hz-20 MPa.

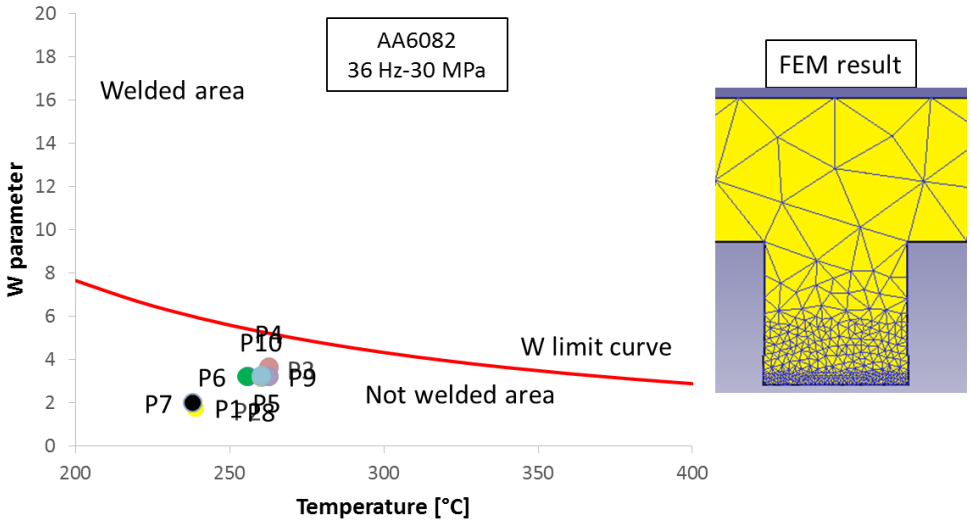

Figure 4.37 Calculated W parameter and threshold value limit curve for the test 36 Hz-30 MPa.

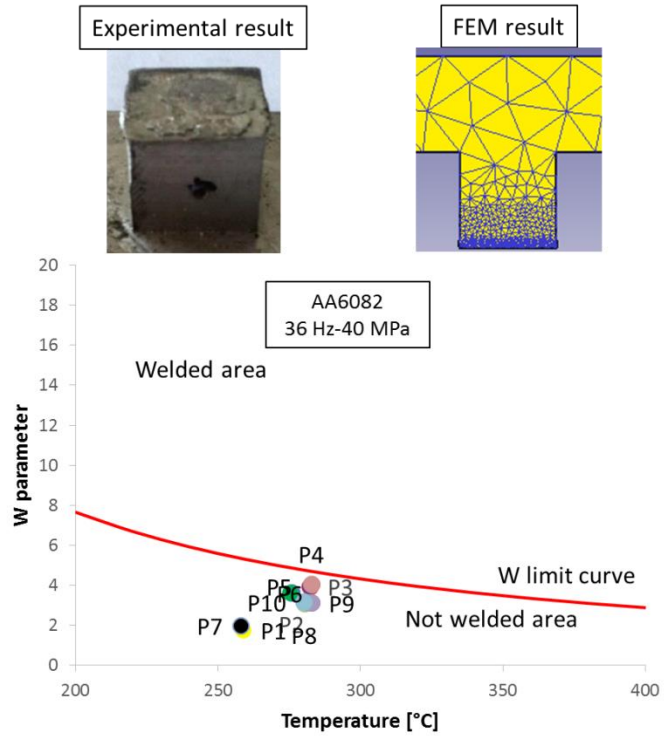

Figure 4.38 Calculated W parameter and threshold value limit curve for the test 36 Hz-40 MPa.

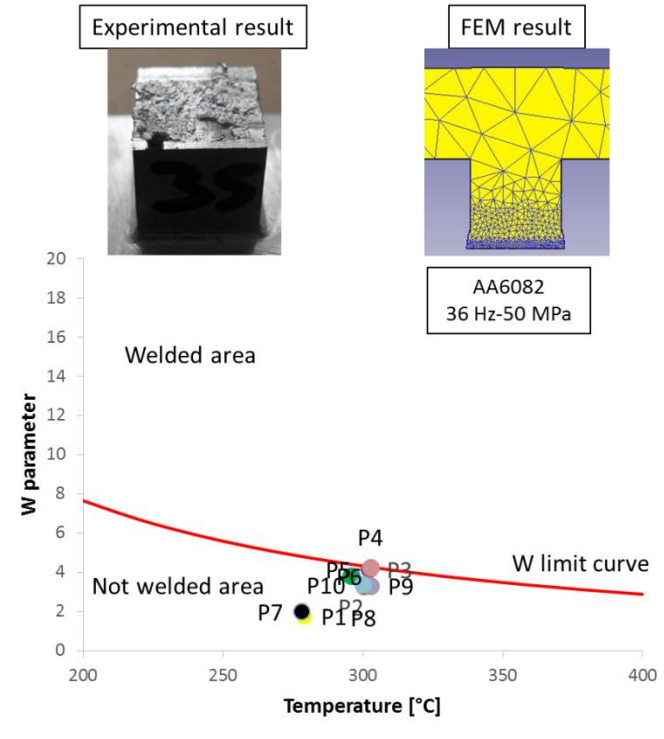

Figure 4.39 Calculated W parameter and threshold value limit curve for the test 36 Hz-50 MPa.

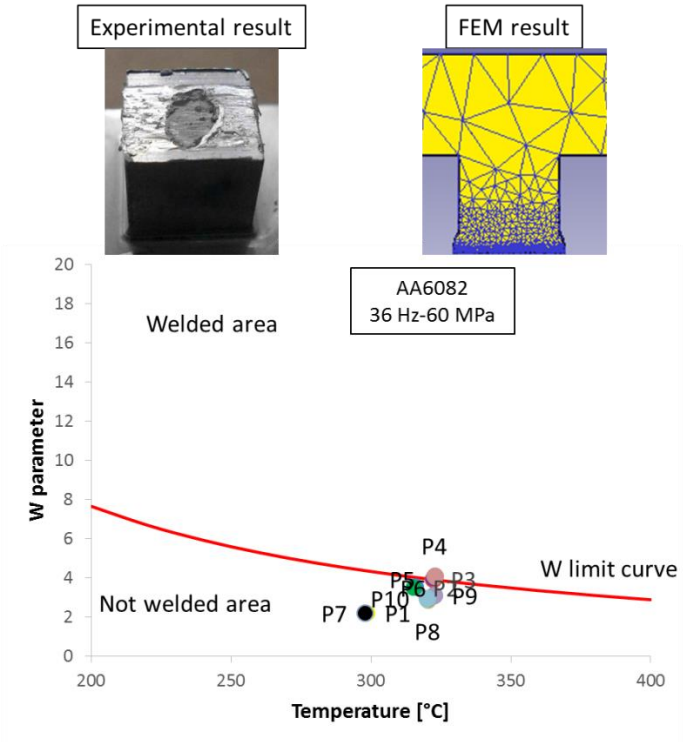

Figure 4.40 Calculated W parameter and threshold value limit curve for the test 36 Hz-60 MPa.

Finally, the weld characterized by 36 Hz of frequency and 60 MPa of contract pressure is characterized by insufficient heat. The experimental observation (Figure 4.10) shows that material continuity is obtained at the center of the transverse section. As it can be seen in the Graph above, the points P3, P4 and P5, i.e. the points laying at the center of the contact area, coincides with the limit curve. The all other points are below the W limit curve. It can be concluded that the prediction of the bonding criterion is correct and accurate.

4.5.2 Time–flow criterion to AA6061

In this paragraph the bonding criterion proposed, i.e. the one based on the Pivnik and Plata criterion, was used to describe the solid bonding phenomenon to a LFW process using an aluminum alloy AA6061.

Differently to the way used for the AA6082, in this case the bonding criterion was applied before the experimental campaign in order to know which process parameters to use experimentally, to obtain a sound weld joint.

To do it, a numerical campaign was conducted using the same process window utilized for the AA6082 (Fig 4.17).

The bonding parameter W was calculated, for the ten observation points highlighted in fig. 4.24, using the numerical results. As far as the W parameter is regarded, a threshold value was taken from literature. In particular, as briefly discussed in the introduction paragraph, Ceretti et al. [161] use droll bonding tests on AA6061 to determine the critical value as a function of temperature. A regression was carried out obtaining the following analytical expression:

$$W_{lim} = 4.9063e^{-0.0017\,T} \quad T > 320°C$$

equation 4.6

The next figures shows the calculated W parameter and the threshold curve for the observation points investigated for each process parameter combination. The temperature corresponding to each point is the average value of the temperatures calculated during the time interval corresponding to non-zero pressure values.

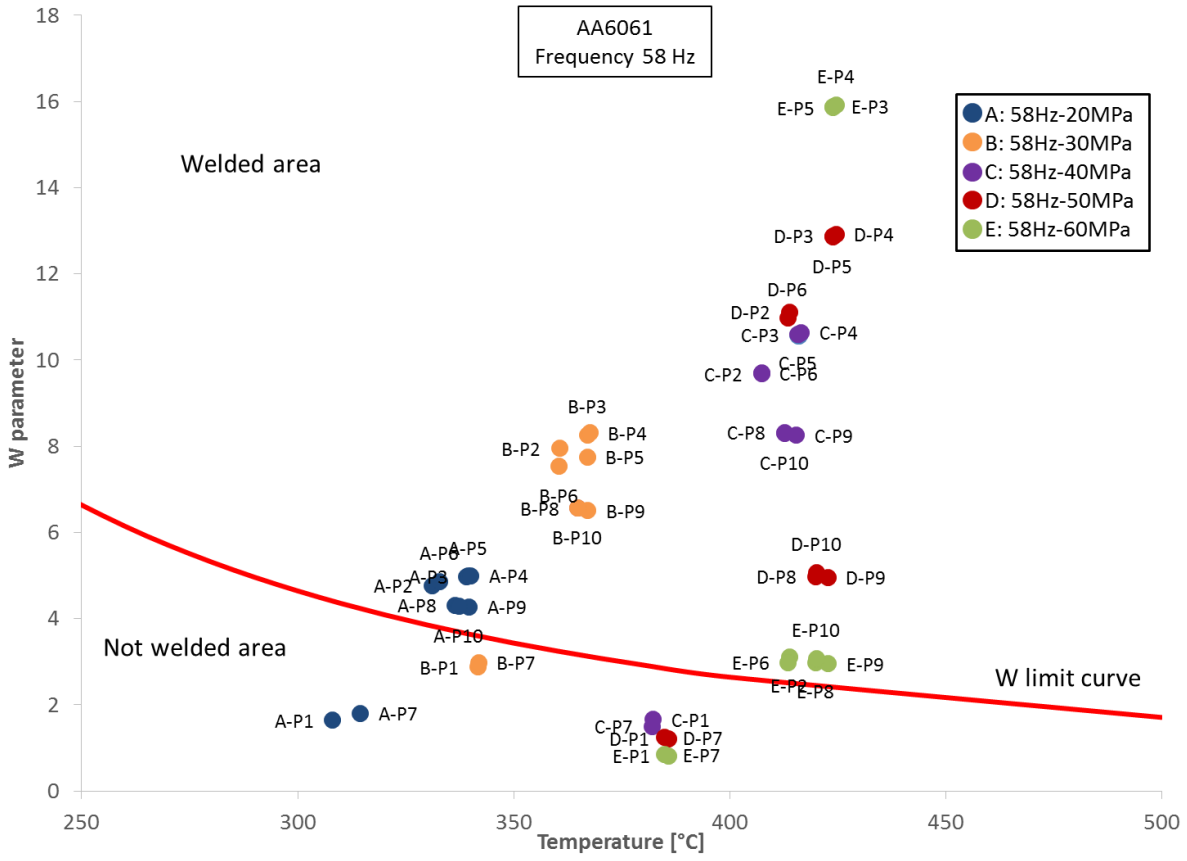

Figure 4.41 Calculated W parameter and threshold value limit curve for the tests 58 Hz.

The weld characterized by 58 Hz of frequency and 20 MPa of contract pressure is characterized by sound test contrary to what happened to the AA6082 using the same process parameter figure 4.26. As it can be seen in the graph 4.41 (points A), all the points are in the welded area of the graph while the points P1 and P7 coincides with the not welded area.

Increasing the contact pressure up to 30 MPa (fig 4.41 points B), 40 MPa (fig 4.41 points C), and 50 MPa (fig 4.41 points D), the sound tests are obtained following the same condition found with the AA6082. All the identified points are in the welded area of the graphs except the points P1 and P7 because are expelled by flash.

The welded joint characterized by 58 Hz of frequency and 60 MPa of contact pressure is an instability test (fig 4.41 points E). The numerical result is characterized by a large amount of flash and axial shortening. In this case the identified points in the central area, P2, P3, P4 are welded. All the other identified points are close the limit curve because are expelled by the generated flash. The points P1 and P7 are not welded.

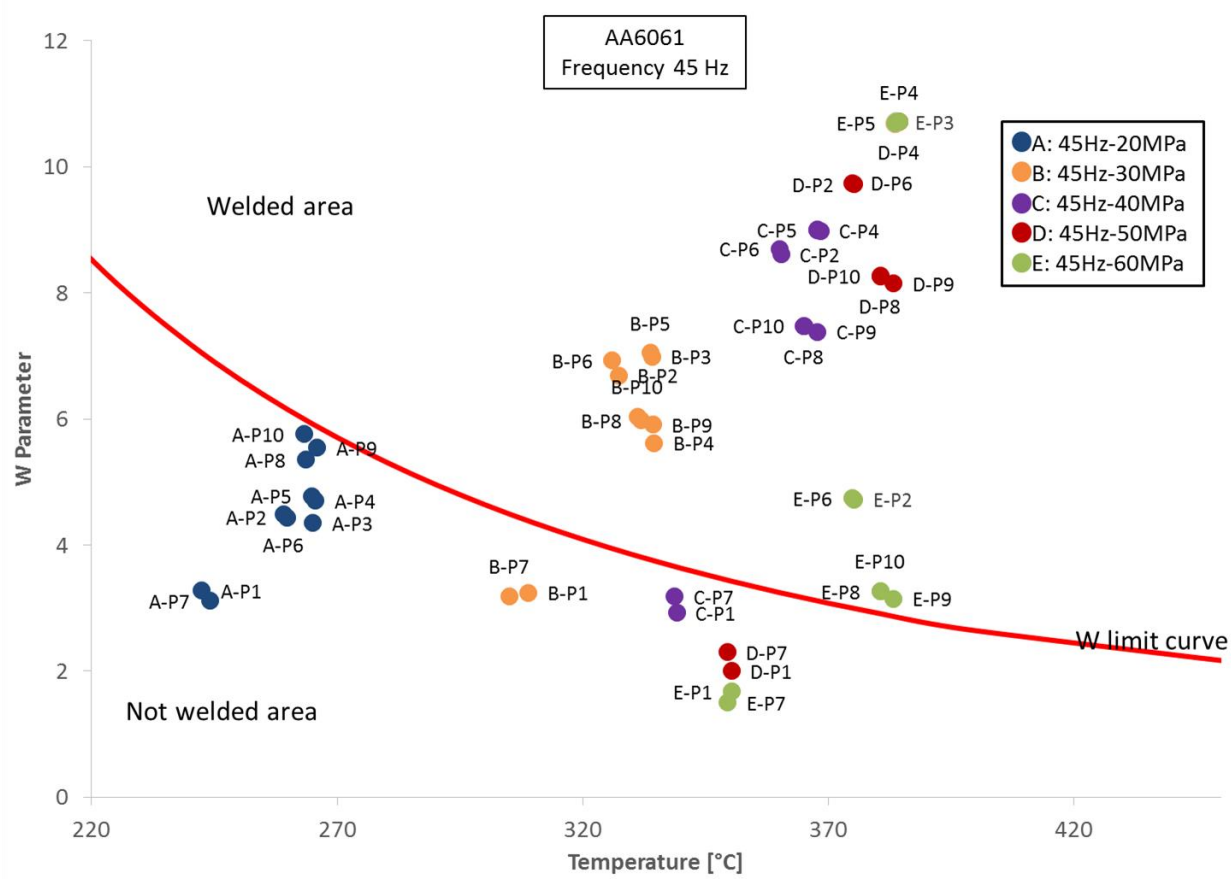

Figure 4.42 Calculated W parameter and threshold value limit curve for the tests 45 Hz.

Regarding the welded joints characterized by 45 Hz of frequency, the results are similar to the results obtained using the AA6082. Insufficient heat condition is obtained with an interface pressure of 20 MPa (figure 4.31). Increasing the contact pressure up to 30 MPa (fig. 4.42 points B), 40 MPa (fig. 4.42 points C) and 50 MPa (fig. 4.42 points D) a sound condition is reached.

Finally, as regards the joints characterized of 45 Hz of frequency, the instability condition is reached increasing the contact pressure up to 60 MPa (fig. 4.42 points E). In this case the identified points in the central area, P2, P3, P4 are welded. All the other identified points are close the limit curve because are expelled by the generated flash. The points P1 and P7 are not welded.

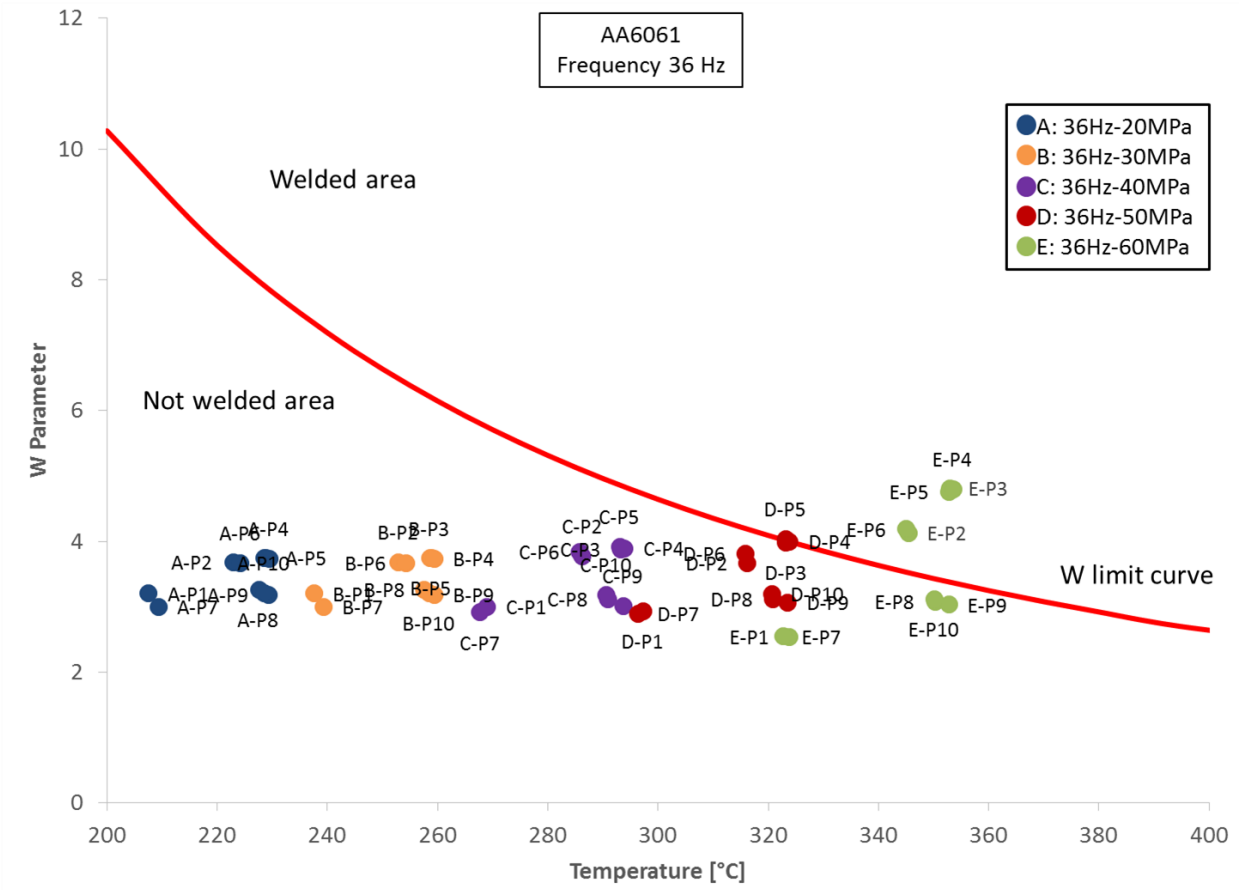

Figure 4.43 Calculated W parameter and threshold value limit curve for the tests 36 Hz.

Finally, as regards the joints characterized of 36 Hz of frequency, the insufficient heat condition is obtained independently of the contact pressure choice. In the figure 4.43, the bonding criterion results of the identified points are shown for each parameter combinations kept the frequency to 36 Hz.

Probably, for this process parameter combination, a partial portion of the interface of the joint will be welded because the points situated in the central part of the interface are welded while the Points P8, P9 P10, P1 and P7 are not welded. Anyway the insufficient heat condition is obtained.

4.6 Neural Networks

In order to build the training data set for the neural network, the value of the welding criterion calculated for each of the observation points and the final position of the observation points highlighted in the paragraph of the application of the time-flow criterion on AA6082 have been used. In this way, 150 values were obtained. As already mentioned, due to the relatively simple material flow, ten tracking point for each process condition were utilized.

The values of temperature, strain and strain rate, during the process, were collected and used to calculate the flow stress σ at each time increment j (Eq. 4.4) The proposed neural network was designed with the aim to get two separated outputs: a qualitative output, indicating if the bonding process occurred for the considered observation point; a quantitative output, indicating the level of “soundness” of the bonding. In order to build the latter indicator, a parameter Q was defined starting from the Piwnik and Plata parameter W for each observed point:

$$Q_i = \frac{W_i}{W_i^{LIM}}$$

equation 4.7

For the considered alloy, the critical value W_{LIM}=W_{LIM}(T) was taken from literature [161] (eq 4.5). The input data set was build calculating an average value of the considered field variable for a specific tracking point (i) and a given process, according to the following:

$$\varepsilon_i = \frac{\int_{t0}^{t1} \varepsilon dt}{t1 - t0} \cong \sum_j \frac{\varepsilon_j \Delta t_j}{t1 - t0}$$

equation 4.8

$$\dot{\varepsilon}_i = \frac{\int_{t0}^{t1} \dot{\varepsilon} dt}{t1 - t0} \cong \sum_j \frac{\dot{\varepsilon}_j \Delta t_j}{t1 - t0}$$

equation 4.9

$$T_i = \frac{\int_{t0}^{t1} T dt}{t1 - t0} \cong \sum_j \frac{T_j \Delta t_j}{t1 - t0}$$

equation 4.10

$$p_i = \frac{\int_{t0}^{t1} p dt}{t1 - t0} \cong \sum_j \frac{p_j \Delta t_j}{t1 - t0}$$

equation 4.11

In this way 150 data have been derived from the process corresponding to 15 process conditions and 10 points for each process. It is worth noticing that, due to the occurring material flow, a few observation points moved towards the edges of the specimen during the process and were finally expelled as flash. These points were not considered for the NN development.

A supervised multilayer feed-forward network based on the back-propagation algorithm was built. The network architecture consists of 5 hidden layers: the input layer is characterized by 4 neurons corresponding to the average values of temperature, strain, strain rate and pressure as calculated in equations 4.8-4.11. Three hidden layers were used, with 5, 4 and 3 neurons, respectively.

Finally an output layer, with 2 neurons corresponding to the qualitative “welded-not welded” output and the quantitative Q parameter is found. All the data were normalized to assume values between -1 and 1. Each layer was fully connected to the next and, according to the back-propagation rule, the weights of the connections linking a neuron belonging to a certain layer to a neuron belonging to the next were adjusted in the learning stage with the aim to minimize the error between the desired output and the calculated one.

The topology of the utilized network, reported in figure 4.44, was determined on the basis of an optimization procedure aimed to improve the network performances.

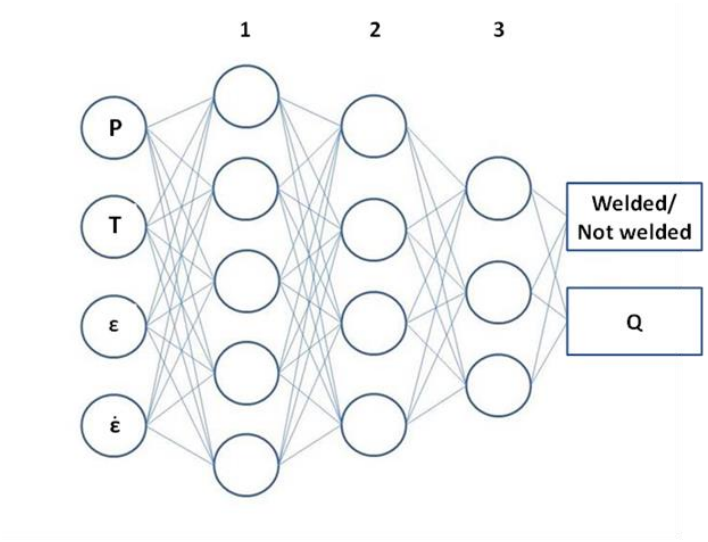

Figure 4.44 Architecture of the Utilized Neural Network

Different networks have been tried with different structures, consist of one, two, three, four and five layers. The number of neurons was gradually increased. If the architecture is too small, the network may not have sufficient degrees of freedom to learn the process correctly. On the other hand, if the network is too large, it may over fit the data. Each network was trained five times by assigning new weights at each training cycle, and the average error was considered to assess the network performance.

The training was carried out providing to the network the input data coming from the simulations. Target data came from both the experimental observations (welded/not-welded qualitative output) and combined experimental and numerical results, i.e. the value of Q. About 10 % of the available input and target data were randomly chosen and used for the test of the network.

The fifteen data randomly chosen to test the network are shown in table 4.4:

Id	*Point*	*Process Parameters*	*Welded*	*Q*
1	P 7	36 Hz-20 MPa	N	0.26
2	P 8	36 Hz-20 MPa	N	0.46
3	P 6	36 Hz-30 MPa	N	0.69
4	P 9	36 Hz-30 MPa	N	0.81

5	P4	36 Hz–60 MPa	Y	1.28
6	P 4	45 Hz-30 MPa	Y	1.98
7	P 8	45 Hz-30 MPa	Y	1.96
8	P 8	45 Hz-40 MPa	Y	2.78
9	P 4	45 Hz–60MPa	Y	6.12
10	P 10	45 Hz–60MPa	Y	5.92
11	P2	58 Hz–30 MPa	Y	3.27
12	P9	58 Hz–30 MPa	Y	3.42
13	P 4	58 Hz-40 MPa	Y	5.26
14	P 3	58 Hz-60 MPa	Y	6.22
15	P 5	58 Hz-60 MPa	Y	5.67

Table 4.4 Observation points randomly selected for the test of the developed Neural Network.

Figure 4.45 shows the comparison between the calculated and observed welding condition. When the Boolean network output is equal to -1, no solid bonding is obtained. On the contrary, an output equal to 1 indicates that solid bonding was obtained.

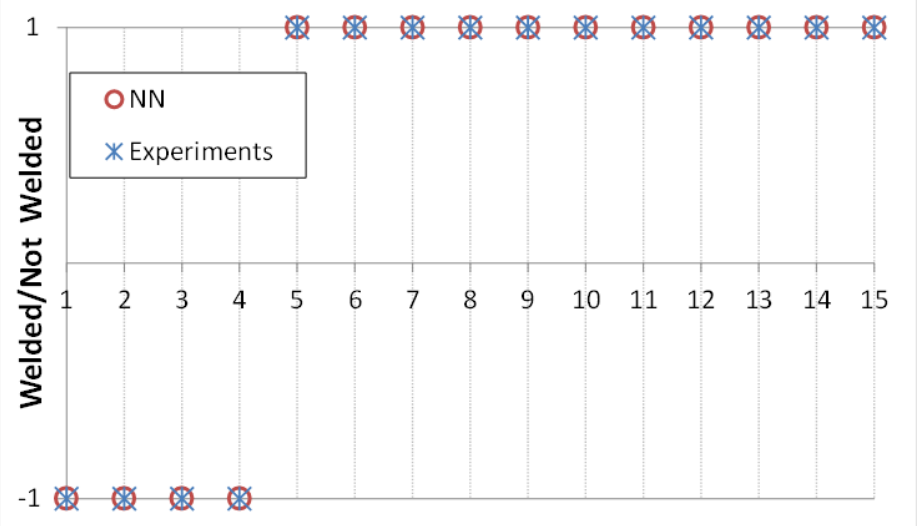

Figure 4.45 Neural Network response: solid bonding occurrence

As it can be observed from the figure, the network can predict correctly the bonding of all the fifteen points analyzed. Figure 4.46 shows the Q parameter, as predicted by the NN and analytically calculated.

The prediction of the network proves to be correct in almost all of the points analyzed, with deviations from the actual values that, for most case studies, do not exceed 5 %. A few observations can be made on these results. First, the insufficient heat area can be identified considering all the points for which Q<1 is obtained. It is noted that ID5 belongs to the joint obtained

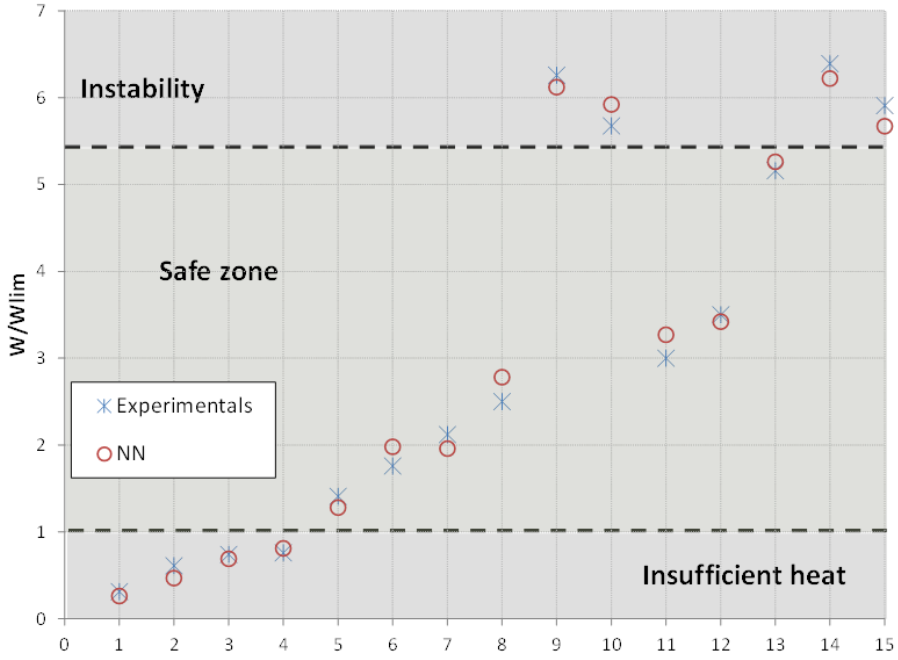

Figure 4.46 Neural Network response: Q parameter

Optical observation (Figure 4.10) shows that material continuity is obtained at the center of the transverse section. Although this is considered a “not welded” joint (Fig. 4.3), as compared to a sound joint (Figure 4.7), it can be stated that solid bonding occurred at the center of the joint. As ID5 corresponds to tracking point P4 (Fig. 4.24), i.e. the point laying at the center of the contact area, it can be concluded that the prediction of the neural network is correct.

Additionally, it is seen that ID 9, 10, 14 and 15 are considered as “welded” by the NN. Looking at the experimental results (Fig. 4.3), it arises that the corresponding welds, i.e. 45 Hz-60 MPa and 58 Hz-60 MPa, are labeled as “instability”: the excess of heat

input causes a complete burn off of the specimen till its collapse under the applied pressure. At these points, the phenomenon of solid bonding occurs experimentally.

However, the calculated parameter Q has a very high value. In this way a further zone, the instability area, can be identified in Figure 4.46. The extension of this area is limited by ID 13, corresponding to the sound joint obtained with 58 HZ and 40 MPa. It is worth noticing that the threshold (dotted black line in Figure 4.46) was identified with an average value of Q=5.4 based also on the NN results obtained with different random tests point sets.

5 Conclusion

A detailed research activity on the solid state welding techniques called Friction Stir Welding and Linear Friction Welding has been carried out with the aim to apply the analytical bonding criteria, originally developed for different manufacturing processes and so to obtain an integrated numerical tool able to predict the occurrence of solid bonding starting from the process input parameters. In particular the research has been developed in three main stages:

- In the first stage, a preliminary analysis of the existing literature on the applicability of the bonding criteria has been made. Aluminum alloys have been mainly chosen, as they are often considered as difficult to weld or "unweldable" by traditional fusion welding processes. In particular, the aluminum alloys AA6082 and AA6061 have been chosen; then the most interesting joint configurations, both from an academic and an industrial point of view, have been considered. In particular, the butt joints for both the processes FSW and LFW; finally the most influent operative parameters, both technological and geometrical, have been selected to be engineered during the subsequent stages of the research work. The full experimental plans have been obtained for both the processes in order to obtain different quality of the welded joints to allow the applicability of the bonding criterion proposed in all welding condition, as final output of this first stage.
- In the second stage attention has been focused on the previously considered case studies: at first the effect of the operative parameters have been studied; then, varying such parameters in proper ranges, the mechanical properties of the joints have been analyzed by ultimate tensile stress tests and microhardness tests. The joint microstructure, the material flow and the deformation and bonding mechanics have also been taken into account and related to the operative parameters on one side, and to the joint final mechanical properties on the other.

  At the same time, a numerical model of the processes has been developed and set up, obtaining information on temperature, strain, strain rate distributions, as well as on forces and on the material flow. Once tested and validated the model effectiveness through several different experimental tests,

the missing link between the input process parameters and the mechanical properties of the joint has been found. The experimental and numerical campaign above described led to an exhaustive knowledge of the material flow phenomena as function of the process operative parameters, thus obtaining effective design tools for both the solid state welding processes.

- In the third and last stage, the applicability of the pressure-time criterion has been tested on the FSW process and LFW process using the two different aluminum alloys. Additionally, a Neural Network was developed able to predict, starting from the evolution of temperature, strain, strain rate and pressure on the bonding line, the occurrence of the solid bonding as well as quantitative parameter Q providing information on the “quality” of the weld.

Regarding a FSW process so, an experimental and numerical campaign was performed on FSW of AA6061 aluminum alloy and AA6082 aluminum alloy. The applicability to FSW of analytical bonding criteria, originally developed for different manufacturing processes, was assessed. FSW experiments were developed with tool rotation and welding speed varying in a wide range in order to obtain different conditions of joint integrity. An already developed and verified numerical model for FSW was used to calculate the main field variables values and the occurring material flow needed to implement the considered criteria. The following main conclusions can be drawn:

- In FSW the material close to the welding line flows around the tool in the retreating side and is eventually left at the advancing side after a few turns depending on the ratio between the tool rotation and welding speed;
- The Pivnik and Plata criterion is suited for FSW. The results of this criterion are consistent with what expected based on the process input parameters are calculated; For the same criterion it was possible to see that just one of the 36 analyzed points for each aluminum alloys, i.e. P6 of test 500 rpm-200 mm/min AA6061, gives back a wrong prediction.

A Neural Network was developed able to predict, starting from the evolution of temperature, strain, strain rate and pressure on the bonding line, the occurrence of the solid binding as well as quantitative parameter Q providing information on the “quality” of the weld. In order to train the network, experimental data have been taken

form literature for Roll Bonding and Porthole Die Extrusion. A numerical model has been set up for each of the two processes and the experiments have been simulated thus obtaining the field variable histories to be used for the training of the network.

On the basis of the obtained results the following conclusion can be drawn:

- For RB and PDE the separation/bonding surface can be easily identified and remains the same during the process. On the contrary, in FSW of butt joints the separation surface, initially vertical, moves due to the thermo-mechanical action of the tool assuming the so called zig-zag shape. The developed model is able to describe the evolution of this line tracking each field variable;
- Although the three processes are characterized by completely different process mechanics, the points involved into the bonding phenomenon show similar trends of temperature, strain, strain rate and normal pressure. This indicates that the microstructural evolutions resulting in the solid bonding are the same; in this way a similar grain morphology and micro and macro mechanical properties can be expected;
- The developed Network is able to correctly predict the occurrence of solid bonding; the use of two output indicators at the same time dissipates all uncertain conditions calculated when the Piwnik & Plata criterion gives values close to threshold conditions.

Regarding a LFW process so, a combined experimental and numerical study on LFW of AA6082-T6 and a numerical campaign was performed on LFW of AA6061 aluminum alloy. The applicability to LFW of analytical bonding criteria was assessed. LFW experiments were developed varying oscillation frequency and interface pressure between the specimens, keeping constant process time, and oscillation amplitude in order to obtain different conditions of joint integrity. The study carried out through the use of thermo-mechanical model showed excellent results compared with the results experimentally obtained. The model is able to predict the effects of process variables, namely pressure and oscillation frequency, on the main field variables distributions a temperature, strain and strain rate.

- The occurrence of the solid bonding is strongly affected by the evolution of temperature, strain, strain rate and pressure in the direction normal to the

separation surface for those points that will be laying along the bonding surface at the end of the considered process;

- For low heat input bonding may occur just at the center of the joints, while, for large heat input, the joint collapses under the applied pressure and an excess of flash is observed.
- The Pivnik and Plata criterion is appropriate for LFW process. The results of this criterion are consistent compared with the experimental results; for this criterion it was possible to see that no one of the 150 analyzed points for each aluminum alloys gives back a wrong prediction.
- The bonding criterion proposed is able to describe, not only the cases in which the bonding occurred, but also the cases study which the solid state bonding condition is verified in a portion of the welding surface due to the special interface condition reached.

An integrated numerical tool able to predict the occurrence of solid bonding starting from the process input parameters was developed. A FEM method was integrated with a dedicated neural network able to predict two parameters: a qualitative one, indicating whether solid bonding take place, and a quantitative one, based on the Pivnik and Plata criterion, providing information on the soundness of the weld produced. Based on the obtained results, the following main conclusions can be drawn:

- Starting from the local values of pressure, temperature, strain and strain rate calculated through the numerical model, the developed nn can effectively predict the occurrence of solid bonding through a qualitative Boolean parameter. This statement holds true also for only partially welded specimens.
- The quantitative nn output allows the identification three different areas and, hence, the prediction of the occurrence of instability or the insufficient heat.

6 Future developments

The results reached with this thesis aims to give a know-how on the raised issues. A few points may give rise to new research starting such as, for example, an experimental campaign using the results of the bonding criterion applied to the LFW of AA6061 aluminum alloy.

Quite interesting, it could be to implement a bonding criteria proposed in this thesis, in other lightweight alloys such as titanium, magnesium or to other aluminum alloys. This new study has to provide to identify a new W limit dependent of the material. A wide experiments campaign have to be perform in order to obtain a solid tool for a process design of experiments such as the ones shown in this thesis.

7 Bibliography

[1] J. Tusek and M. Suban, "Hybrid welding with arc and laser beam," *Science and Technology of Welding and Joining,* vol. 4, pp. 308-311, 1999.

[2] A. Heinz, A. Haszler, C. Keidel, S. Moldenhauer, R. Benedictus, and W. S. Miller, "Recent development in aluminium alloys for aerospace applications," *Materials Science and Engineering A,* vol. 280, pp. 102-107, 2000.

[3] h. e. e. e. c. p. t. v. c. i. e. h. (16.09.2014).

[4] J. C. Lippold, *Welding Metallurgy and Weldability*, 2014.

[5] M. P. Matheny and K. F. Graff, "Ultrasonic welding of metals," in *Power Ultrasonics: Applications of High-Intensity Ultrasound*, ed, 2014, pp. 259-293.

[6] A. A. A. Mousavi and S. T. S. Al-Hassani, "Numerical and experimental studies of the mechanism of the wavy interface formations in explosive/impact welding," *Journal of the Mechanics and Physics of Solids,* vol. 53, pp. 2501-2528, 2005.

[7] A. S. Bahrani and B. Crossland, "SOLID-PHASE WELDING PROCESSES - 3. FRICTION WELDING," *Chart Mech Eng,* vol. 23, pp. 61-63, 65, 1976.

[8] T. Aizawa, M. Kashani, and K. Okagawa, "Application of magnetic pulse welding for aluminum alloys and SPCC steel sheet joints," *Welding Journal (Miami, Fla),* vol. 86, pp. 119-s-124-s, 2007.

[9] J. Muehlhause, S. Gall, and S. Mueller, "Simulation of the co-extrusion of hybrid Mg/Al profiles," in *Key Engineering Materials*, pp. 113-119, 2010.

[10] P. G. Partridge and C. M. Ward-Close, "Diffusion bonding of advanced materials," *Metals and materials Bury St Edmunds,* vol. 5, pp. 334-339, 1989.

[11] A. S. Rogachev, "Exothermic reaction waves in multilayer nanofilms," *Russian Chemical Reviews,* vol. 77, pp. 21-37, 2008.

[12] A. Nikanorov, E. Baake, H. Brauer, and C. Weil, "Approaches for coupled numerical simulation of high frequency tube welding process," in *COUPLED PROBLEMS 2015 - Proceedings of the 6th International Conference on Coupled Problems in Science and Engineering*, pp. 657-665, 2015.

[13] H. J. Kim and S. K. Youn, "Three dimensional analysis of high frequency induction welding of steel pipes with impeder," *Journal of Manufacturing Science and Engineering, Transactions of the ASME,* vol. 130, pp. 0310051-0310057, 2008.

[14] H. Valberg, "Extrusion welding in aluminium extrusion," *International Journal of Materials and Product Technology,* vol. 17, pp. 497-556, 2002.

[15] N. Tsuji, Y. Saito, H. Utsunomiya, and S. Tanigawa, "Ultra-fine grained bulk steel produced by accumulative roll-bonding (ARB) process," *Scripta Materialia,* vol. 40, pp. 795-800, 1999.

[16] H. Valberg and T. Malvik, "Experimental investigation of the material flow inside the bearing channel in aluminium extrusion," *International Journal of Materials and Product Technology,* vol. 9, pp. 428-463, 1994.

[17] R. Z. Valiev, "Structure and mechanical properties of ultrafine-grained metals," *Materials Science and Engineering A,* vol. 234-236, pp. 59-66, 1997.

[18] Z. Y. Ma, "Friction stir processing technology: A review," *Metallurgical and Materials Transactions A: Physical Metallurgy and Materials Science,* vol. 39 A, pp. 642-658, 2008.

[19] B. Crossland, "Friction welding," *Contemp Phys,* vol. 12, pp. 559-574, 1971.

[20] E. D. Nicholas and W. M. Thomas, "A review of friction processes for aerospace applications," *International Journal of Materials and Product Technology,* vol. 13, pp. 45-55, 1998.
[21] W. S. Miller, L. Zhuang, J. Bottema, A. J. Wittebrood, P. De Smet, A. Haszler, and A. Vieregge, "Recent development in aluminium alloys for the automotive industry," *Materials Science and Engineering A,* vol. 280, pp. 37-49, 2000.
[22] E. Ceretti, L. Mazzoni, and C. Giardini, "Simulation of metal flow and welding prediction in porthole die extrusion: The influence of the geometrical parameters," *International Journal of Material Forming,* vol. 2, pp. 101-104, 2009.
[23] R. Akeret, "Extrusion welds-quality aspects are now center stage," *Proceedings of the Fifth International Aluminum Extrusion Technology Seminar,* vol. 1, pp. 319-336, 1992.
[24] B. Bourqui, A. Huber, C. Moulin, and A. Bunetti, "Improved weld seam quality using 3D FEM simulations in correlation with practice," in *Proceedings of First EAA (European Aluminum Association-Extruders Division)*, Montichiari BS, 2002.
[25] M. Plata and J. Piwnik, "Theoretical and experimental analysis of seam weld formation in hot extrusion of aluminum alloys," *7th International Aluminum Extrusion Technology,* vol. 1, pp. 205-211, 2000.
[26] S. Støren, "The theory of extrusion-Advances and challenges," *International Journal of Mechanical Sciences,* vol. 35, pp. 1007-1020, 1993.
[27] J. X. Xie, T. Murakami, K. Ikeda, and H. Takahashi, "Experimental simulation of metal flow in porthole-die extrusion," *Journal of Materials Processing Tech.,* vol. 49, pp. 1-11, 1995.
[28] G. Liu, J. Zhou, and J. Duszczyk, "FE analysis of metal flow and weld seam formation in a porthole die during the extrusion of a magnesium alloy into a square tube and the effect of ram speed on weld strength," *Journal of Materials Processing Technology,* vol. 200, pp. 185-198, 2008.
[29] Y. T. Kim and K. Ikeda, "Flow behavior of the billet surface layer in porthole die extrusion of aluminum," *Metallurgical and Materials Transactions A: Physical Metallurgy and Materials Science,* vol. 31, pp. 1635-1643, 2000.
[30] R. K. Uyyuru and H. Valberg, "Physical and numerical analysis of the metal flow over the punch head in backward cup extrusion of aluminium," *Journal of Materials Processing Technology,* vol. 172, pp. 312-318, 2006.
[31] Y. T. Kim, K. Ikeda, and T. Murakami, "Metal flow in porthole die extrusion of aluminium," *Journal of Materials Processing Technology,* vol. 121, pp. 107-115, 2002.
[32] Y. F. He, S. S. Xie, L. Cheng, G. J. Huang, and Y. Fu, "FEM simulation of aluminum extrusion process in porthole die with pockets," *Transactions of Nonferrous Metals Society of China (English Edition),* vol. 20, pp. 1067-1071, 2010.
[33] L. Donati, L. Tomesani, M. Schikorra, N. Ben Khalifa, and A. E. Tekkaya, "Friction model selection in FEM simulations of aluminium extrusion," *International Journal of Surface Science and Engineering,* vol. 4, pp. 27-41, 2010.
[34] T. Kloppenborg, M. Schwane, N. B. Khalifa, A. E. Tekkaya, and A. Brosius, "Experimental and numerical analysis of material flow in porthole die extrusion," in *Key Engineering Materials*, pp. 97-104, 2012.

[35] F. Gagliardi, G. Ambrogio, and L. Filice, "On the die design in AA6082 porthole extrusion," *CIRP Annals - Manufacturing Technology,* vol. 61, pp. 231-234, 2012.
[36] G. Buffa, L. Donati, L. Fratini, and L. Tomesani, "Solid state bonding in extrusion and FSW: Process mechanics and analogies," *Journal of Materials Processing Technology,* vol. 177, pp. 344-347, 2006.
[37] F. Micari, *Processi di formatura dei metalli*. Palermo: Flaccovio Dario, 2004.
[38] M. Ruppert, W. Böhm, H. Nguyen, H. W. Höppel, M. Merklein, and M. Göken, "Influence of upscaling accumulative roll bonding on the homogeneity and mechanical properties of AA1050A," *Journal of Materials Science,* vol. 48, pp. 8377-8385, 2013.
[39] N. Takata, S. H. Lee, and N. Tsuji, "Ultrafine grained copper alloy sheets having both high strength and high electric conductivity," *Materials Letters,* vol. 63, pp. 1757-1760, 2009.
[40] N. Tsuji, Y. Ito, Y. Saito, and Y. Minamino, "Strength and ductility of ultrafine grained aluminum and iron produced by ARB and annealing," *Scripta Materialia,* vol. 47, pp. 893-899, 2002.
[41] http://www.totalmateria.com. (01 March 2015).
[42] N. Tsuji, Y. Saito, S. H. Lee, and Y. Minamino, "ARB (accumulative roll-bonding) and other new techniques to produce bulk ultrafine grained materials," *Advanced Engineering Materials,* vol. 5, pp. 338-344, 2003.
[43] I. Topic, H. W. Höppel, D. Staud, M. Merklein, M. Geiger, and M. Göken, "Formability of accumulative roll bonded aluminum AA1050 and AA6016 investigated using bulge tests," *Advanced Engineering Materials,* vol. 10, pp. 1101-1109, 2008.
[44] A. Azushima, R. Kopp, A. Korhonen, D. Y. Yang, F. Micari, G. D. Lahoti, P. Groche, J. Yanagimoto, N. Tsuji, A. Rosochowski, and A. Yanagida, "Severe plastic deformation (SPD) processes for metals," *CIRP Annals - Manufacturing Technology,* vol. 57, pp. 716-735, 2008.
[45] N. Bay, A. Azushima, P. Groche, I. Ishibashi, M. Merklein, M. Morishita, T. Nakamura, S. Schmid, and M. Yoshida, "Environmentally benign tribo-systems for metal forming," *CIRP Annals - Manufacturing Technology,* vol. 59, pp. 760-780, 2010.
[46] J. Y. Huang, Y. T. Zhu, H. Jiang, and T. C. Lowe, "Microstructures and dislocation configurations in nanostructured Cu processed by repetitive corrugation and straightening," *Acta Materialia,* vol. 49, pp. 1497-1505, 2001.
[47] A. Korbel and H. Dybiec, "The problem of the negative strain-rate sensitivity of metals under the portevin-lechatelier deformation conditions," *Acta Metallurgica,* vol. 29, pp. 89-93, 1981.
[48] S. Mizunuma, "Large straining behavior and microstructure refinement of several metals by torsion extrusion process," in *Materials Science Forum*, pp. 185-190, 2006.
[49] K. Nakamura, K. Neishi, K. Kaneko, M. Nakagaki, and Z. Horita, "Development of severe torsion straining process for rapid continuous grain refinement," *Materials Transactions,* vol. 45, pp. 3338-3342, 2004.
[50] R. Z. Valiev, "The new trends in fabrication of bulk nanostructured materials by SPD processing," *Journal of Materials Science,* vol. 42, pp. 1483-1490, 2007.
[51] Y. Saito, H. Utsunomiya, N. Tsuji, and T. Sakai, "Novel ultra-high straining process for bulk materials development of the accumulative roll-bonding (ARB) process," *Acta Materialia,* vol. 47, pp. 579-583, 1999.

[52] Y. Saito, N. Tsuji, H. Utsunomiya, T. Sakai, and R. G. Hong, "Ultra-fine grained bulk aluminum produced by accumulative roll-bonding (ARB) process," *Scripta Materialia,* vol. 39, pp. 1221-1227, 1998.
[53] C. C. Koch, D. G. Morris, K. Lu, and A. Inoue, "Ductility of nanostructured materials," *MRS Bulletin,* vol. 24, pp. 54-58, 1999.
[54] N. Tsuji, "Ultrafine grained steels managing both high strength and ductility," *Journal of Physics: Conference Series,* vol. 165, 2009.
[55] M. Kadkhodaee, M. Babaiee, H. D. Manesh, M. Pakshir, and B. Hashemi, "Evaluation of corrosion properties of Al/nanosilica nanocomposite sheets produced by accumulative roll bonding (ARB) process," *Journal of Alloys and Compounds,* vol. 576, pp. 66-71, 2013.
[56] I. Salvatori, "Ultra grain refinement of low C steels by accumulative roll bonding," in *Materials Science Forum* vol. 503-504, ed, 2006, pp. 311-316.
[57] M. Eizadjou, A. Kazemi Talachi, H. Danesh Manesh, H. Shakur Shahabi, and K. Janghorban, "Investigation of structure and mechanical properties of multi-layered Al/Cu composite produced by accumulative roll bonding (ARB) process," *Composites Science and Technology,* vol. 68, pp. 2003-2009, 2008.
[58] M. C. Chen and W. Wu, "Microstructure changed during Accumulative roll bonding of Al/Mg composite," in *Solid State Phenomena* vol. 124-126, ed, 2007, pp. 1445-1448.
[59] S. Roy, B. R. Nataraj, S. Suwas, S. Kumar, and K. Chattopadhyay, "Accumulative roll bonding of aluminum alloys 2219/5086 laminates: Microstructural evolution and tensile properties," *Materials and Design,* vol. 36, pp. 529-539, 2012.
[60] M. W. Thomas, Nicholas, E.D., Needham, J.C., Murch, M.G., Templesmith, P., Dawes, C.J., GB Patent, December 1991.
[61] B. London, M. Mahoney, W. Bingel, M. Calabrese, R. H. Bossi, and D. Waldron, "Material flow in friction stir welding monitored with Al-SiC and Al-W composite markers," in *TMS Annual Meeting*, pp. 3-12, 2003.
[62] W. D. Lockwood, B. Tomaz, and A. P. Reynolds, "Mechanical response of friction stir welded AA2024: Experiment and modeling," *Materials Science and Engineering A,* vol. 323, pp. 348-353, 2002.
[63] T. Hirata, T. Oguri, H. Hagino, T. Tanaka, S. W. Chung, Y. Takigawa, and K. Higashi, "Influence of friction stir welding parameters on grain size and formability in 5083 aluminum alloy," *Materials Science and Engineering A,* vol. 456, pp. 344-349, 2007.
[64] M. Cabibbo, H. J. McQueen, E. Evangelista, S. Spigarelli, M. Di Paola, and A. Falchero, "Microstructure and mechanical property studies of AA6056 friction stir welded plate," *Materials Science and Engineering A,* vol. 460-461, pp. 86-94, 2007.
[65] G. Liu, L. E. Murr, C. S. Niou, J. C. McClure, and F. R. Vega, "Microstructural aspects of the friction-stir welding of 6061-T6 aluminum," *Scripta Materialia,* vol. 37, pp. 355-361, 1997.
[66] M. Mahoney, R. S. Mishra, T. Nelson, J. Flintoff, R. Islamgaliev, and Y. Hovansky, "High strain rate, thick section superplasticity created via friction stir processing," in *Friction Stir Welding and Processing*, pp. 183-194, 2001.
[67] M. Geiger, F. Micari, M. Merklein, L. Fratini, D. Contorno, A. Giera, and D. Staud, "Friction Stir Knead Welding of steel aluminium butt joints," *International Journal of Machine Tools and Manufacture,* vol. 48, pp. 515-521, 2008.

[68] G. Buffa, L. Fratini, T. Gnibl, M. Wieland, and M. Merklein, "Process mechanics in friction stir welding of magnesium alloys: Experimental and numerical analysis," in *Key Engineering Materials*, pp. 735-740, 2012.
[69] G. Buffa, L. Fratini, T. Gnibl, M. Wieland, and M. Merklein, "On the friction stir welding of titanium alloys: Experimental measurements and FEM model fine tuning," *Steel Research International,* vol. SPL. ISSUE, pp. 591-594, 2012.
[70] R. John, K. V. Jata, and K. Sadananda, "Residual stress effects on near-threshold fatigue crack growth in friction stir welds in aerospace alloys," *International Journal of Fatigue,* vol. 25, pp. 939-948, 2003.
[71] http://www.twi-global.com/. (01 April 2015).
[72] http://www.frictionstirlink.com/. (30 April 2015).
[73] A. Askari, S. Silling, B. London, and M. Mahoney, "Modeling and analysis of friction stir welding processes," in *Friction Stir Welding and Processing*, pp. 43-54, 2001.
[74] N. Afrin, D. L. Chen, X. Cao, and M. Jahazi, "Microstructure and tensile properties of friction stir welded AZ31B magnesium alloy," *Materials Science and Engineering A,* vol. 472, pp. 179-186, 2008.
[75] W. B. Lee, Y. M. Yeon, and S. B. Jung, "The joint properties of dissimilar formed Al alloys by friction stir welding according to the fixed location of materials," *Scripta Materialia,* vol. 49, pp. 423-428, 2003.
[76] R. S. Mishra and Z. Y. Ma, "Friction stir welding and processing," *Materials Science and Engineering R: Reports,* vol. 50, pp. 1-78, 2005.
[77] G. Çam, "Friction stir welded structural materials: Beyond Al-alloys," *International Materials Reviews,* vol. 56, pp. 1-48, 2011.
[78] M. W. Mahoney, C. G. Rhodes, J. G. Flintoff, R. A. Spurling, and W. H. Bingel, "Properties of friction-stir-welded 7075 T651 aluminum," *Metallurgical and Materials Transactions A: Physical Metallurgy and Materials Science,* vol. 29, pp. 1955-1964, 1998.
[79] A. P. Reynolds, W. D. Lockwood, and T. U. Seidel, "Processing-property correlation in friction stir welds," *Materials Science Forum,* vol. 331, p. II/, 2000.
[80] B. Heinz, B. Skrotzki, and G. Eggeler, "Microstructural and mechanical characterization of a friction stir welded Al-alloy," *Materials Science Forum,* vol. 331, p. II/, 2000.
[81] K. A. A. Hassan, P. B. Prangnell, A. F. Norman, D. A. Price, and S. W. Williams, "Effect of welding parameters on nugget zone microstructure and properties in high strength aluminium alloy friction stir welds," *Science and Technology of Welding and Joining,* vol. 8, pp. 257-268, 2003.
[82] V. Balasubramanian, "Relationship between base metal properties and friction stir welding process parameters," *Materials Science and Engineering A,* vol. 480, pp. 397-403, 2008.
[83] S. Rajakumar and V. Balasubramanian, "Establishing relationships between mechanical properties of aluminium alloys and optimised friction stir welding process parameters," *Materials and Design,* vol. 40, pp. 17-35, 2012.
[84] Y. S. Sato and H. Kokawa, "Distribution of tensile property and microstructure in friction stir weld of 6063 aluminum," *Metallurgical and Materials Transactions A: Physical Metallurgy and Materials Science,* vol. 32, pp. 3023-3031, 2001.

[85] L. B. Johannes, I. Charit, R. S. Mishra, and R. Verma, "Enhanced superplasticity through friction stir processing in continuous cast AA5083 aluminum," *Materials Science and Engineering A,* vol. 464, pp. 351-357, 2007.
[86] S. H. C. Park, S. Hirano, K. Okamoto, W. Gan, R. H. Wagoner, K. Chung, and C. Kim, "Characterization of dual phase steel friction-stir weld for tailor-welded blank applications," in *TMS Annual Meeting*, pp. 253-260, 2007.
[87] T. J. Lienert, W. L. Stellwag Jr, B. B. Grimmett, and R. W. Warke, "Friction stir welding studies on mild steel," *Welding Journal (Miami, Fla),* vol. 82, pp. 1/s-9/s, 2003.
[88] W. B. Lee, Y. M. Yeon, and S. B. Jung, "Joint properties of friction stir welded AZ31B - H24 magnesium alloy," *Materials Science and Technology,* vol. 19, pp. 785-790, 2003.
[89] R. L. Goetz and K. V. Jata, "Modeling friction stir welding of titanium and aluminum alloys," in *Friction Stir Welding and Processing*, pp. 35-42, 2001.
[90] P. Ulysse, "Three-dimensional modeling of the friction stir-welding process," *International Journal of Machine Tools and Manufacture,* vol. 42, pp. 1549-1557, 2002.
[91] R. Nandan, G. G. Roy, and T. Debroy, "Numerical simulation of three dimensional heat transfer and plastic flow during friction stir welding," *Metallurgical and Materials Transactions A: Physical Metallurgy and Materials Science,* vol. 37, pp. 1247-1259, 2006.
[92] R. Nandan, G. G. Roy, T. J. Lienert, and T. Debroy, "Three-dimensional heat and material flow during friction stir welding of mild steel," *Acta Materialia,* vol. 55, pp. 883-895, 2007.
[93] G. Buffa, J. Hua, R. Shivpuri, and L. Fratini, "A continuum based fem model for friction stir welding - Model development," *Materials Science and Engineering A,* vol. 419, pp. 389-396, 2006.
[94] L. Fratini, G. Buffa, D. Palmeri, J. Hua, and R. Shivpuri, "Material flow in FSW of AA7075-T6 butt joints: Numerical simulations and experimental verifications," *Science and Technology of Welding and Joining,* vol. 11, pp. 412-421, 2006.
[95] S. Xu, X. Deng, A. P. Reynolds, and T. U. Seidel, "Finite element simulation of material flow in friction stir welding," *Science and Technology of Welding and Joining,* vol. 6, pp. 191-193, 2001.
[96] Z. Zhang and J. T. Chen, "The simulation of material behaviors in friction stir welding process by using rate-dependent constitutive model," *Journal of Materials Science,* vol. 43, pp. 222-232, 2008.
[97] C. M. Chen and R. Kovacevic, "Finite element modeling of friction stir welding - Thermal and thermomechanical analysis," *International Journal of Machine Tools and Manufacture,* vol. 43, pp. 1319-1326, 2003.
[98] Y. H. Zhao, S. B. Lin, F. X. Qu, and L. Wu, "Influence of pin geometry on material flow in friction stir welding process," *Materials Science and Technology,* vol. 22, pp. 45-50, 2006.
[99] V. Soundararajan, S. Zekovic, and R. Kovacevic, "Thermo-mechanical model with adaptive boundary conditions for friction stir welding of Al 6061," *International Journal of Machine Tools and Manufacture,* vol. 45, pp. 1577-1587, 2005.
[100] M. Guerra, C. Schmidt, J. C. McClure, L. E. Murr, and A. C. Nunes, "Flow patterns during friction stir welding," *Materials Characterization,* vol. 49, pp. 95-101, 2002.

[101] H. Schmidt and J. Hattel, "A local model for the thermomechanical conditions in friction stir welding," *Modelling and Simulation in Materials Science and Engineering,* vol. 13, pp. 77-93, 2005.
[102] G. Buffa, J. Hua, R. Shivpuri, and L. Fratini, "Design of the friction stir welding tool using the continuum based FEM model," *Materials Science and Engineering A,* vol. 419, pp. 381-388, 2006.
[103] R. Nandan, T. DebRoy, and H. K. D. H. Bhadeshia, "Recent advances in friction-stir welding - Process, weldment structure and properties," *Progress in Materials Science,* vol. 53, pp. 980-1023, 2008.
[104] X. Cao, M. Jahazi, and M. Guerin, "Friction stir welding of an aerospace magnesium alloy," in *TMS Annual Meeting*, Orlando, FL; United States, pp. 213-222, 2007.
[105] W. M. Thomas and E. D. Nicholas, "Friction stir welding for the transportation industries," *Materials and Design,* vol. 18, pp. 269-273, 1997.
[106] W. Richter, "Herbeifuehrung einer haftverbindung zwischen plaettchen aus werkzeugstahl und deren traegern nach art einer schweissung oder loetung," *Patent No. DE477084,* 1929.
[107] A. W. E. Nentwig and L. Appel, "Untersuchungen zum linear-reibschweißen von metallen," *Schweiss. Schneid.,* vol. 47, pp. 648-653, 1995.
[108] R. Maurya and J. Kauzlarich, "Bonding apparatus - Friction welding by reciprocal motion," *Patent Nos. US3420428-A DE1552871-A CA844858-A,* 1969.
[109] http://www.twi-global.com, 01 April 2015.
[110] A. Vairis and M. Frost, "On the extrusion stage of linear friction welding of Ti 6a1 4V," *Materials Science and Engineering A,* vol. 271, pp. 477-484, 1999.
[111] A. Vairis and M. Frost, "High frequency linear friction welding of a titanium alloy," *Wear,* vol. 217, pp. 117-131, 1998.
[112] A. Vairis and M. Frost, "Modelling the linear friction welding of titanium blocks," *Materials Science and Engineering A,* vol. 292, pp. 8-17, 2000.
[113] A. T. Bikmeyev, A. Vairis, R. K. Gazizov, and A. M. Yamileva, "Modeling the temperature distribution in the contact area of a moving object in the case of linear friction welding," in *ASME International Mechanical Engineering Congress and Exposition, Proceedings (IMECE)*, p. V08AT09A038, 2013.
[114] P. Wanjara and M. Jahazi, "Linear friction welding of Ti-6Al-4V: Processing, microstructure, and mechanical-property inter-relationships," *Metallurgical and Materials Transactions A: Physical Metallurgy and Materials Science,* vol. 36, pp. 2149-2164, 2005.
[115] Y. Guo, T. Jung, Y. L. Chiu, H. Li, S. Bray, and P. Bowen, "Microstructure and microhardness of Ti6246 linear friction weld," *Materials Science and Engineering A,* vol. 562, pp. 17-24, 2013.
[116] Y. Guo, Y. Chiu, M. M. Attallah, H. Li, S. Bray, and P. Bowen, "Characterization of dissimilar linear friction welds of α-β Titanium alloys," *Journal of Materials Engineering and Performance,* vol. 21, pp. 770-776, 2012.
[117] A. C. Addison, "Linear friction welding of engineering metals," TWI Ltd, Cambridge, UK2008.
[118] I. Bhamji, M. Preuss, P. L. Threadgill, and A. C. Addison, "Solid state joining of metals by linear friction welding: A literature review," *Materials Science and Technology,* vol. 27, pp. 2-12, 2011.

[119] S. Caldara, "Blisks-an Investigation into the Linear Friction Welding of Titanium Alloy IMI 318," department of mechanical and manufacturing engineering University of Bristol, Bristol, 1987.
[120] A. C. Addison, "Linear friction welding information for production engineering," TWI Ltd, Cambridge, UK2010.
[121] A. Mateo, "On the feasibility of BLISK produced by linear friction welding," *Revista de Metalurgia,* vol. 50, p. e023, 2014.
[122] W. Li, J. Suo, T. Ma, Y. Feng, and K. Kim, "Abnormal microstructure in the weld zone of linear friction welded Ti-6.5Al-3.5Mo-1.5Zr-0.3Si titanium alloy joint and its influence on joint properties," *Materials Science and Engineering A,* vol. 599, pp. 38-45, 2014.
[123] A. M. Korsunsky, K. E. James, and M. R. Daymond, "Intergranular stresses in polycrystalline fatigue: Diffraction measurement and self-consistent modelling," *Engineering Fracture Mechanics,* vol. 71, pp. 805-812, 2004.
[124] X. Song, M. Xie, F. Hofmann, T. S. Jun, T. Connolley, C. Reinhard, R. C. Atwood, L. Connor, M. Drakopoulos, S. Harding, and A. M. Korsunsky, "Residual stresses in Linear Friction Welding of aluminium alloys," *Materials and Design,* vol. 50, pp. 360-369, 2013.
[125] F. Schröder, R. M. Ward, A. R. Walpole, R. P. Turner, M. M. Attallah, J. C. Gebelin, and R. C. Reed, "Linear friction welding of Ti6Al4V: Experiments and modelling," *Materials Science and Technology (United Kingdom),* vol. 31, pp. 372-384, 2015.
[126] R. Bayindir and H. Ates, "Comparison of the constructed control methods for a friction-welding machine," *Materials and Manufacturing Processes,* vol. 20, pp. 131-146, 2005.
[127] M. Sahin, "Joining with friction welding of high-speed steel and medium-carbon steel," *Journal of Materials Processing Technology,* vol. 168, pp. 202-210, 2005.
[128] Y. T. M. Corzo, M. Anglada and A. Mateo, "FRACTURE BEHAVIOUR OF LINEAR FRICTION WELDS IN TITANIUM ALLOYS," *Anales de la Mecánica de Fractura,* vol. Vol 1, 2007.
[129] M. J. Corzo M., Villechaise P., Rebours C., Ferte J.-P., Gach E., Roder O., Llanes L., Anglada M. y Mateo A.,, "High-cycle fatigue performance of dissimilar linear friction welds of titanium alloys," presented at the Proceedings of the 9th International Fatigue Congress, Atlanta, USA, 2006.
[130] T. Ma, W. Y. Li, Q. Xu, Y. Zhang, J. Li, S. Yang, and H. Liao, "Microstructure evolution and mechanical properties of linear friction welded 45 steel joint," *Advanced Engineering Materials,* vol. 9, pp. 703-707, 2007.
[131] W. Y. Li, T. J. Ma, S. Q. Yang, Q. Z. Xu, Y. Zhang, J. L. Li, and H. L. Liao, "Effect of friction time on flash shape and axial shortening of linear friction welded 45 steel," *Materials Letters,* vol. 62, pp. 293-296, 2008.
[132] W. Y. Li, T. Ma, and J. Li, "Numerical simulation of linear friction welding of titanium alloy: Effects of processing parameters," *Materials and Design,* vol. 31, pp. 1497-1507, 2010.
[133] B. Lang, T. C. Zhang, X. H. Li, and D. L. Guo, "Microstructural evolution of a TC11 titanium alloy during linear friction welding," *Journal of Materials Science,* vol. 45, pp. 6218-6224, 2010.
[134] J. Romero, M. M. Attallah, M. Preuss, M. Karadge, and S. E. Bray, "Effect of the forging pressure on the microstructure and residual stress development in Ti-6Al-4V linear friction welds," *Acta Materialia,* vol. 57, pp. 5582-5592, 2009.

[135] A. Chamanfar, M. Jahazi, J. Gholipour, P. Wanjara, and S. Yue, "Suppressed liquation and microcracking in linear friction welded WASPALOY," *Materials and Design,* vol. 36, pp. 113-122, 2012.
[136] C. Mary and M. Jahazi, "Multi-scale analysis of IN-718 microstructure evolution during linear friction welding," *Advanced Engineering Materials,* vol. 10, pp. 573-578, 2008.
[137] F. Rotundo, L. Ceschini, A. Morri, T. S. Jun, and A. M. Korsunsky, "Mechanical and microstructural characterization of 2124Al/25 vol.%SiC p joints obtained by linear friction welding (LFW)," *Composites Part A: Applied Science and Manufacturing,* vol. 41, pp. 1028-1037, 2010.
[138] T. S. Jun, F. Rotundo, L. Ceschini, and A. M. Korsunsky, "A study of residual stresses in Al/SiCp linear friction weldment by energy-dispersive neutron diffraction," in *Key Engineering Materials*, pp. 517-520, 2008.
[139] T. S. Jun, F. Rotundo, X. Song, L. Ceschini, and A. M. Korsunsky, "Residual strains in AA2024/AlSiCp composite linear friction welds," *Materials and Design,* vol. 31, pp. S117-S120, 2010.
[140] L. Ceschini, A. Morri, F. Rotundo, A. Korsunsky, and T. S. Jun, "Linear Friction Welding (LFW) of metal matrix composites," *Metallurgia Italiana,* vol. 102, pp. 23-30, 2010.
[141] R. Turner, J. C. Gebelin, R. M. Ward, and R. C. Reed, "Linear friction welding of Ti-6Al-4V: Modelling and validation," *Acta Materialia,* vol. 59, pp. 3792-3803, 2011.
[142] R. Turner, R. M. Ward, R. March, and R. C. Reed, "The magnitude and origin of residual stress in Ti-6Al-4V linear friction welds: An investigation by validated numerical modeling," *Metallurgical and Materials Transactions B: Process Metallurgy and Materials Processing Science,* vol. 43, pp. 186-197, 2012.
[143] A. R. McAndrew, P. A. Colegrove, A. C. Addison, B. C. D. Flipo, and M. J. Russell, "Modelling the influence of the process inputs on the removal of surface contaminants from Ti-6Al-4V linear friction welds," *Materials and Design,* vol. 66, pp. 183-195, 2015.
[144] F. Schroeder, R. M. Ward, R. P. Turner, M. M. Attallah, J. C. Gebelin, R. C. Reed, and A. R. Walpole, "Linear friction welding of titanium alloys for aeroengine applications: Modelling and validation," in *ASM Proceedings of the International Conference: Trends in Welding Research*, pp. 886-892, 2013.
[145] E. Ceretti, L. Fratini, C. Giardini, and D. La Spisa, "Numerical modelling of the linear friction welding process," *International Journal of Material Forming,* vol. 3, pp. 1015-1018, 2010.
[146] M. Grujicic, G. Arakere, B. Pandurangan, C. F. Yen, and B. A. Cheeseman, "Process modeling of Ti-6Al-4V linear friction welding (LFW)," *Journal of Materials Engineering and Performance,* vol. 21, pp. 2011-2023, 2012.
[147] M. Grujicic, R. Yavari, J. S. Snipes, S. Ramaswami, C. F. Yen, and B. A. Cheeseman, "Linear friction welding process model for carpenter custom 465 precipitation-hardened martensitic stainless steel," *Journal of Materials Engineering and Performance,* vol. 23, pp. 2182-2198, 2014.
[148] J. Sorina-Müller, M. Rettenmayr, D. Schneefeld, O. Roder, and W. Fried, "FEM simulation of the linear friction welding of titanium alloys," *Computational Materials Science,* vol. 48, pp. 749-758, 2010.

[149] M. Vaziri, S. Berg, D. Sandberg, and I. T. Gheinani, "Three-dimensional finite element modelling of heat transfer for linear friction welding of Scots pine," *Wood Material Science and Engineering,* vol. 9, pp. 102-109, 2014.
[150] A. Chamanfar, M. Jahazi, J. Gholipour, P. Wanjara, and S. Yue, "Mechanical property and microstructure of linear friction welded WASPALOY," *Metallurgical and Materials Transactions A: Physical Metallurgy and Materials Science,* vol. 42, pp. 729-744, 2011.
[151] M. Karadge, M. Preuss, C. Lovell, P. J. Withers, and S. Bray, "Texture development in Ti-6Al-4V linear friction welds," *Materials Science and Engineering A,* vol. 459, pp. 182-191, 2007.
[152] L. Donati and L. Tomesani, "The effect of die design on the production and seam weld quality of extruded aluminum profiles," *Journal of Materials Processing Technology,* vol. 164-165, pp. 1025-1031, 2005.
[153] H. H. Jo, C. S. Jeong, S. K. Lee, and B. M. Kim, "Determination of welding pressure in the non-steady-state porthole die extrusion of improved Al7003 hollow section tubes," *Journal of Materials Processing Technology,* vol. 139, pp. 428-433, 2003.
[154] L. Donati and L. Tomesani, "The prediction of seam welds quality in aluminum extrusion," *Journal of Materials Processing Technology,* vol. 153-154, pp. 366-373, 2004.
[155] H. Valberg, "Extrusion welding in porthole die extrusion," *Proc. 6th Int. Al. Extr. Techn. Sem.,* vol. 2, pp. 213-224, 1996.
[156] H. Y. Wu, S. Lee, and J. Y. Wang, "Solid-state bonding of iron-based alloys, steel-brass, and aluminum alloys," *Journal of Materials Processing Technology,* vol. 75, pp. 173-179, 1998.
[157] R. Akeret, "Properties of pressure welds in extruded aluminium alloy sections," *Journal of the Institute of Metals,* vol. 100, pp. 202-207, 1972.
[158] C. Y. Barlow, P. Nielsen, and N. Hansen, "Multilayer roll bonded aluminium foil: Processing, microstructure and flow stress," *Acta Materialia,* vol. 52, pp. 3967-3972, 2004.
[159] R. Jamaati and M. R. Toroghinejad, "Investigation of the parameters of the cold roll bonding (CRB) process," *Materials Science and Engineering A,* vol. 527, pp. 2320-2326, 2010.
[160] L. Donati, L. Tomesani, and G. Minak, "Characterization of seam weld quality in AA6082 extruded profiles," *Journal of Materials Processing Technology,* vol. 191, pp. 127-131, 2007.
[161] E. Ceretti, L. Fratini, F. Gagliardi, and C. Giardini, "A new approach to study material bonding in extrusion porthole dies," *CIRP Annals - Manufacturing Technology,* vol. 58, pp. 259-262, 2009.
[162] G. D'Urso, M. Longo, E. Ceretti, and C. Giardini, "Coupled simulative-experimental procedure for studying the solid state bonding phenomena," in *Key Engineering Materials*, pp. 181-188, 2012.
[163] G. D'Urso, C. Giardini, M. Longo, and A. Segatori, "Microstructural evaluation of solid state welds obtained by means of flat rolling process," *Metallurgia Italiana,* vol. 107, pp. 31-37, 2015.
[164] G. Buffa, L. Fratini, S. Pellegrino, and F. Micari, "On the field variables influence on bonding phenomena during FSW processes: Experimental and numerical study," in *Key Engineering Materials*, pp. 484-491, 2013.

[165] L. Donati and L. Tomesani, "Seam welds modeling and mechanical properties prediction in the extrusion of AA6082 alloy," in *Key Engineering Materials*, pp. 125-136, 2008.
[166] G. Buffa, S. Pellegrino, and L. Fratini, "Analytical bonding criteria for joint integrity prediction in friction stir welding of aluminum alloys," *Journal of Materials Processing Technology,* vol. 214, pp. 2102-2111, 2014.
[167] L. Fu, *Neural Networks in Computer Intelligence,* 1994.
[168] H. Ney, "On the Probabilistic Interpretation of Neural Network Classifiers and Discriminative Training Criteria," *IEEE Transactions on Pattern Analysis and Machine Intelligence,* vol. 17, pp. 107-119, 1995.
[169] L. Frosini and G. Petrecca, "Neural networks for load torque monitoring of an induction motor," *Applied Soft Computing,* vol. 1, pp. 215-223, 2001.
[170] B. Ayhan, M. Y. Chow, and M. H. Song, "Multiple discriminant analysis and neural-network-based monolith and partition fault-detection schemes for broken rotor bar in induction motors," *IEEE Transactions on Industrial Electronics,* vol. 53, pp. 1298-1308, 2006.
[171] H. Okuyucu, A. Kurt, and E. Arcaklioglu, "Artificial neural network application to the friction stir welding of aluminum plates," *Materials and Design,* vol. 28, pp. 78-84, 2007.
[172] E. Boldsaikhan, E. M. Corwin, A. M. Logar, and W. J. Arbegast, "The use of neural network and discrete Fourier transform for real-time evaluation of friction stir welding," *Applied Soft Computing Journal,* vol. 11, pp. 4839-4846, 2011.
[173] S. Malinov and W. Sha, "Application of artificial neural networks for modelling correlations in titanium alloys," *Materials Science and Engineering A,* vol. 365, pp. 202-211, 2004.
[174] G. Buffa, L. Fratini, and F. Micari, "Mechanical and microstructural properties prediction by artificial neural networks in FSW processes of dual phase titanium alloys," *Journal of Manufacturing Processes,* vol. 14, pp. 289-296, 2012.
[175] G. Buffa, G. Patrinostro, and L. Fratini, "Using a neural network for qualitative and quantitative predictions of weld integrity in solid bonding dominated processes," *Computers and Structures,* vol. 135, pp. 1-9, 2014.
[176] H. B. Chen, K. Yan, T. Lin, S. B. Chen, C. Y. Jiang, and Y. Zhao, "The investigation of typical welding defects for 5456 aluminum alloy friction stir welds," *Materials Science and Engineering A,* vol. 433, pp. 64-69, 2006.
[177] N. N:, "Tensile testing - Part 2: Method of test at elevated temperature (ISO 6892-2:2011)," Beuth-Verlag, Germany, 2011.
[178] J. E. Hockett and O. D. Sherby, "Large strain deformation of polycrystalline metals at low homologous temperatures," *Journal of the Mechanics and Physics of Solids,* vol. 23, pp. 87-98, 1975.
[179] *ASTM Standards,* 1994.
[180] D. Staud and M. Merklein, "Zug-Druck-Versuche an Miniaturproben zur Erfassung von Parametern fur kinematische Verfestigungsmodelle," *Tagungsband Werkstoffprüfung,* vol. 2, pp. 211-218, 2009.
[181] S. Bouvier, H. Haddadi, P. Levée, and C. Teodosiu, "Simple shear tests: Experimental techniques and characterization of the plastic anisotropy of rolled sheets at large strains," *Journal of Materials Processing Technology,* vol. 172, pp. 96-103, 2006.

[182] M. Merklein and M. Biasutti, "Forward and reverse simple shear test experiments for material modeling in forming simulations," in *Special Edition: 10th International Conference on Technology of Plasticity, ICTP 2011*, pp. 702-707, 2011.
[183] M. Merklein and M. Biasutti, "Development of a biaxial tensile machine for characterization of sheet metals," *Journal of Materials Processing Technology,* vol. 213, pp. 939-946, 2013.
[184] F. Barlat, Y. Maeda, K. Chung, M. Yanagawa, J. C. Brem, Y. Hayashida, D. J. Lege, K. Matsui, S. J. Murtha, S. Hattori, R. C. Becker, and S. Makosey, "Yield function development for aluminum alloy sheets," *Journal of the Mechanics and Physics of Solids,* vol. 45, pp. 1727-1763, 1997.
[185] R. Hill, "Constitutive modelling of orthotropic plasticity in sheet metals," *Journal of the Mechanics and Physics of Solids,* vol. 38, pp. 405-417, 1990.
[186] J. E. Hatch, *Aluminum: Properties and Physical Metallurgy,* 1984.
[187] L. Fratini, S. Beccari, and G. Buffa, "Friction stir welding fem model improvement through inverse thermal characterization," in *Transactions of the North American Manufacturing Research Institute of SME*, pp. 259-266, 2005.
[188] F.-C. Chen and H. K. Khalil, "Adaptive control of nonlinear systems using neural networks," *International Journal of Control,* vol. 55, pp. 1299-1317, 1992.
[189] L. Fratini, G. Buffa, D. Campanella, and D. La Spisa, "Investigations on the linear friction welding process through numerical simulations and experiments," *Materials and Design,* vol. 40, pp. 285-291, 2012.
[190] G. Buffa, M. Cammalleri, D. Campanella, and L. Fratini, "Shear coefficient determination in linear friction welding of aluminum alloys," *Materials and Design,* vol. 82, pp. 238-246, 2015.